TITLE:	**NISP Instrument Thermal design, Justification file and FEM study**		
Date:	14/03/2014	**Issue:**	2.0
Reference:	EUCL-IBO-RP-7-002		
Custodian:	A. De Rosa		

Authors :	**Function:**	**Date:**	**Signature:**
A. De Rosa	NISP Thermal Engineer	14.03.2014	DocuSigned by: A. G. De Rosa 337AE19382FD4C5...
G. Morgante	NISP Thermal Architect	14.03.2014	DocuSigned by: G. Morgante CB3619E10F5F40E...
Contributors :	**Function:**	**Date:**	**Signature:**
Laurent Martin	AMT		
Rafael Toledo	C&C Architect		
Leonardo Corcione	Electrical Architect		
Tony Pamplona	NI-SA Manager		
Carlotta Bonoli	OBSW Architect		
Frank Grupp	Optical Architect		
Jean-Claude Clemens	Detector Chain Architect		
Marco Riva	Mechanism Architect		
Felix Hormuth	Calibration Architect		
Fabio Bortoletto	Data Process Architect		
Sebastiano Ligori	Harness Architect		
Massimo Trifoglio	EGSE Architect		
Approved by:	**Function:**	**Date:**	**Signature:**
E. Prieto	NISP System Manager	14.03.2014	DocuSigned by: E. Prieto 84C1917795BF434...
T. Maciaszek	NISP Instrument PM	14.03.2014	
Authorised by:	**Function:**	**Date:**	**Signature:**
T. Maciaszek	NISP Instrument PM	14.03.2014	DocuSigned by: T Maciaszek 610833C2BF2E41D...

Change Log

Issue	Date	Page	Description Of Change
0.1	23/07/13		First draft of the doc
1.0	09/10/13	all	General review of the document. Comments received integrated. More figures and tables added
2.0	05/03/14	all	General review of the document. Modified materials for some components. Modified idealization of Mylar shields insulation. Performed transient analysis on NI-DS, added chapter with results. Added design justification for the NISP thermal design.

Table of Contents

1. Purpose and Scope 5
2. Documents 6
2.1. Applicable documents 6
2.2. Reference documents 6
3. Acronyms 6
4. NISP Thermal Architecture 7
4.1. Thermal Requirements 7
4.2. NI-OMA thermal design 9
4.2.1. The Filter and Grism Wheel Assembly (FWA/GWA) 11
4.2.2. The Collimator Lens Assembly (CoLA) and Camera Lens Assembly (CaLA) 11
4.2.3. Calibration Unit (CU) 12
4.3. NI-DS 12
5. Input CAD model 14
6. Units 14
7. Materials 15
8. FEM model 25
8.1. Imported CAD model and shields: geometry 25
8.2. Idealization 27
8.3. Contact interactions 31
8.4. MLI insulation idealization [added in rev. 2] 31
8.5. Radiative interactions 32
8.6. View factor calculation 33
8.7. Mesh statistics 33
8.8. Mesh images 33
9. Loads and Boundary conditions 35
9.1. Loads 35
9.1.1. Sidecars 36
9.1.2. Detectors 36
9.1.3. FWA motor (for steady state analysis) 37
9.1.4. GWA motor (for steady state analysis) 37
9.1.5. FWA-GWA (transient analysis) 38
9.2. Boundary conditions 41
9.2.1. Bipods (BP1, BP2, BP3, BP4, BP5, BP6) 41
9.2.2. Detector flange (CSS) 41
9.2.3. Sidecars mainframe (SSS) 42
9.2.4. External box 43
10. Simulation runs 45
10.1. Steady state analysis 45
10.2. Transient analysis 45
10.3. Summary tables of the performed jobs 46
10.3.1. Steady state 46

11. Paths 47

12. Detectors and sidecars numeration 62

13. Results 63

13.1. Job 11 – Steady state analysis, Nominal Case, Instrument Off, Not-OP mode 63

13.1.1. JOB 11 temperature profiles on optical units 88

13.1.2. JOB 11 Heat Loads 94

13.2. Job 12 – Steady state analysis, Max T Case, Instrument Off, Not-OP mode 96

13.2.1. JOB 12 temperature profiles on optical units 121

13.2.2. JOB 12 Heat Loads 127

13.3. Job 13 – Steady state analysis, Min T Case, Instrument Off, Not-OP mode 129

13.3.1. JOB 13 temperature profiles on optical units 154

13.3.2. JOB 13 Heat Loads 160

13.4. Job 14 - Steady state analysis, Nominal Case, Instrument On, OP mode 162

13.4.1. JOB 14 temperature profiles on bipods and optical units 187

13.4.2. JOB 14 Heat Loads 193

13.5. Job 15 – Steady state analysis, Max T Case, Instrument On, OP mode 196

13.5.1. JOB 15 temperature profiles on bipods and optical units 221

13.5.2. JOB 15 Heat Loads 227

13.6. Job 16 – Steady state analysis, Min T Case, Instrument On, OP mode 229

13.6.1. JOB 16 temperature profiles on bipods and optical units 254

13.6.2. JOB 16 Heat Loads 260

14. Heat load results comparison 262

14.1. Bipods comparison 262

14.1.1. All motors off (case 11,12,13) – Not OP mode 263

14.1.2. All motors on (case 14,15,16) – OP mode 263

15. Transient Analysis 264

15.1. Transient analysis results 265

15.1.1. Job-46 – 15mK increment and asymptotic equilibrium 266

15.1.2. Job-45 – dynamic response to curve 1 267

15.1.3. Job-48 – sinusoidal excitation: period 30s; amplitude 1K 268

15.1.4. Job-47 – sinusoidal excitation: period 60s, amplitude 1K 269

15.1.5. Job-52 – sinusoidal excitation: period 120s ; amplitude 1K 270

15.1.6. Job-53 – sinusoidal excitation: period 240s ; amplitude 1K 271

15.1.7. Job-54 – sinusoidal excitation: period 480s ; amplitude 1K 272

15.1.8. Job-55 – sinusoidal excitation: period 960s ; amplitude 1K 273

15.1.9. Job-50 – sinusoidal excitation: period 3600s [1h]; amplitude 1K 274

15.1.10. Job-51 – sinusoidal excitation: period 36000s [10h]; amplitude 1K 275

15.2. Damping Factor estimation 276

1. Purpose and Scope

This document describes the NISP thermal architecture and the justification of its design. The demonstration of the validity of such design in terms of meeting the baseline requirements relies on the results of the detailed thermal FEM analysis of the instrument.

The thermal architecture is based on the Instrument PLM thermo-mechanical configuration and on the favourable conditions of the L2 thermal environment. For this reason the driving objective of the NIP thermal design is to maximize exploitation of passive cooling and instrument performances while minimizing design complexity.

The analysis has been performed using a finite elements code (Abaqus). The NISP CAD model has been imported in the Abaqus environment and detailed with a fine mesh structure (around 10^5 nodes): both the conductive and radiative heat transfer in operational and non-operational conditions has been simulated in three main thermal cases, Hot, Nominal and Cold conditions. Results in terms of heat loads at the main internal and external interfaces are reported together with the temperature distribution of the instrument units.

This document shall be used as a reference for the NISP thermal design and FEM simulation, as it contains a description of all assumptions and definitions for the model.

2. Documents

2.1. Applicable documents

AD	Title / Author	Document Reference	Issue	Date
1	Euclid EID-A	EUCL-EST-EID-3-001	1.3	27/05/2013
2	PERD Payload Elements Requirements Document	EUCL-EST-RD-3-002	1.1	18/11/2013
3	NISP Instrument Interface Control Document (ICD)	EUCL-LAM-ICD-7-001	2.0	13/12/2013
4	NISP Instrument Description document	EUCL-LAM-OTH-7-001	1.0	14/06/2013
5	NI-SA Design Definition File and Trade off	EUCL-LAM-RP-7-006	1.1	18/11/2013

2.2. Reference documents

RD	Title / Author	Document Reference	Issue	Date
0	Euclid Consortium Acronyms List	EUCL-IAP-LI-1-001	2.02	28/02/2014
1	NI-TC Design Definition File and Trade off	EUCL-LAM-RP-7-010	PDR	14/04/2014
2	NISP Instrument Design Justification File	EUCL-LAM-OTH-7-004	1.0	14/06/2013
3	NI-TC Design Justification Report	EUCL-IBO-NPS-RP-00299	1.0	06404/2012
4	NI-SA to wheel IF thermal transient analysis	EUCL-IBO-NPS-RP-00224	1.0	17/12/2012

3. Acronyms

See RD0

4. NISP Thermal Architecture

The PLM thermal design for the NISP instrument is based on a purely passive configuration: radiators coupled to cold space, exploiting the favorable conditions of the L2 thermal environment, will provide the main temperature references for the NI-OMA structure and the NI-DS. The NISP thermal architecture is schematically shown in Figure 4-1. There are three main general boundaries of the instrument thermal architecture:

1. the PLM Instrument Cavity (IC);
2. the Baseplate (BP);
3. the PLM Thermal Interfaces (TIF1 and 2) for the Detector System (SCS and SCA)

The first item defines the radiative environment, while the other two the conductive boundaries.

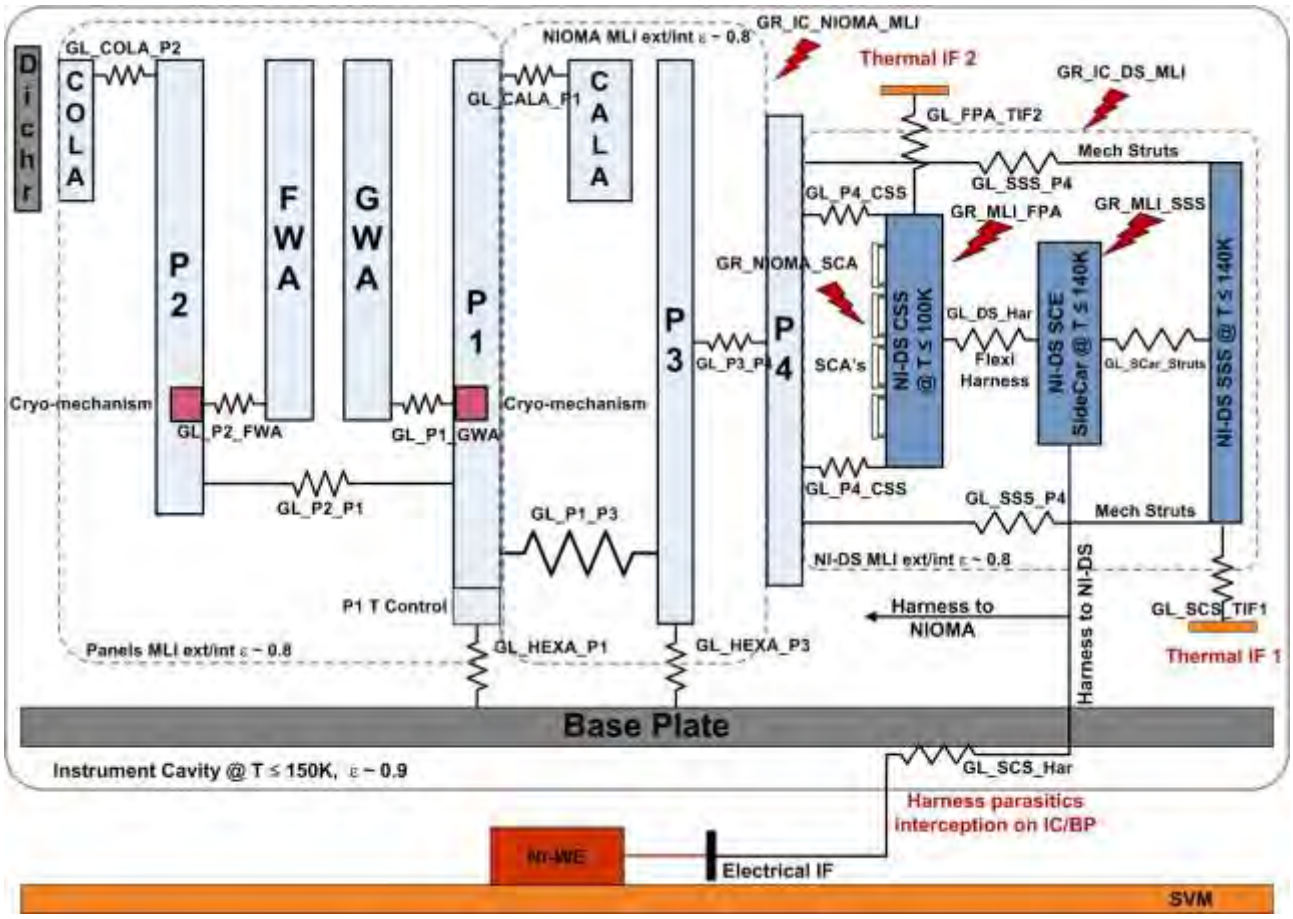

Figure 4-1. NISP thermal concept

4.1. Thermal Requirements

The NIPS thermal design shall be compliant to the general thermal requirements. All the NISP units shall meet all performance requirements in the acceptance and qualification operational spacecraft interface temperature ranges, derived from the operational design spacecraft interface temperature ranges, including their guaranteed temperature stability and temperature gradients, as defined in the table below extracted from the [AD1].

		NI-OMADA Mounting	NI-SSS	NI-CSS
Conductive I/F Temperatures				
T_{min} Operation [1, 2]	[K]	120	120	80
T_{max} Operation [1, 2]	[K]	135	135	95
T_{min} non-op. [1]	[K]	120	120	80
T_{max} non-op. [1]	[K]	313	313	313
T_{min} switch-on	[K]	= Tmin non-op	= Tmin non-op	= Tmin non-op
T_{max} switch-on	[K]	= Tmax op.	= Tmax op.	= Tmax op.
T_{min} ground AFT [4]	[K]	288	288	288
T_{max} ground AFT [(3, 4)]	[K]	313	313	313
Conductive I/F Temperature Stability				
short term [4]	[K]	+/- 0.2	+/- 0.8	+/- 0.1
ref. time short	[s]	11000	11000	11000
mid term	[K]	N/A	N/A	+/- 0.5 (TBC)
ref. time mid	[days]	N/A	N/A	30
long term	[K]	+/- 2.0	+/- 2.0	+/- 2.0
Conductive I/F Temperature Gradients				
Overall	[K]	+/- 2.0	+/- 1.0	+/- 0.5
Conductive I/F Couplings				
Area	[cm^2]	30 (TBC)	7.5	7.5
Number	[-]	6 (TBC)	4	4
Radiative I/F Virtual Box				
Dimension	[-]	Dimensions and geometry defined in the NISP ICD [AD7]		
Radiative I/F Temperatures				
T_{min} Operation [1]	[K]	120		
T_{max} Operation [1]	[K]	150		
T_{min} non-op. [1]	[K]	120		
T_{max} non-op. [1]	[K]	150		
T_{min} switch-on	[K]	= Tmin non-op		
T_{max} switch-on	[K]	= Tmax op.		
T_{min} ground AFT [4]	[K]	288		
T_{max} ground AFT [3, 4]	[K]	313		
Radiative I/F Temperature Stability				
short term	[K]	+/- 0.5		

ref. time	[s]	11000		
long term	[K]	+/- 2.0		
Radiative I/F Temperature Gradients				
Overall	[K]	+/- 7.0		
Radiative I/F Couplings				
MLI		Yes	Yes	Yes

Table 4-1. NISP to PLM Interface Temperatures, Gradients, Stabilities and Couplings

Table notes:

1. Temperature range compliant to the required temperature stability is ensured by the PLM within these specified limits. The temperature limits are to be considered as average values at the interface.
2. These interface operational temperatures shall be selected at the end of phase B. The selected value shall be compatible with the minimum and maximum values of **Errore. L'origine riferimento non è stata trovata.** that shall never been exceeded during the full mission duration taking into account the maximum allowed TIF's temperature variations of ±2K over the full mission duration.
3. Bake-out can be performed at temperatures above the non-op ground temperature limits specified to limit its duration as allowed by the specific unit design.
4. The op. ground AFT temperature limits apply to Ambient Functional Tests. It represents the ranges where the units can be switched on and operated with degraded performance. For cold performance test on ground the operational limits apply. The temperature limits experienced by instrument units when unpowered during ground testing are specified in requirements EIR-738 and EIR-739

The allocated heat loads for the NISP instrument at the thermal interfaces are reported in the next table:

Interface	Max heat load @ IF (W)	Min heat load @ IF (W)
NIOMADA mounting	1.0	0.0
NI-SSS	5.0	3.2
NI-CSS (Detectors)	2.7	1.7

Table 4-2. NIPS allocated loads at PLM interfaces

4.2. NI-OMA thermal design

Operating temperature and thermal stability of the units are the key drivers for the instrument architecture: the structure (NI-SA) is by design thermally insulated from the main mechanical interface (the Baseplate) through the struts that support panels P1 and P3. In such a way the heat exchanged conductively with the Baseplate should be minimized (theoretically tending to zero). In this configuration the units inside the NI-OMA, and the optical lenses especially, are less sensitive to fluctuations and can exploit the whole instrument thermal mass to operate in a more stable condition. Cooling at the required operating temperatures is provided mainly by heat extraction through the two thermal interfaces (TIF1 and TIF2) and, partially, by radiative exchange with PLM background. Thermal InterFace 1 (TIF1) and 2 are the interfaces dedicated to export the loads generated by the two main active units the Sidecars (on TIF1) and the detectors (TIF2). With the structure insulated from the Baseplate, TIF1 and 2 are also responsible for extracting the heat generated by all the active units inside the NI-OMA (cryo-mechanisms and calibration unit) as only a small amount of load fluxes through the two NI-SA P1 Invar bipods and the two P3 Invar monopods (Figure 4-2). The Invar pods from P1 and P3 allow to reach low conductance values, on the order of 0.0084 W/K per leg. The total conductance from P1 and P3 to the Baseplate is respectively around 0.035 W/K and less than 0.01 W/K.

The structure entirely made of SiC, given the good thermal conductivity of this material, ensures a good temperature uniformity and an efficient heat extraction towards the main conductive interfaces.

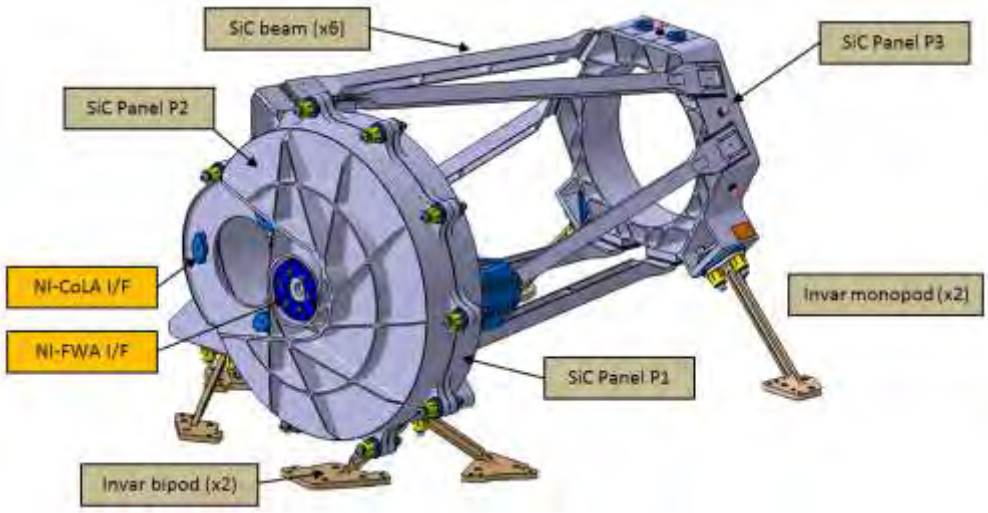

Figure 4-2. Mechanical configuration of NI-SA

A control heater is integrated on both P1 to bipods interfaces in order to keep P1 and P2 temperature within the required stability level of the optical units (CoLA and CaLA, see 4.2.2).

Radiative exchange with the PLM environment is regulated by a radiative shroud that encloses the full instrument. A 10-layers aluminized MLI blanket (with Dacron as insulating medium) shields the NISP units from the external radiation and ensures a very efficient cooling of the units. As the emissivity of all units inside the PLM cavity, due to optical stray light minimization, is required to be as high as possible, both external surfaces of the MLI blanket are black coated. For the same reason all the instrument units shall have high external emissivity.

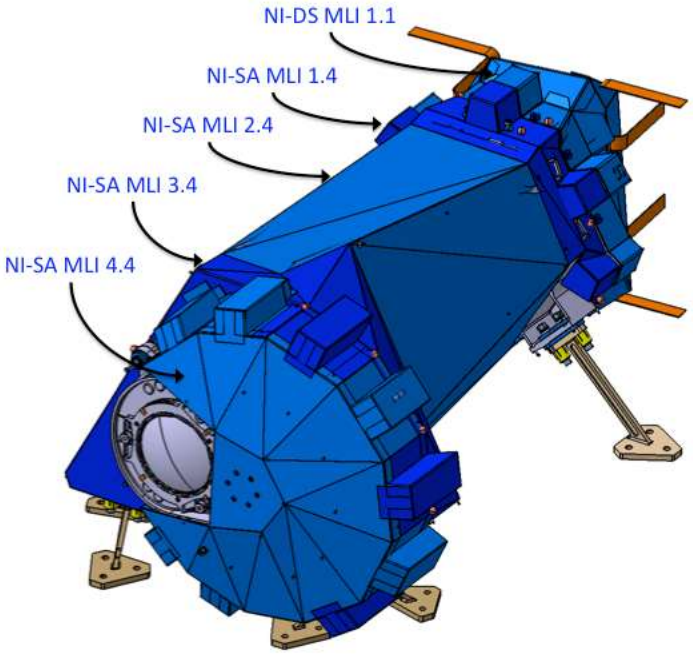

Figure 4-3. NISP MLI blanket latest design

The MLI blanket has also the task to minimize the thermal gradient that could be introduced on instrument units by the PLM radiative background. It has been estimated (see Table 4-1) that the instrument cavity in the PLM can show up to 14K gradient in the spatial temperature distribution from the coldest point to the warmest. According the PLM Prime Contractor evaluation all radiative exchange simulations shall be performed assuming a +7K and -

7K respectively on the top and bottom sides of the instrument cavity with respect to the lateral surface average temperature (see 9.2.4).

All harness from SVM to NI-OMA or NI-DS shall be thermally coupled to a 135K passive stage (Baseplate, for example) to ensure maximum parasitic loads interception.

4.2.1. The Filter and Grism Wheel Assembly (FWA/GWA)

The only active units in the NI-OMA, with the exception of the control heaters, are the cryo-mechanisms that rotate the filter and grism wheels. The transient dissipation of these motors is the major disturbance to the wheels units (filters and grisms) and to the optical lenses of CoLA and CaLA (see next paragraph).

The estimated worst case power profile is based on a spike load of 20W applied for a very short time (less than 0.05 s) followed by 6W applied for 8s and by 1W applied for 8.5s (equivalent to a total heat injection of about 60J). The mechanisms load is mainly dissipated by the stators which are thermally anchored to the relative NI-OMA panels (P1 for the GWA and P2 for the FWA) with a conductance value of around 0.7 W/K. This value ensures that the load is quickly extracted away from critical items such as the filters and grisms. Thanks to the units thermal inertia filtering, the disturbance transmitted to the optical units is minimized. This can be checked by a simple evaluation: even in the worst case of the full load being dissipated directly on the wheels, taking into account their thermal inertia, the ΔT induced on the filters/grisms by the heat injected is on the order of 15 mK for both wheels. This is confirmed by the Finite Element Model results (see Chapter 13).
In the steady-state simulations the loads induced by the two cryo-motors have been considered as a constant contribution by integrating their power profile over a full observation cycle (around 1100 s) and averaging according to their activations in a cycle. With the FWA activated twice than the GWA in each observation cycle, the estimated average power used in the simulations are respectively 0.208W and 0.104W.

4.2.2. The Collimator Lens Assembly (CoLA) and Camera Lens Assembly (CaLA)

The most challenging requirements of the whole thermal design is the temperature stability needed on the CoLA and CaLA lenses during the full mission operational life. The NI-OA design operational temperature shall be:

- NI-CoLA: 135K (TBC) +/-0.3K (TBC)
- NI-CaLA: 135K (TBC) +/-0.3K (average over the unit) (TBC)

The absolute temperature value depends on the NI-OMA structure thermal balance and will be adjusted according to the boundary conditions (Table 4-1) changes, if any, until the manufacturing will start. At that time the operating T values of the lenses shall be known with a high degree of confidence.
The main requirement on thermal stability defines a maximum temperature variation of ±0.3K of the CoLA and CaLA units during operations over the full mission. For this requirement NISP cannot rely on interfaces temperature (Table 4-1), as they can change by ± 2K during operations inducing excessive fluctuations on the two optical systems. At steady state such changes cannot be filtered by a purely passive damping due to the system thermal inertia and requires an active control on the optical units. Both units are partially decoupled from the NI-OMA panels (K≤ 0.1W/K TBC) to exploit the thermal RC constant to filter out at least the higher frequency oscillations. In order to cope with the ground/BOL and EOL long period evolution of the interface temperatures (± 2K), a control heater is integrated at the P1 hexapods interface to maintain the NI-OMA optical units at the their required operational T temperature ±0.3K during mission. During mission operations control heater power can be adjusted proportionally from ground on the basis of the thermal trend indicated by the temperature monitoring of the units. Control heater power range is 0-10W and can also be used for decontamination purposes during cooldown.
In steady-state conditions the main perturbation to the thermal status of both unit lenses is the dissipation of the FWA and GWA cryo-mechanisms that is expected to dominate over the expected fluctuations of the TIFs and environment. Applying the cryo-mechanisms transient power profile for several observation runs in a row to the NI-OMA panels P2 and P1, a steady-state constant DT is asymptotically reached on the CoLA and CaLA units. Across the conductance to the panels (K≤ 0.1W/K) this induced DT for the CoLA and CaLA is on the order of 30 mK and less than 10mK respectively (CaLA thermal inertia is on the order of 3 to 4 times the CoLA one), an order of magnitude below the required 0.3 K.

This transient simulations show that the assumption of an average constant load applied to the cryo-motors during the model runs in steady-state conditions is correct.

4.2.3. Calibration Unit (CU)

The calibration unit consists of an aluminum structure mounted, through a bipod support, on panel P1, close to the Camera Lens Assembly CaLA, with a total conductance higher than 0.5 W/K . The source is based on 5 LEDs (plus a redundant set), providing an indirect and nearly homogeneous illumination of the detector plane. With a maximum power dissipation of 200mW, the Calibration Unit's contribution to the NISP thermal budget is negligible. Moreover the thermal load is present only during the activation of the unit in a calibration run and therefore it is not expected to be a disturbance to the thermal balance of the NISP Instrument during observations.

4.3. NI-DS

The NI-DS (Detector System) is a mosaic of 16 triplets referred as SCS's, each triplet being composed of a H2RG detectors (SCA's), a proximity read-out electronics built around a dedicated ASIC, called SIDECAR (SCE's) and the flexible cable which connect SCA and SCE together (often called "flexi cable"). A drawing of this arrangement is shown in Figure 4-4. A mechanical structure (called the CSS), made of molybdenum, supports the 16 SCA's arranged in a 4x4 mosaic that constitutes the Focal Plane of the instrument. The SCE's are mounted on a different mechanical structure (the SSS), and are connected to the SCA by the flexi harness. Both structures are supported on the NI-SA Panel P4 with insulating stands that provide a total conductance of around 0.1 W/K for the SSS and 0.015 W/K for the CSS.
The thermal scheme of the NIPS Detector System is shown in Figure 4-5 and is based on maximizing the insulation from P4 on one side (for the CSS especially) and the thermal coupling with the thermal interfaces on the other side: TIF1 for the SCE's on the SSS and TIF2 for the SCA's on the CSS (Figure 4-4). On both supporting structures (SSS and CSS) the interfaces are split in four contact areas to maximize the contact surface. In the conservative assumption that a 1000 $W/m^2/K$ contact surface conductance can be achieved at the thermo-mechanical interfaces, the coupling to the TIF's is designed as follows:

- TIF 1 to SideCar Structure (NI-DS SSS)
  - 4 conductive IFs on the SSS of ≈5 cm^2 each (20 cm^2 total area) providing 0.5 W/K per contact area for a total of 2 W/K
- TIF 2 to Detectors Structure (NI-DS CSS)
  - 4 conductive IFs on CSS of ≈8 cm^2 each (32 cm^2 total area) providing 0.8 W/K per contact area for a total of 3.2 W/K

The operating temperature of the SCA and SCE will be around 95K and 140K respectively. Detectors stability is a key issue for instrumental performance and requires a careful design of a proper thermal control system. Thermal control is achieved by a combination of passive and active systems. The passive component exploits thermal masses and resistances of the components (struts and flanges) to damp temperature oscillations during their propagation from the instability source (TIF2) to the detectors. In order to cope with the ground/BOL and EOL long period evolution of the interface temperatures (± 2K), a control heater is integrated on the CSS to ensure NI-DS optimized performance in any boundary conditions status. This active control, as for the NI-OMA, relies on a simple proportional control operated from ground following thermal trend analysis. Heater power range is 0-6W and can also be used for decontamination purposes during cooldown.
A set of transient simulation runs dedicated to analyze the response of the NI-DS system to temperature fluctuations induced by TIF2 has been carried out with the FEM. Results and indications are reported in the last chapter of this document.

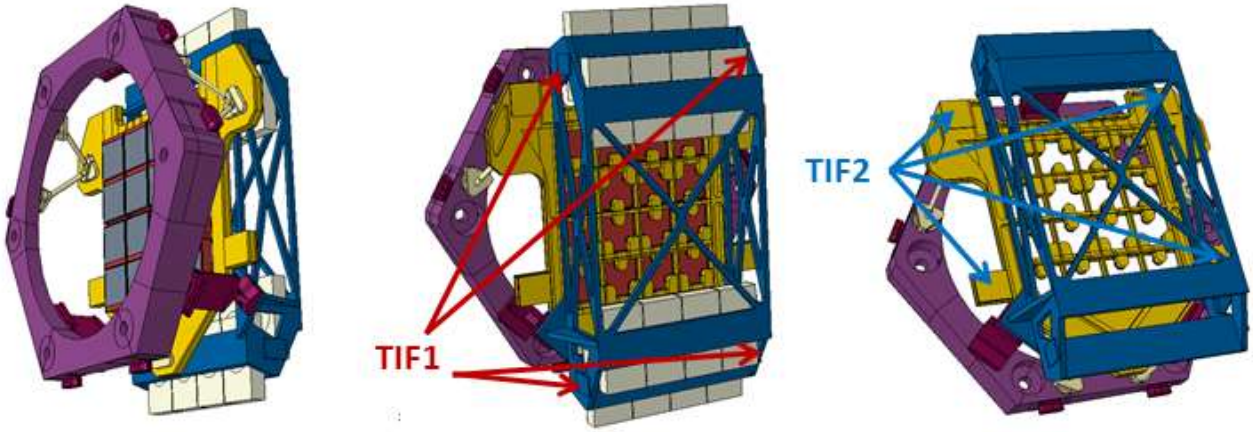

Figure 4-4. NI-DS CAD drawing

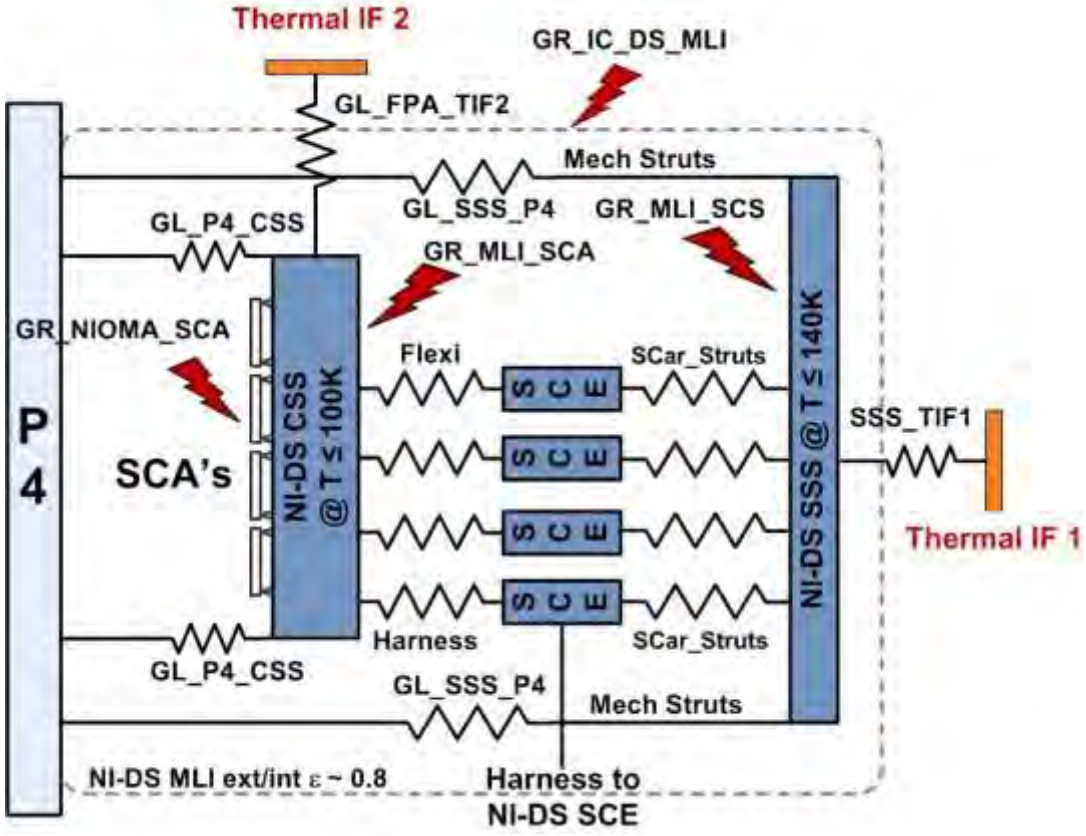

Figure 4-5. NI-DS thermal scheme

5. Input CAD model

The CAD model used as input for the analysis is the step file named NIDS_Detail_3D.stp received on March 11 2013. Some rounds, holes and chamfers have been removed from the fem model in order to optimize the mesh quality, reducing the overall number of nodes, and to have the capability of using isoparametric elements in almost all the units of the instrument. This step is necessary to get a FEM model with good convergence properties, and with relatively small computational time even in the transient analysis cases. The overall change in shape and mass due to these minor modifications is negligible for this kind of analysis.

In the input CAD model the FWA step motor is missing. It is then assumed that the FWA motor is identical to the GWA motor and with the same mechanical fixation to its panel. The FWA motor has then been obtained mirroring the GWA motor.

In the input CAD model the FWA wheel and the GWA wheel were misaligned with respect to the optical system. In order to simulate the instrument in a realistic observational condition a rotation of -15deg (x-axis) is imposed to the FWA and a rotation of +75deg (x-axis) is imposed to the GWA.

6. Units

The Units system adopted for this analysis is mm-t-s-mJ-K.

Length	Mm
Mass	Tonne
Time	Second
Temperature	Kelvin
Energy	mJ
Power	mW
Thermal conductivity	mW/(mm-K)
Specific heat	mJ/(tonne-K)

The physical constants of interest are assumed to be:

Absolute Zero	0.0K
Stephan-Boltzmann	5.67037e-11

7. Materials

The material properties are summarized in the following tables. For this study the thermal properties have been considered constant over the temperature (small) variations around the equilibrium points of the units during the simulations.

AISI440C

Thermal Conductivity [mmW/(mm-K)]	25
Mass density [t/mm^2]	7.8E-009
Specific heat [mJ/(tonne-K)]	350000000

Al-6061

Thermal Conductivity [mmW/(mm-K)]	115
Mass density [t/mm^2]	2.75E-009
Specific heat [mJ/(tonne-K)]	660000000

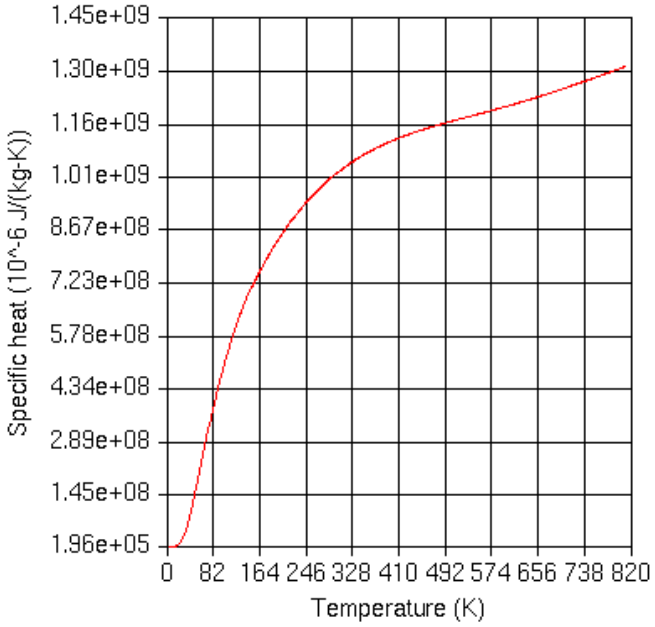

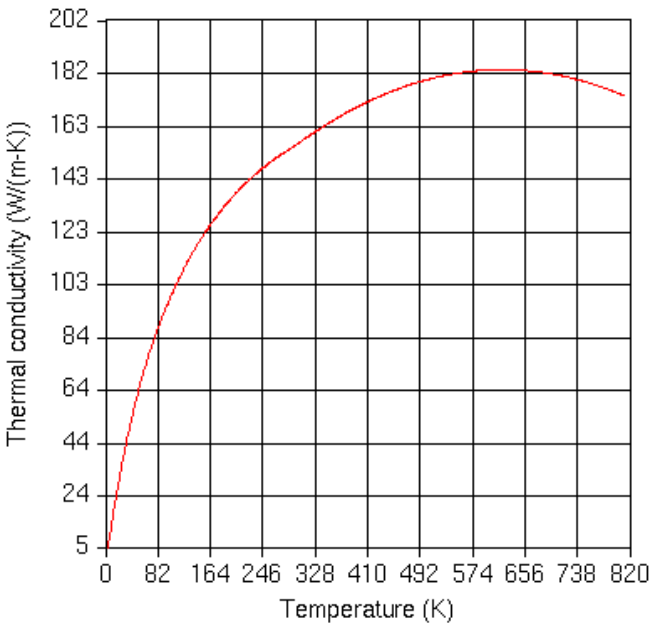

Al-7075

Thermal Conductivity [mmW/(mm-K)]	85
Mass density [t/mm^2]	2.75E-009
Specific heat [mJ/(tonne-K)]	620000000

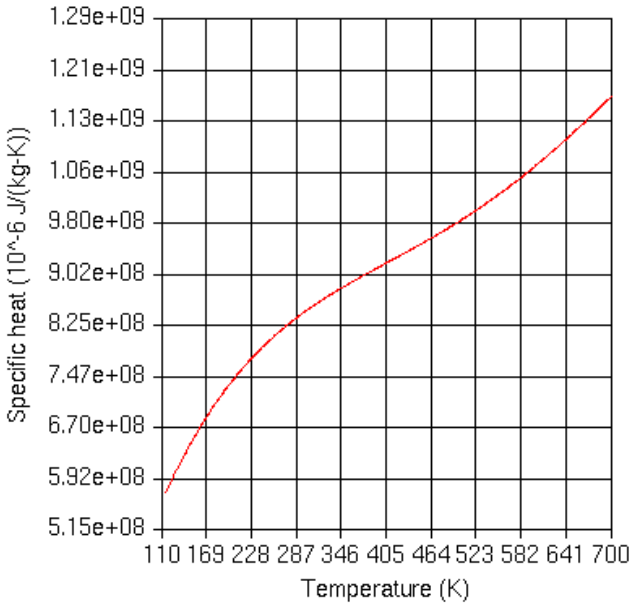

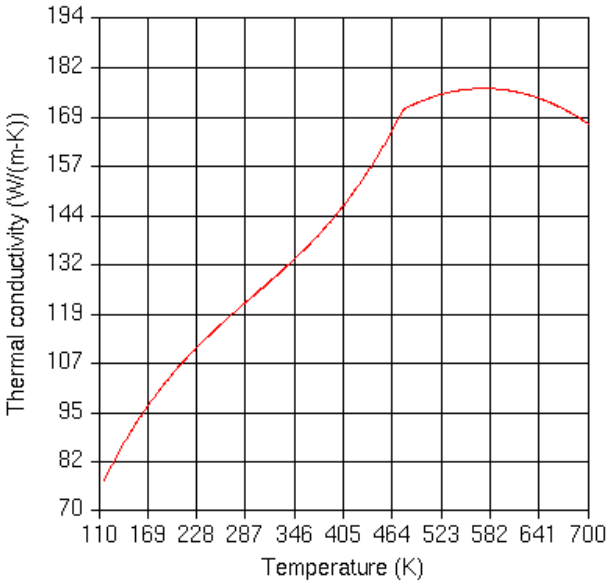

Al5N

Thermal Conductivity [mmW/(mm-K)]	225
Mass density [t/mm^2]	1e-9
Specific heat [mJ/(tonne-K)]	630000000

Armco

Thermal Conductivity [mmW/(mm-K)]	88
Mass density [t/mm^2]	7.9E-009
Specific heat [mJ/(tonne-K)]	330000000

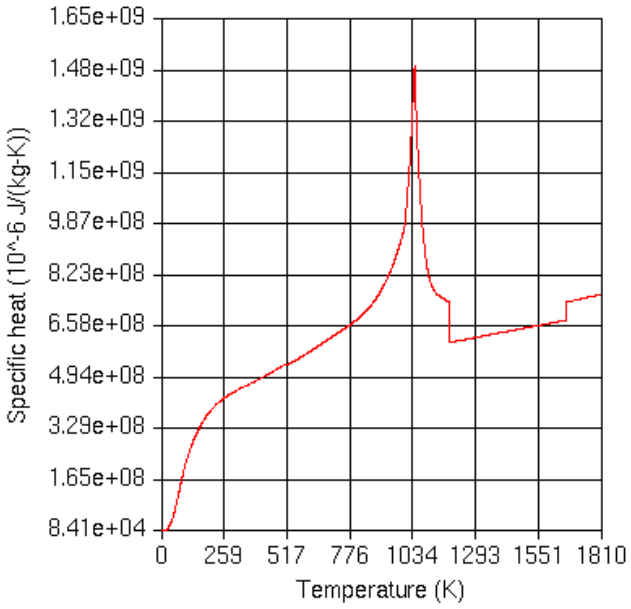

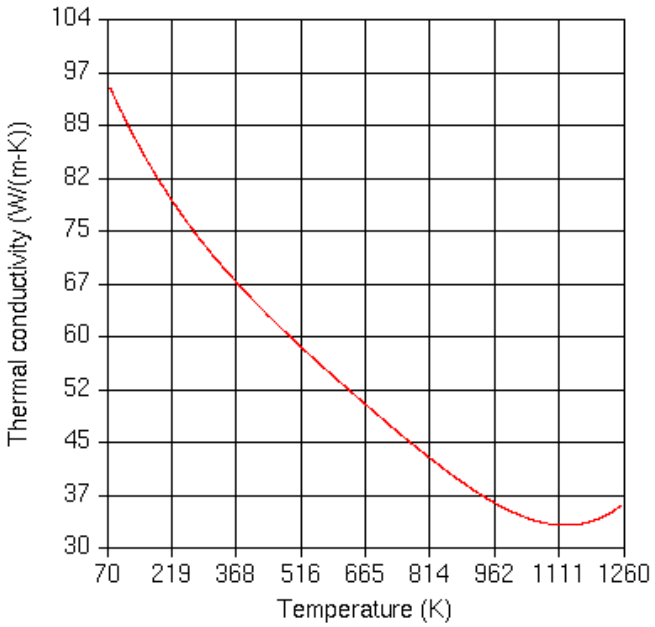

CUC1

Thermal Conductivity [mmW/(mm-K)]	400
Mass density [t/mm^2]	9E-009
Specific heat [mJ/(tonne-K)]	310000000

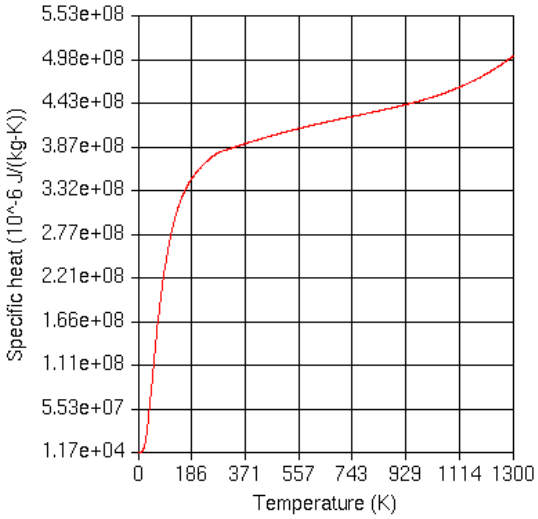

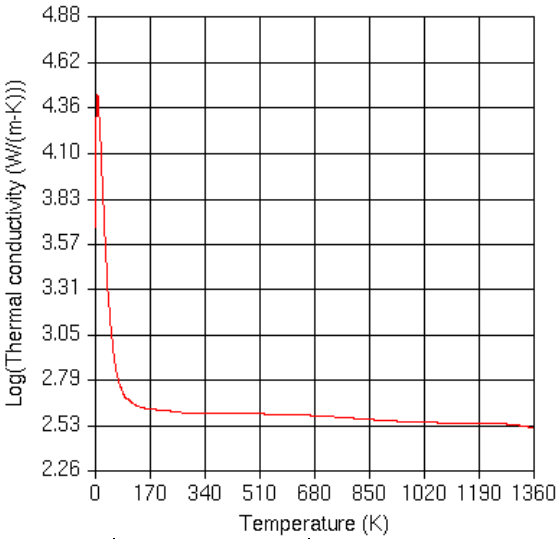

CaF2

Thermal Conductivity [mmW/(mm-K)]	24
Mass density [t/mm^2]	3.2E-009
Specific heat [mJ/(tonne-K)]	540000000

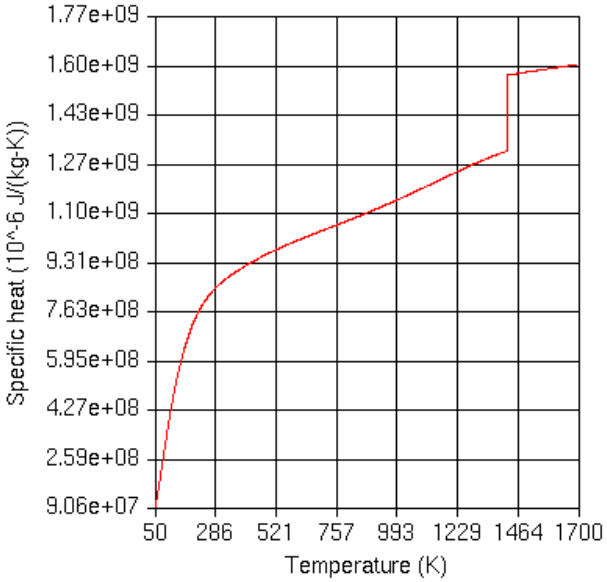

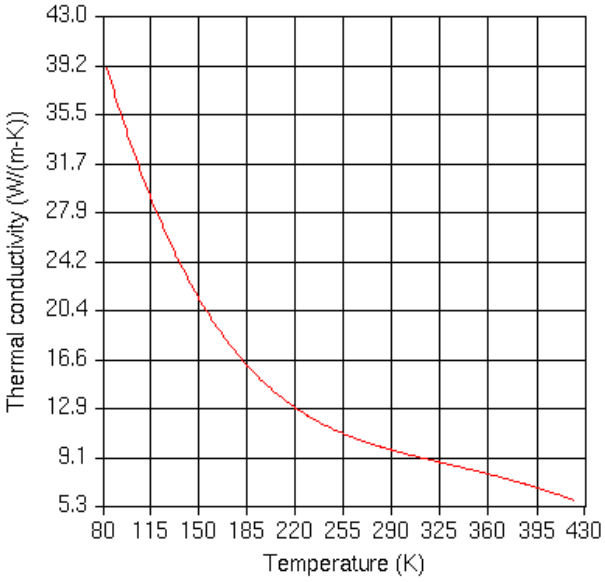

CuCr1Zr

Thermal Conductivity [mmW/(mm-K)]	290
Mass density [t/mm^2]	8.9E-009
Specific heat [mJ/(tonne-K)]	310000000

Fused-Silica

Thermal Conductivity [mmW/(mm-K)]	0.88
Mass density [t/mm^2]	2.2E-009
Specific heat [mJ/(tonne-K)]	370000000

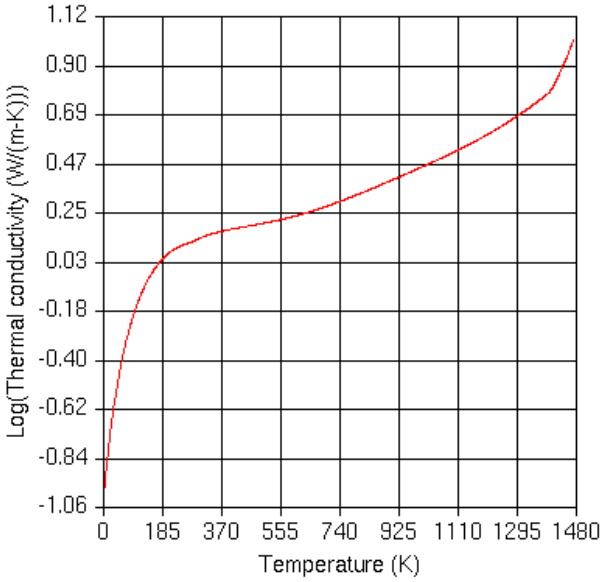
1.12
0.90
0.69
0.47
0.25
0.03
-0.18
-0.40
-0.62
-0.84
-1.06
Log(Thermal conductivity (W/(m-K)))
0
185
370
555
740
925
1110
1295
1480
Temperature (K)

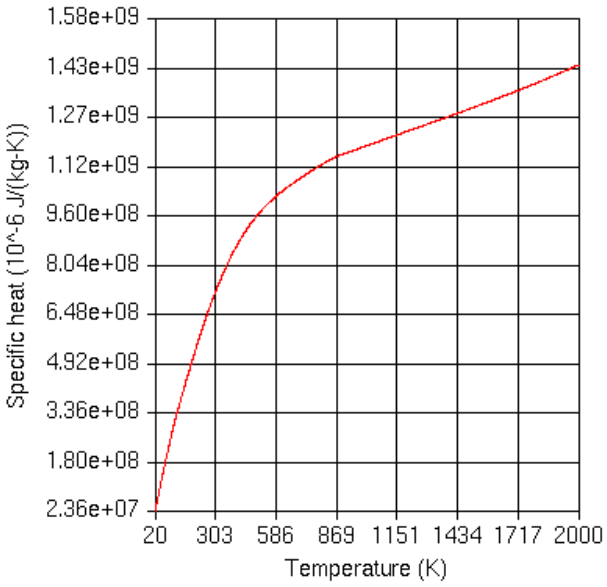
1.58e+09
1.43e+09
1.27e+09
1.12e+09
9.60e+08
8.04e+08
6.48e+08
4.92e+08
3.36e+08
1.80e+08
2.36e+07
Specific heat (10^-6 J/(kg-K))
20
303
586
869
1151
1434
1717
2000
Temperature (K)

INVAR

Thermal Conductivity [mmW/(mm-K)]	9.5
Mass density [t/mm^2]	8.1E-009
Specific heat [mJ/(tonne-K)]	320000000

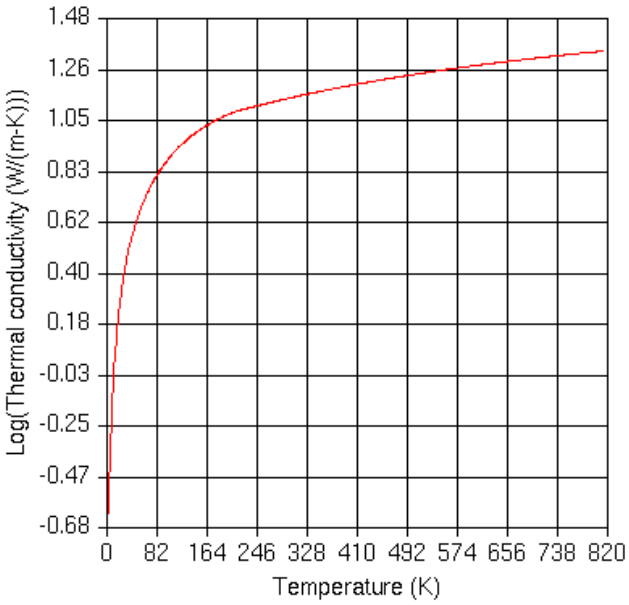

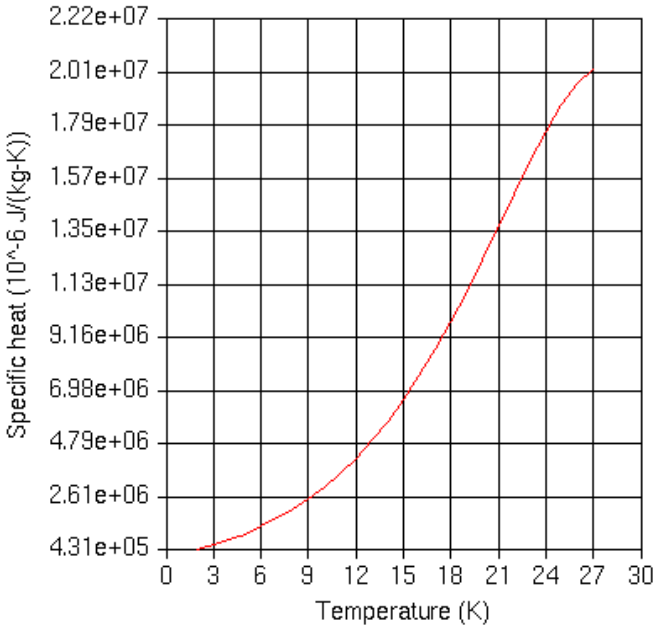

LF5G15

Thermal Conductivity [mmW/(mm-K)]	1
Mass density [t/mm^2]	3.2E-009
Specific heat [mJ/(tonne-K)]	400000000

Mo

Thermal Conductivity [mmW/(mm-K)]	155
Mass density [t/mm^2]	1.02E-008
Specific heat [mJ/(tonne-K)]	183000000

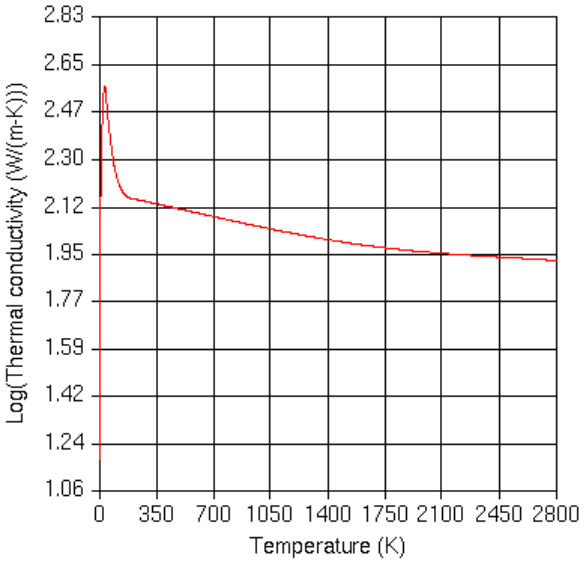

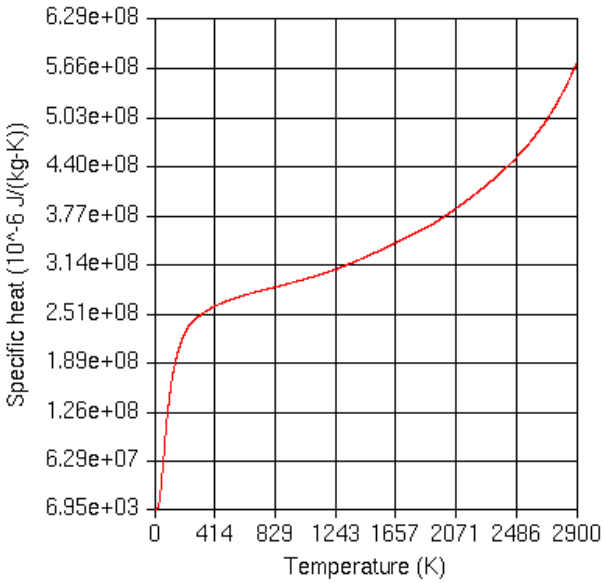

Mylar (isotropic properties)

Thermal Conductivity [mmW/(mm-K)]	0.15
Mass density [t/mm^2]	1.4E-009

Specific heat [mJ/(tonne-K)]	230000000

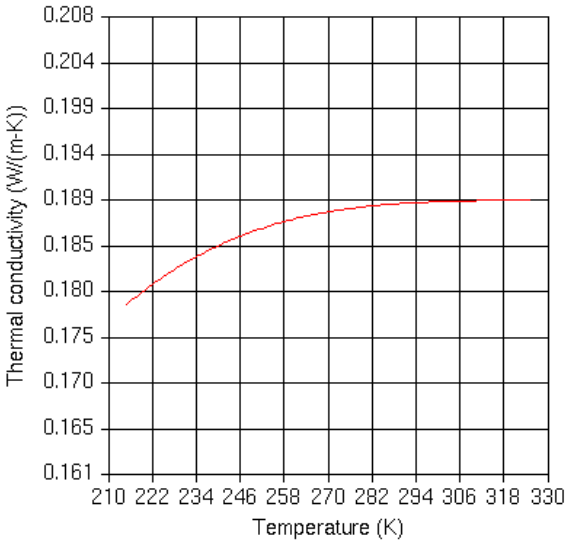

Si

Thermal Conductivity [mmW/(mm-K)]	500
Mass density [t/mm^2]	2.3E-009
Specific heat [mJ/(tonne-K)]	380000000

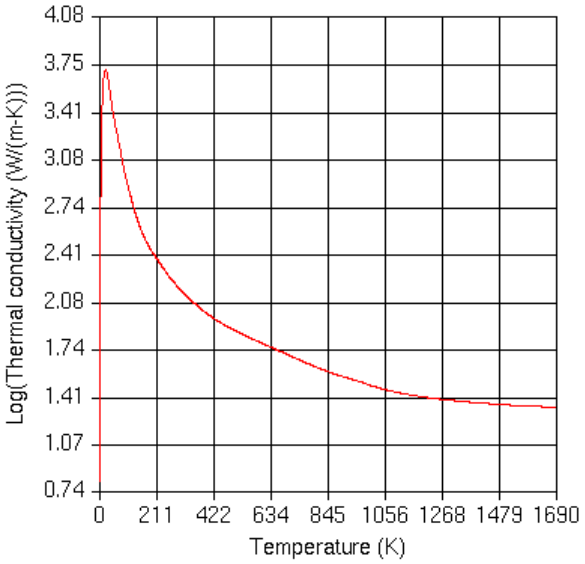
4.08
3.75
3.41
3.08
2.74
2.41
2.08
1.74
1.41
1.07
0.74
Log(Thermal conductivity (W/(m-K)))
0
211
422
634
845
1056
1268
1479
1690
Temperature (K)

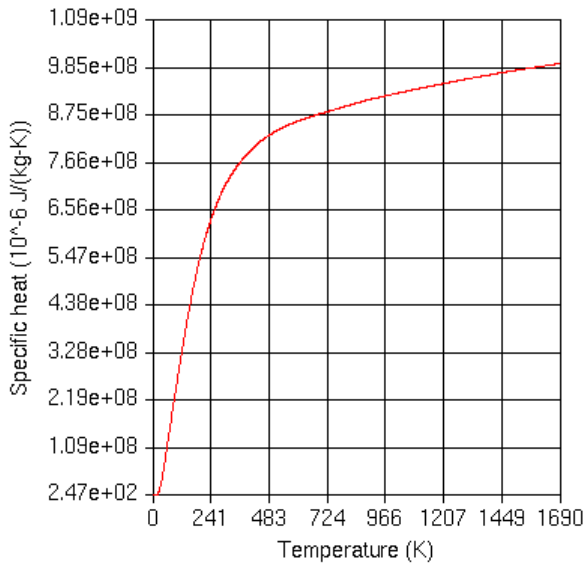
1.09e+09
9.85e+08
8.75e+08
7.66e+08
6.56e+08
5.47e+08
4.38e+08
3.28e+08
2.19e+08
1.09e+08
2.47e+02
Specific heat (10^-6 J/(kg-K))
0
241
483
724
966
1207
1449
1690
Temperature (K)

SiC

Thermal Conductivity [mmW/(mm-K)]	150
Mass density [t/mm^2]	3E-009
Specific heat [mJ/(tonne-K)]	220000000

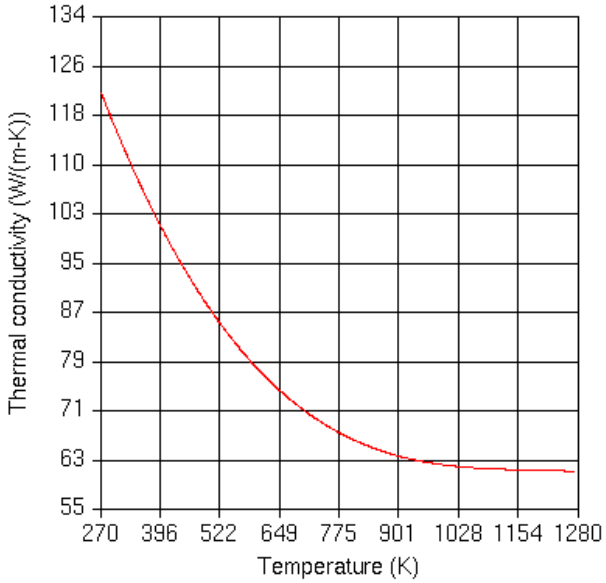

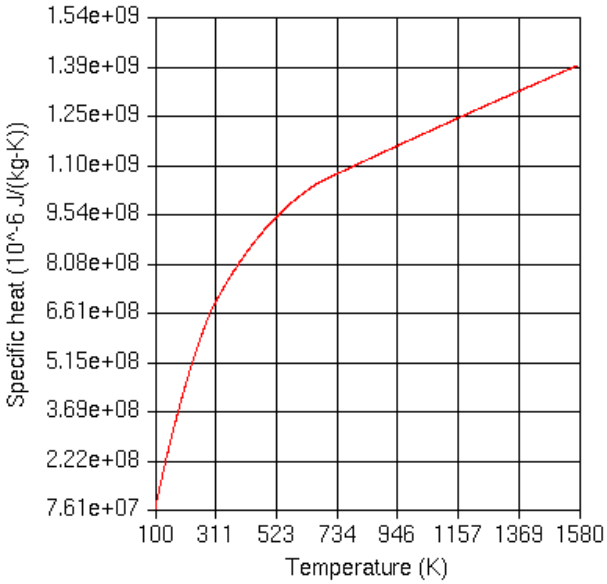

Ti6Al4V

Thermal Conductivity [mmW/(mm-K)]	6.1
Mass density [t/mm^2]	4.5E-009
Specific heat [mJ/(tonne-K)]	390000000

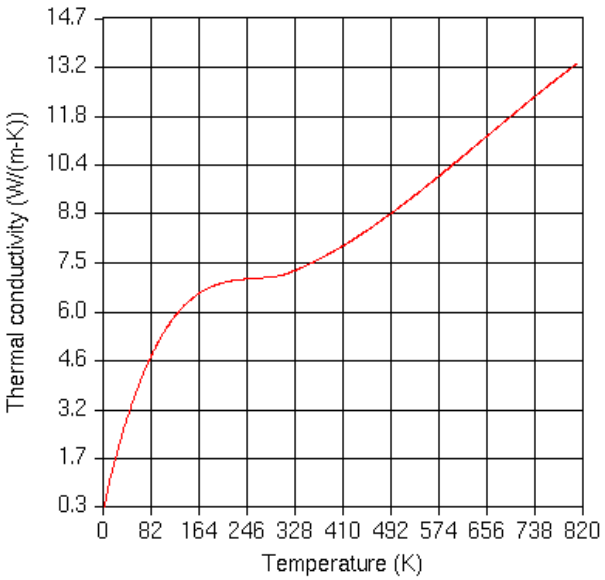

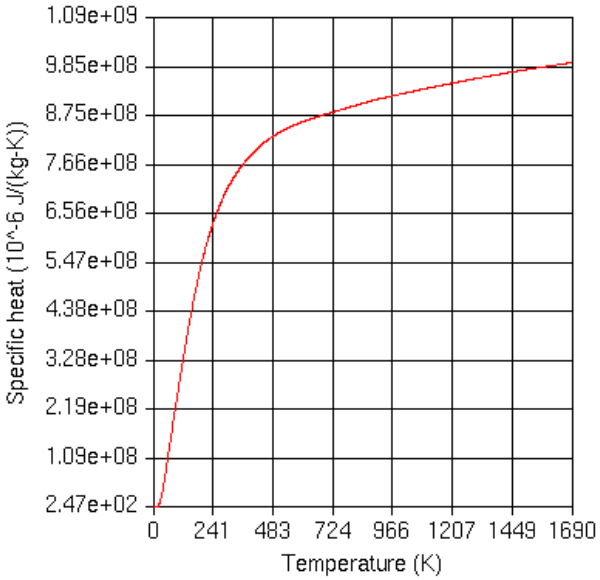

Copper

Thermal Conductivity [mmW/(mm-K)]	403
Mass density [t/mm^2]	8.96E-009
Specific heat [mJ/(tonne-K)]	302170000

8. FEM model

8.1. Imported CAD model and shields: geometry

All the imported parts are shown in the following images.

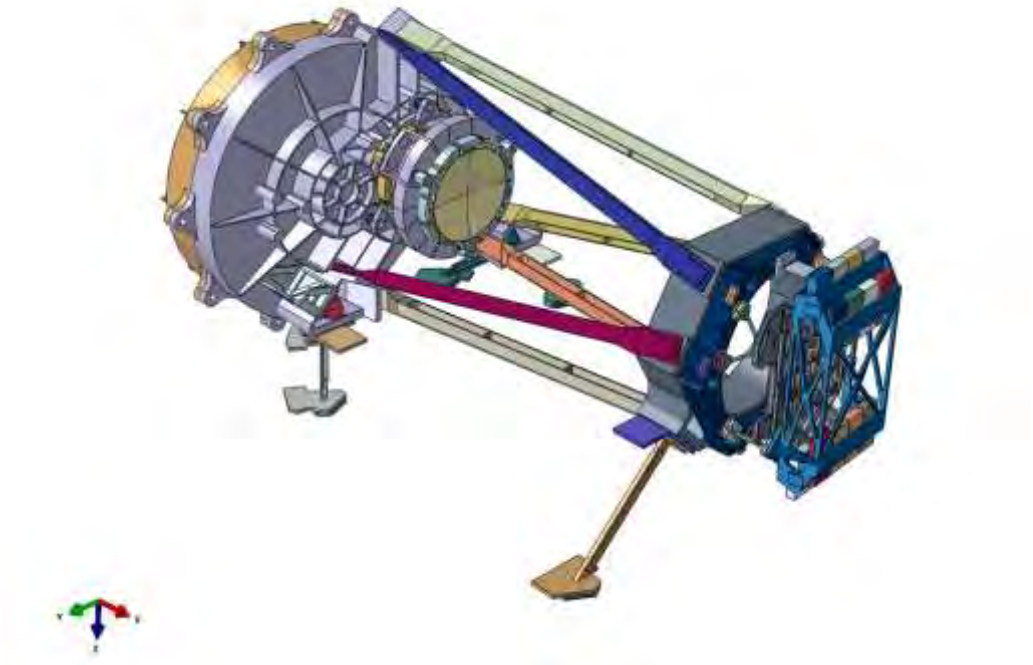

Figure 8-1 imported geometry

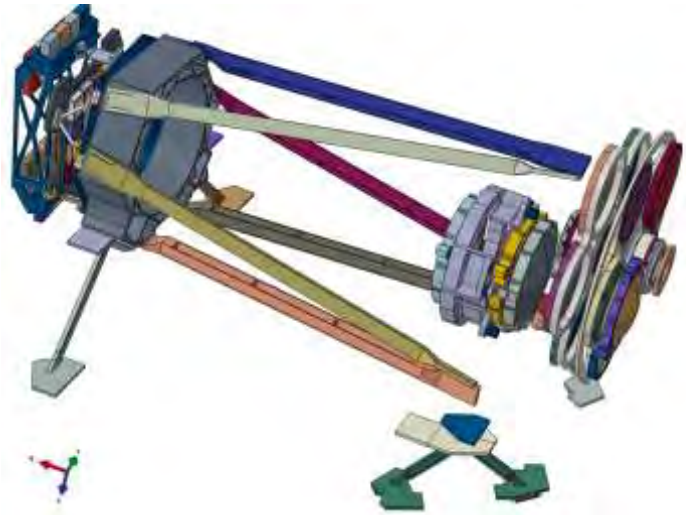

Figure 8-2 details of wheels and lenses imported

In order to simulate the actual radiative coupling of the instrument with the PLM environment, a radiative shroud, missing in the CAD model, has been added. A black (high emissivity) coated shield split in three sections, modelled with simple geometric surfaces, simulates the effect of the MLI shroud of the instrument.

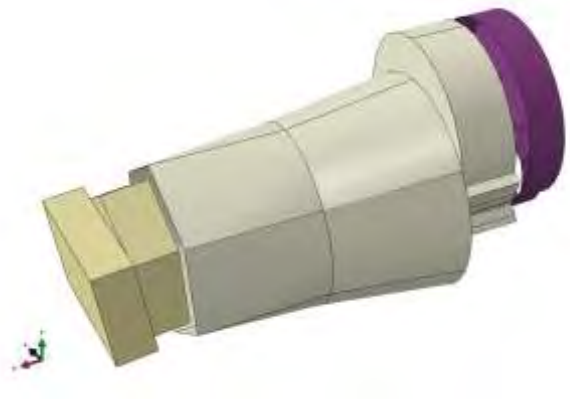

Figure 8-3 Shield idealization

The instrument external environment in the PLM is represented with a box.

Figure 8-4 External PLM box idealization

8.2. Idealization

The elements used for this analysis are heat transfer elements (only one degree of freedom), linear, with full integration. 3D elements are used for all the instrument parts (hexa or tetra). 2D shell elements are used for the shields. 1D elements are used for the NI-DS flexi cables idealization.

In the table are reported the materials assigned to the main units.

Label	Material	m (10^{-3} tonne)
P1	SiC	7
P1 T Ctrl 1	Ti	0.107
P1 T Ctrl 2	Ti	0.107
P2	SiC	3.3
P3	SiC	2.75
P4	SiC	2.75
FMech	SiC/SS	2
FWheel	INVAR36	5.5
GMech	SiC/SS	2
GWheel	INVAR36	7.5
CoLA Ring	Invar	0.65
CoLA Lens	Fused Silica	0.6

CaLA Barrel	Ti	1.85
CaLA Ring L1	CuCr1Zr	0.95
Lens L1	CaF2	1.25
CaLA Ring L2	Ti	0.65
Lens L2	LF5G15	1.72
CaLA Ring L3	Ti	0.65
Lens L3	LF5G15	1.41
SCar SSS	Al	1
SideCars	CE9	2.5
DS-CSS Plate	Molybdenum	1.8
DS-Baffle	Mo	0.275
Detectors	Mo/Si	2
Calib. Unit	Al (6061)	0.5
MLI NIOMA ext.	Mylar/Al	0.3
MLI NIOMA int.	Mylar/Al	0.3
MLI DS int	Mylar/Al	0.1
MLI DS ext	Mylar/Al	0.1
MLI Panel ext	Mylar/Al	0.175
MLI Panel int	Mylar/Al	0.175
BasePlate 1	Boundary	
BP2	"	
BP3	"	
BP4	"	
BP5	"	
BP6	"	
Cavity (box)	"	
TIF1.1 SCS	"	
TIF1.2	"	
TIF1.3	"	
TIF1.4	"	
TIF2.1 DS	"	
TIF2.2	"	
TIF2.3	"	
TIF2.4	"	
Dichroic	"	

Table 8-1. Materials assumptions on main units

In the following images the units of the assembly are painted with different colours indicating the material type.

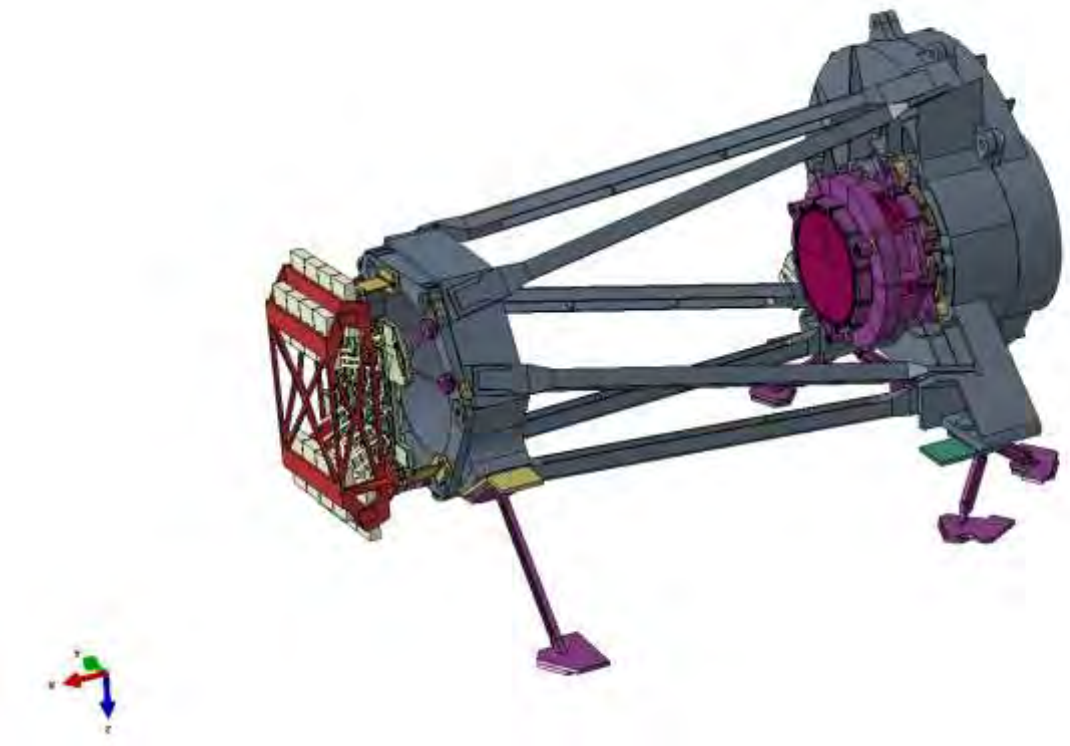

Figure 8-5 Assembly painted by material type

Figure 8-6 Wheels and lenses painted by material type

The NI-DS flexi cable connection is modelled using truss elements, neglecting the radiative effect caused by the blocking surface due to the cables between the detectors and the external shield.

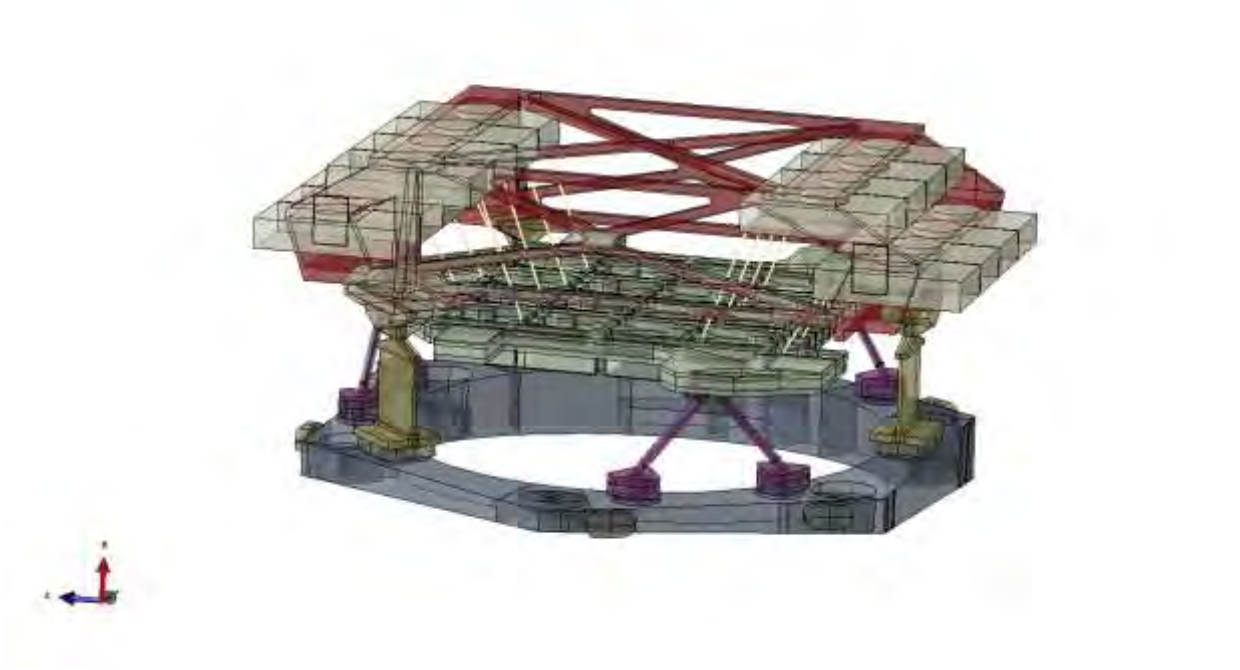

Figure 8-7 Sidecar and detector assembly

The cross section area of the truss is computed assuming a thermal conductance of 1.5 mW/K per cable. The short truss are length 45 mm, the long truss are 75 mm.

Assuming that:

C = lambda*A/L
A = C*L/lambda

then

A_{short} = 1.5*45/403 = 0.17mm^2
A_{long} = 1.5*75/403 = 0.28mm^2

The motor bearings are simplified connecting the external ring to the internal with a small circular section (1 mm thick). In the following image are shown the couple of bearings between the stator and the rotor of each motor.

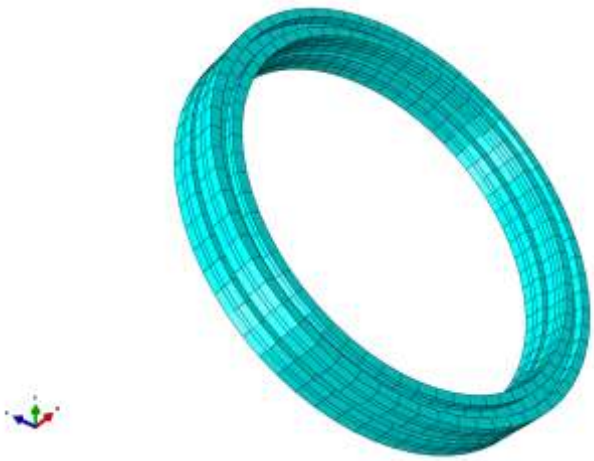

Figure 8-8 Ball bearing idealization

In the CAD model the sidecars are represented as simple 3D solid boxes. For this reason, missing a detailed model of the unit, they are modelled as 3D solid boxes, assuming a combination of materials (Al and Si) able to reproduce approximated thermal properties of these electronic devices.

Figure 8-9 Sidecar

8.3. Contact interactions

The parts in contact are imposed at the start of the analysis, and cannot change during the simulation. The Abaqus tie algorithm is used: master and slave surfaces are defined with the appropriate distance tolerance for the coupling. This step is necessary due to the tolerance of the imported CAD model and in all cases that require the exclusion of washers from the analysis. The interaction property is defined without contact thermal resistance, in order to reduce the overall number of equations, and to avoid the introduction of too many uncertainties in the model. More detailed thermal contact properties will be added in the next issues of the model, once they will be frozen and defined. The contact properties are strictly dependent from the contact pressure, that is defined by the screw type, the torque and the surface finishing. For this early stage of the analysis it has been decided to neglect errors due to such uncertainties.

8.4. MLI insulation idealization [added in rev. 2]

In this new issue of the document the MLI insulation blanket has been idealized in a different way with respect to the first one. In the first simulation the MLI insulation was modelled as an isotropic material (shell elements). In this revision of the analysis, the Mylar insulation is modelled by a multi isotropic layers configuration. The full blanket is simulated by 5 layers:

1. Aluminium layer: thickness=0.2 [mm];
2. Insulating layer: thickness = 5 [mm];
3. Aluminium layer: thickness = 0.2 [mm];
4. Insulating layer: thickness = 5 [mm];
5. Aluminium layer: thickness = 0.2 [mm];

With this idealization it is possible to modify, independently, both the "in plane" and the transversal thermal conductivity property. The middle aluminium layer is added in order to redistribute the thermal load between the insulating layers interfaces. The thickness and physical properties of the layers inside the two external surfaces have been chosen to simulate the expected thermal conductance across and along the shroud layers.
The emissivity of the external radiative exchanging surfaces (top and bottom ones) is e=0.88 to replicate the black Kapton properties.

A more detailed and realistic idealization will be possible once the aluminized Mylar insulation design will be defined and frozen in the mechanical model.

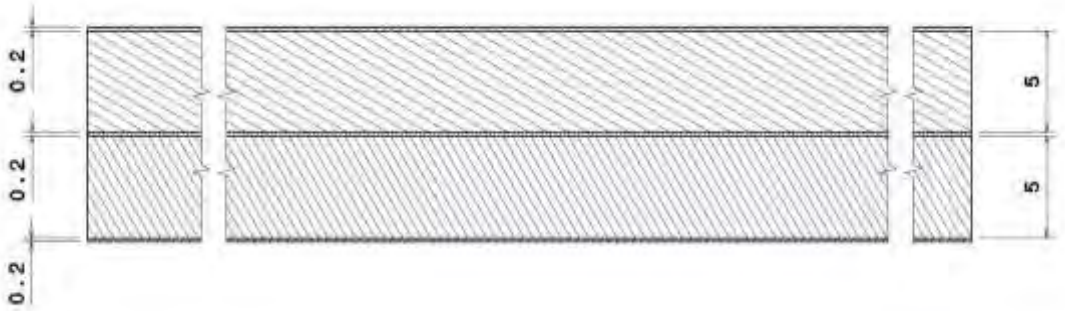

8.5. Radiative interactions

In order to reduce the overall computational cost of the simulation, only some surfaces are assumed to participate and actively contribute to the radiative exchange.

The following radiative couplings are defined in the analysis:

1. External box – Mylar shield
2. Sidecars shield – instrument (all the sidecars, all the detectors, the mainframe of the sidecar SSS, the plate of the detector CSS)
3. All the detectors, the shield around the invar connecting rod, the lens CaLA 3
4. Lenses CaLA3 - CaLA2
5. Lenses CaLA2 – CaLA1
6. Lense CaLA1 - GWA Filter
7. GWA Filter-FWA Filter
8. FWA Filter - CoLA
9. CoLA – external

Due to the consideration that the working wavelength of Euclid NISP is the near infrared, it is assumed in all the analysis that the efficiency of the lenses is very high in this band. In the hypothesis that the materials are heated mainly by this IR radiation, the emissivity factor for all the surfaces of the lenses is assumed as 0.98. The radiative model used in Abaqus (as usual for the FEM models) is based on the relation emissivity-reflectivity and does not take into account the transmittance factor.

8.6. View factor calculation

In order to achieve more realistic results, every radiative cavity is defined as closed, even if the overall sum of the radiation factors inside the cavity is less than 1. Abaqus algorithm for the estimation of the view factor is based on geometric calculation, the algorithm is then forced to avoid a too simplified evaluation by modifying all the tolerances and limits.
A parallel algorithm is used to optimize performance. To be able to use the parallel algorithm for the calculation of the view factors, few small changes in the surface definition of the filter and grism aligned for the simulation are required. An external annulus of 1 mm on the optical surface with no thermal radiative exchange is needed to decouple the radiative surface from the side cylindrical conductive area. The choice of this kind of domain decomposition is based on the assumption that the conductive effect is leading with respect to the radiative one: a change in the conductive interaction has a stronger impact than a little change in the radiative interaction. The temperature difference between the surfaces is less than 1K at any time.

8.7. Mesh statistics

In the following table are reported the type of elements used in the analysis and their overall numbers. Tetrahedral elements are used for NIOMA P1, P2, P3 due to the imprecisions of the imported surfaces. Hexa elements will be used once these errors will be corrected.

ELEM NAME	TYPE	ORDER	NUMBER
DC3D4	tetrahedral	linear	86729
DC3D8	hexahedral	linear	319070
DC1D2	line	linear	120
DS4	quadrilateral	linear	7457
DS3	triangular	linear	71

Table 8-2. Mesh elements type

8.8. Mesh images

In this paragraph are reported some images of the mesh, to show the accuracy used for the model.

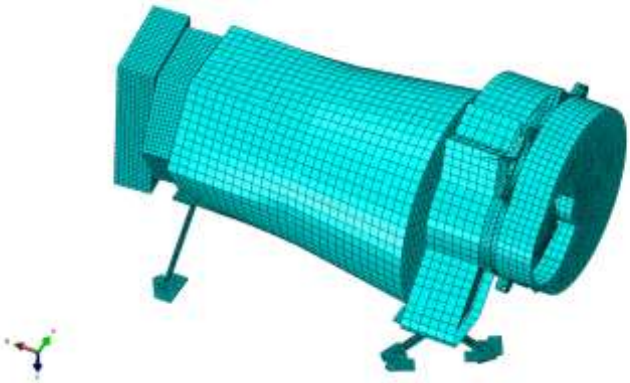

Figure 8-10 Mylar shields mesh

Figure 8-11 Instrument mesh

Figure 8-12 Instrument mesh without P1 and P2

Figure 8-13 Lenses and wheels meshed

Figure 8-14 Lenses with radiative interaction

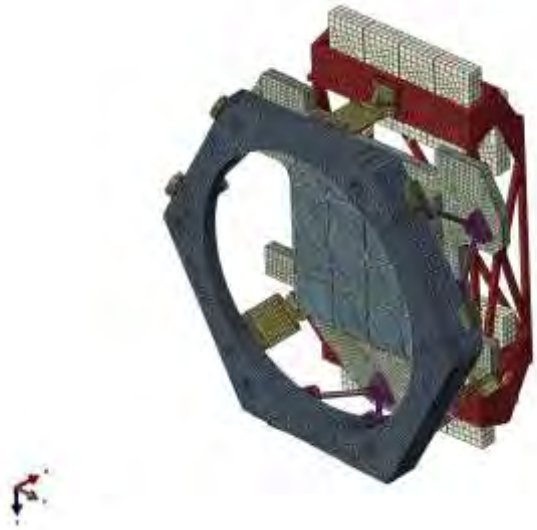

Figure 8-15 Detectors and sidecars mesh

9. Loads and Boundary conditions

9.1. Loads

The thermal loads are defined as surface fluxes, uniformly distributed over the surface, and defined in terms of total surface flux. This load condition could be changed to flux generated per unit volume for the sidecar, once a detailed model of these units will be available.
In the motors the coils are not represented at this time, and so the thermal flux is simulated as surface thermal flux on the area on which the coils are winded up.
In the following subsections are reported the descriptions of each load condition.

9.1.1. Sidecars

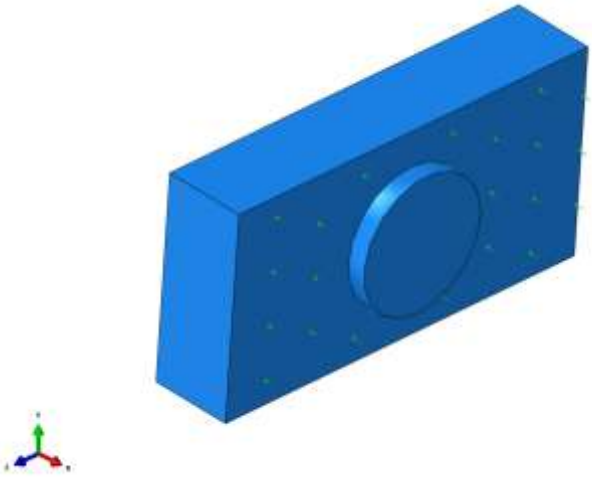

Figure 9-1 Sidecar uniform distribution load on surface

The total flux on the surface of a single Sidecar is **350mW**.

9.1.2. Detectors

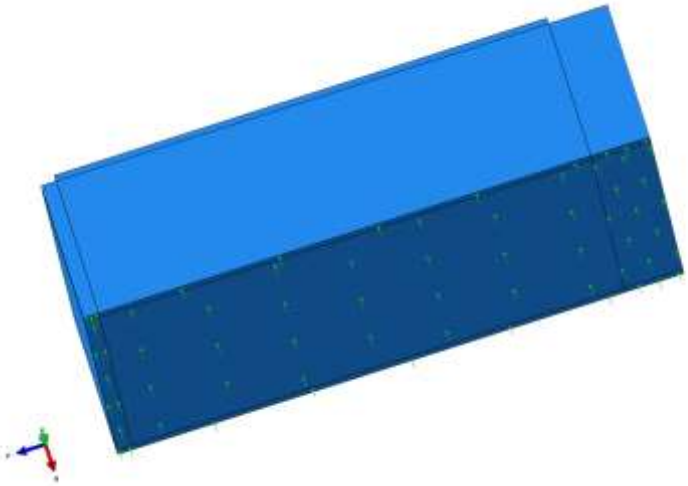

Figure 9-2 Detector uniform distribution load on surface

The total flux on the surface of the single detector is **8mW**.

9.1.3. FWA motor (for steady state analysis)

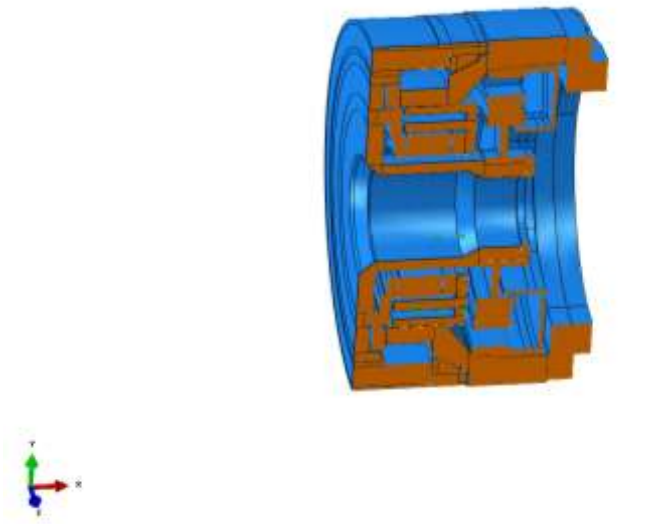

Figure 9-3 Uniform surface load on FWA motor

For the steady state analysis it is assumed that the overall thermal power generated by the motor is uniformly distributed over time. Only one surface is defined for the thermal flux exchange, and so the different position of thermal load due to the clutch coils and the motor coils is neglected.
The total flux on the surface is **208mW.** This flux is the average constant power calculated by diluting the cryo-mechanism power profile over a typical observation cycle.

9.1.4. GWA motor (for steady state analysis)

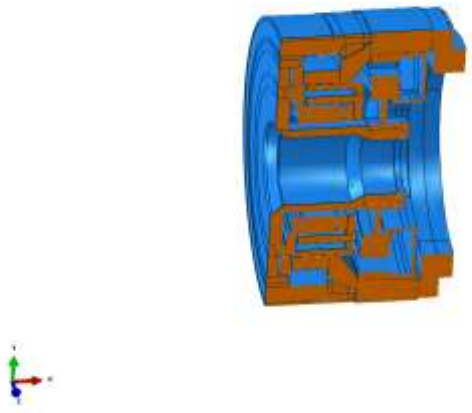

Figure 9-4 Uniform surface load on GWA motor

For the steady state analysis it is supposed that the overall thermal power generated by the motor is uniformly distributed over the time. Only one surface is defined for the thermal flux exchange, and so the different position of thermal load due to the clutch coils and the motor coils is neglected.
The total flux on the surface is **104mW.** This flux is the average constant power, half of FWA motor value as in the same time interval, the GWA cryo-mechanism is activated half the times.

In the figure below are indicated all the applied loads in the steady state analysis.

Figure 9-5 All loads applied on steady state analysis

9.1.5. FWA-GWA (transient analysis)

For the transient analysis it is considered that the clutch coil and the motor coil have different positions. The load is then applied in the right position according to the duty cycle of the cryomechanism activation.
The duty cycle curve is discussed in chapter 9.2.

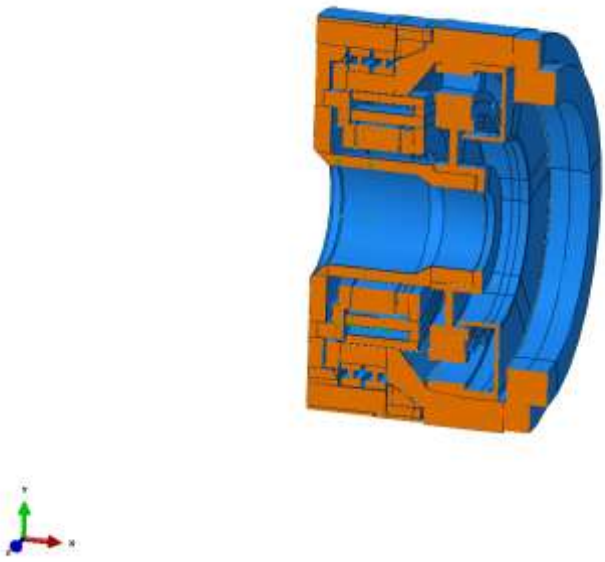

Figure 9-6 Clutch coil interaction during transient analysis

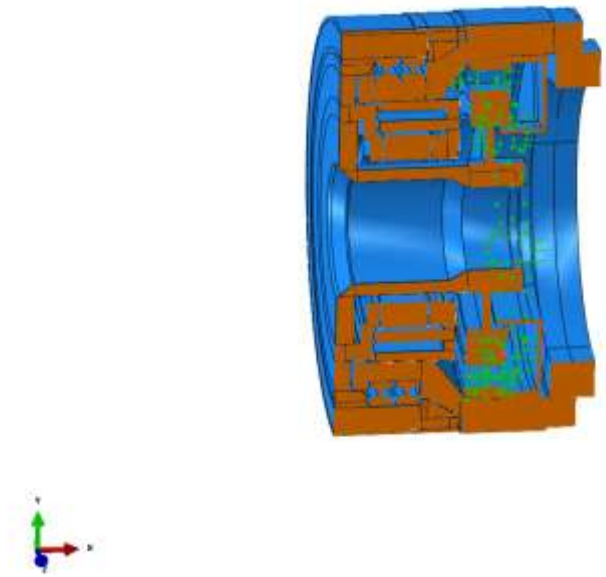

Figure 9-7 Motor coil interaction during transient analysis

The loads generated by the cryo-mechanism at the level of the Motor Coil and Clutch Coil have been simulated with periodical functions that approximate the FWA operations in a typical observation cycle, as reported in the latest version of the EID-B (AD2) In the model the FWA CM outputs the following loads in one activation:

Time (s)	Motor load (W)	Clutch load (W)	Comments
0	0	20	The clutch activation peak is applied for one sec (worst case) instead of the actual 0.05 s
1-8	6	1	The continuous 6W are applied for 8 s
9	0	1	CM is kept unclutched for another s
10	0	0	Observation start

Table 9-1. Motor activation cycle steps

The following two Figures (taken from RD4) show in more detail the sequence of the motor activation:

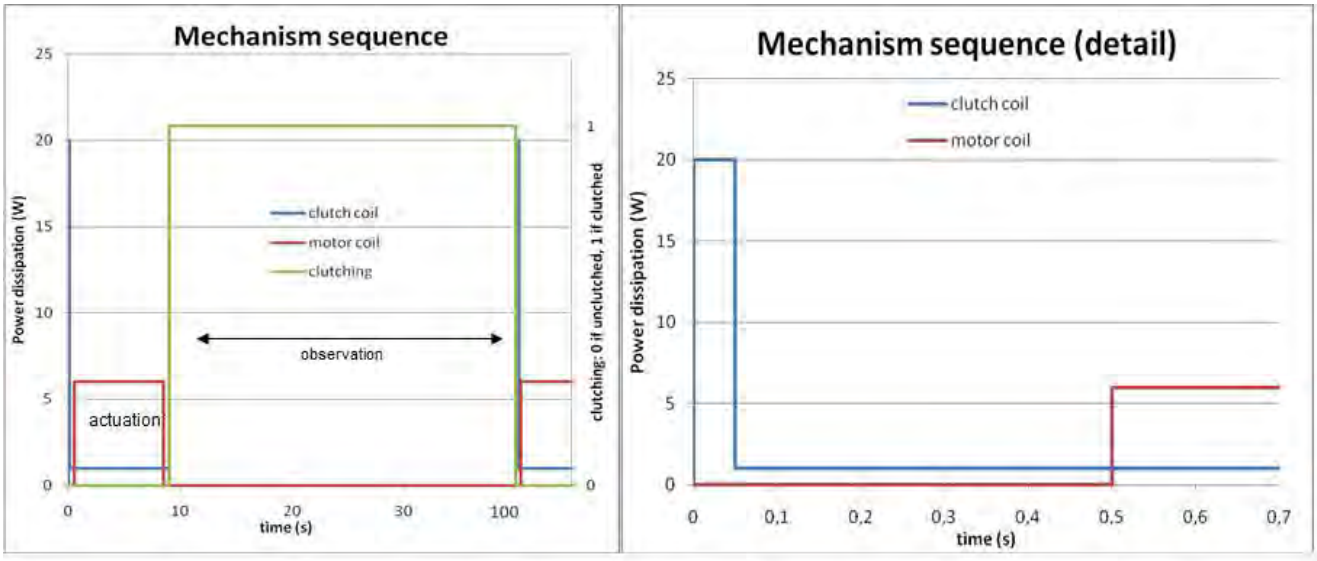

The full cycle of one observation is reported in the table below:

Time (s)	Duration (s)	Operational State
0	10	FWA cryo-mech activation
10	130	Observation for 130 s
140	10	FWA cryo-mech activation
150	126	Observation for 126 s
276	10	FWA cryo-mech activation
286	101	Observation for 101 s
387	10	FWA cryo-mech activation
397	55	Observation for 55 s
452	10	FWA cryo-mech activation
462	650	Observation for 650 s
1112	10	Cycle restarts with CM activation after 1113s (period)

Table 9-2. Full cycle of observation assumed for transient analysis

9.2. Boundary conditions

The boundary conditions at the thermo-mechanical interfaces are reported in this Chapter.

9.2.1. Bipods (BP1, BP2, BP3, BP4, BP5, BP6)

Figure 9-8 Bipods Thermal bounday condition surfaces

These boundary conditions are defined as fixed temperatures over the entire 6 surfaces. The values assumed in the thermal cases analysed are reported in the following table.

Minimum T Case [K]	**120**
Nominal Case [K]	**135**
Maximum T Case[K]	**135**

Table 9-3. NI-OMA bipods boundary conditions for each thermal case

9.2.2. Detector flange (CSS)

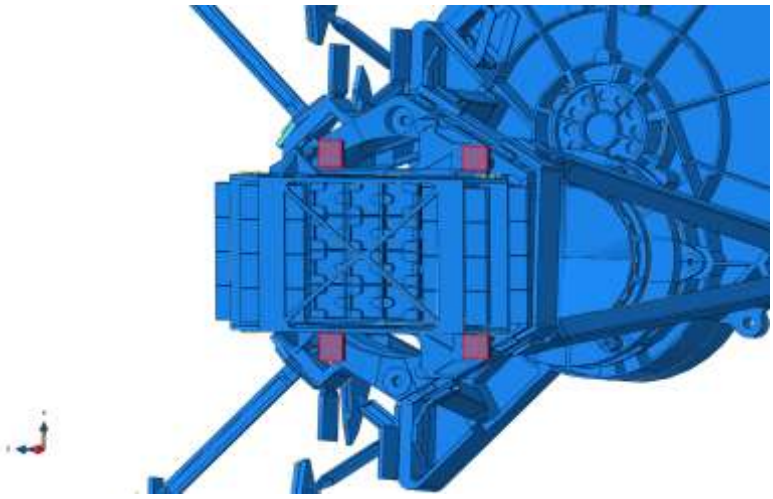

Figure 9-9 CSS Thermal boundary condition surfaces

The boundary conditions are defined as fixed temperatures over all the 4 surfaces. The values assumed in the thermal cases analysed are reported in the following table.

Min T Case [K]	**80**
Nominal Case [K]	**95**
Max T Case[K]	**95**

Table 9-4. CSS boundary conditions for each thermal case

9.2.3. Sidecars mainframe (SSS)

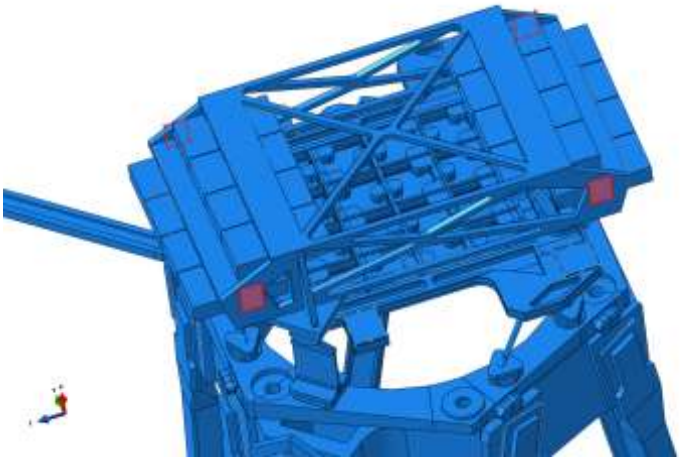

Figure 9-10 SSS Thermal boundary condition surfaces

The boundary conditions are defined as fixed temperature over all the 4 contact surfaces. The values assumed in the thermal cases analysed are reported in the following table.

Min T Case [K]	**120**
Nominal Case [K]	**135**
Max T Case[K]	**135**

Table 9-5. SSS boundary conditions for each thermal case

9.2.4. External box

According to PLM Prime predictions, a 14K gradient has to be assumed across the instrument radiative environment. The top and bottom surfaces of the radiative box should be set at a temperature that is respectively 7K lower and higher than the side surface.

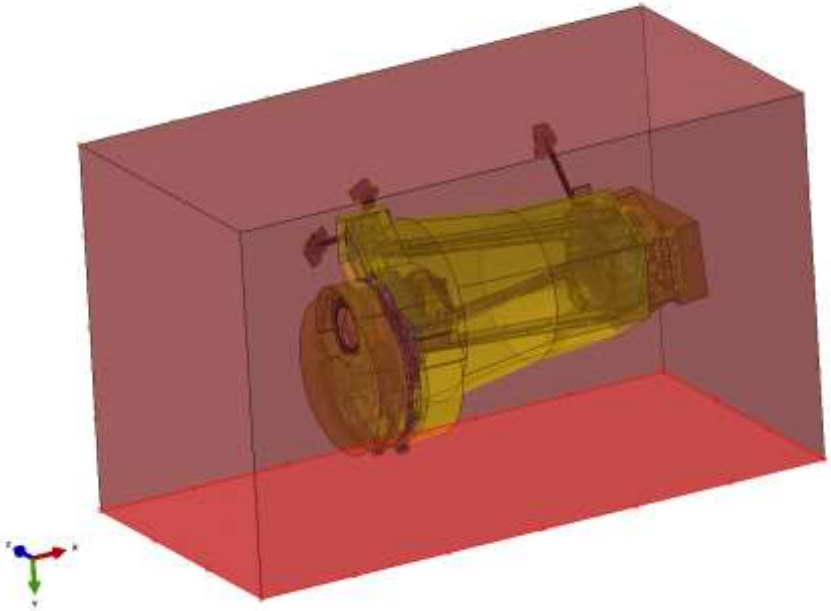

Figure 9-11 Box lower surface

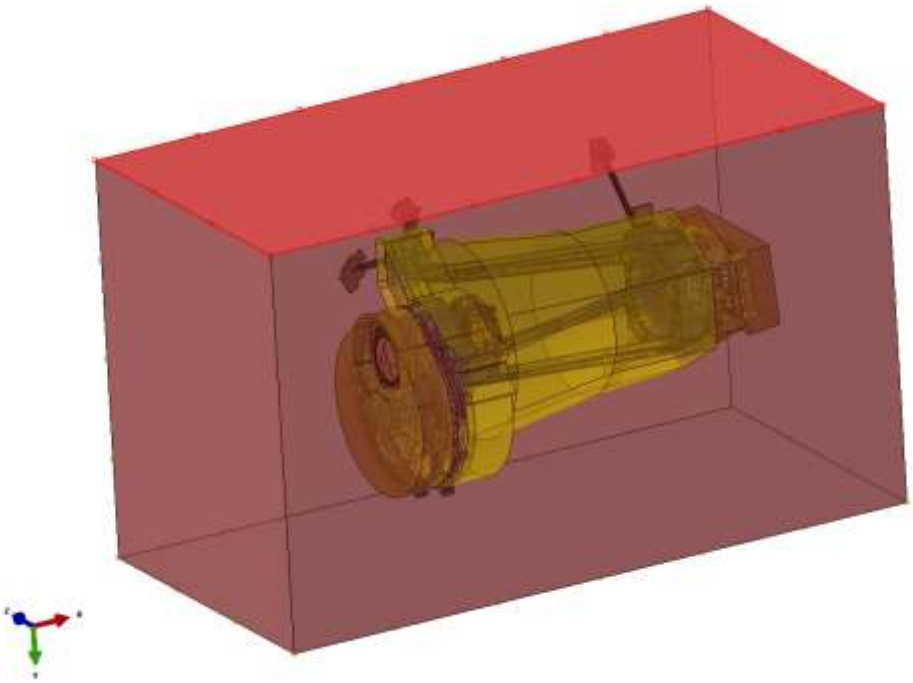

Figure 9-12 Box upper surface

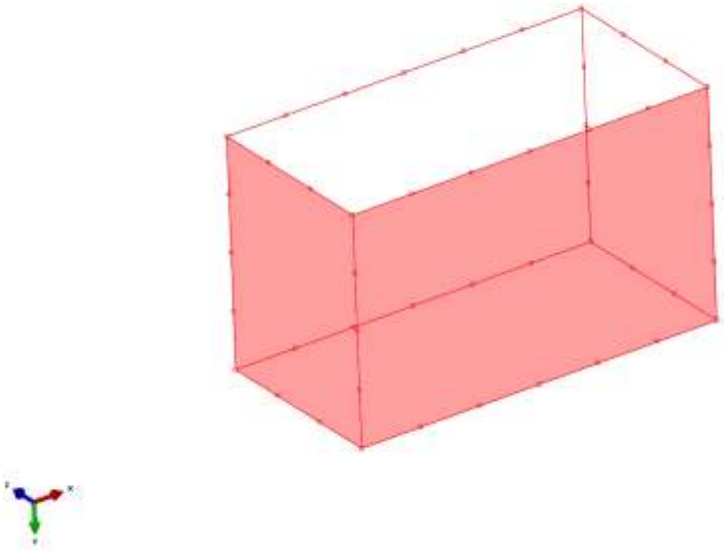

Figure 9-13 Box side surface

All the boundary conditions are imposed as fixed temperature surfaces. In the following table are summarized the values assumed for each of them.

	Box Lower	Box Upper	Box Side
Min T Case [K]	**127**	**113**	**120**
Nominal Case [K]	**142**	**128**	**135**
Max T Case [K]	**157**	**143**	**150**

Table 9-6. Instrument cavity environment boundary conditions for each thermal case

10. Simulation runs

10.1. Steady state analysis

Due to the presence of an efficient radiative shielding (MLI shroud), coupled to both the external environment and the instrument, the simulations have executed using 100 iterations, considering at the same time the conductive and the radiative interactions. The loads are applied as a linear ramp over the iterations.
The direct solver method is used for all these analyses, with hybrid parallelization.
The load cases studied are a combination of the boundary condition state (Max, Nominal, Min) and the instrument state (On or Off). In the Instrument Off state all active loads are set to zero; in the Instrument ON condition the nominal active loads are assumed. In the chapter 10.3 are reported the results for all the combinations and the relative job reference numbers.

10.2. Transient analysis

After the study of the instrument thermal status at equilibrium, a set of analysis runs have been performed in order to define the transient behaviour of the system after a variation of the boundary interface of the CSS flange. The following simulated fluctuations have been imposed at the TIF2 contact areas:

1. Single step increment of the boundary temperature of the CSS interface of 15mK; [Job-46]
2. Increment of the boundary temperature of the CSS interface following the curve 1; [Job-45]
3. Sinusoidal fluctuation of the boundary temperature of the CSS interface [period 30s; Amplitude 1K; sampling time 1s]; [Job-48]
4. Sinusoidal fluctuation of the boundary temperature of the CSS interface [period 60s; Amplitude 1K; sampling time 1s]; [Job-47]
5. Sinusoidal fluctuation of the boundary temperature of the CSS interface [period 120s; Amplitude 1K; sampling time 1s]; [Job-52]
6. Sinusoidal fluctuation of the boundary temperature of the CSS interface [period 240s; Amplitude 1K; sampling time 1s]; [Job-53]
7. Sinusoidal fluctuation of the boundary temperature of the CSS interface [period 480s; Amplitude 1K; sampling time 1s]; [Job-54]
8. Sinusoidal fluctuation of the boundary temperature of the CSS interface [period 960s; Amplitude 1K; sampling time 1s]; [Job-55]
9. Sinusoidal fluctuation of the boundary temperature of the CSS interface [period 3600s; Amplitude 1K; sampling time 10s]; [Job-50]
10. Sinusoidal fluctuation of the boundary temperature of the CSS interface [period 36000s; Amplitude 1K; sampling time 100s]; [Job-51]

All these analysis are performed starting from the steady-state solution for the nominal case with the instrument in operational mode.

10.3. Summary tables of the performed jobs

10.3.1. Steady state

Summary table of the steady state analysis job id's:

Case	Instrument Off	Instrument On
Nominal Case	11	14
Max T Case	12	15
Min T Case	13	16

Table 10-1. FEM simulations runs job ID's

11. Paths

In order to represent the temperature distribution on the different units, resulting from the simulations, some paths have been defined. The Figures of this Chapter show all the paths on the mesh used to report the gradients in the graphic displays that show temperature distribution on lenses and bipods: all the temperature profiles shown in Chapter 13 are based on these paths.

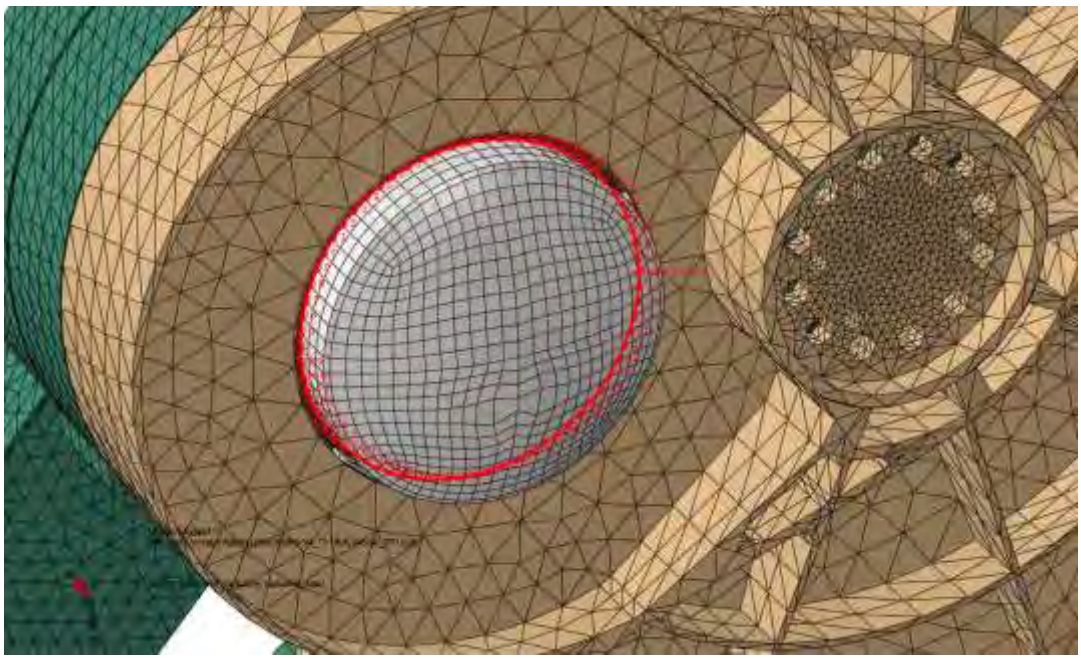

Figure 11-1 CoLA lens internal circumference 1 (ColA circ1)

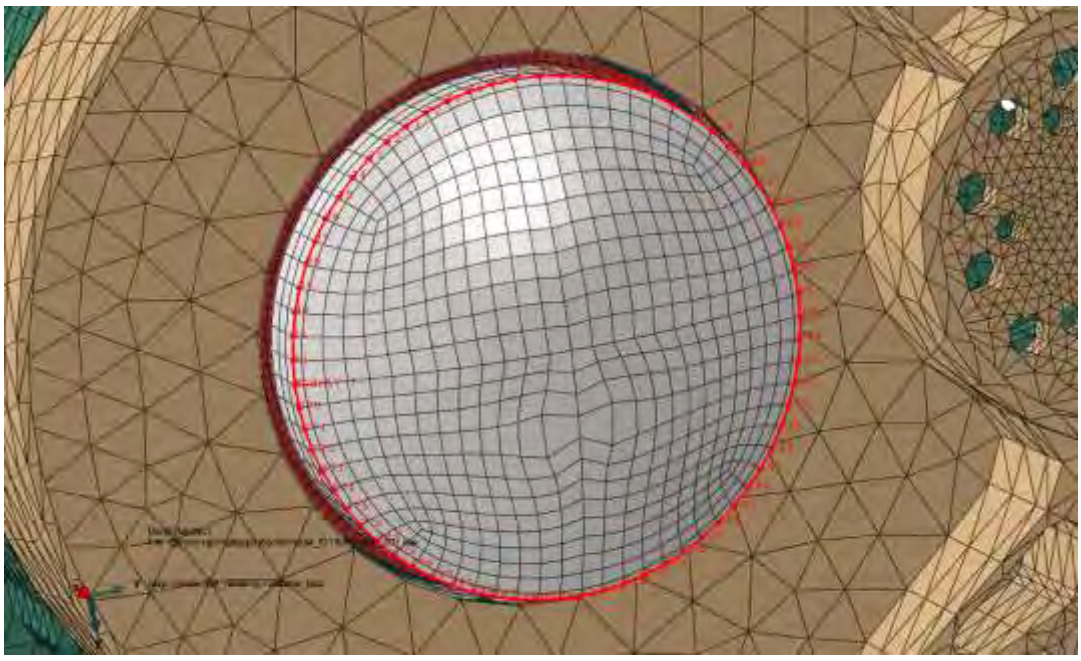

Figure 11-2 CoLA lens external circumference 2 (CoLA circ2)

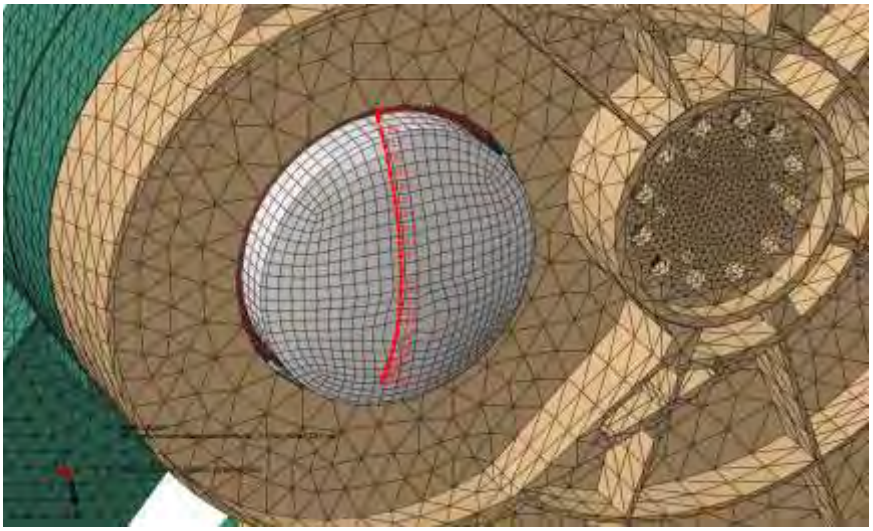

Figure 11-3 CoLA lens internal diameter 1 (CoLA diam1)

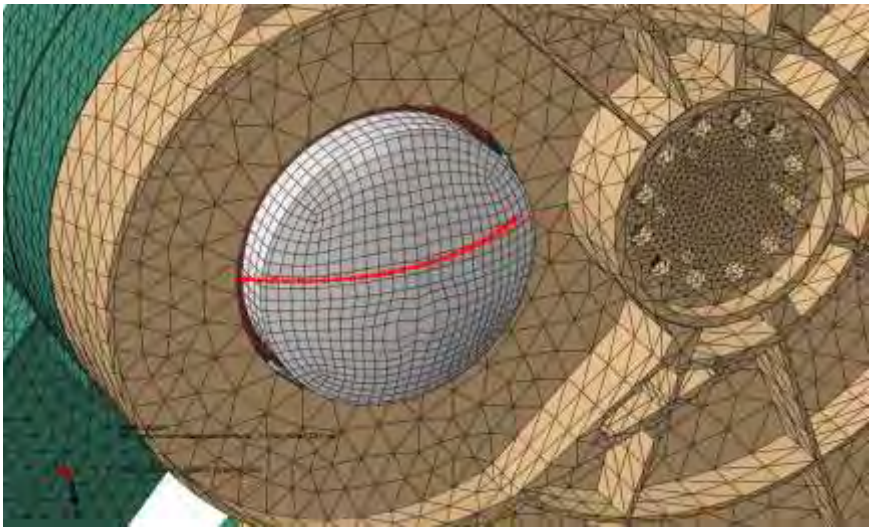

Figure 11-4 CoLA lens internal diameter 2 (CoLA diam2)

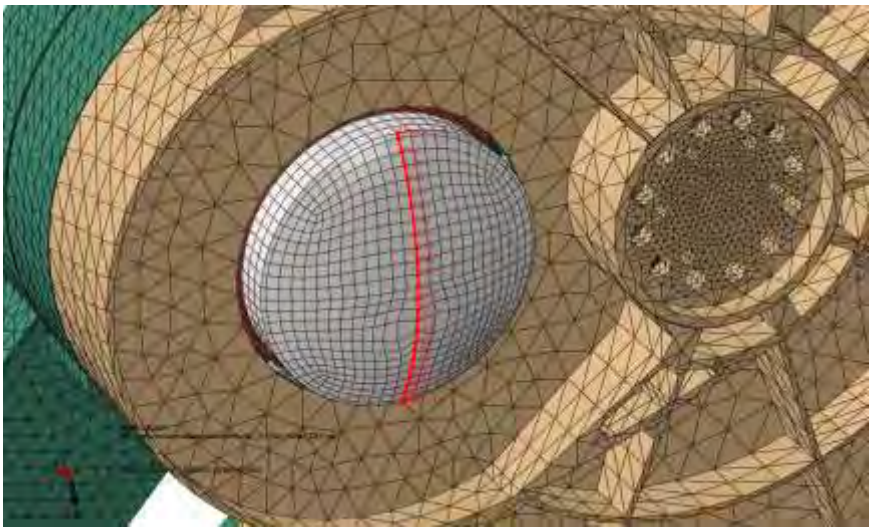

Figure 11-5 CoLA lens external diameter 3 (CoLA diam3)

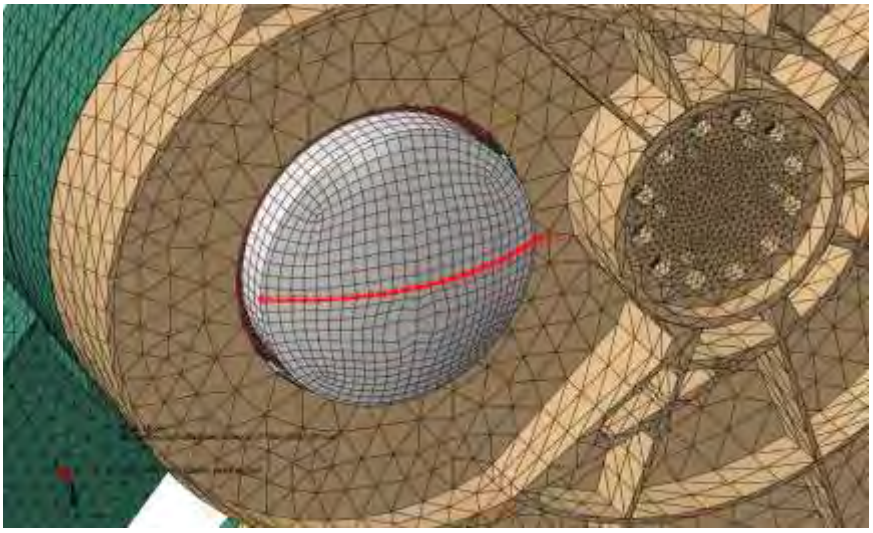

Figure 11-6 CoLA lens external diameter 4 (CoLA diam4)

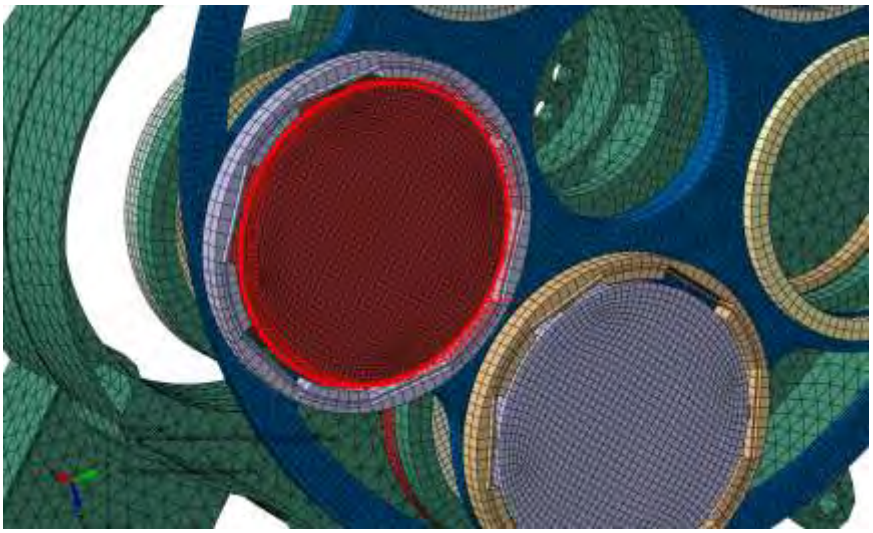

Figure 11-7 Filter front circumference 1 (FWA circ1)

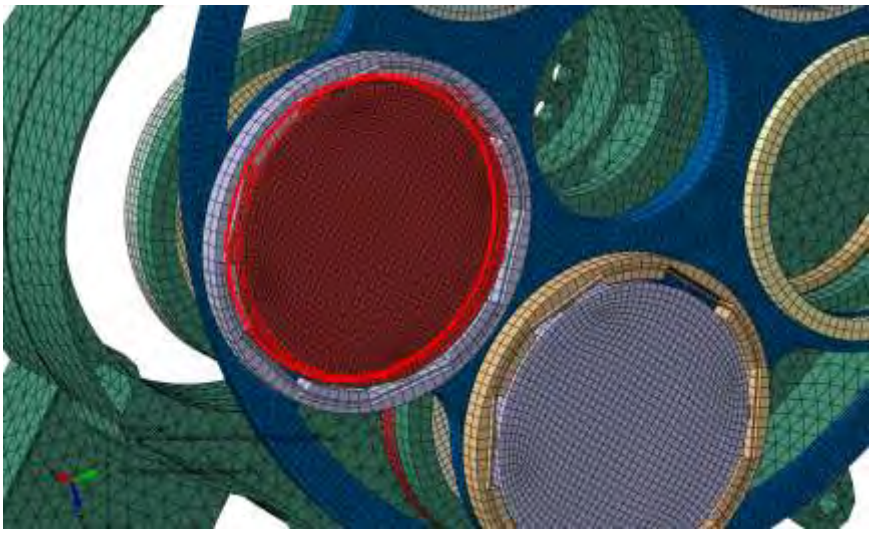

Figure 11-8 Filter back circumference 2 (FWA circ2)

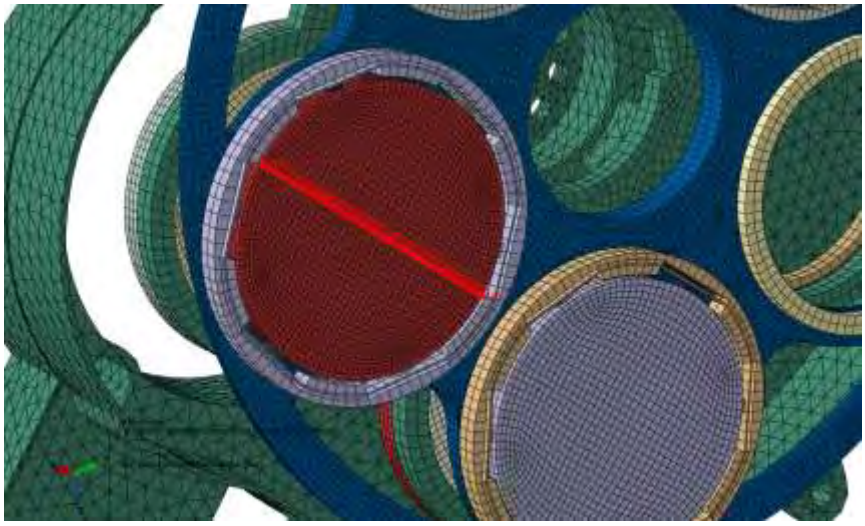

Figure 11-9 Filter front diameter 1 (FWA diam 1)

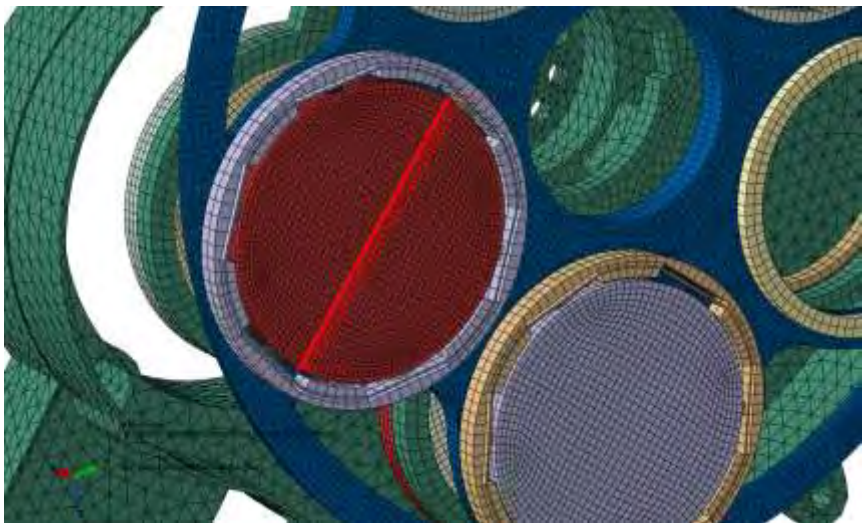

Figure 11-10 Filter front diameter 2 (FWA diam2)

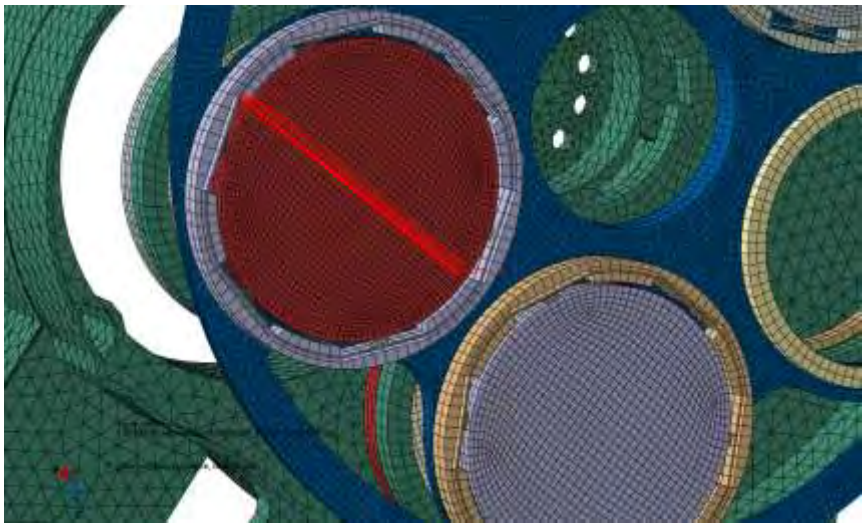

Figure 11-11 Filter back diameter 3 (FWA diam3)

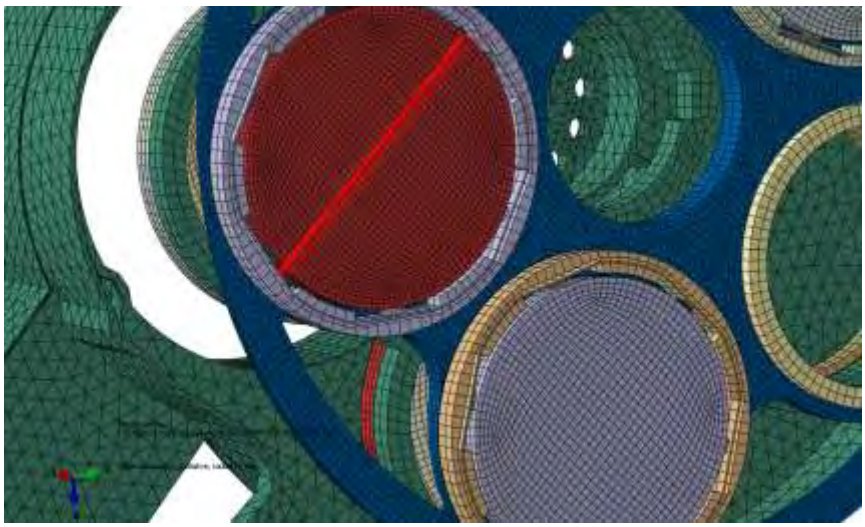

Figure 11-12 Filter back diameter 4 (FWA diam4)

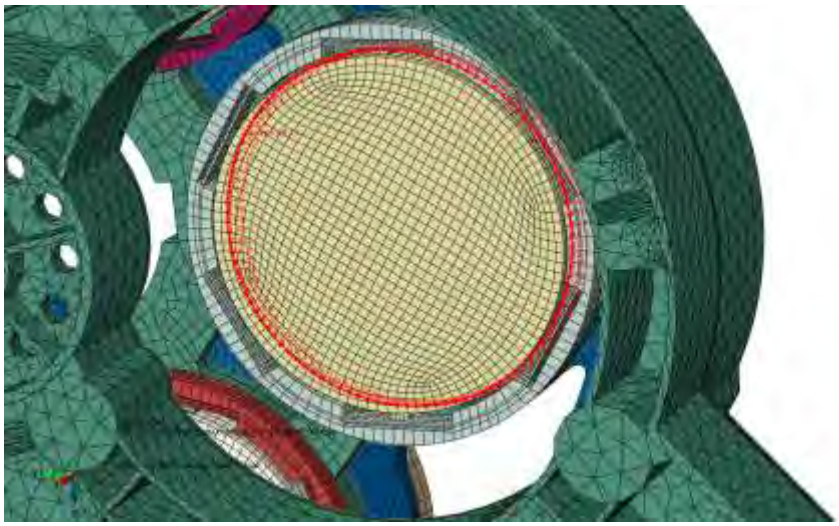

Figure 11-13 Grism front circumference 1 (GWA cir1)

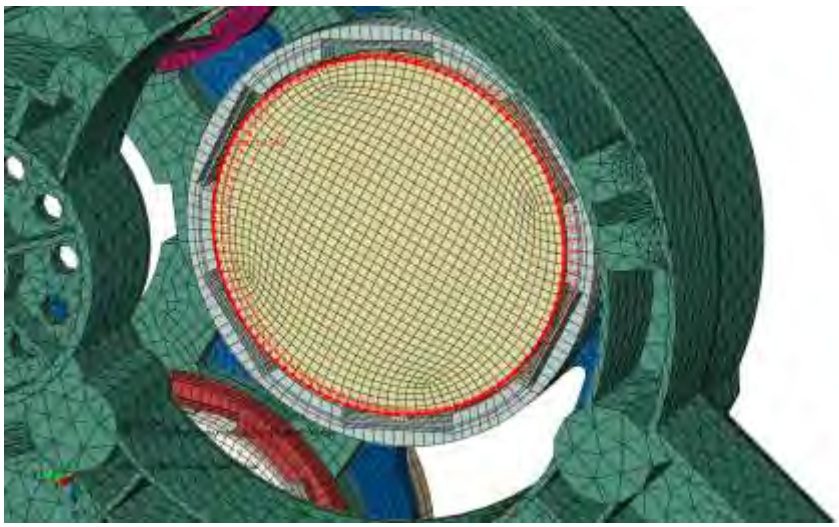

Figure 11-14 Grism back circumference 2 (GWA circ2)

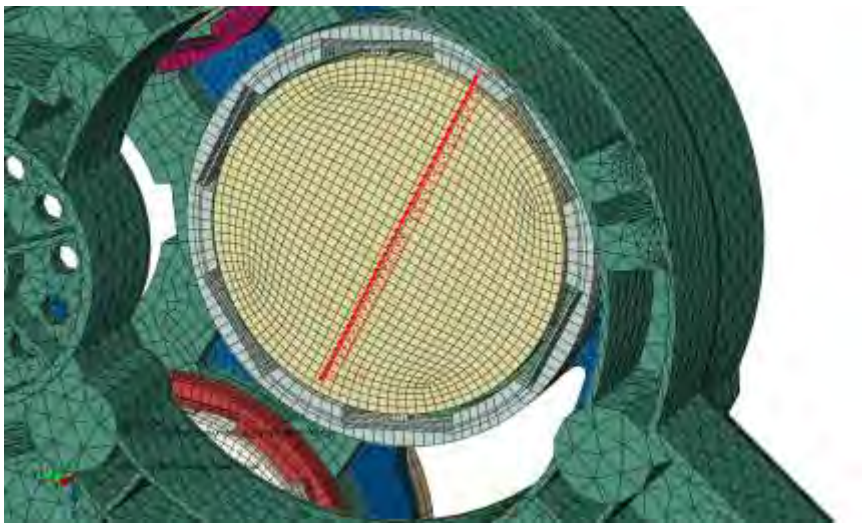

Figure 11-15 Grism front diameter 1 (GWA diam1)

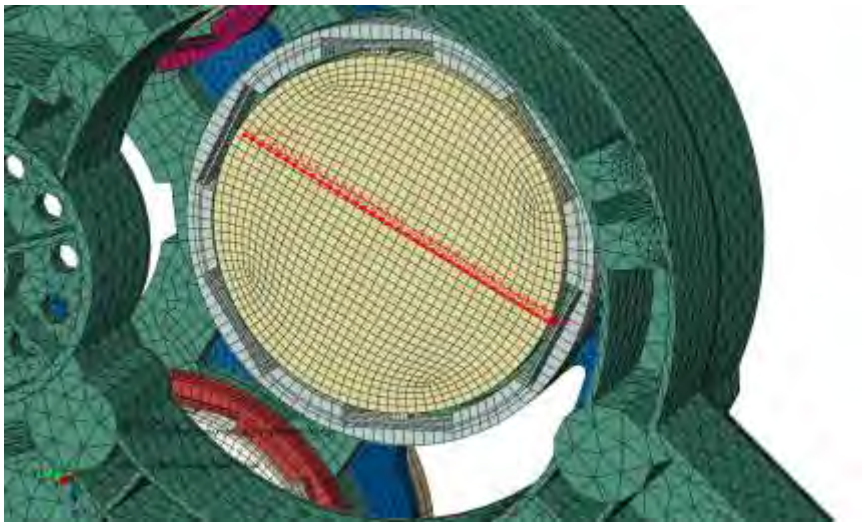

Figure 11-16 Grism front diameter 2 (GWA diam2)

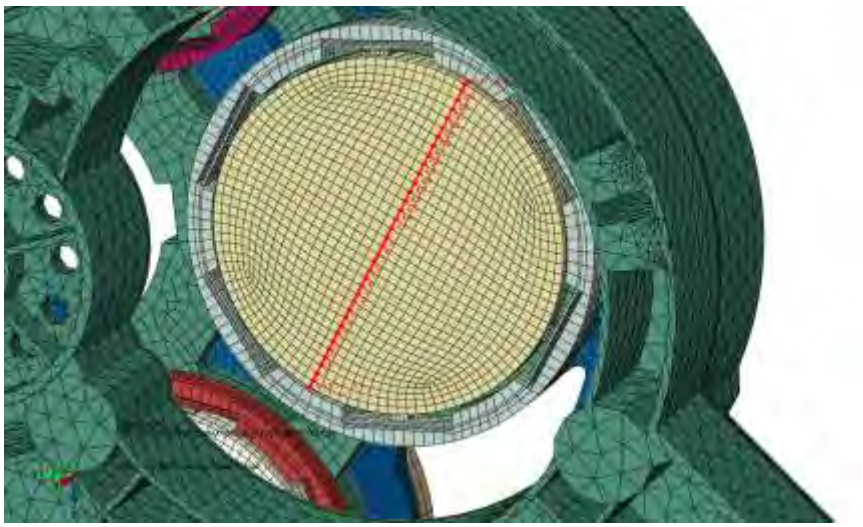

Figure 11-17 Grism back diameter 3 (GWA diam3)

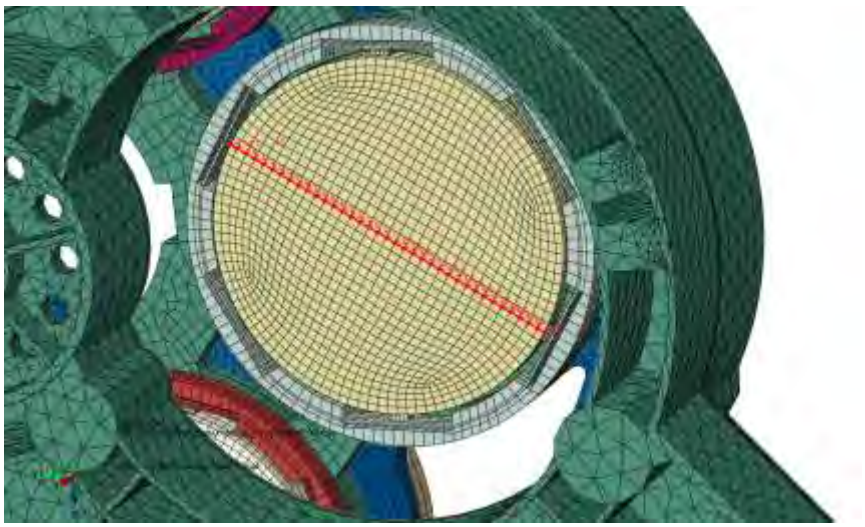

Figure 11-18 Grism back diameter 4 (GWA diam4)

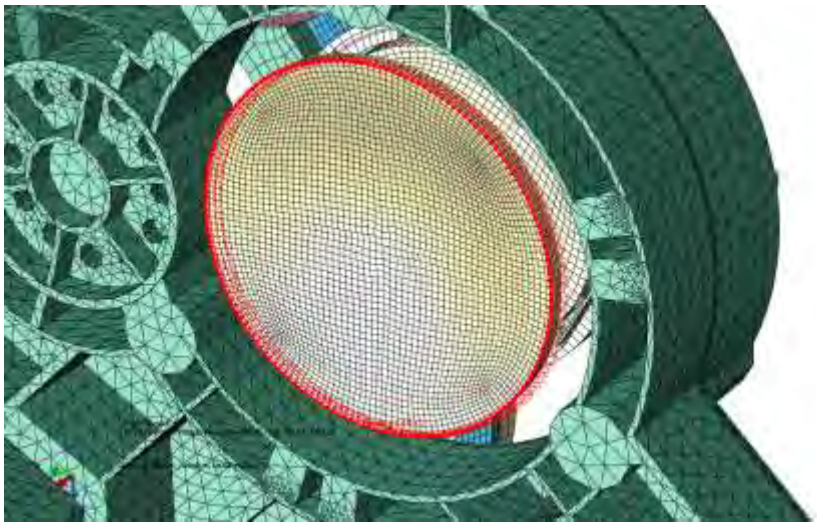

Figure 11-19 CaLA Lens 1 back circumference 1 (CaLA1 circ1)

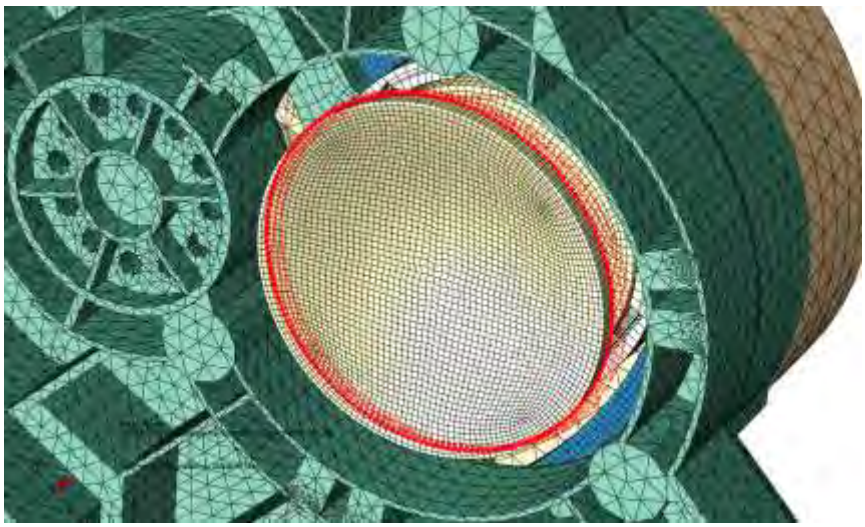

Figure 11-20 CaLA Lens 1 front circumference2 (CaLA1 circ2)

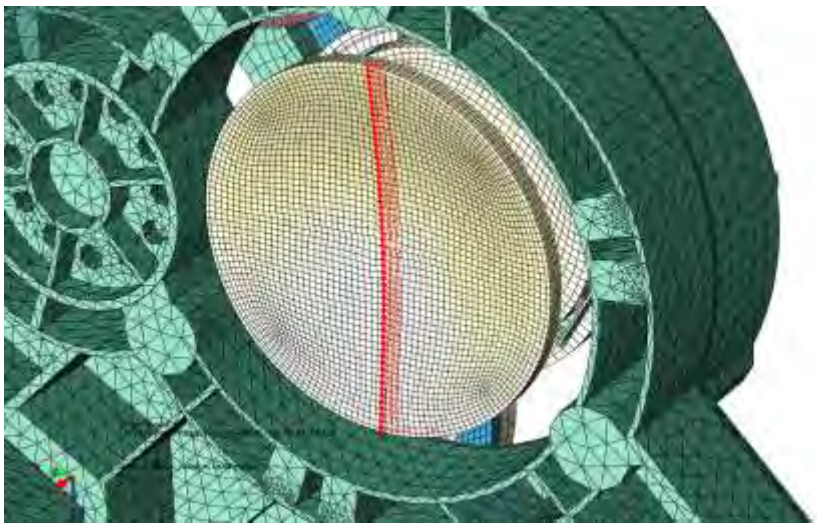

Figure 11-21 CaLA Lens 1 back diameter 1 (CaLA1 diam1)

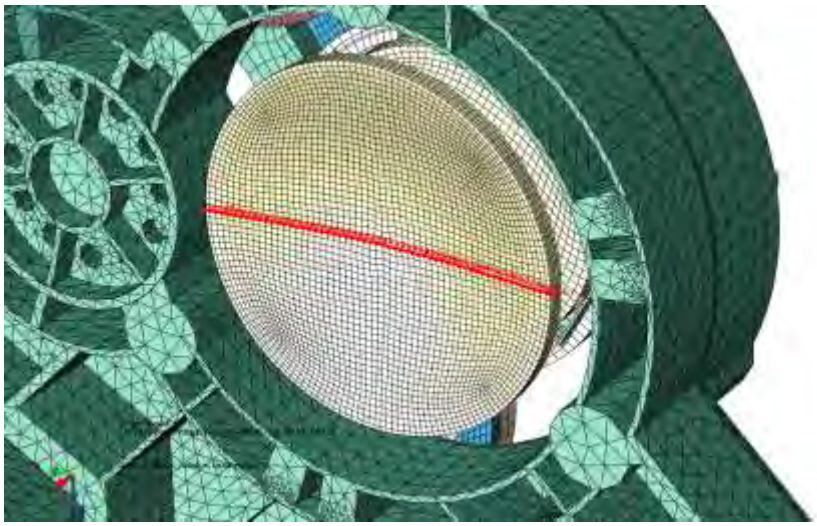

Figure 11-22 CaLA Lens 1 back diameter 2 (CaLA1 diam2)

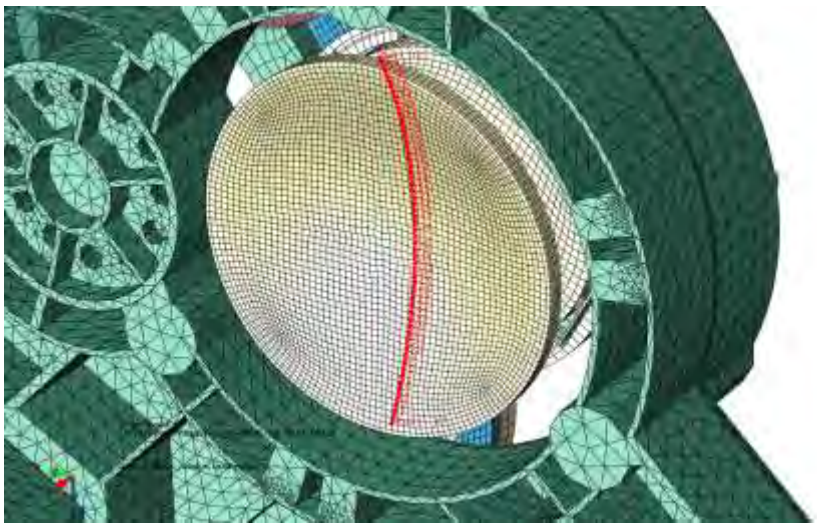

Figure 11-23 CaLA Lens 1 front diameter 3 (CaLA1 diam3)

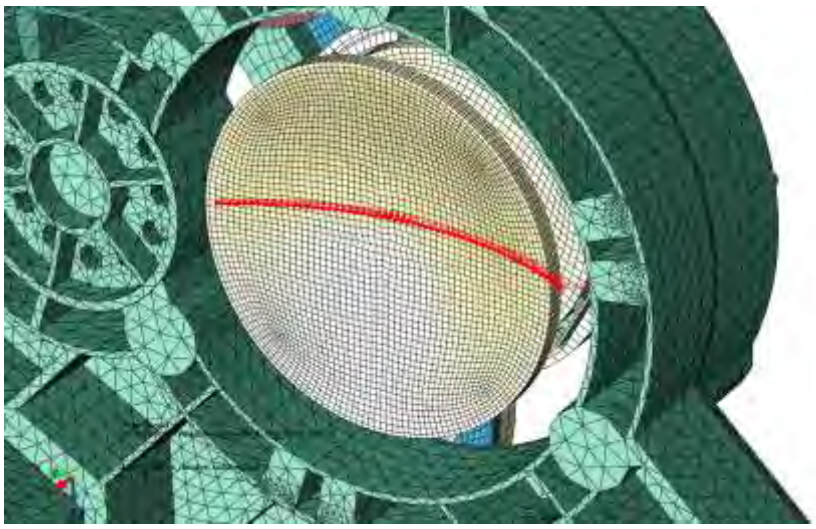

Figure 11-24 CaLA Lens 1 front diameter 4 (CaLA1 diam4)

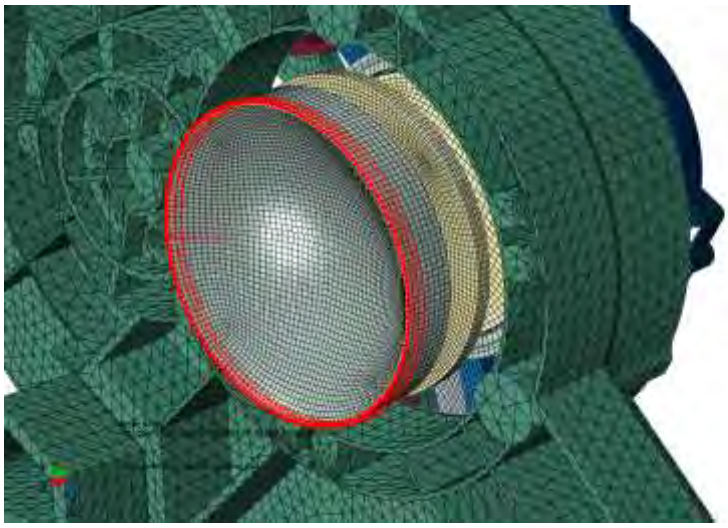

Figure 11-25 CaLA Lens 2 back circumference 1 (CaLA2 circ1)

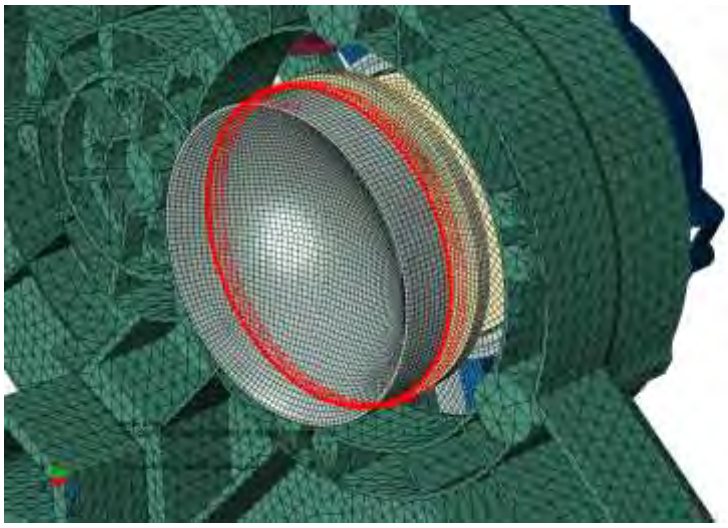

Figure 11-26 CaLA Lens 2 front circumference 2 (CaLA2 circ2)

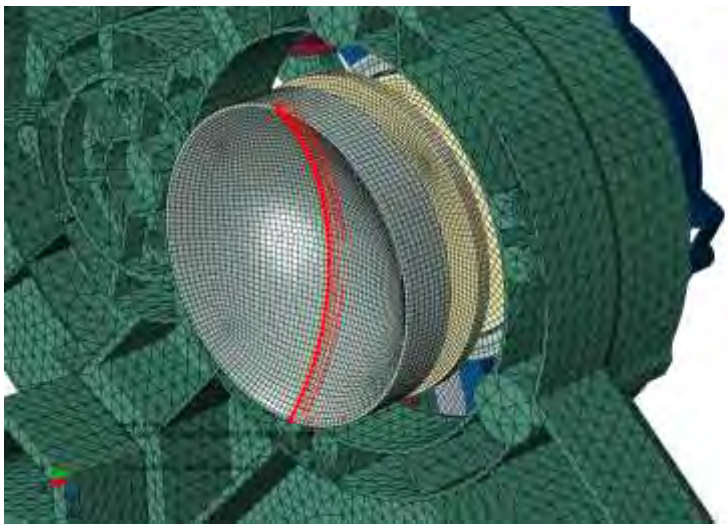

Figure 11-27 CaLA Lens 2 back diameter 1 (CaLA2 diam1)

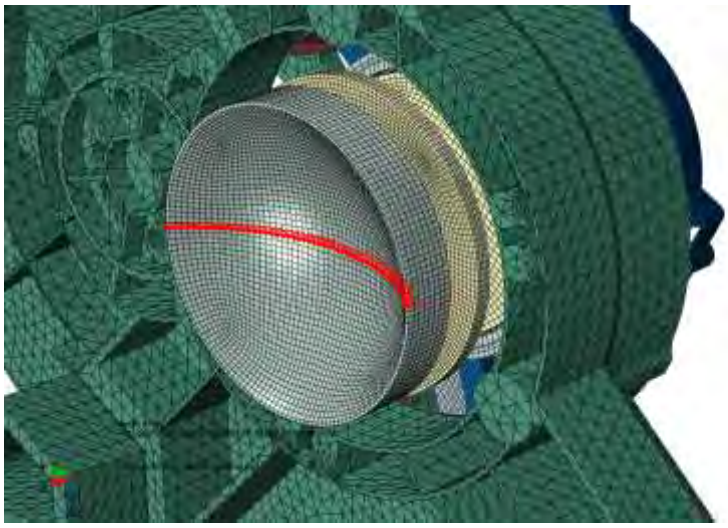

Figure 11-28 CaLA Lens 2 back diameter 2 (CaLA2 diam2)

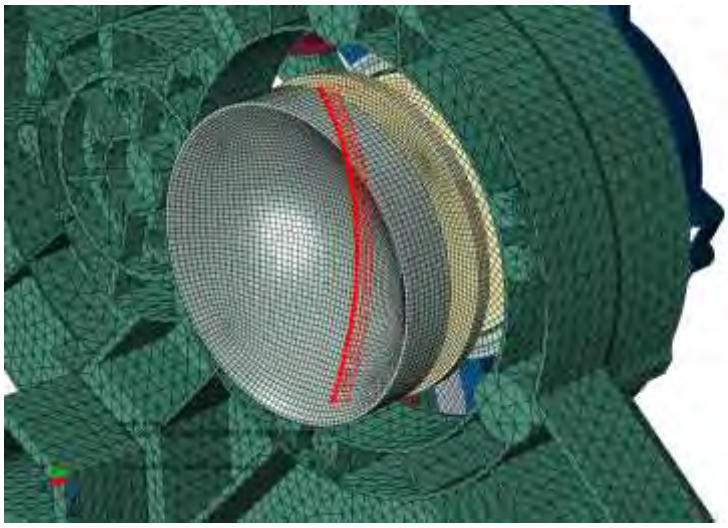

Figure 11-29 CaLA Lens 2 front diameter 3 (CaLA2 diam3)

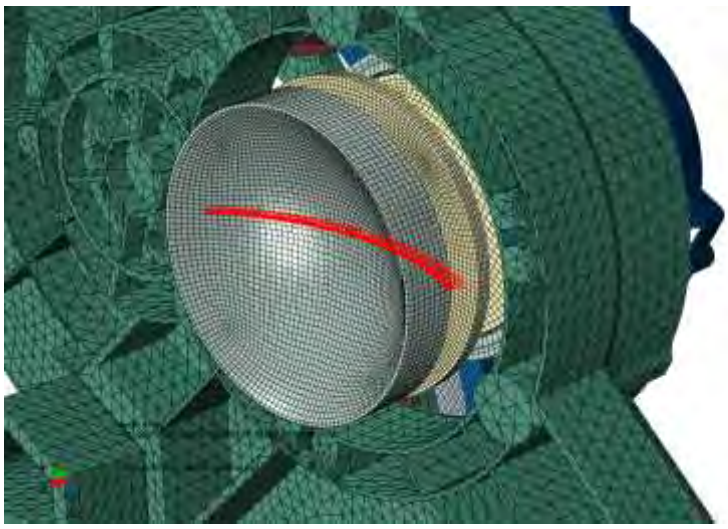

Figure 11-30 CaLA Lens 2 front diameter 4 (CaLA2 diam4)

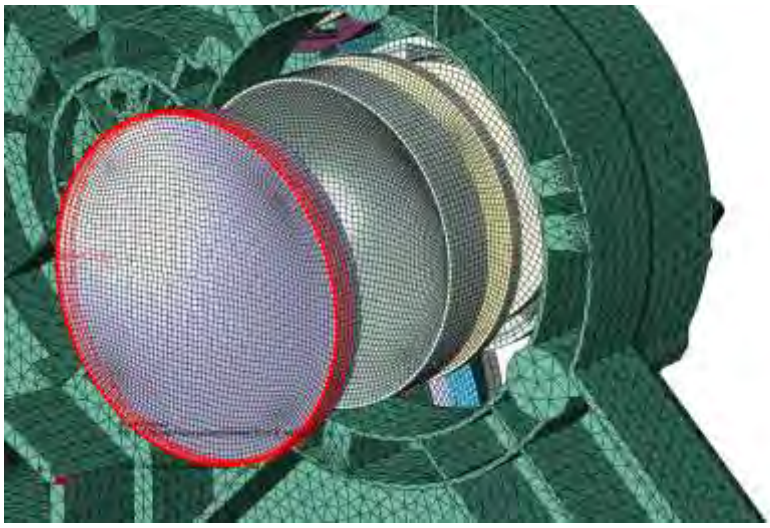

Figure 11-31 CaLA Lens 3 back circumference 1 (CaLA3 circ1)

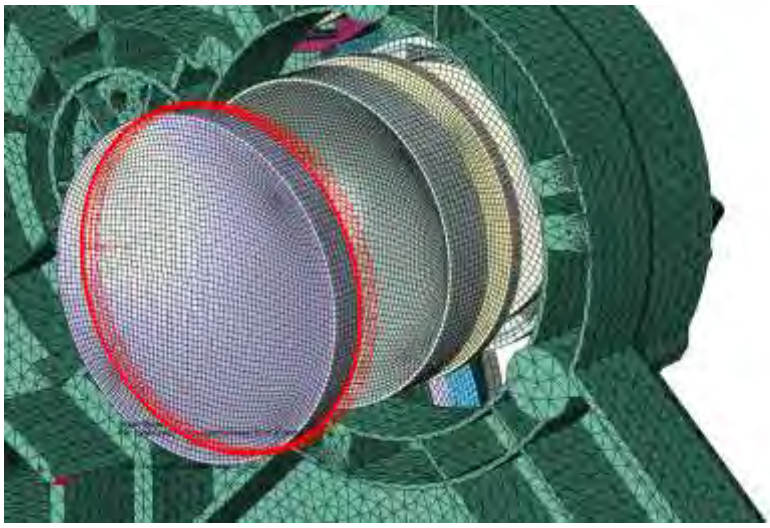

Figure 11-32 CaLA Lens 3 front circumference 2 (CaLA3 circ2)

Figure 11-33 CaLA Lens 3 back diameter 1 (CaLA3 diam1)

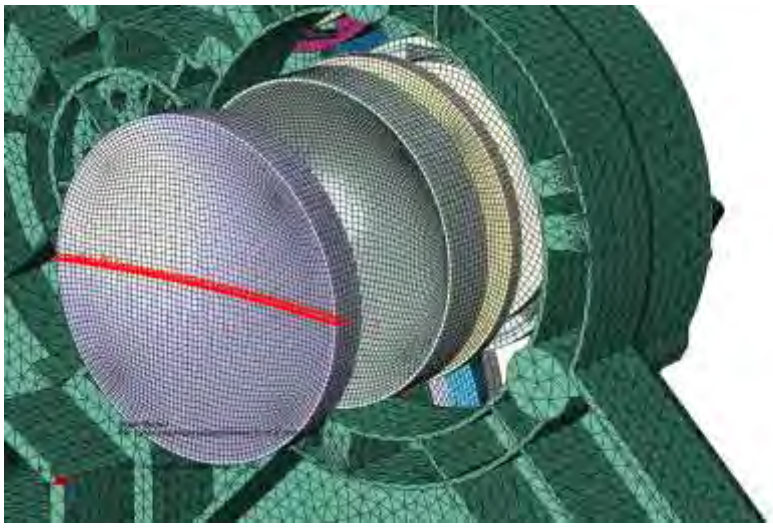

Figure 11-34 CaLA Lens 3 back diameter 2 (CaLA3 diam2)

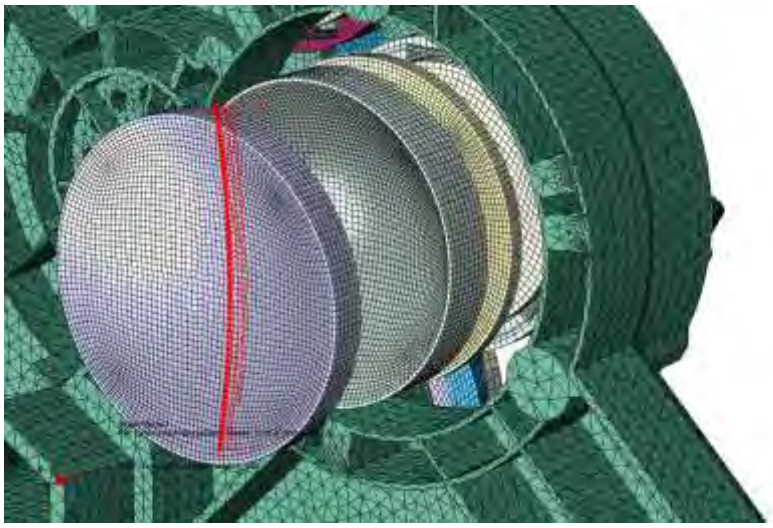

Figure 11-35 CaLA Lens 3 front diameter 3 (CaLA3 diam3)

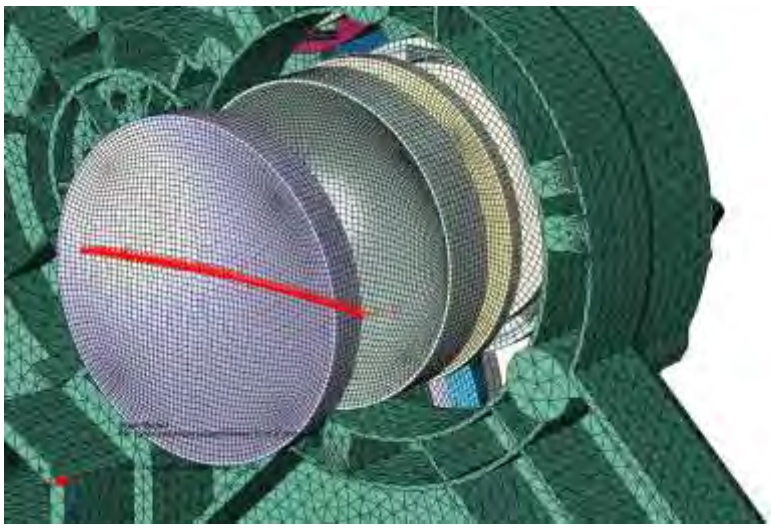

Figure 11-36 CaLA Lens 3 front diameter 4 (CaLA3 diam4)

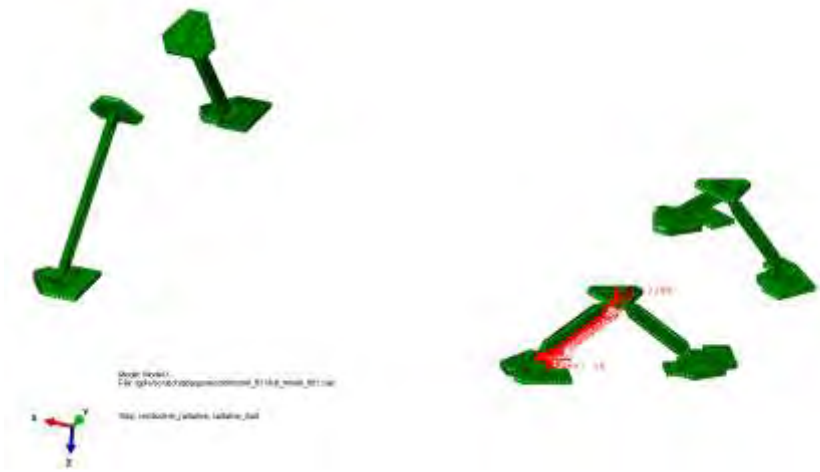

Figure 11-37 Bipods 1 (BP1)

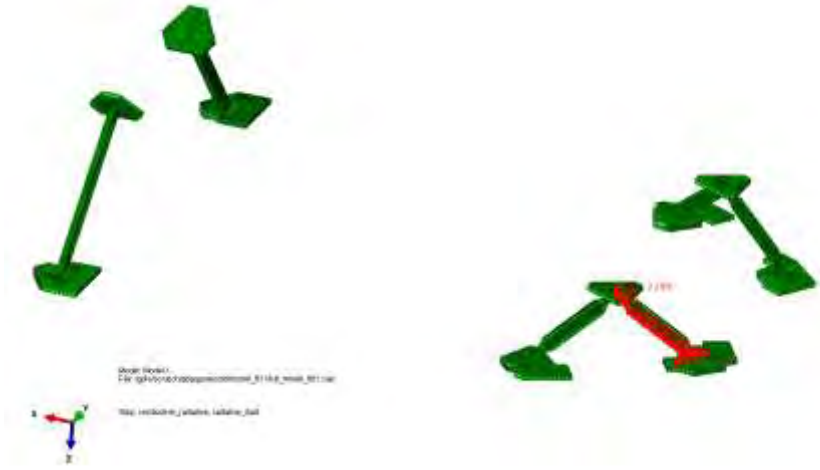

Figure 11-38 Bipods 2 (BP2)

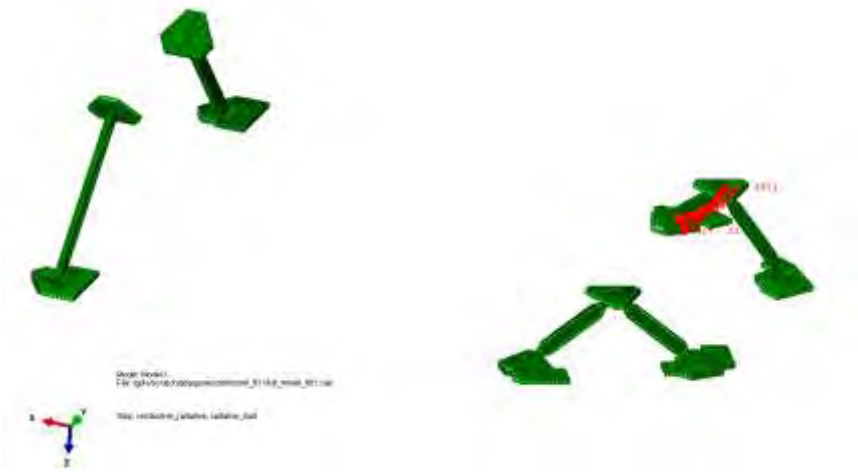

Figure 11-39 Bipods 3 (BP3)

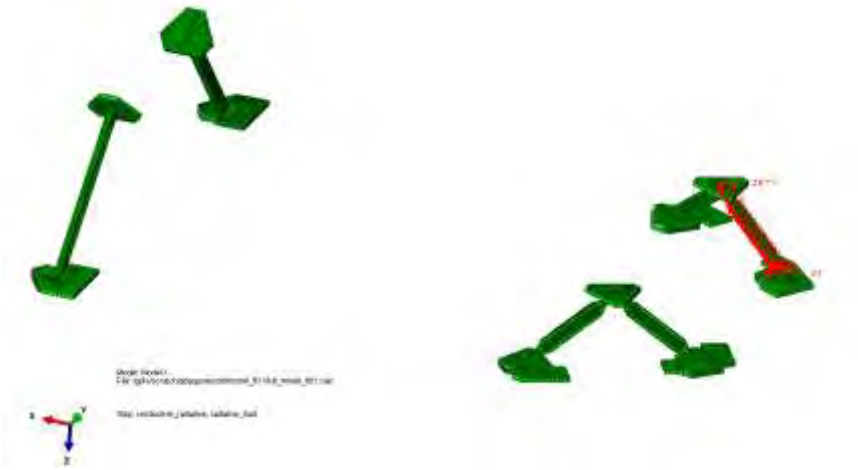

Figure 11-40 Bipods 4 (BP4)

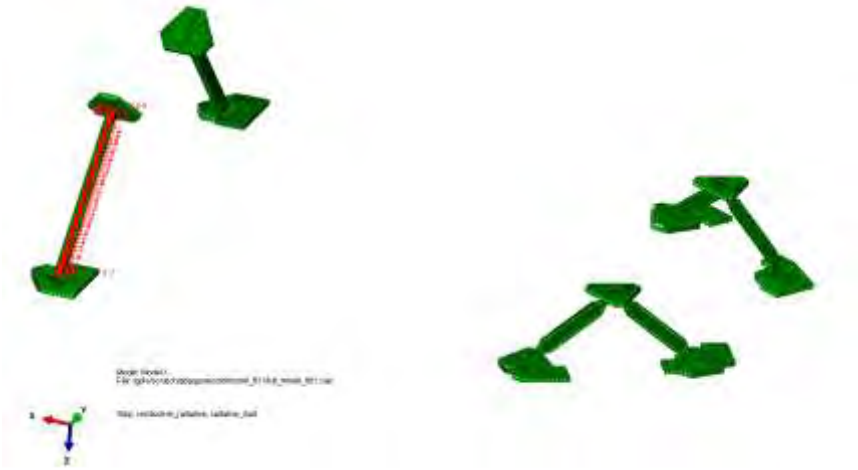

Figure 11-41 Bipods 5 (BP5)

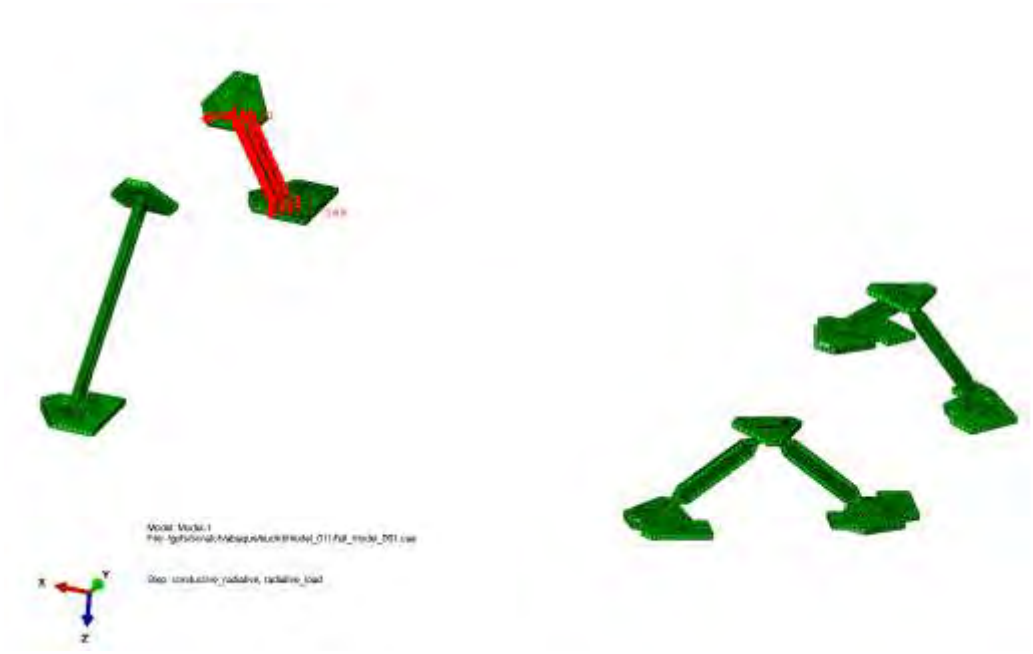

Figure 11-42 Bipods 6 (BP6)

12. Detectors and sidecars numeration

To simplify the results summary for each sidecar and detector, it is needed to define a standard numbering of these components. It has been decided to use the part number assigned by the cad during the importation step.

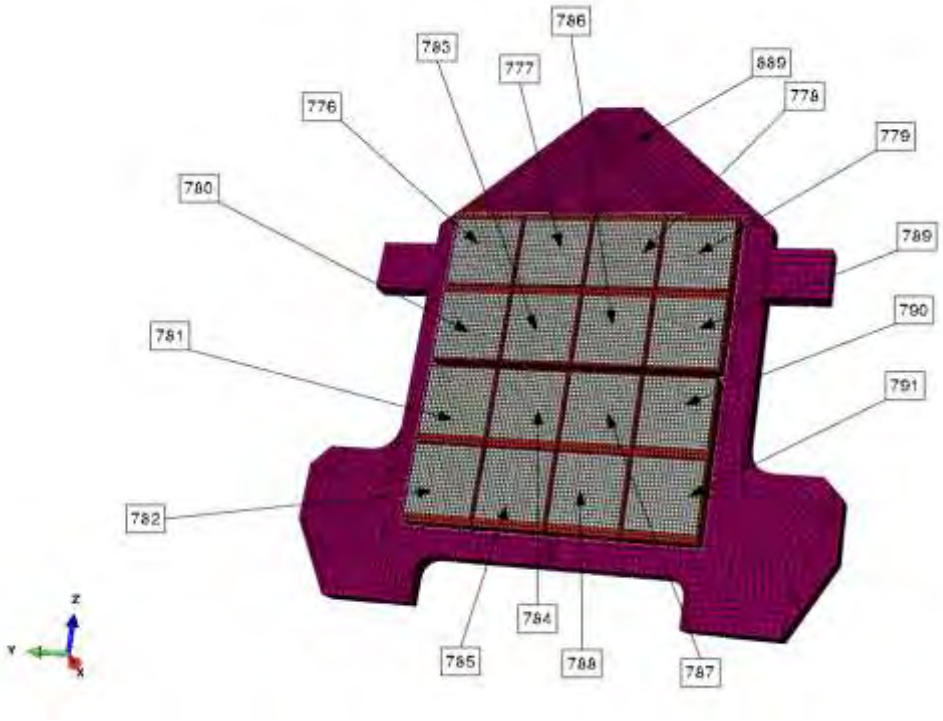

Figure 12-1 Detectors CAD reference number

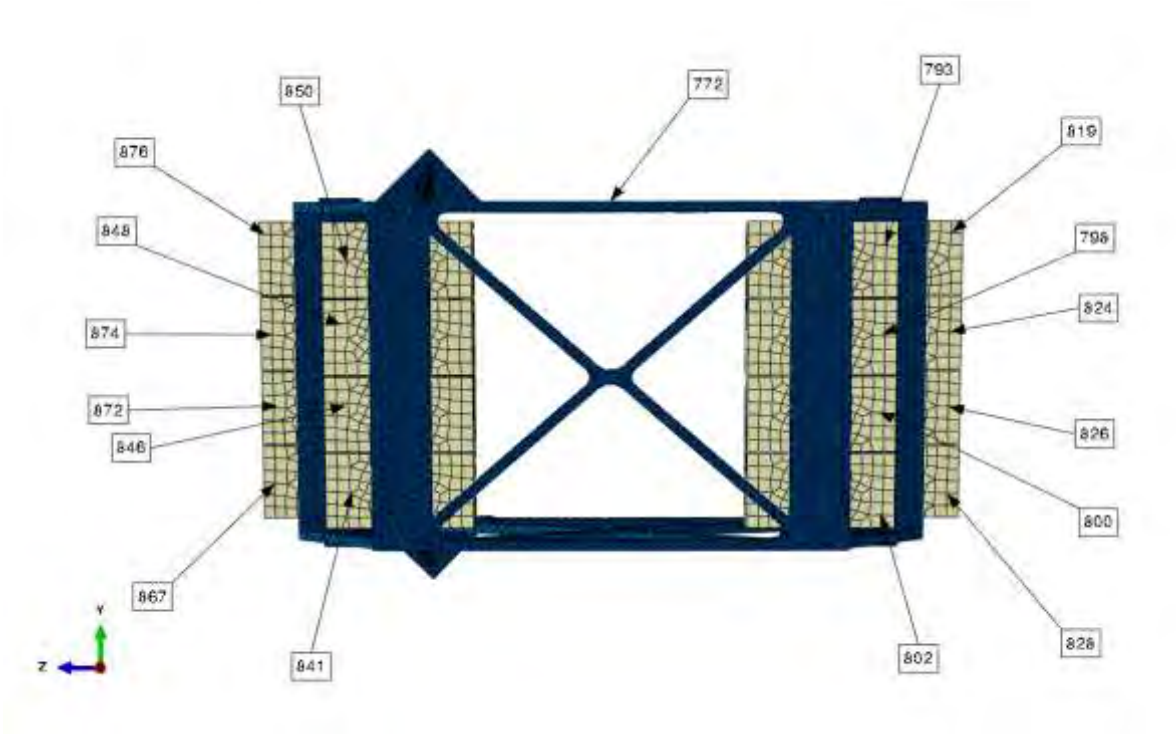

Figure 12-2 Sidecars CAD reference number

13. Results

In this Chapter are reported all the results of the steady-state analysis runs (Jobs 11-16). For each main unit the temperature distribution, the view factors and the heat fluxes are represented. Each graphic display is self-explaining.
To show a more readable representation of temperature distributions and view factors, the range of all the images is built with 24 colours table and the numbers are written with a fixed number of digits, in this case 5. This choice has been done taking into account the nearly isothermal condition of some components. All the results are to be assumed as deterministic and it was not performed a statistic analysis of the uncertain effect present in the material properties (the main uncertainty present in the model definition). So the number of digits present in the figures is the number of significant digits of the model, discarding any kind of uncertainty, and the use is limited to illustrate the distribution of the variables on the components.

13.1. Job 11 – Steady state analysis, Nominal Case, Instrument Off, Not-OP mode

In the followings images are reported the temperature distributions, the view factors and the radiative fluxes for the instruments, and in particular for the lenses, the detectors and the sidecars.

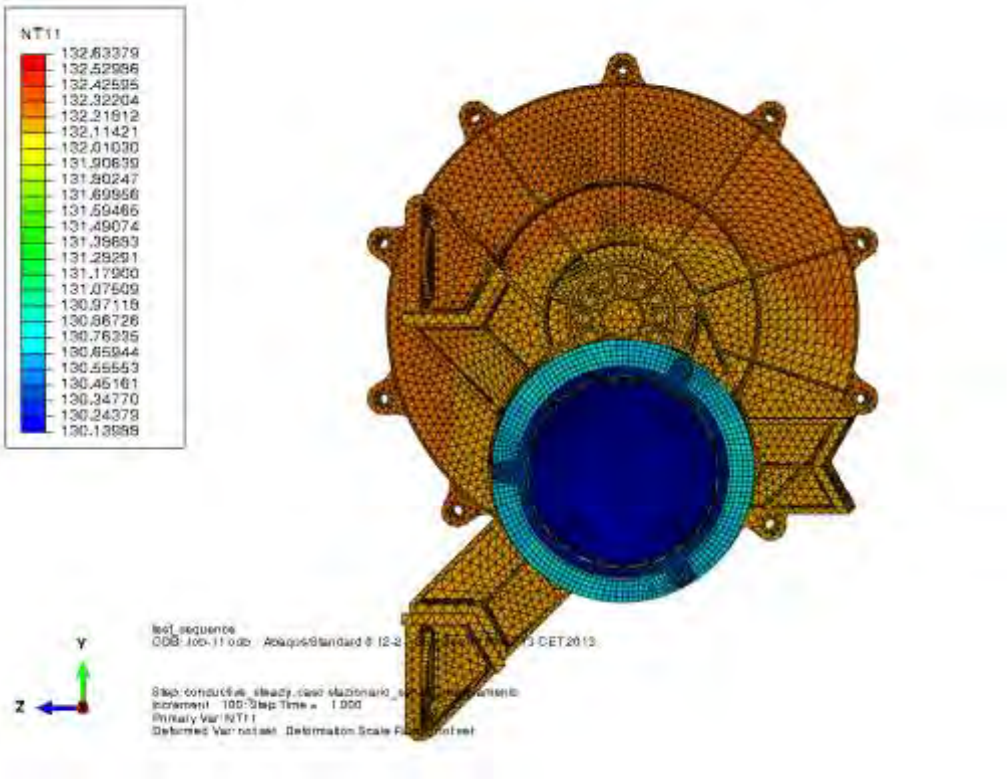

Figure 13-1 P1 and CaLA assembly temperature distribution [K]

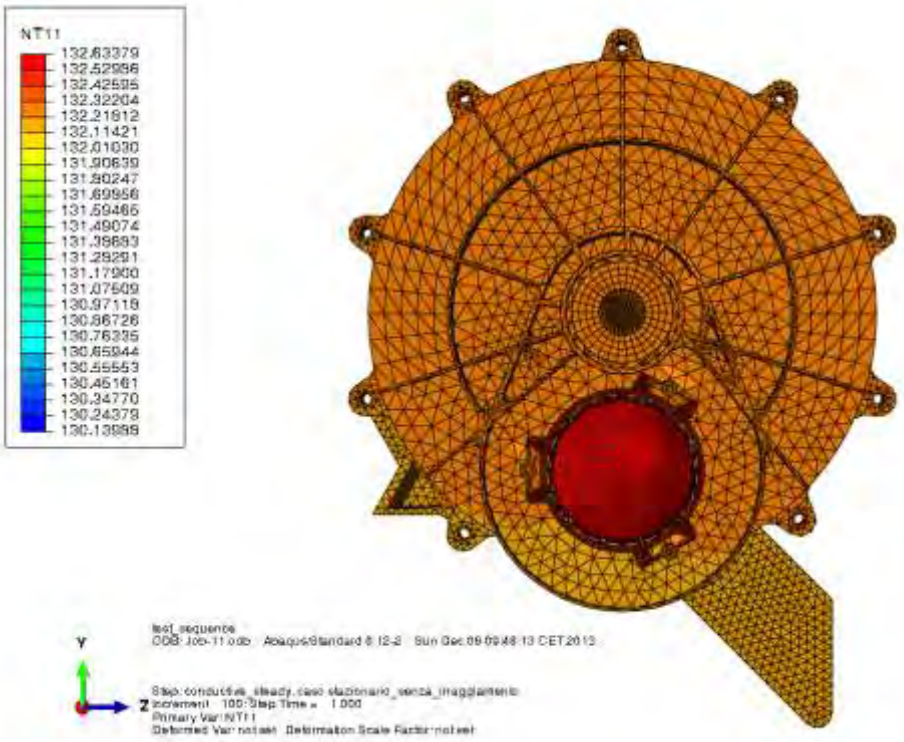

Figure 13-2 P2 and CoLA temperature distribution [K]

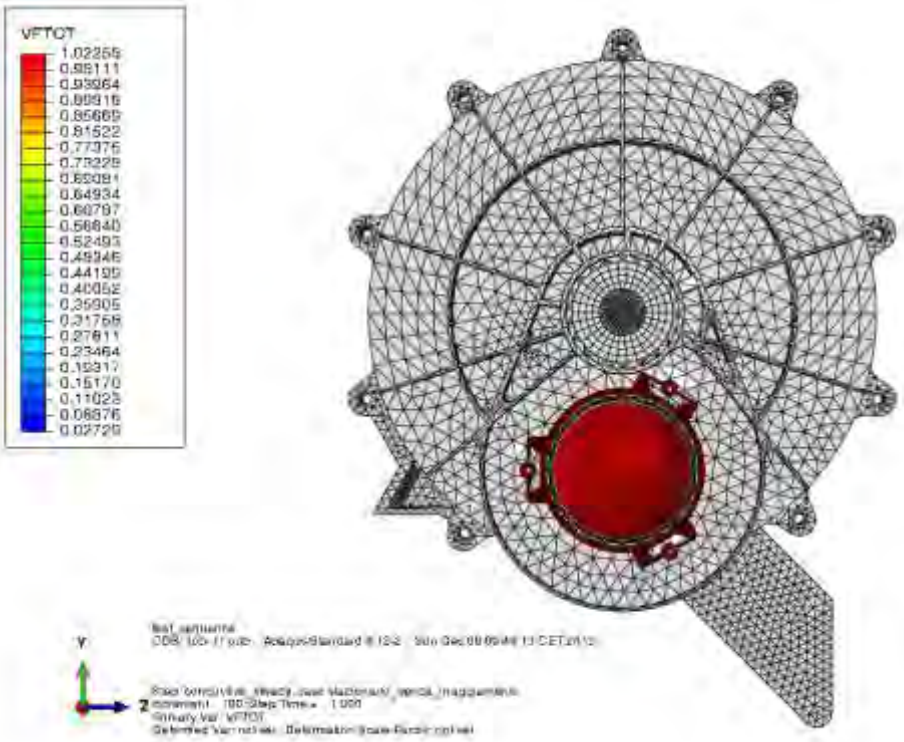

Figure 13-3 CoLA View Factor

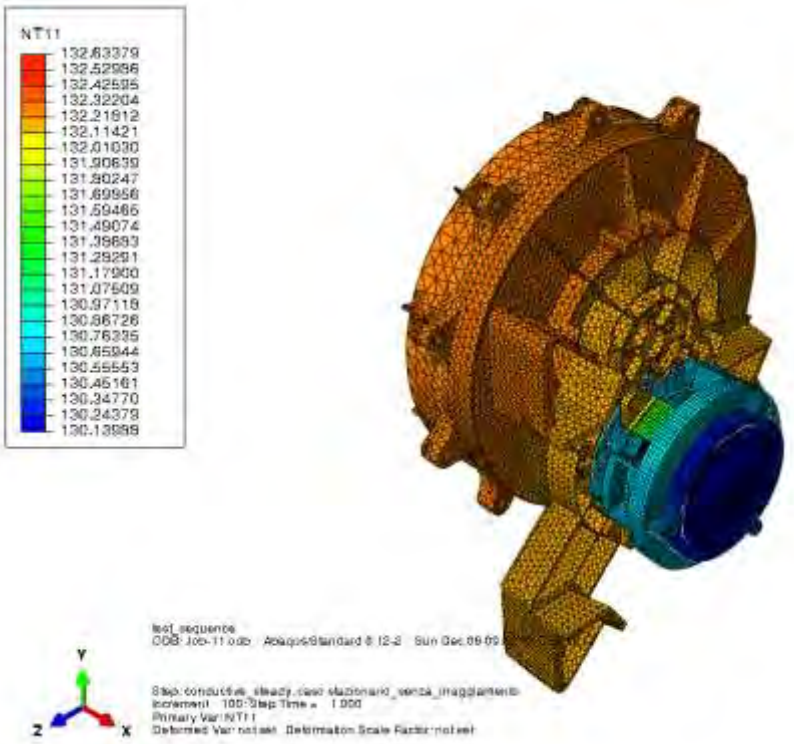

Figure 13-4 P1, P2 and CaLA assembly temperature distribution [K]

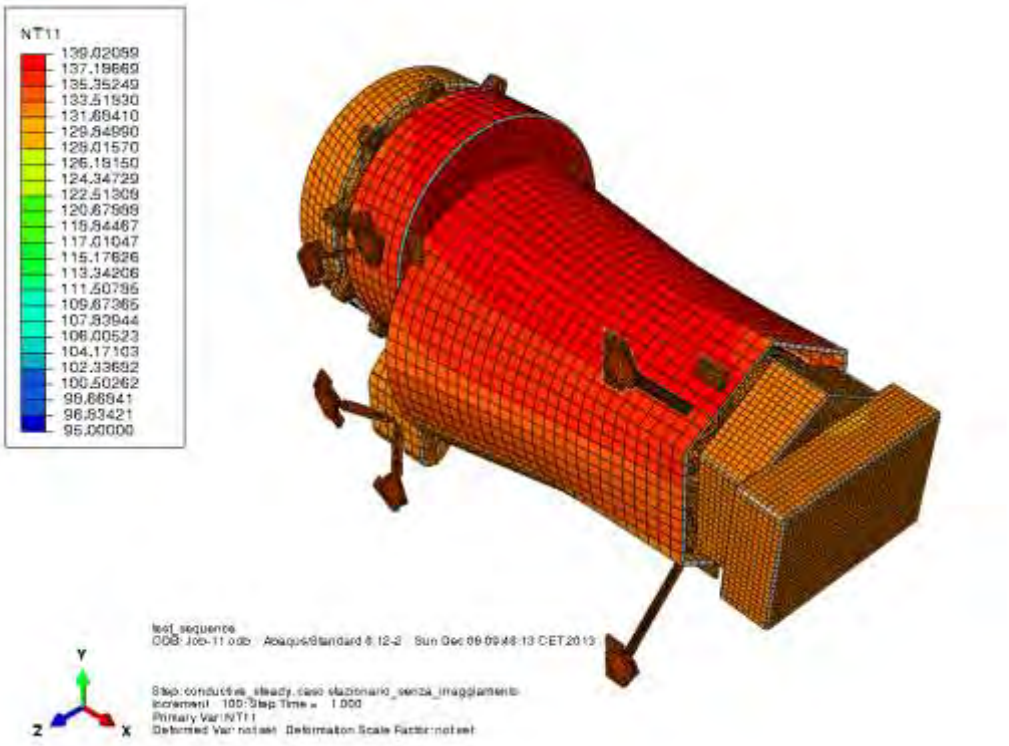

Figure 13-5 Full instrument assembly, with shrouds, temperature distribution [K]

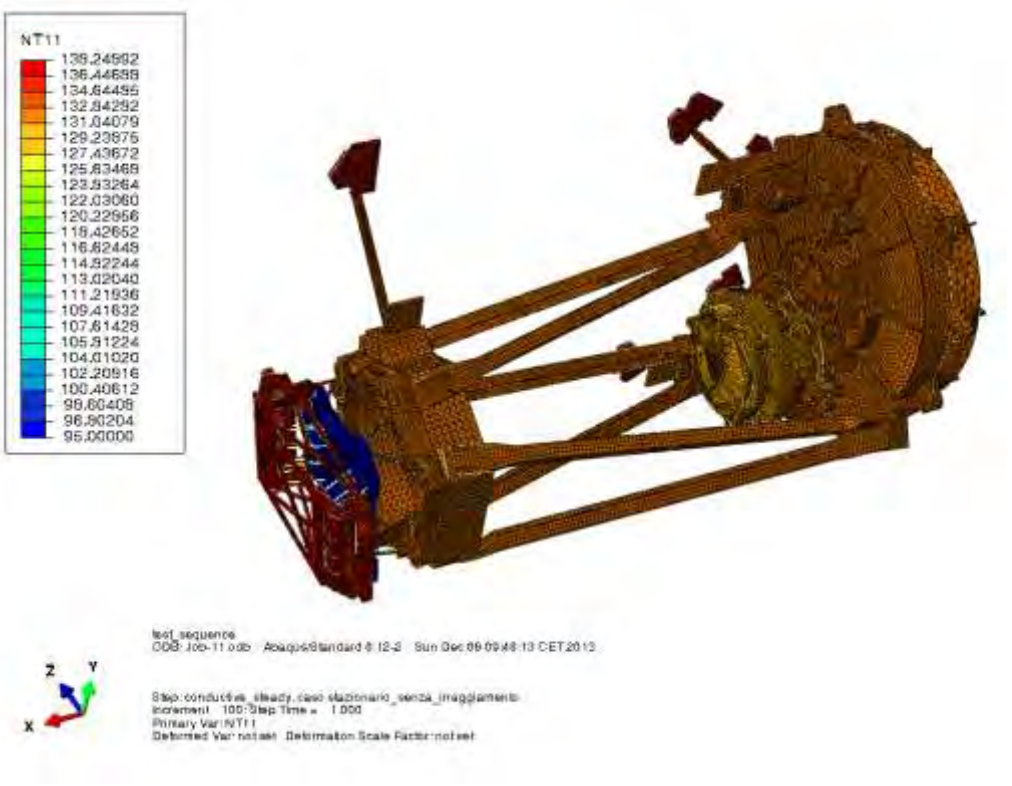

Figure 13-6 Full Assembly temperature distribution [K]

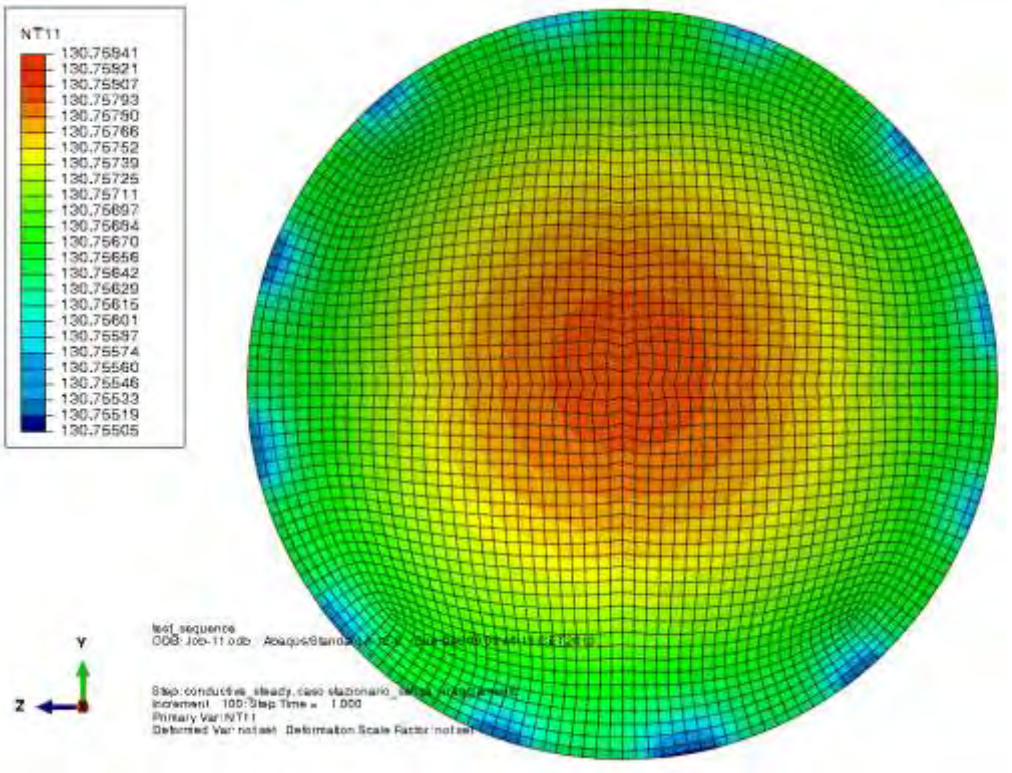

Figure 13-7 CaLA Lens 1 back temperature distribution [K]

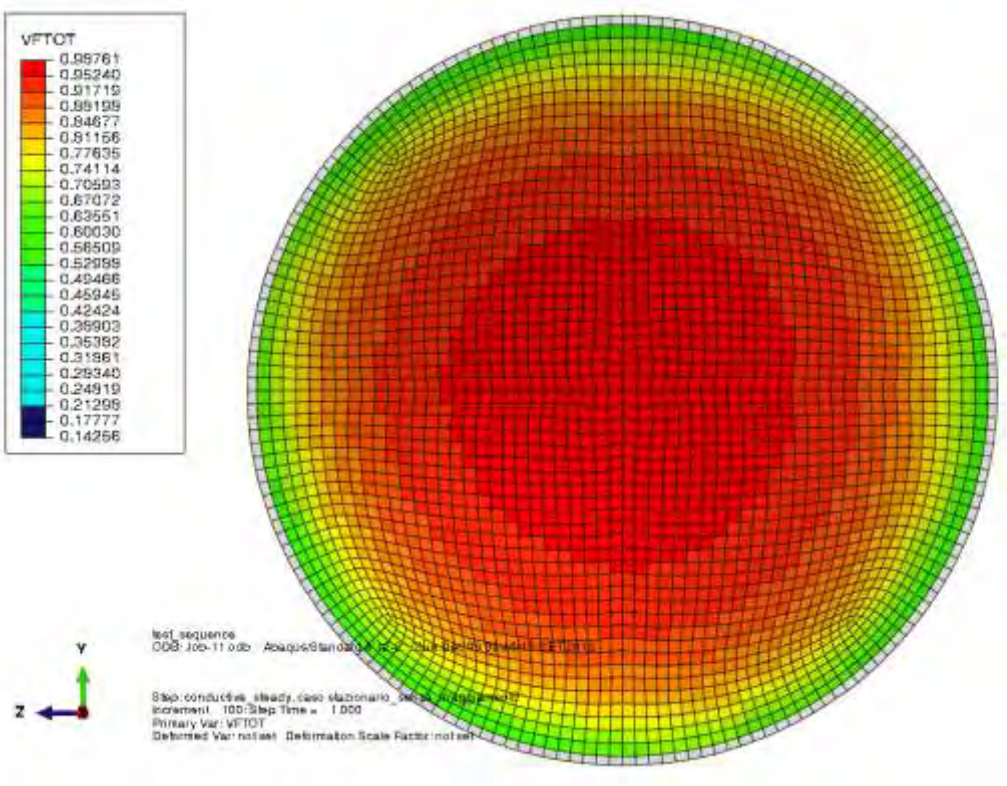

Figure 13-8 CaLA Lens 1 back view factor

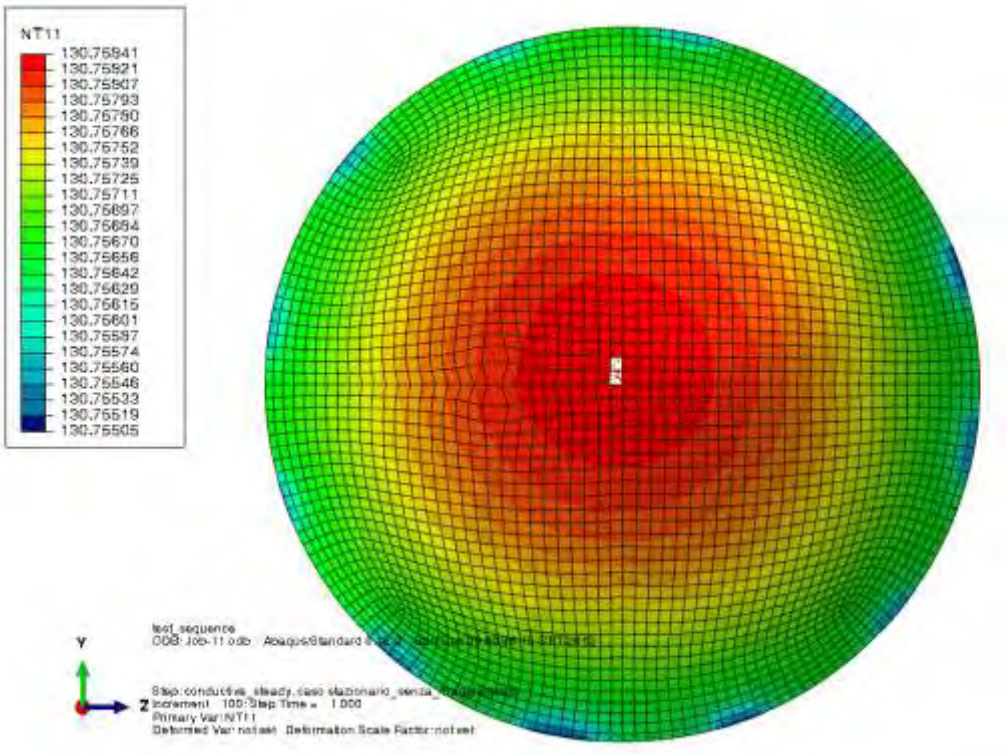

Figure 13-9 CaLA Lens 1 front temperature distribution [K]

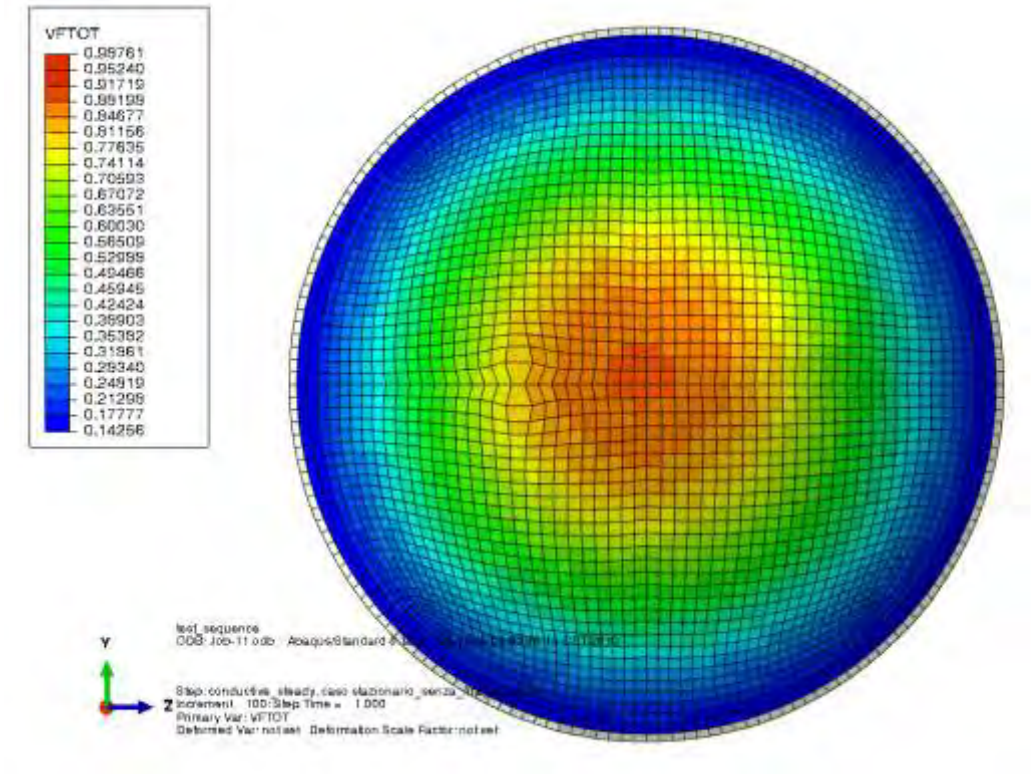

Figure 13-10 CaLA Lens 1 front view factor

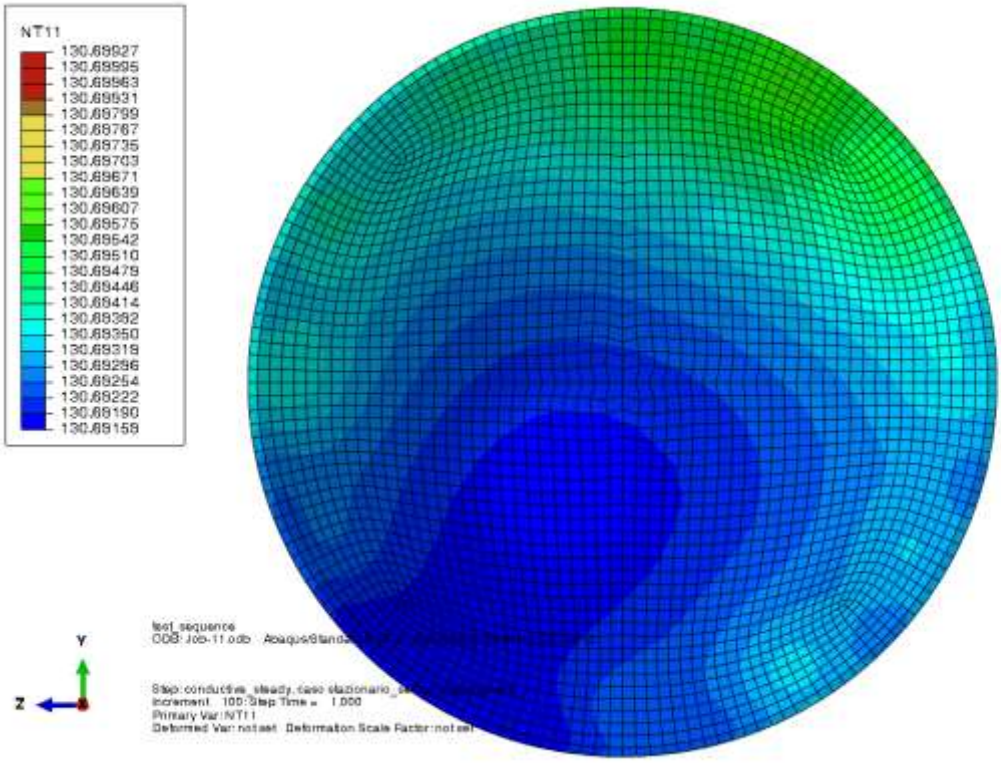

Figure 13-11 CaLA Lens 2 back temperature distribution [K]

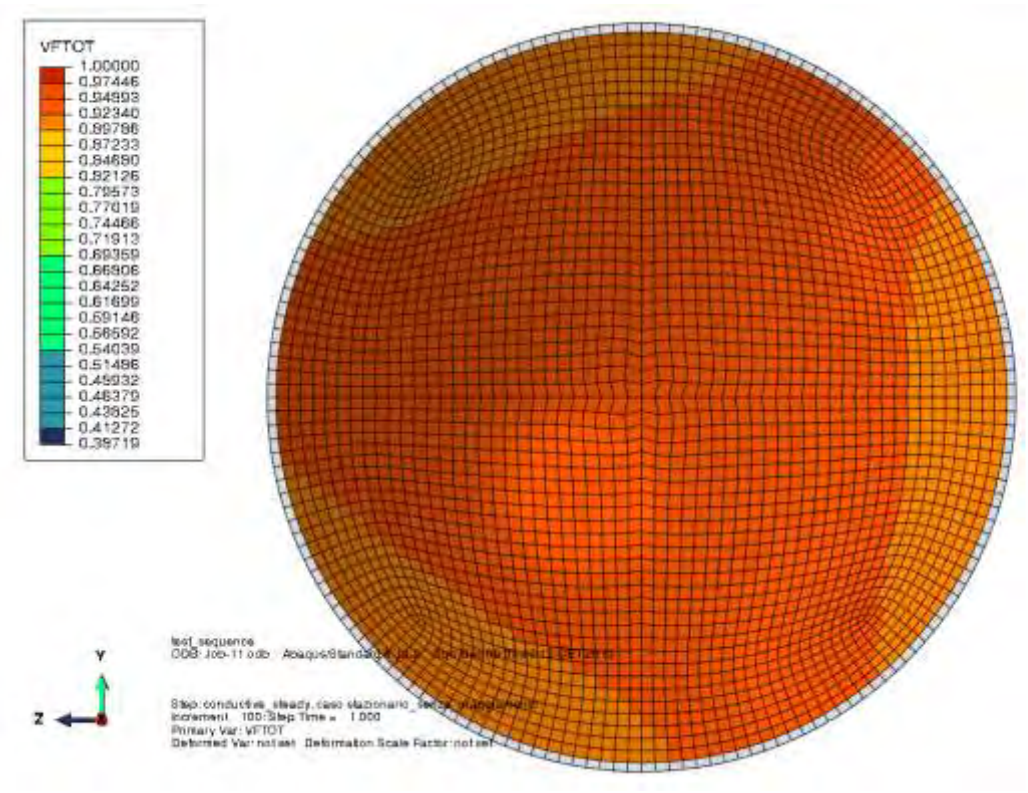

Figure 13-12 CaLA Lens 2 back view factor

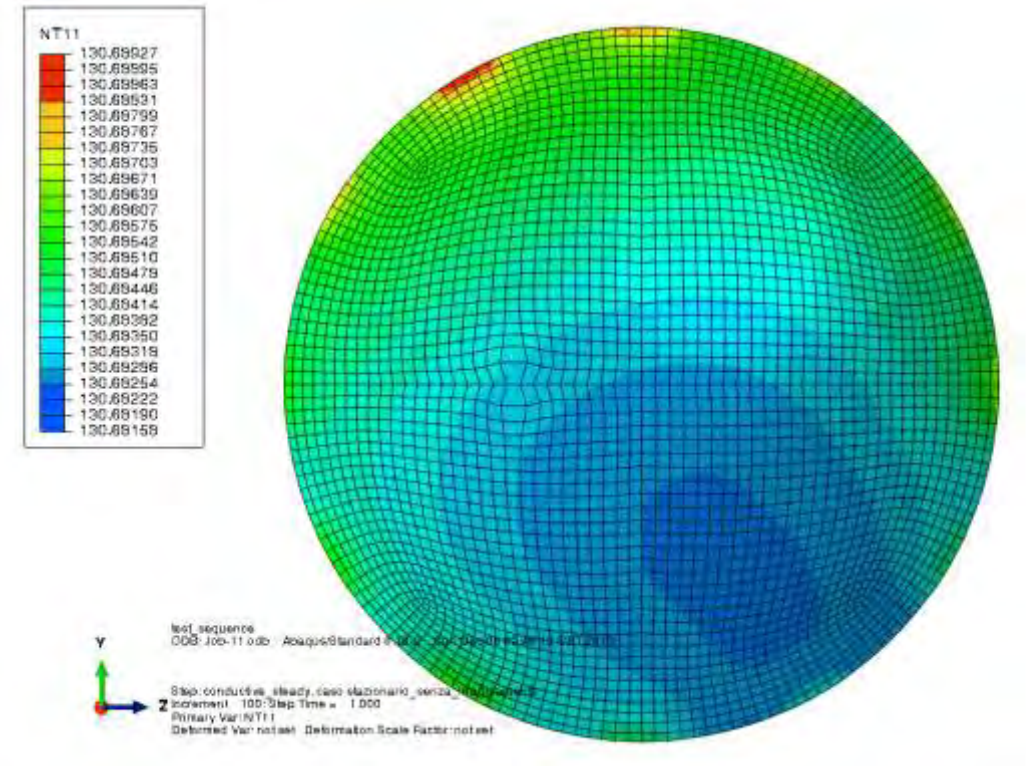

Figure 13-13 CaLA Lens 2 front temperature distribution [K]

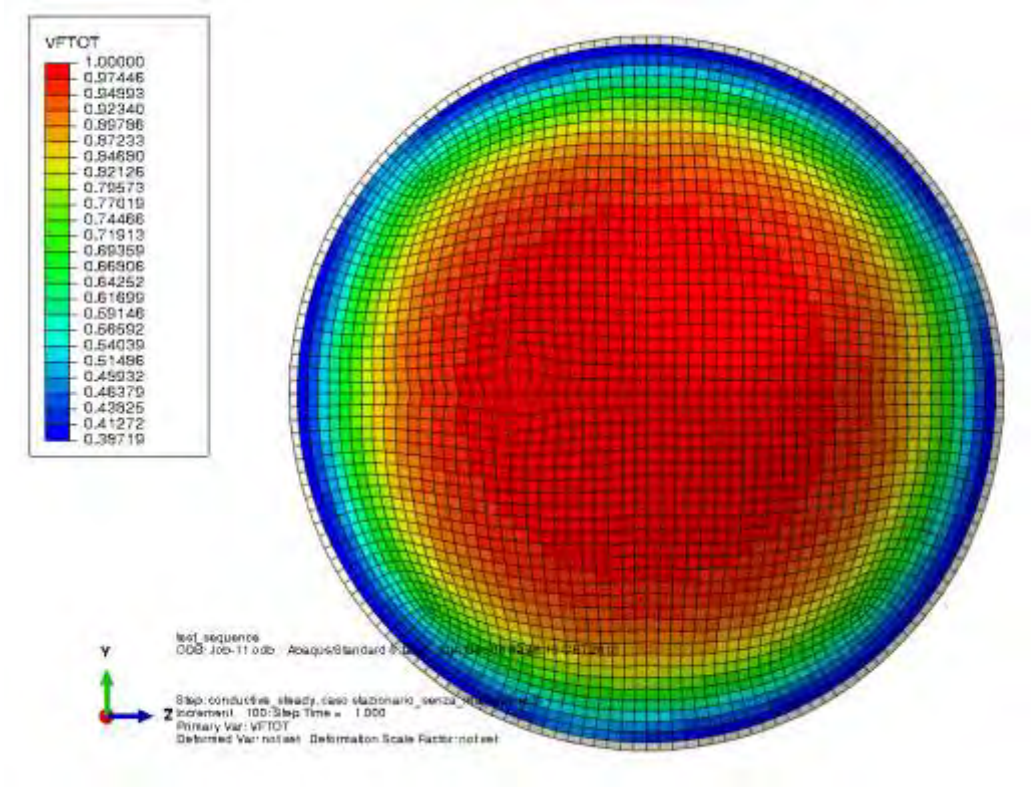

Figure 13-14 CaLA Lens 2 front view factor

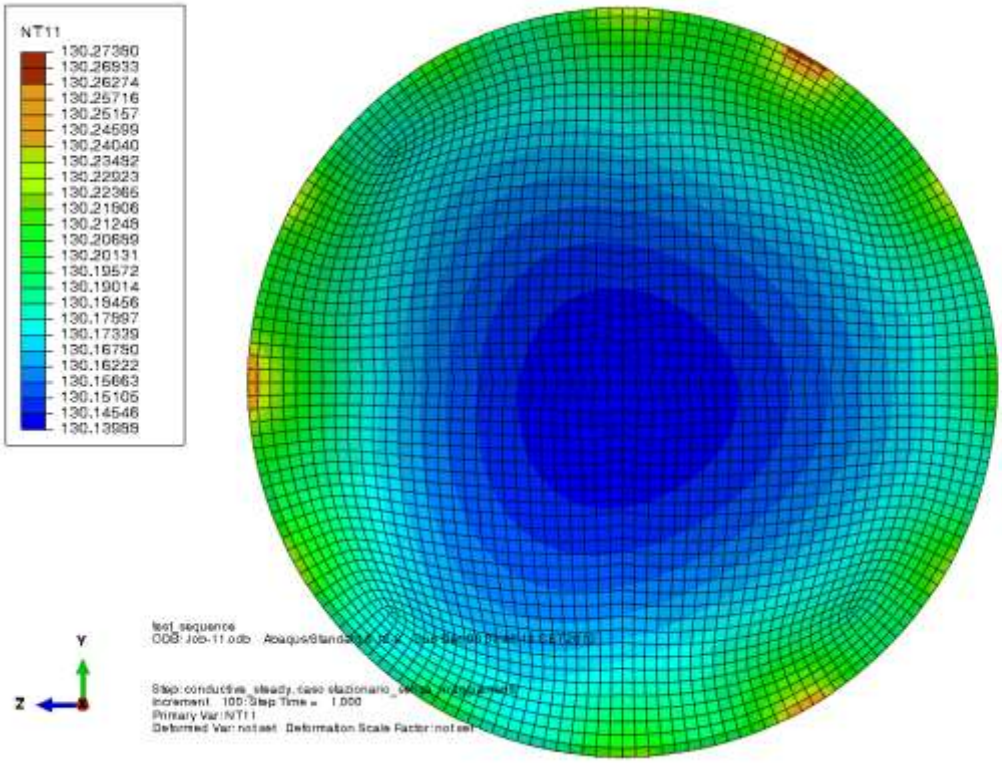

Figure 13-15 CaLA Lens 3 back temperature distribution [K]

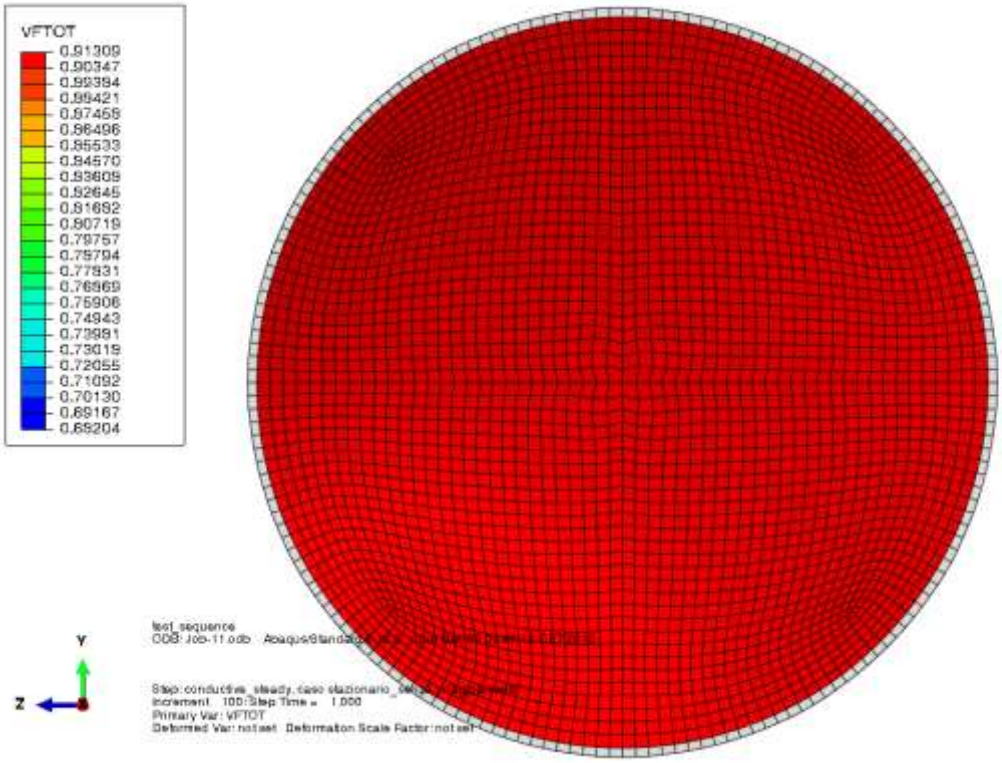

Figure 13-16 CaLA Lens 3 back view factor

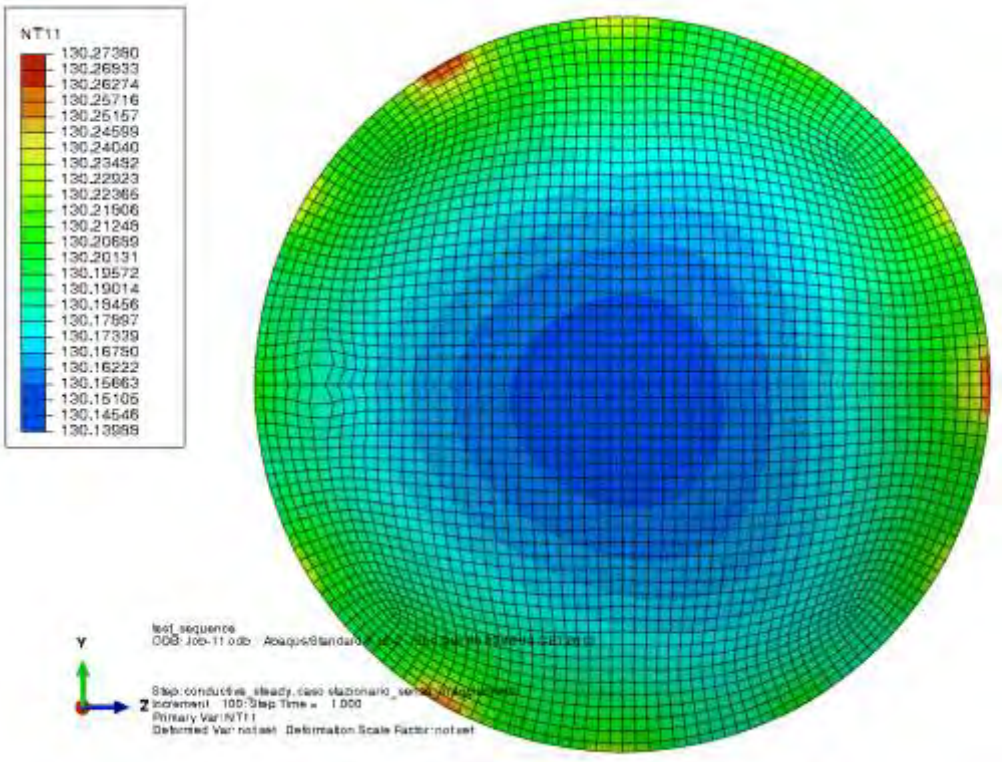

Figure 13-17 CaLA Lens 3 front temperature distribution [K]

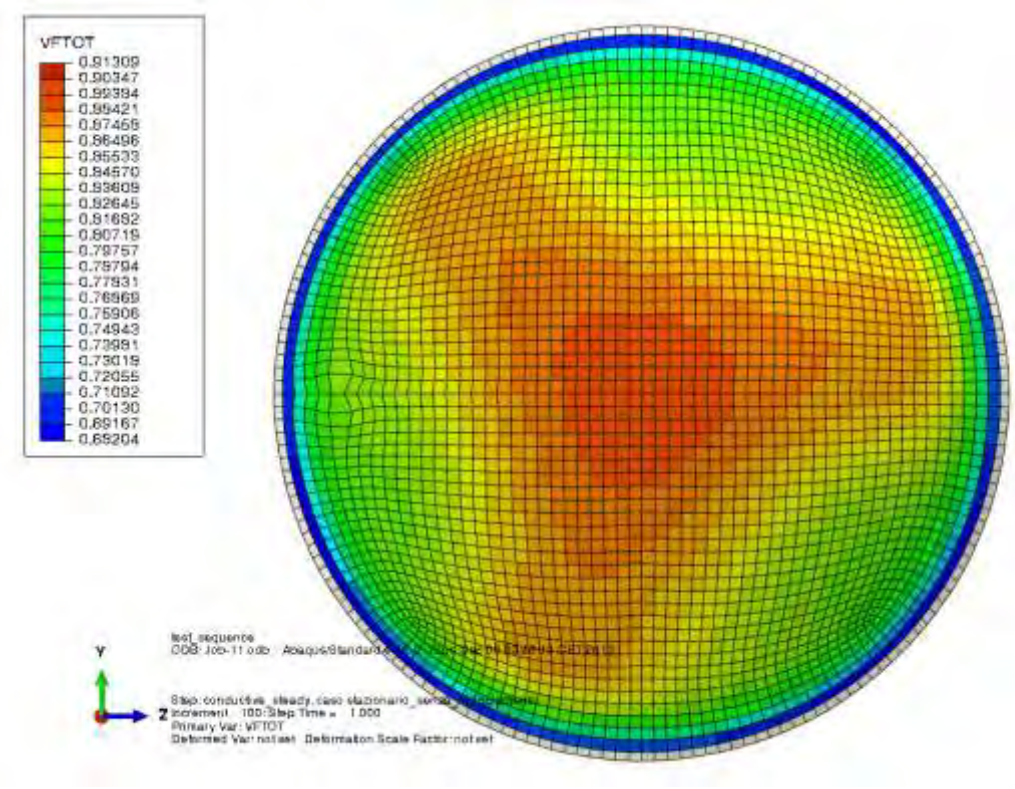

Figure 13-18 CaLA Lens 3 front view factor

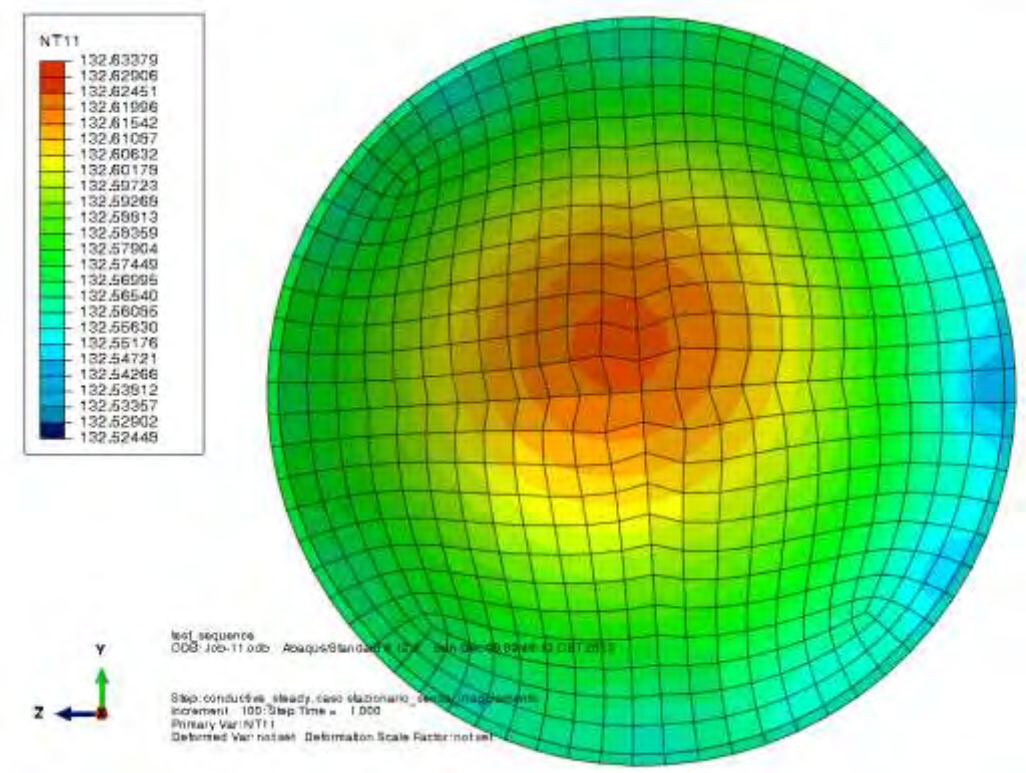

Figure 13-19 CoLA Lens back temperature distribution [K]

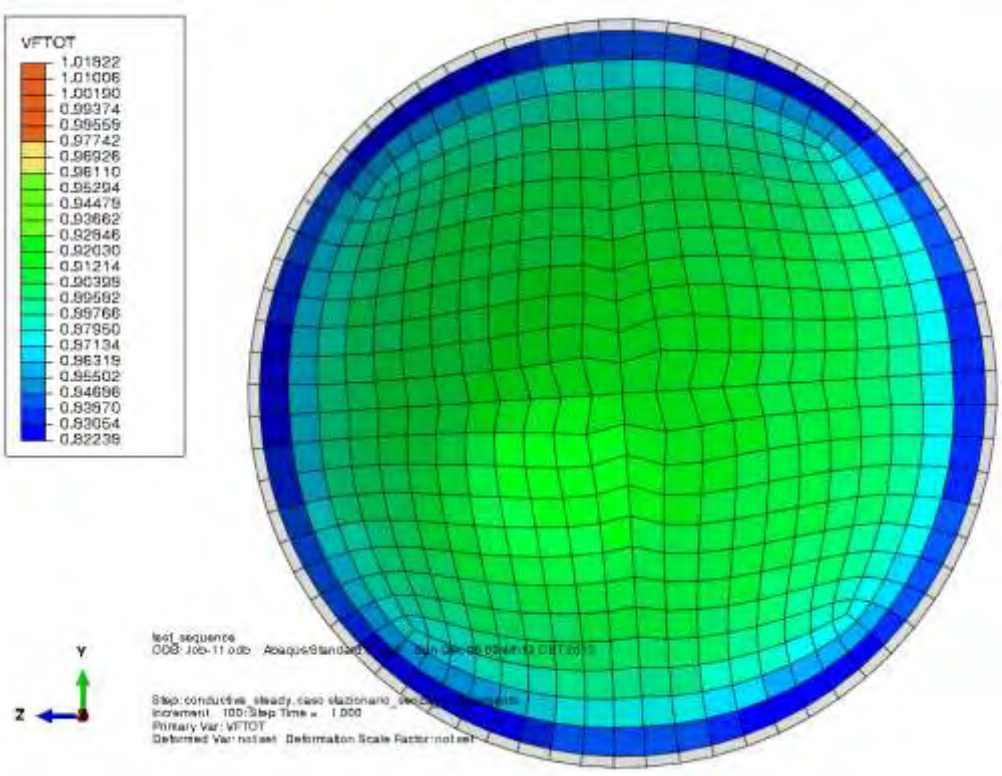

Figure 13-20 CoLA Lens back view factor

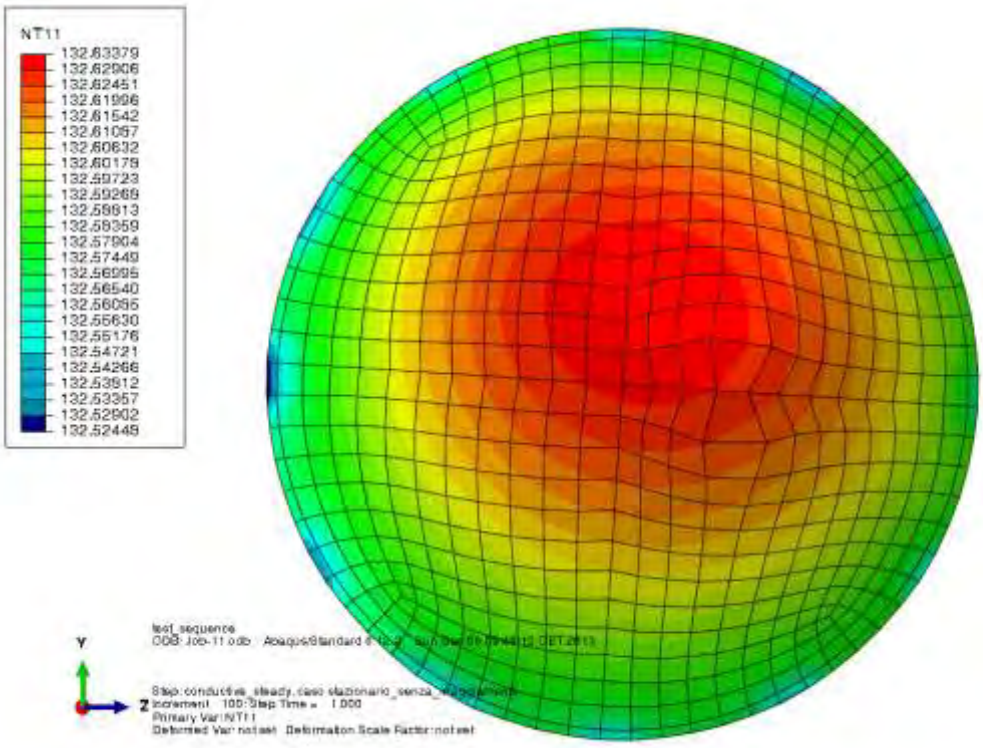

Figure 13-21 CoLA Lens front temperature distribution [K]

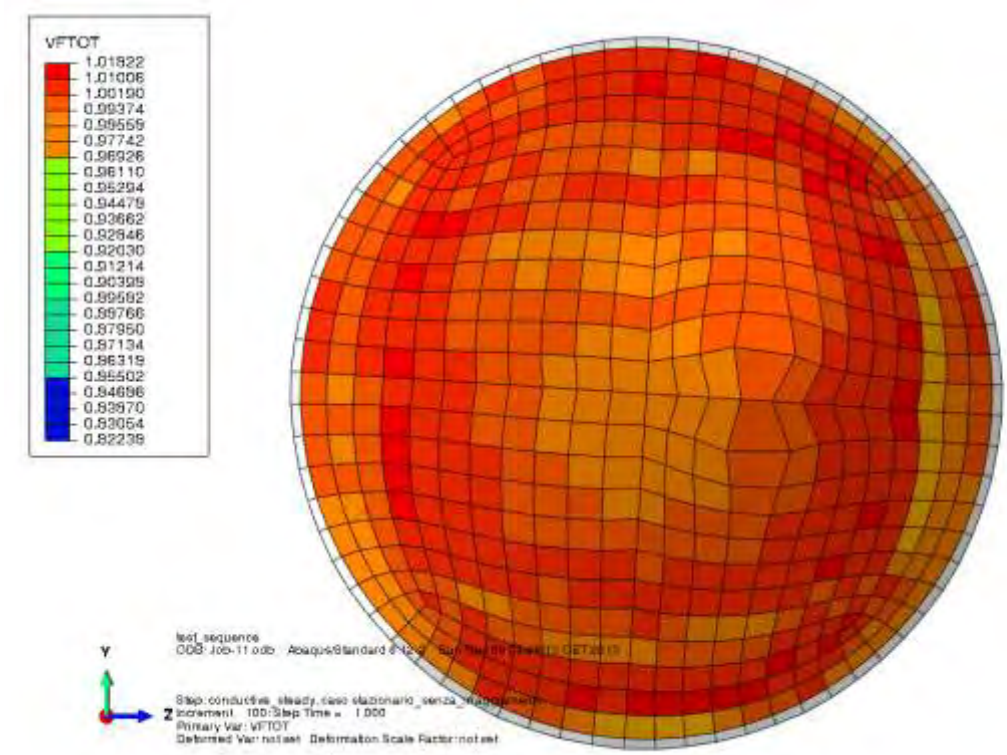

Figure 13-22 CoLA Lens front view factor

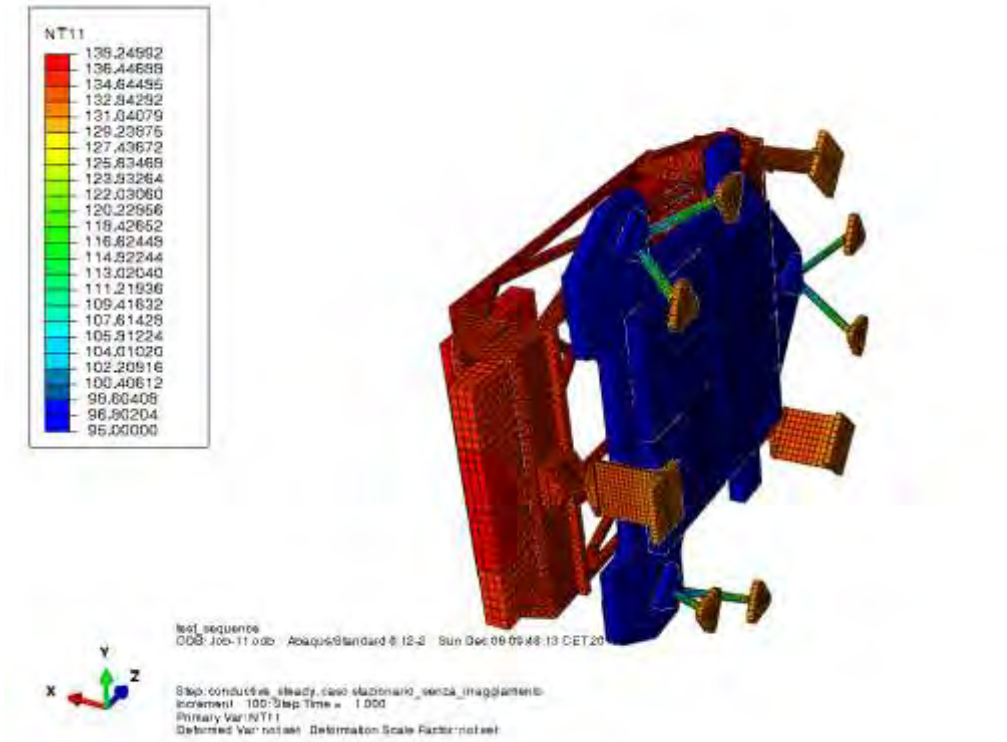

Figure 13-23 Sidecars and detectors assembly [K]

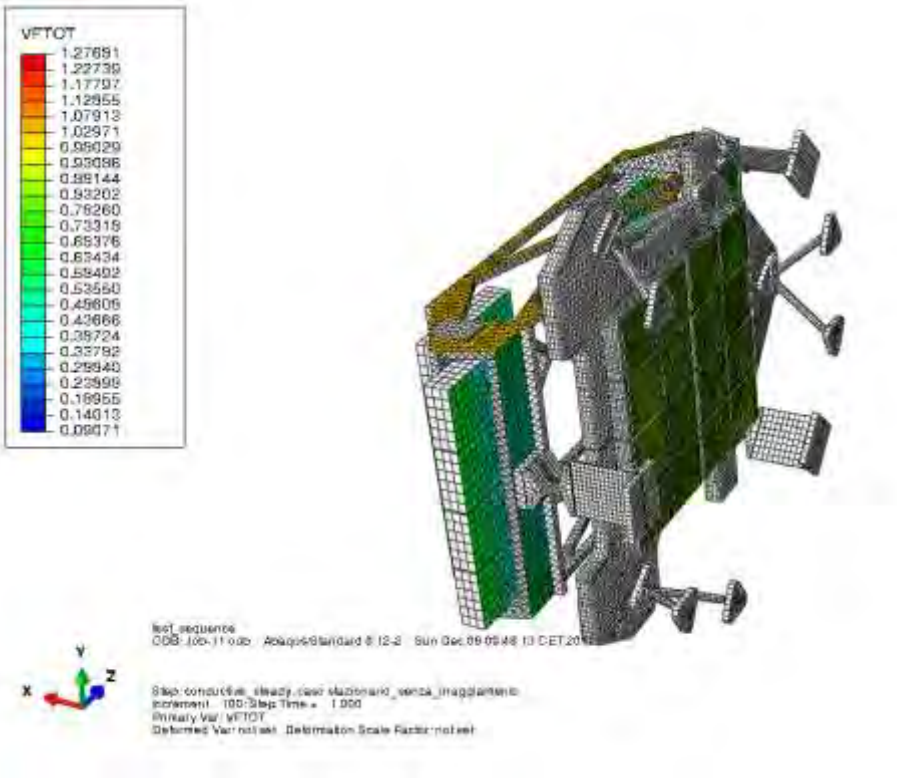

Figure 13-24 Sidecars and Detectors view factor

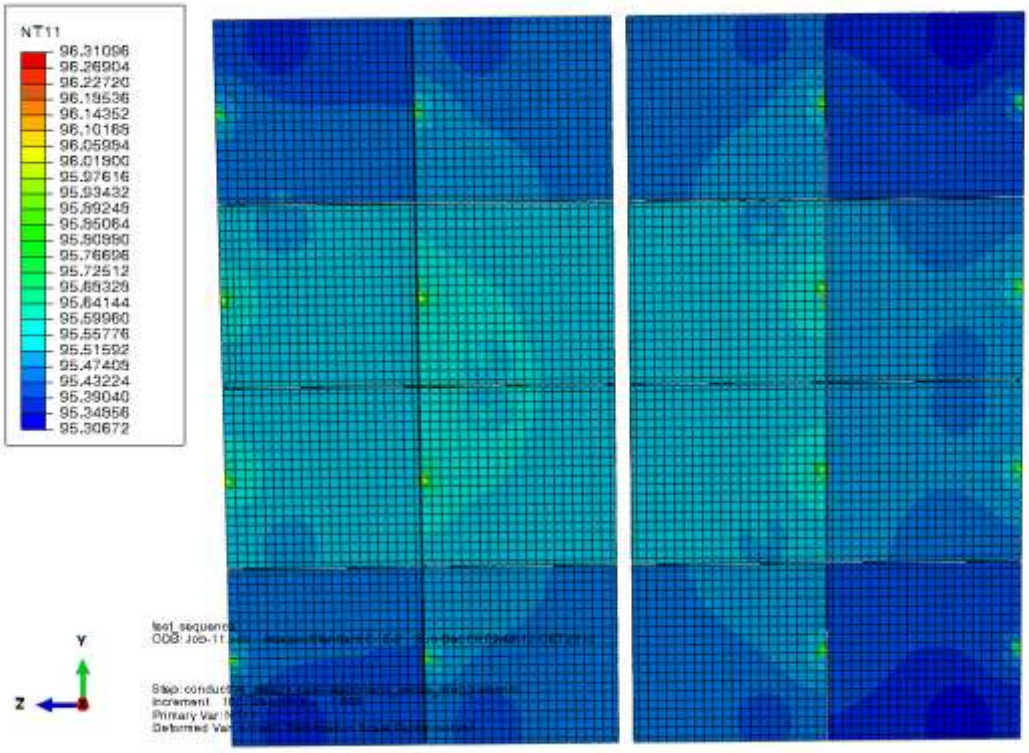

Figure 13-25 detectors back temperature distribution [K]

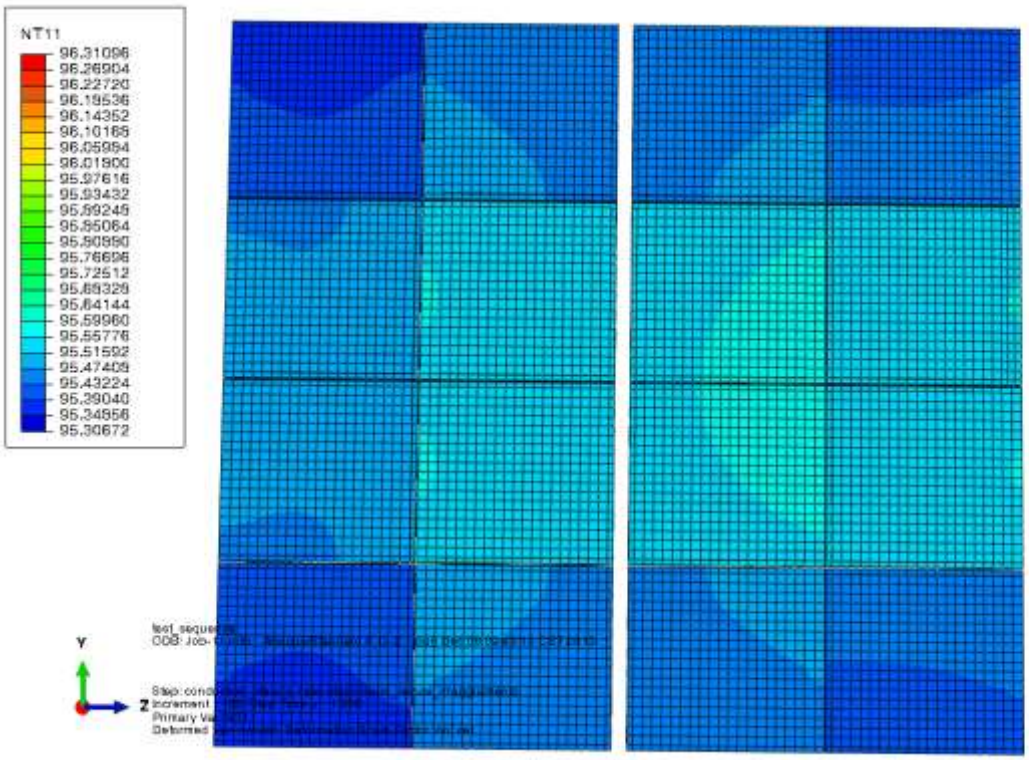

Figure 13-26 Detectors front temperature distribution [K]

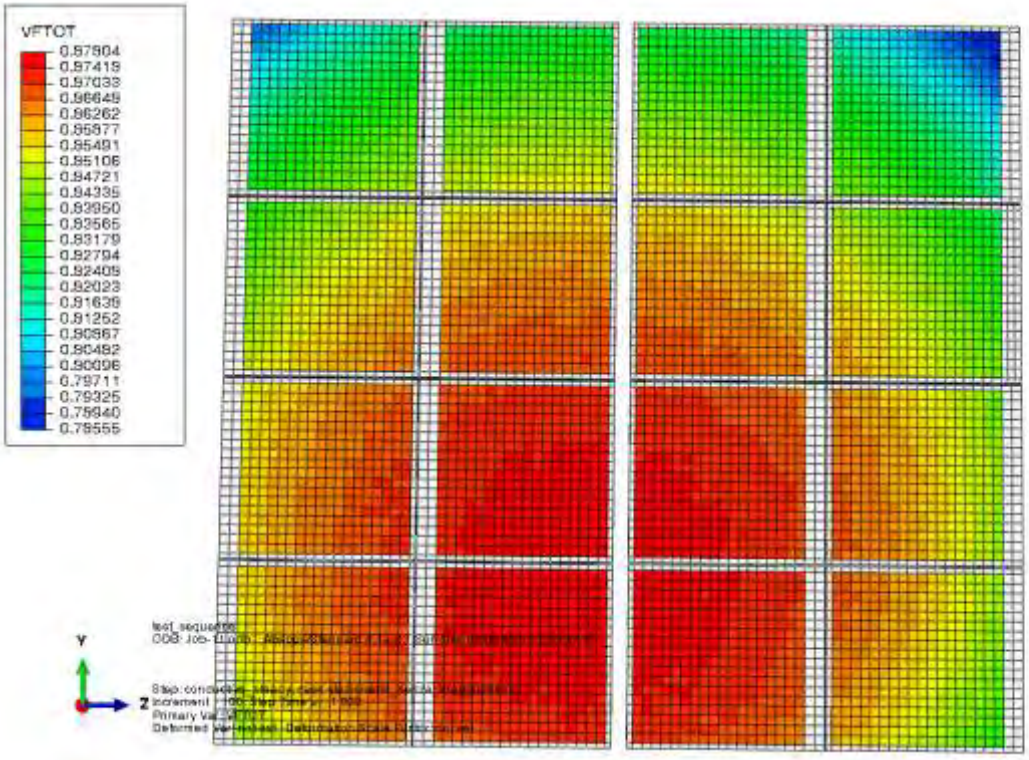

Figure 13-27 Detectors view factor

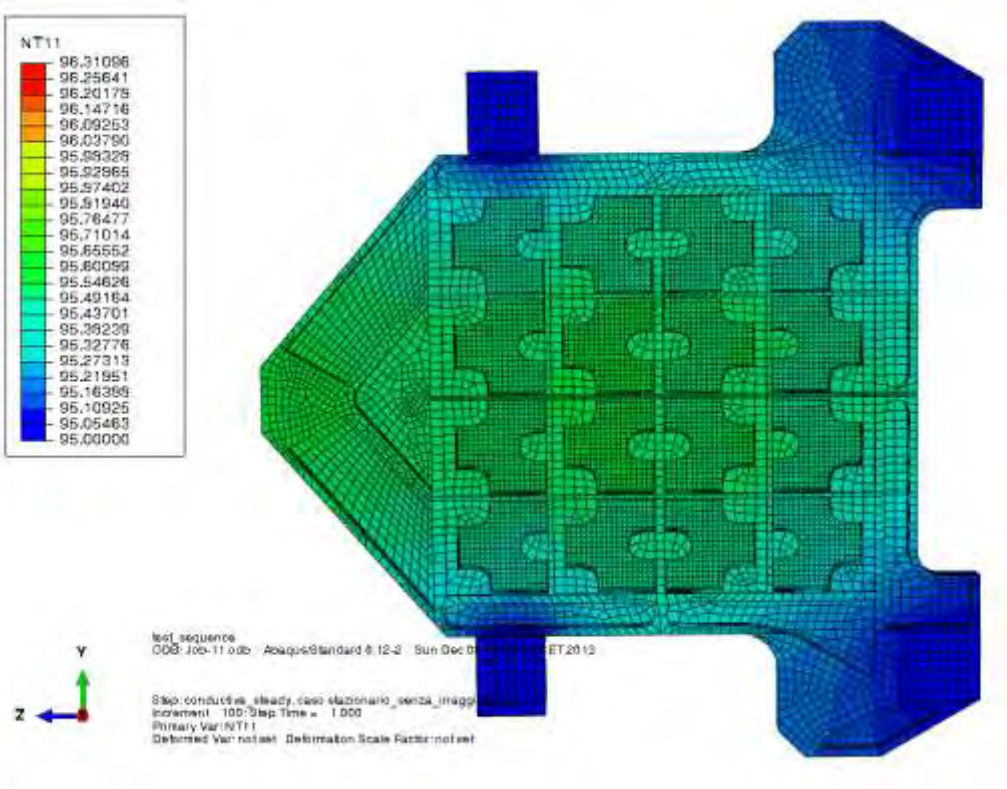

Figure 13-28 Detectors and CSS back temperature distribution [K]

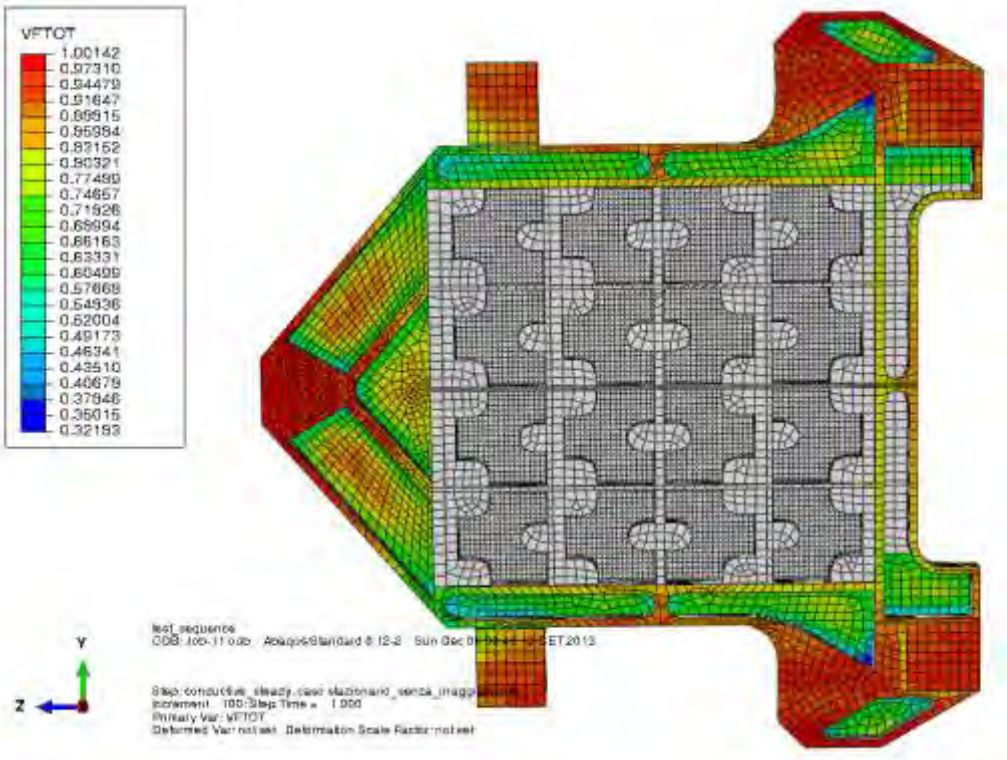

Figure 13-29 Detectors and CSS back view factor

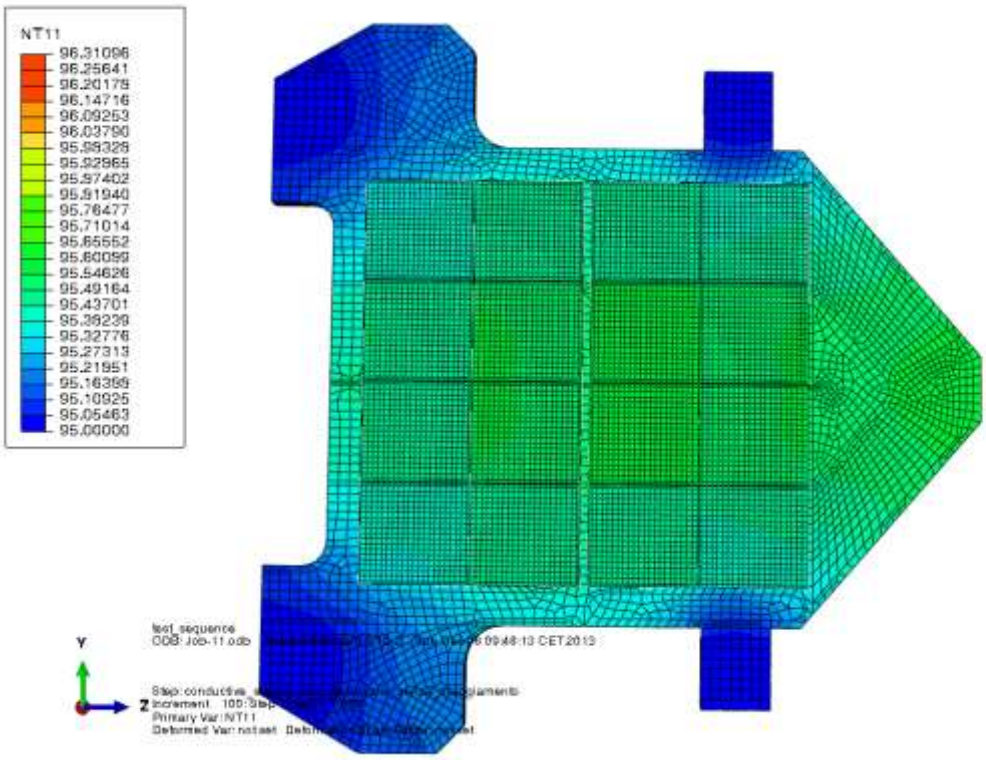

Figure 13-30 Detectors and CSS front temperature distribution [K]

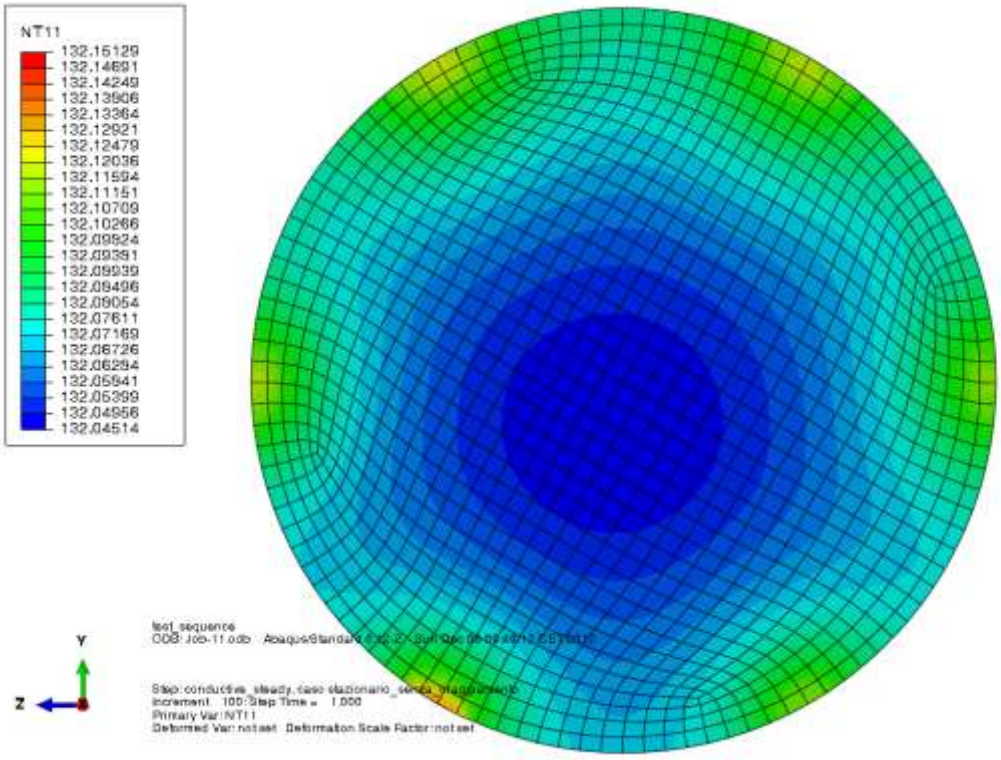

Figure 13-31 Filter front temperature distribution [K]

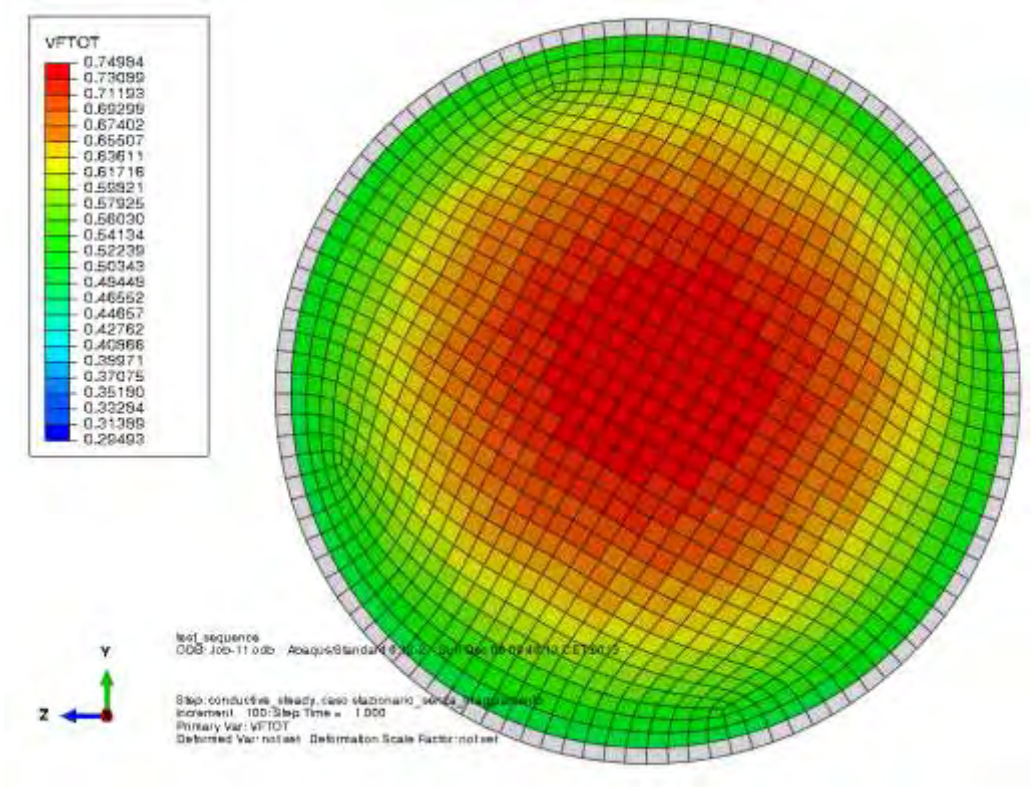

Figure 13-32 Filter front view factor

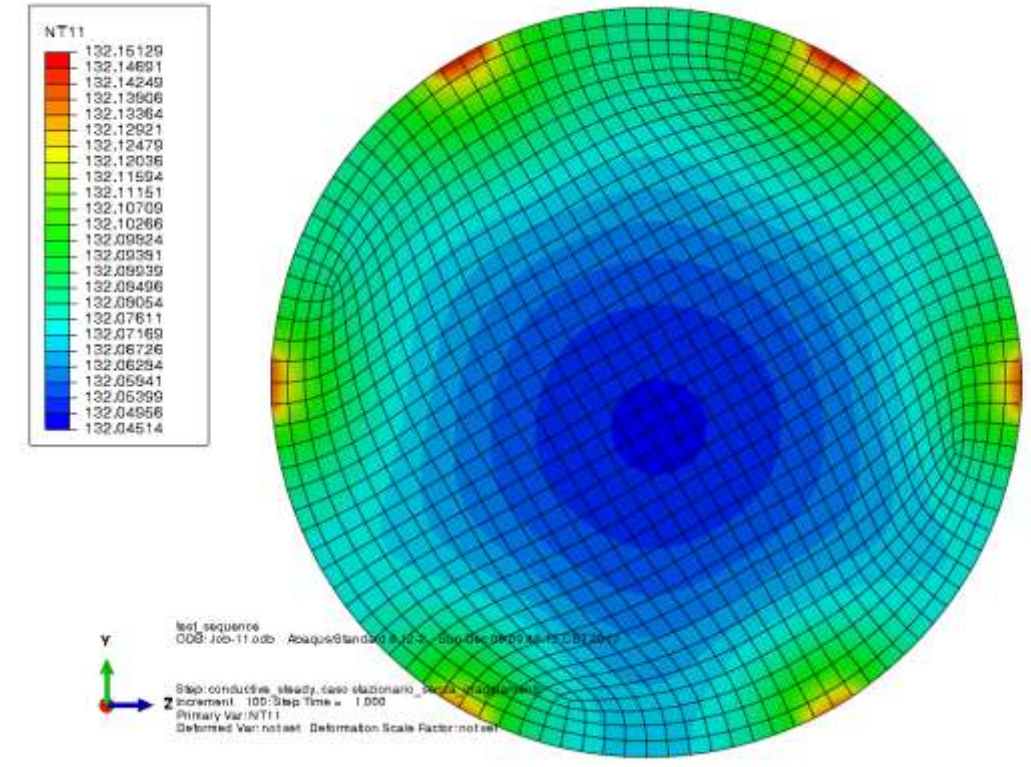

Figure 13-33 Filter back temperature distribution [K]

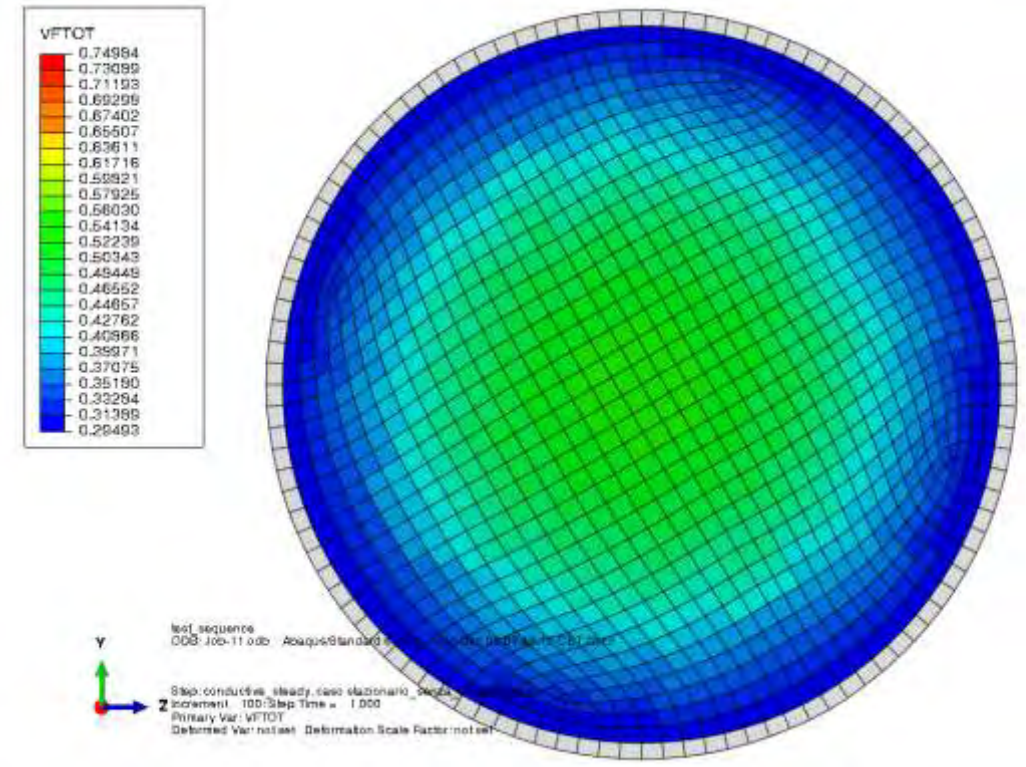

Figure 13-34 Filter back view factor

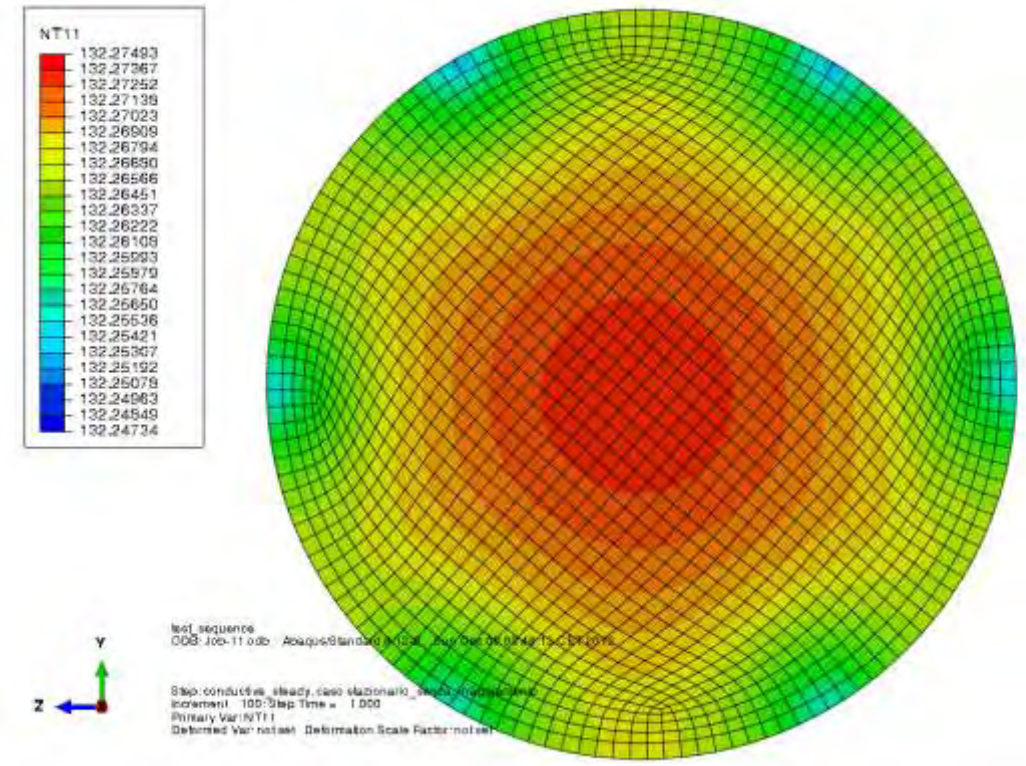

Figure 13-35 Grism front temperature distribution [K]

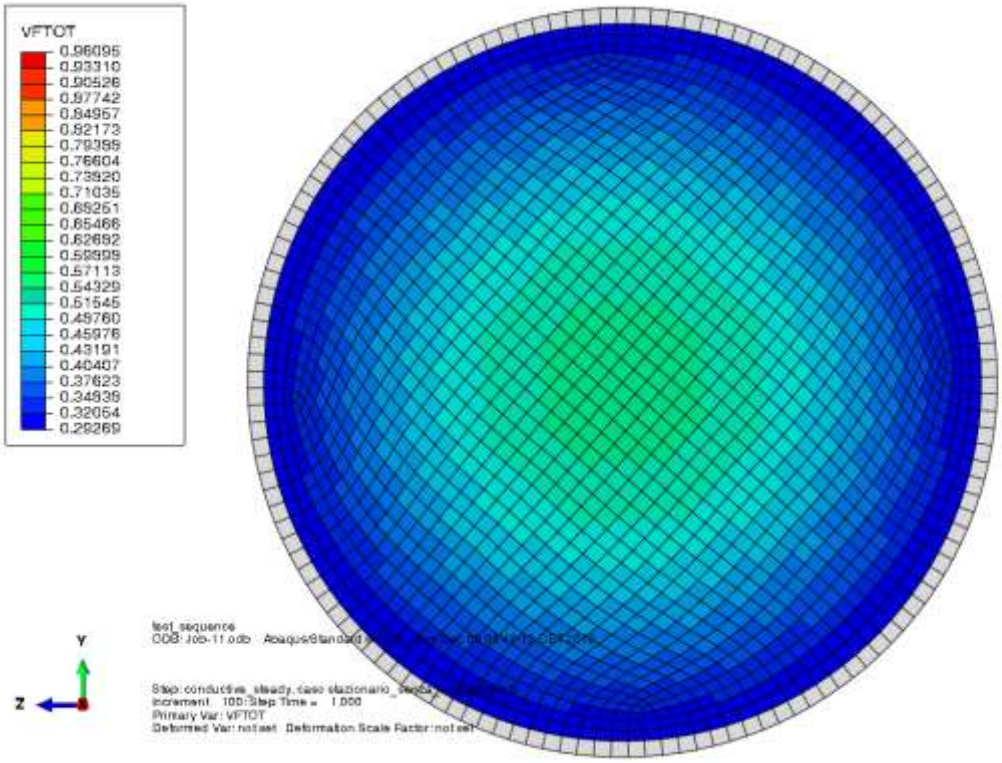

Figure 13-36 Grism front view factor

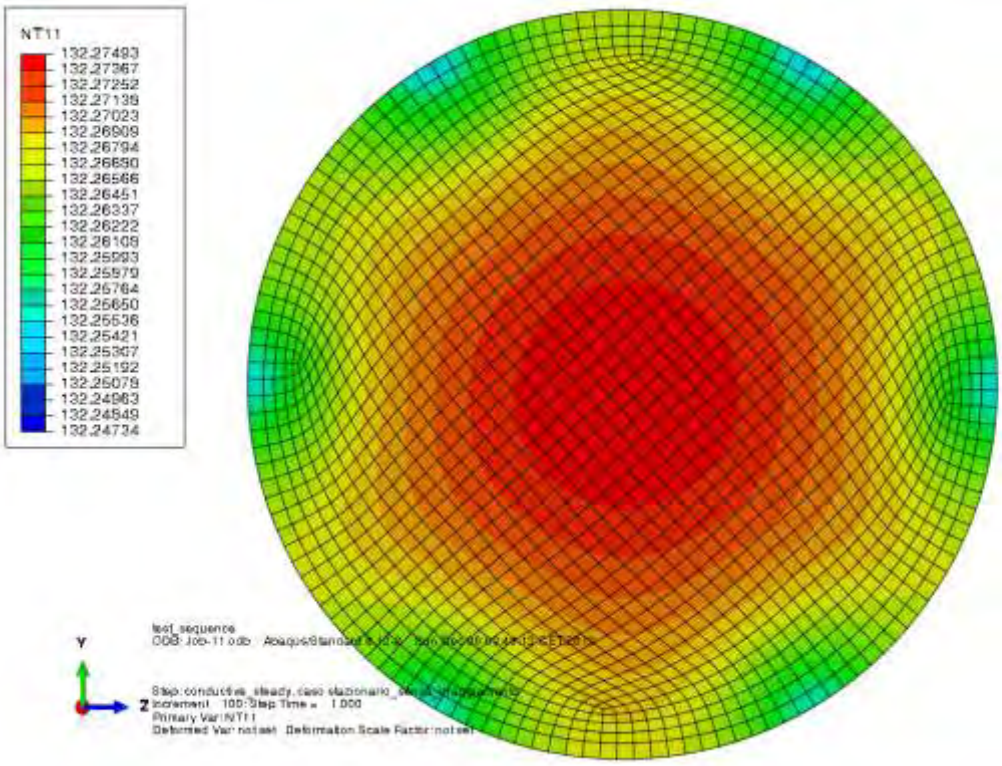

Figure 13-37 Grism back temperature distribution [K]

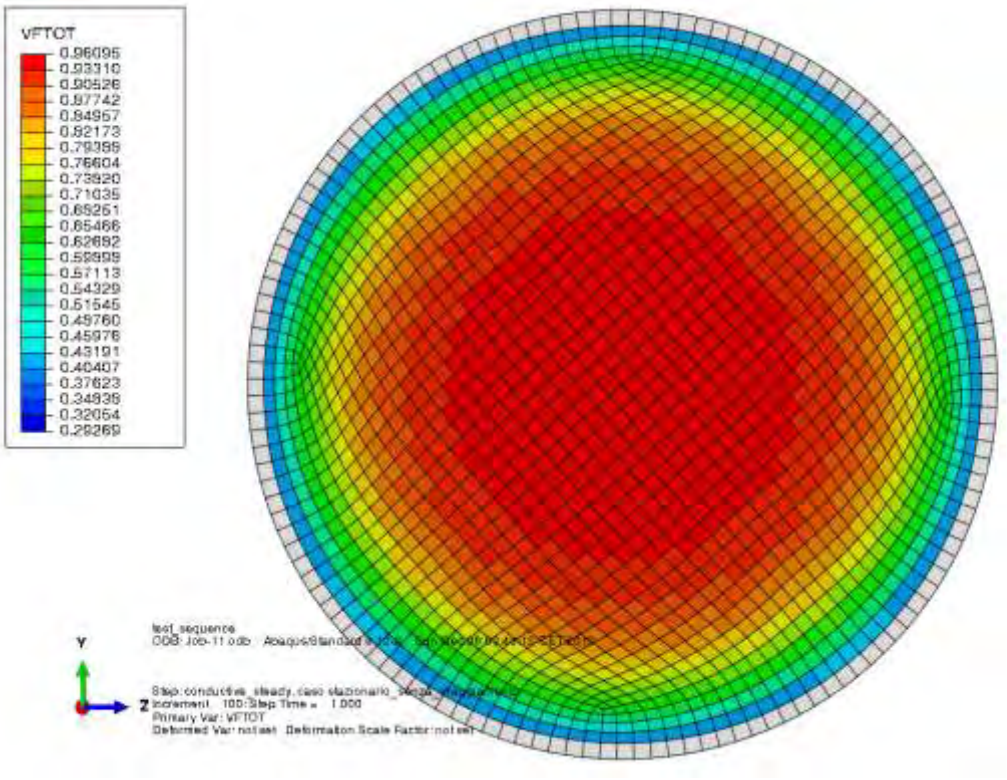

Figure 13-38 Grism back view factor

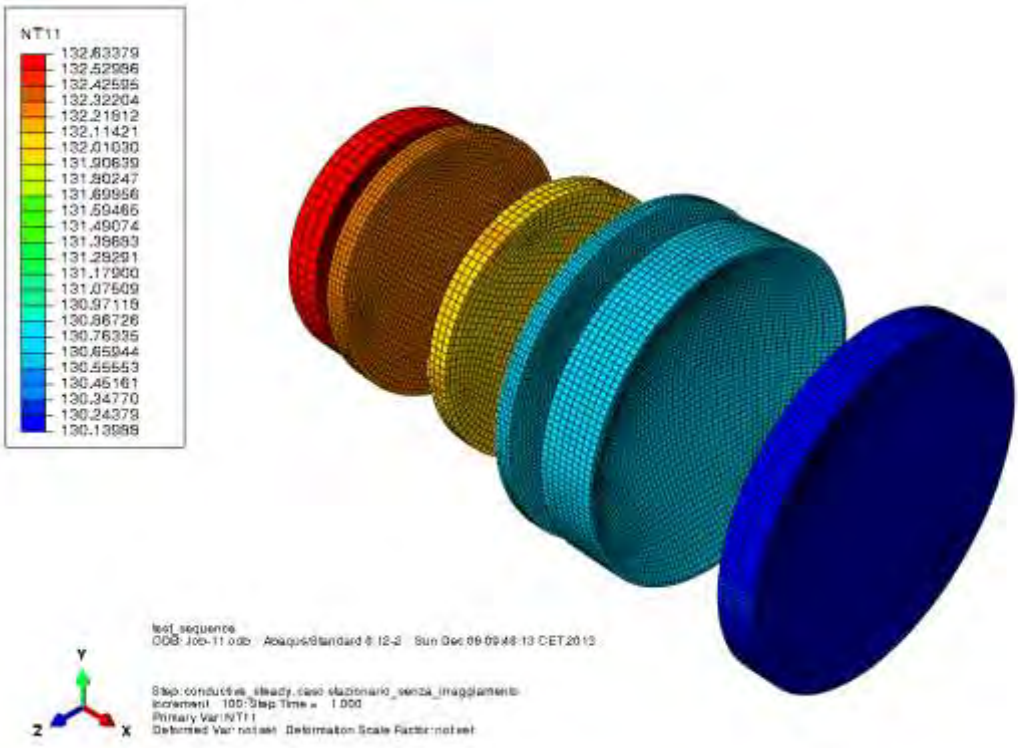

Figure 13-39 NI-OA lenses temperature distribution [K]

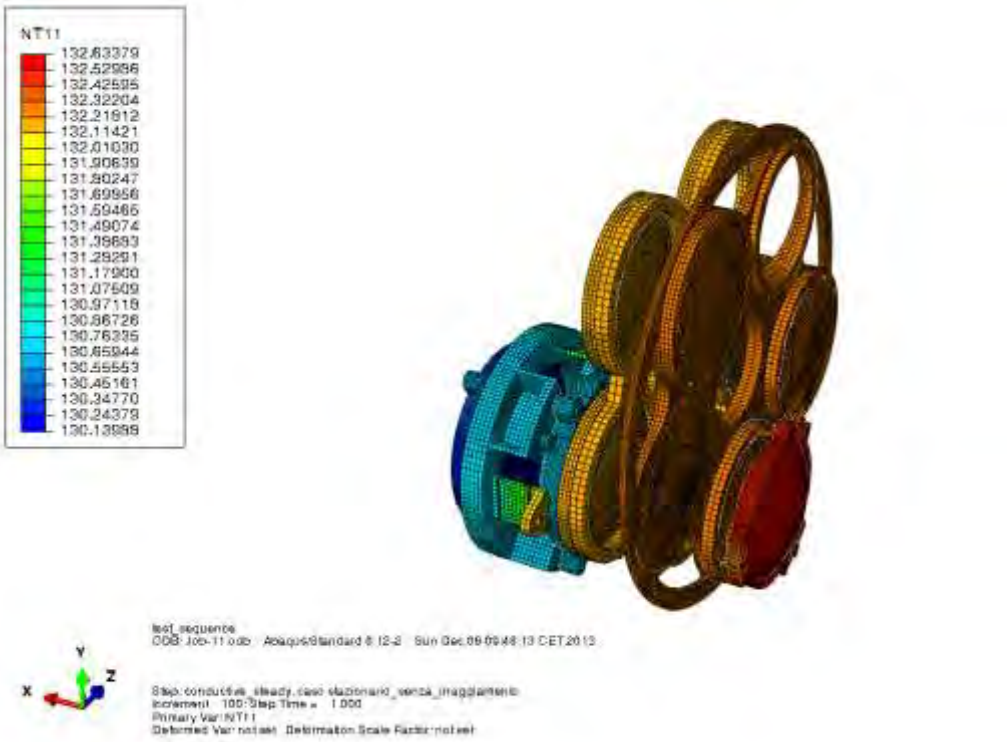

Figure 13-40 Wheels and lenses temperature distribution [K]

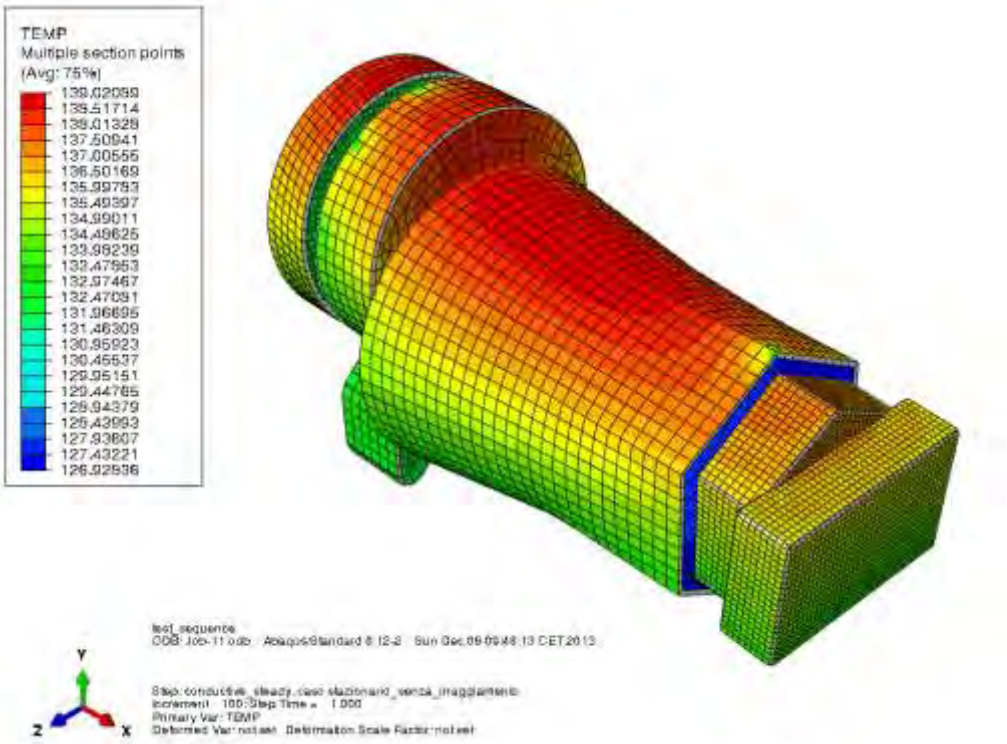

Figure 13-41 MLI Shields temperature distribution [K]

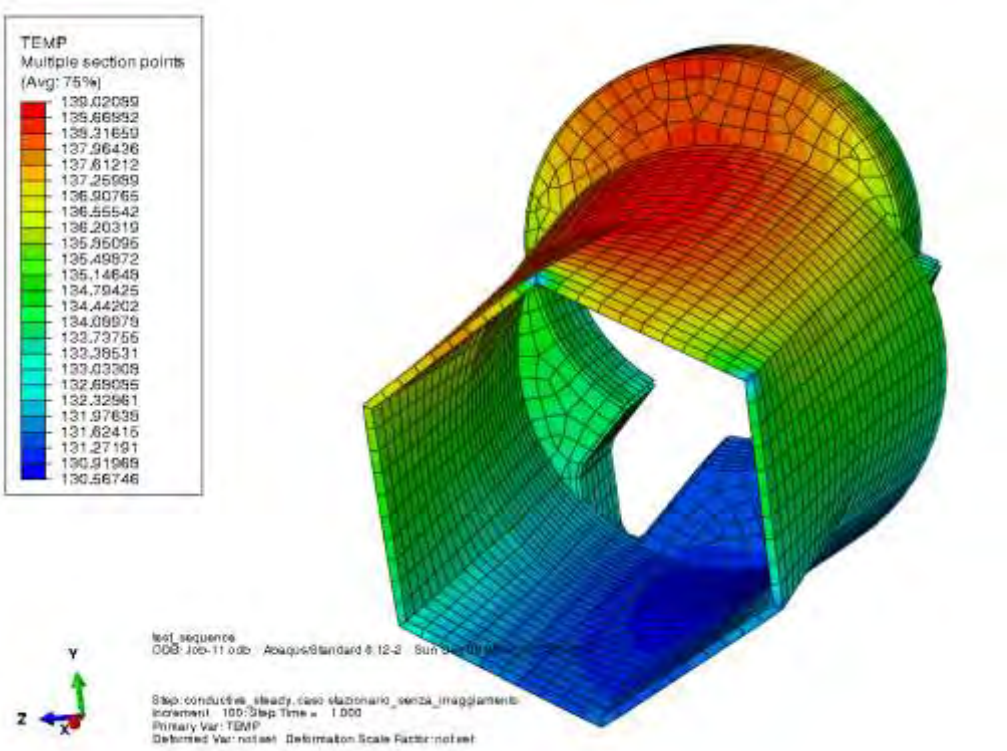

Figure 13-42 Main MLI Shield external temperature distribution [K]

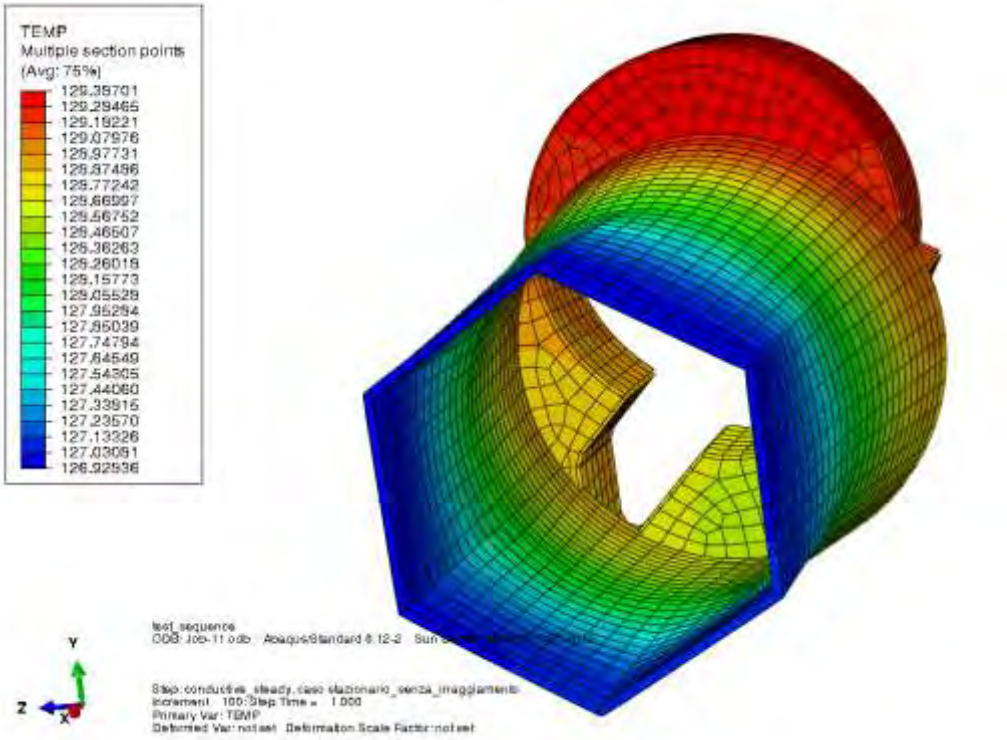

Figure 13-43 Main MLI Shield internal temperature distribution [K]

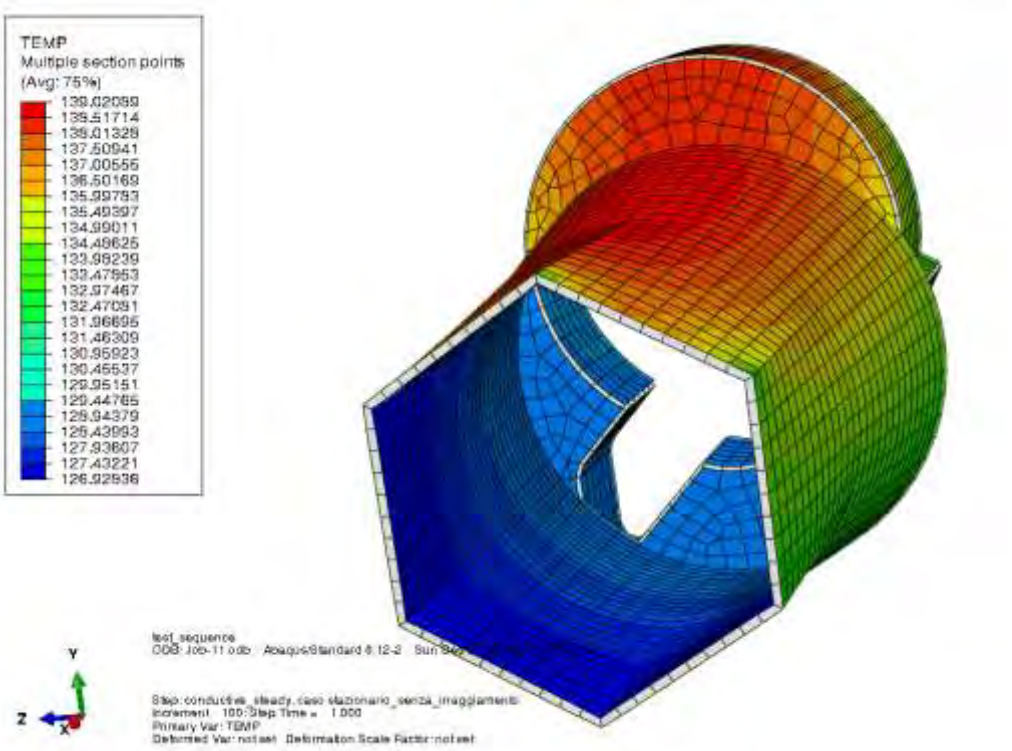

Figure 13-44 Main MLI Shield internal and external temperature distribution [K]

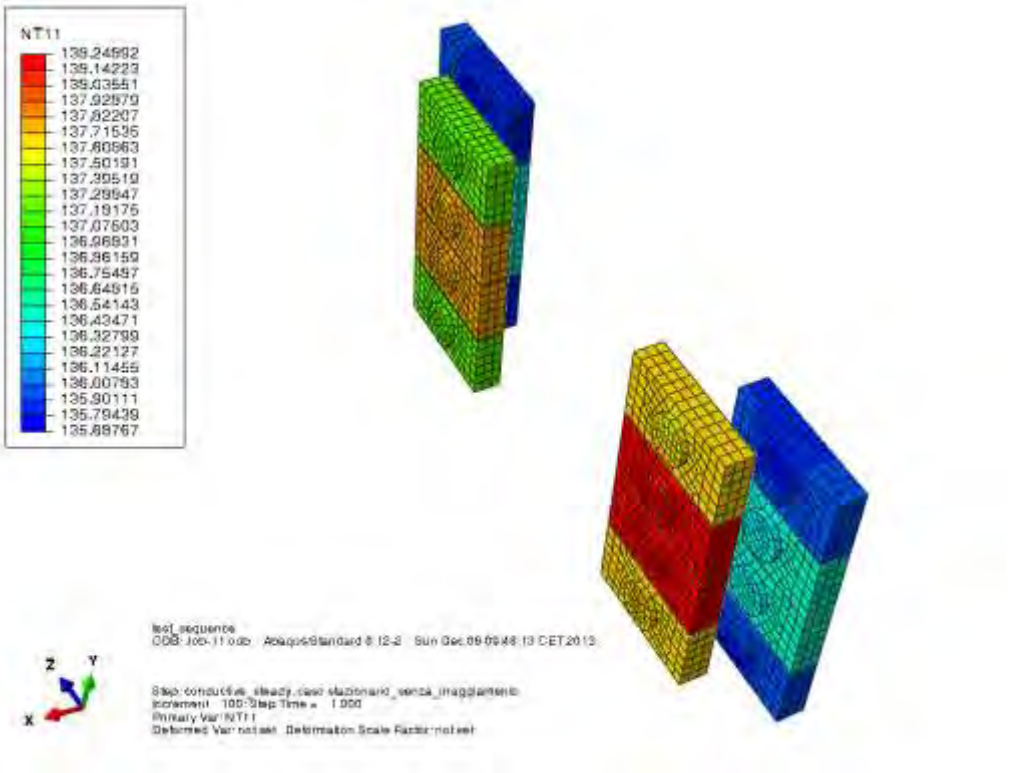

Figure 13-45 Sidecars temperature distribution [K]

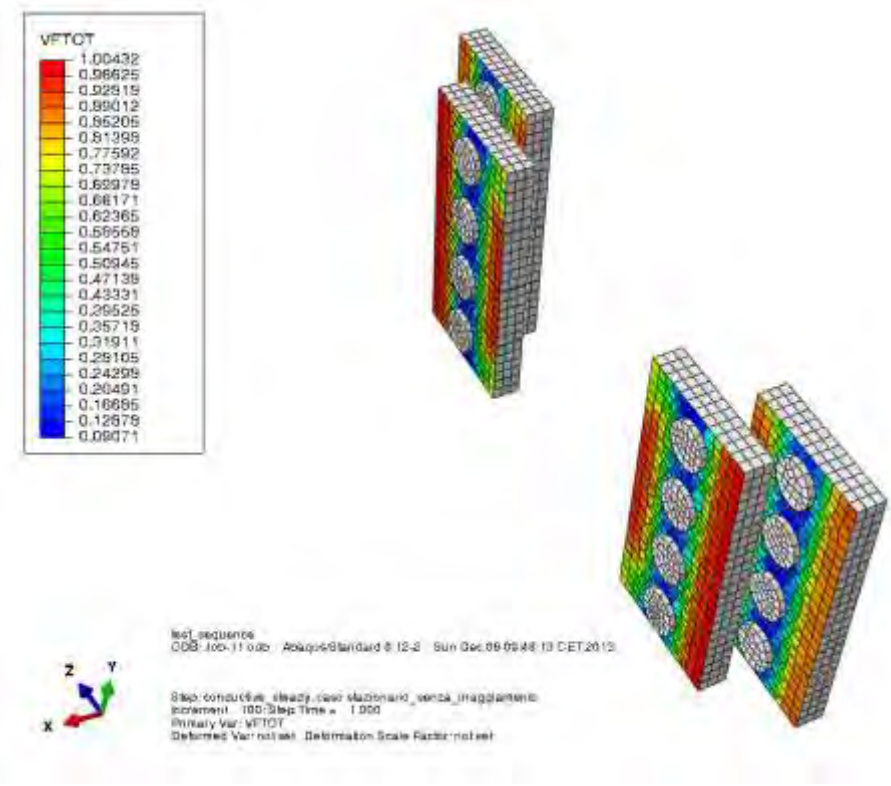

Figure 13-46 Sidecars view factors

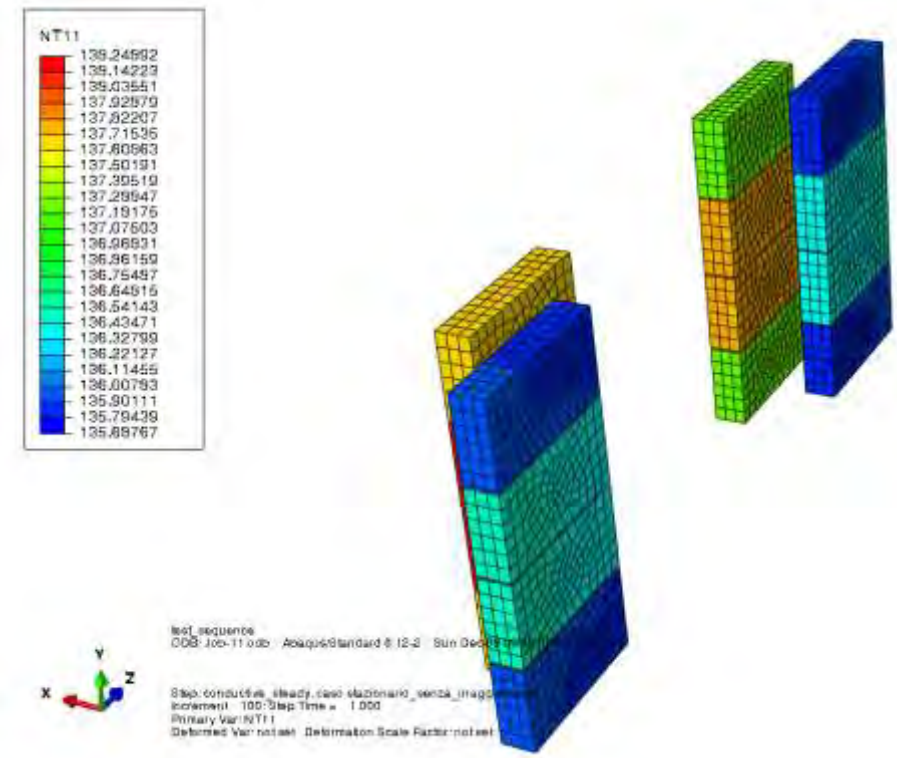

Figure 13-47 Sidecars temperature distribution [K]

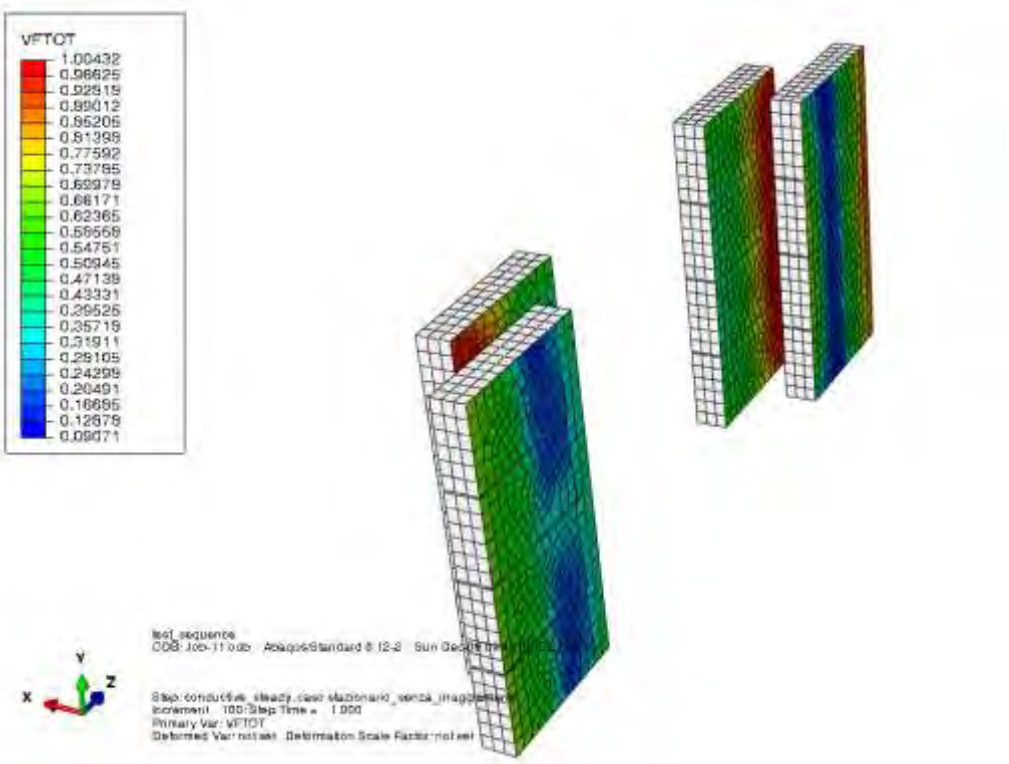

Figure 13-48 Sidecars view factors

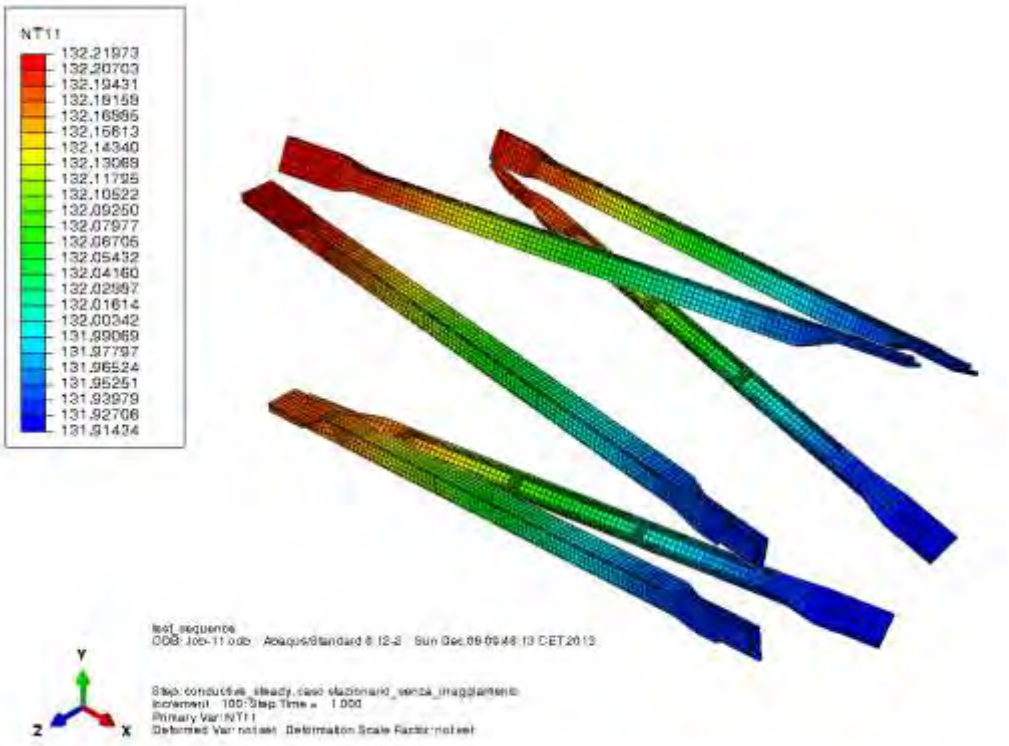

Figure 13-49 Structural beams temperature distribution [K]

13.1.1. JOB 11 temperature profiles on optical units

All the temperature profiles on the different units, calculated along the paths indicated in Chapter 11, are now shown in the next Figures. Captions and unit names are reported directly in the figures.

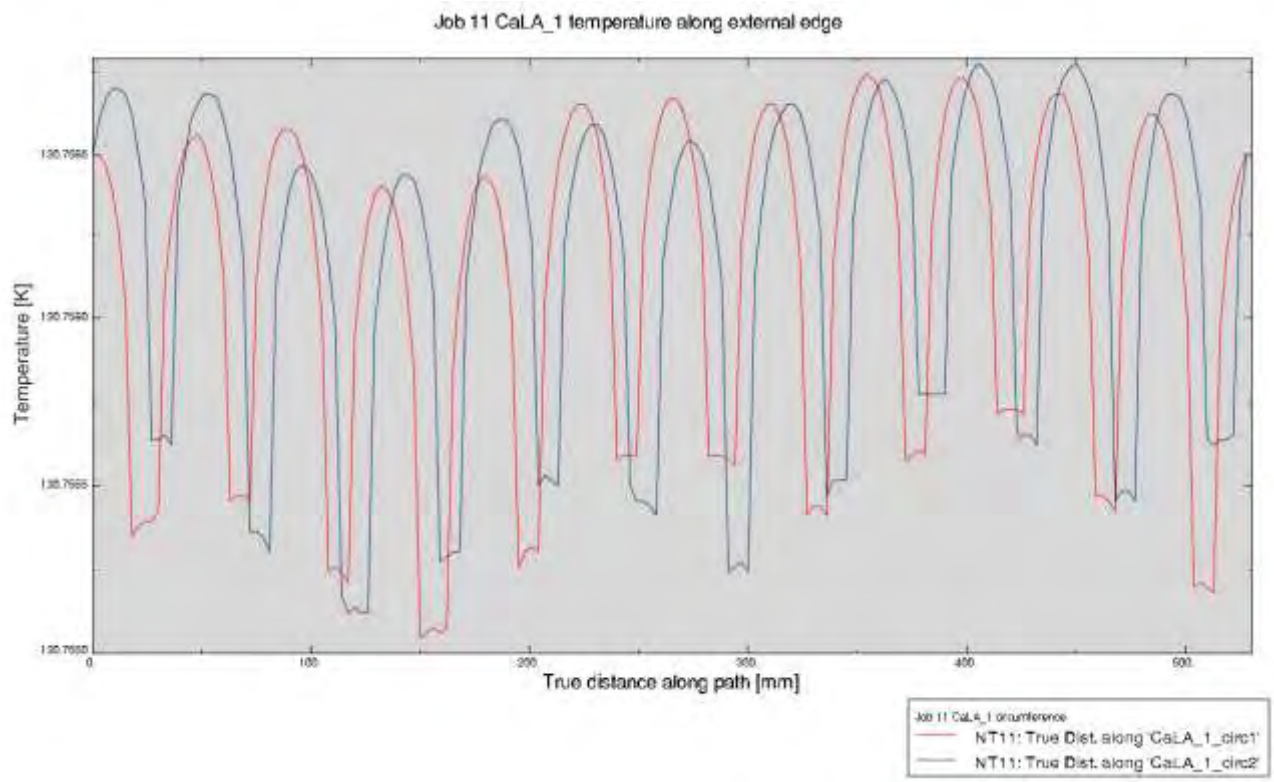

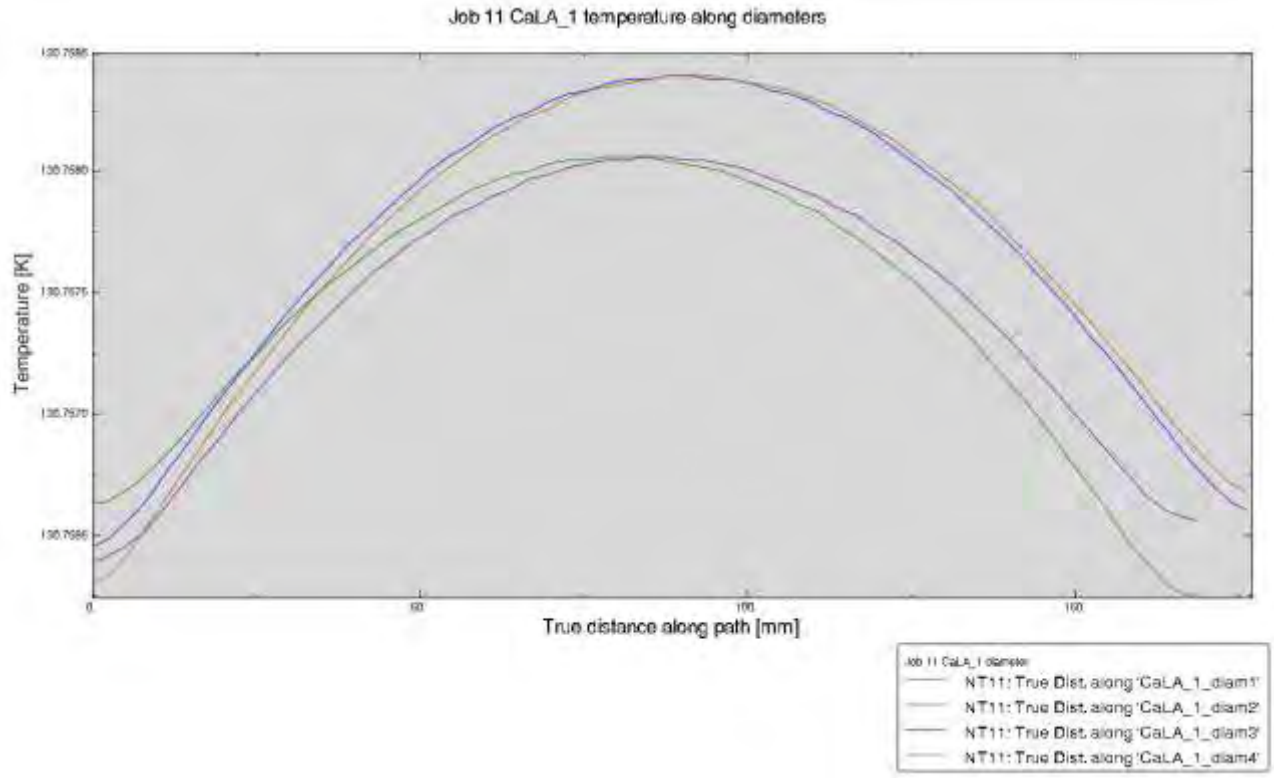

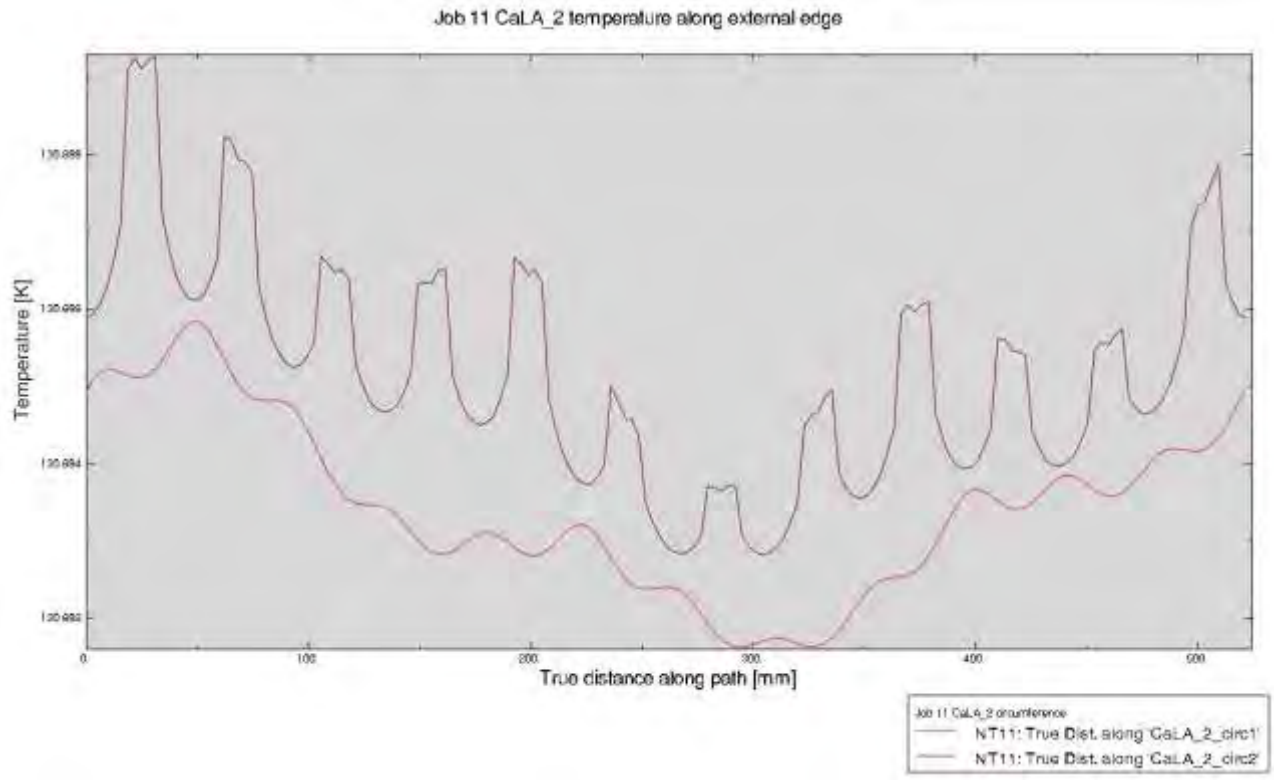
Job 11 CaLA_2 temperature along external edge
Temperature [K]
True distance along path [mm]
Job 11 CaLA_2 circumference
NT11: True Dist. along 'CaLA_2_circ1'
NT11: True Dist. along 'CaLA_2_circ2'

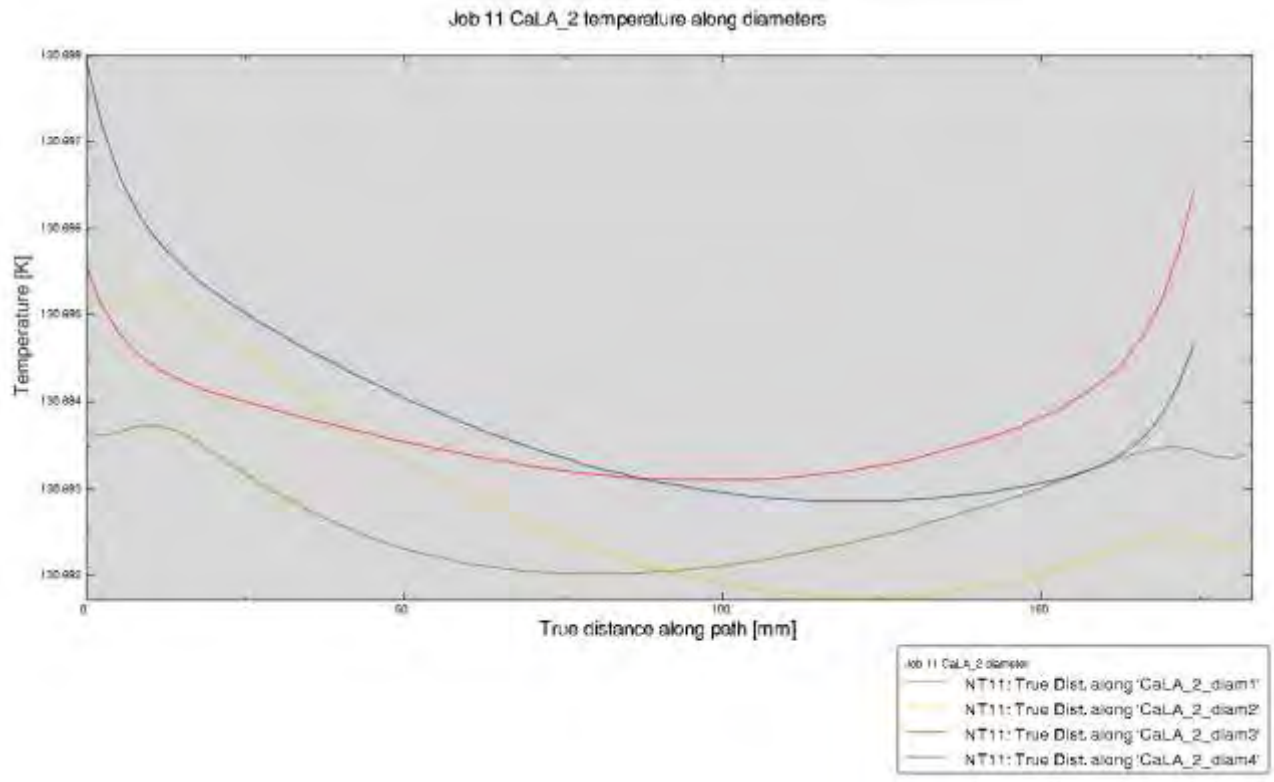
Job 11 CaLA_2 temperature along diameters
Temperature [K]
True distance along path [mm]
Job 11 CaLA_2 diameter
NT11: True Dist. along 'CaLA_2_diam1'
NT11: True Dist. along 'CaLA_2_diam2'
NT11: True Dist. along 'CaLA_2_diam3'
NT11: True Dist. along 'CaLA_2_diam4'

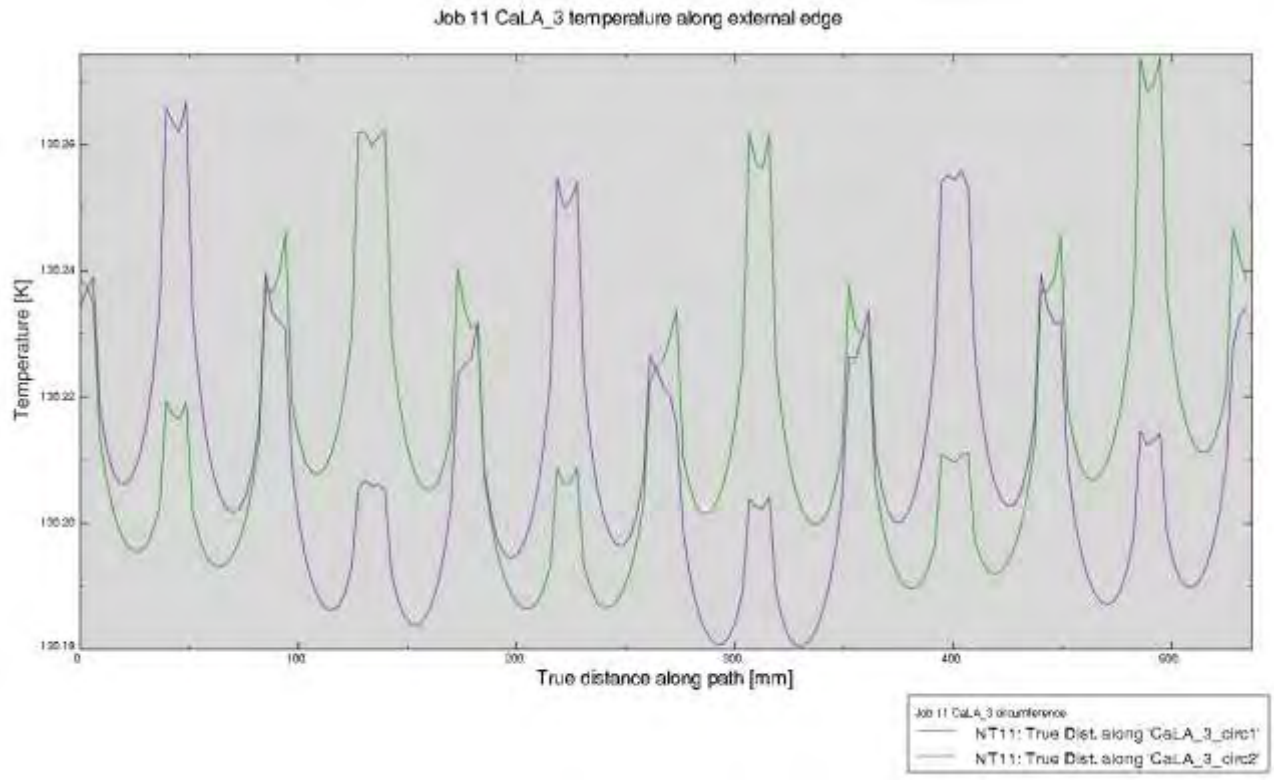
Job 11 CaLA_3 temperature along external edge
Temperature [K]
True distance along path [mm]
Job 11 CaLA_3 circumference
NT11: True Dist. along 'CaLA_3_circ1'
NT11: True Dist. along 'CaLA_3_circ2'

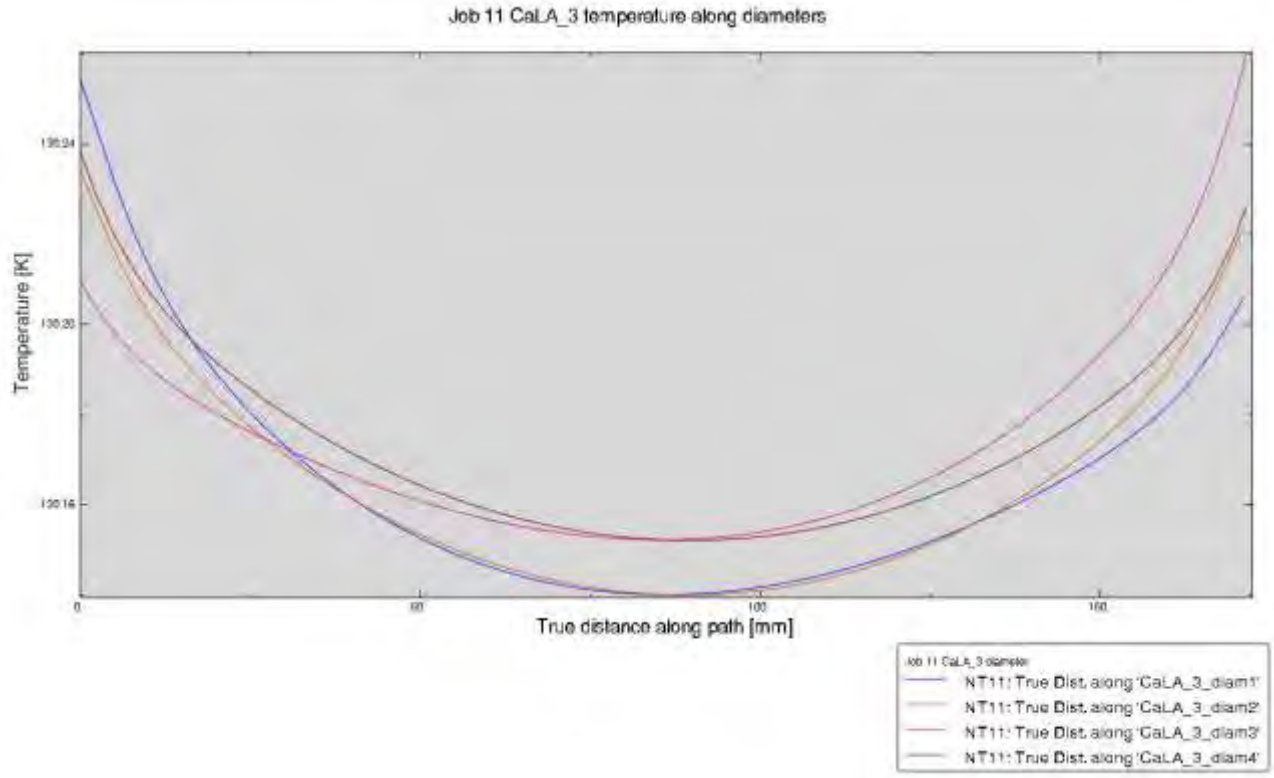
Job 11 CaLA_3 temperature along diameters
Temperature [K]
True distance along path [mm]
Job 11 CaLA_3 diameter
NT11: True Dist. along 'CaLA_3_diam1'
NT11: True Dist. along 'CaLA_3_diam2'
NT11: True Dist. along 'CaLA_3_diam3'
NT11: True Dist. along 'CaLA_3_diam4'

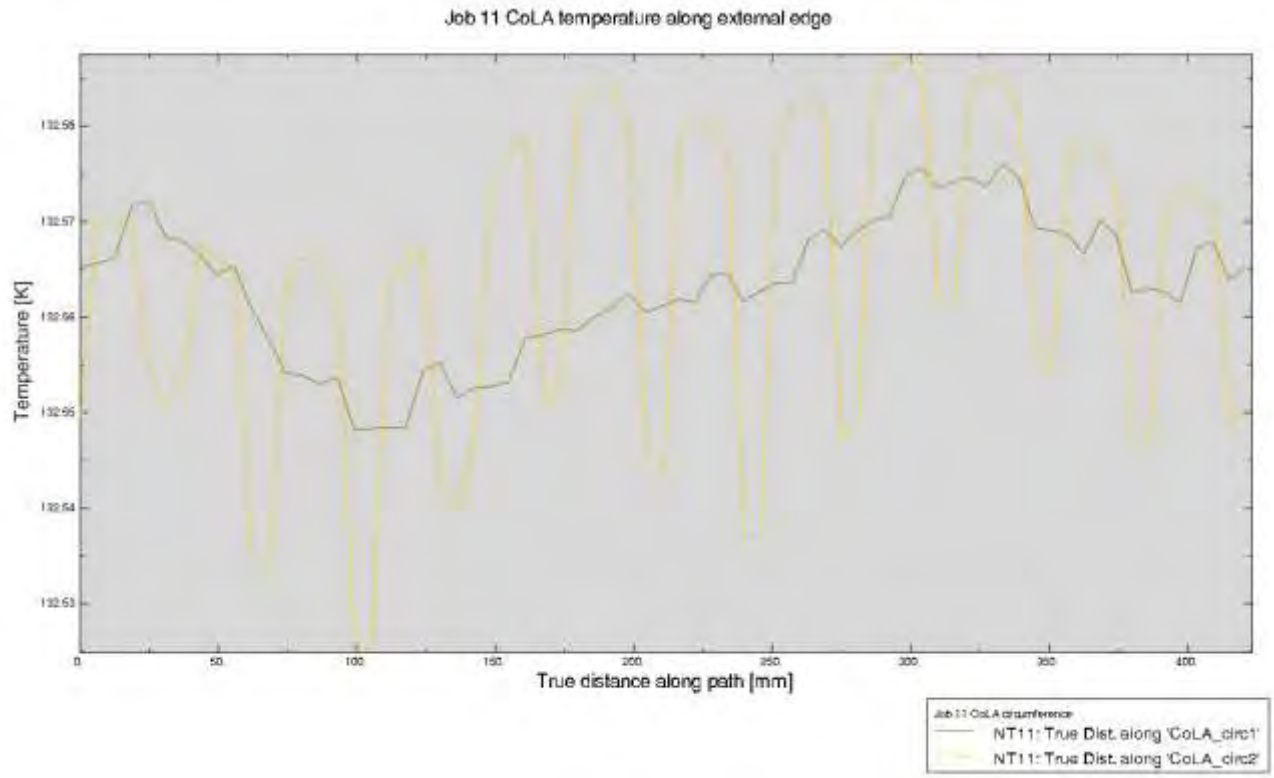
Job 11 CoLA temperature along external edge
Temperature [K]
True distance along path [mm]
Job 11 CoLA circumference
NT11: True Dist. along 'CoLA_circ1'
NT11: True Dist. along 'CoLA_circ2'

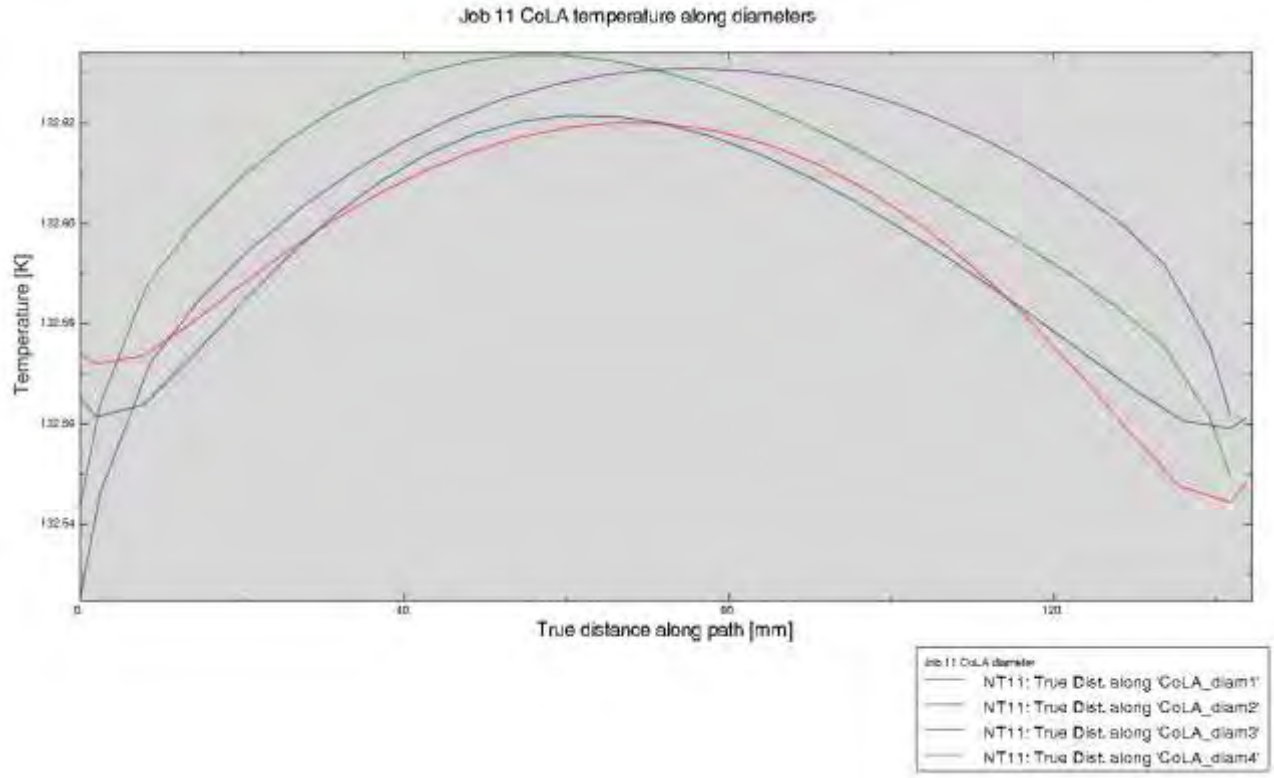
Job 11 CoLA temperature along diameters
Temperature [K]
True distance along path [mm]
Job 11 CoLA diameter
NT11: True Dist. along 'CoLA_diam1'
NT11: True Dist. along 'CoLA_diam2'
NT11: True Dist. along 'CoLA_diam3'
NT11: True Dist. along 'CoLA_diam4'

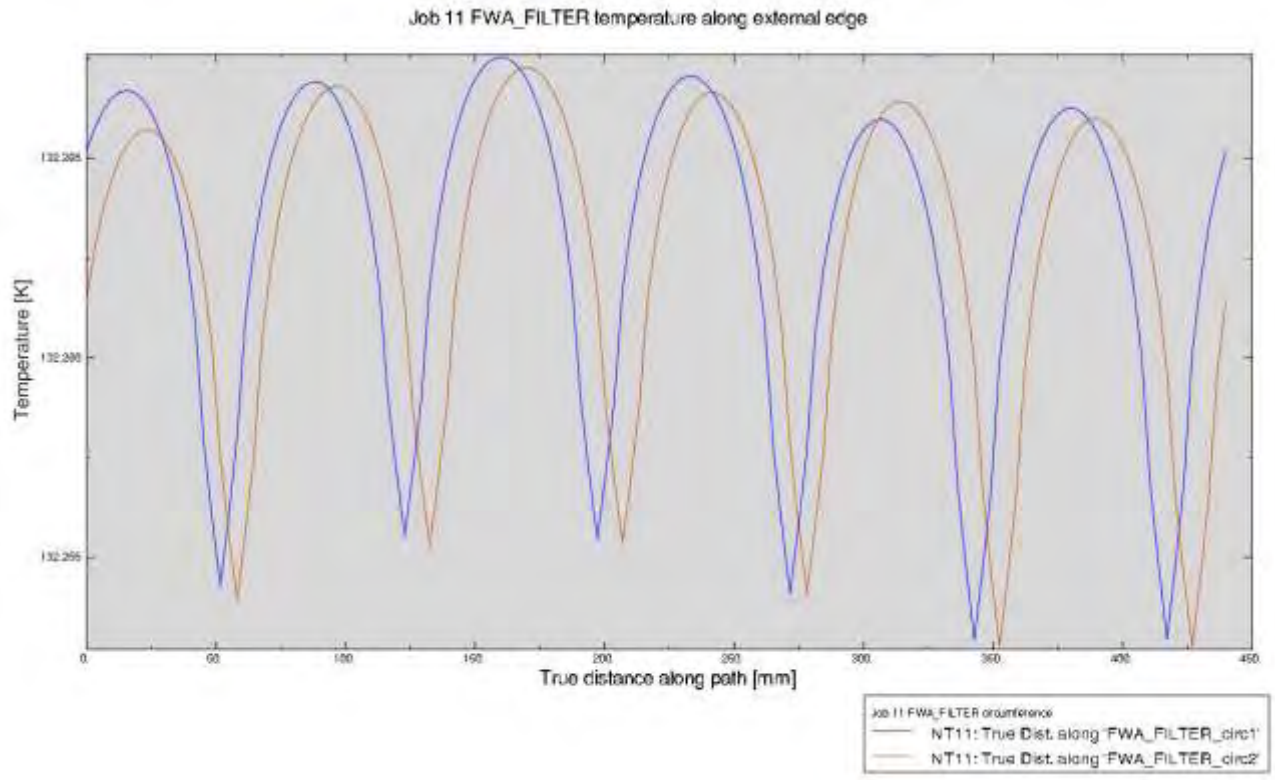
Job 11 FWA_FILTER temperature along external edge
Temperature [K]
True distance along path [mm]
Job 11 FWA_FILTER circumference
NT11: True Dist. along 'FWA_FILTER_circ1'
NT11: True Dist. along 'FWA_FILTER_circ2'

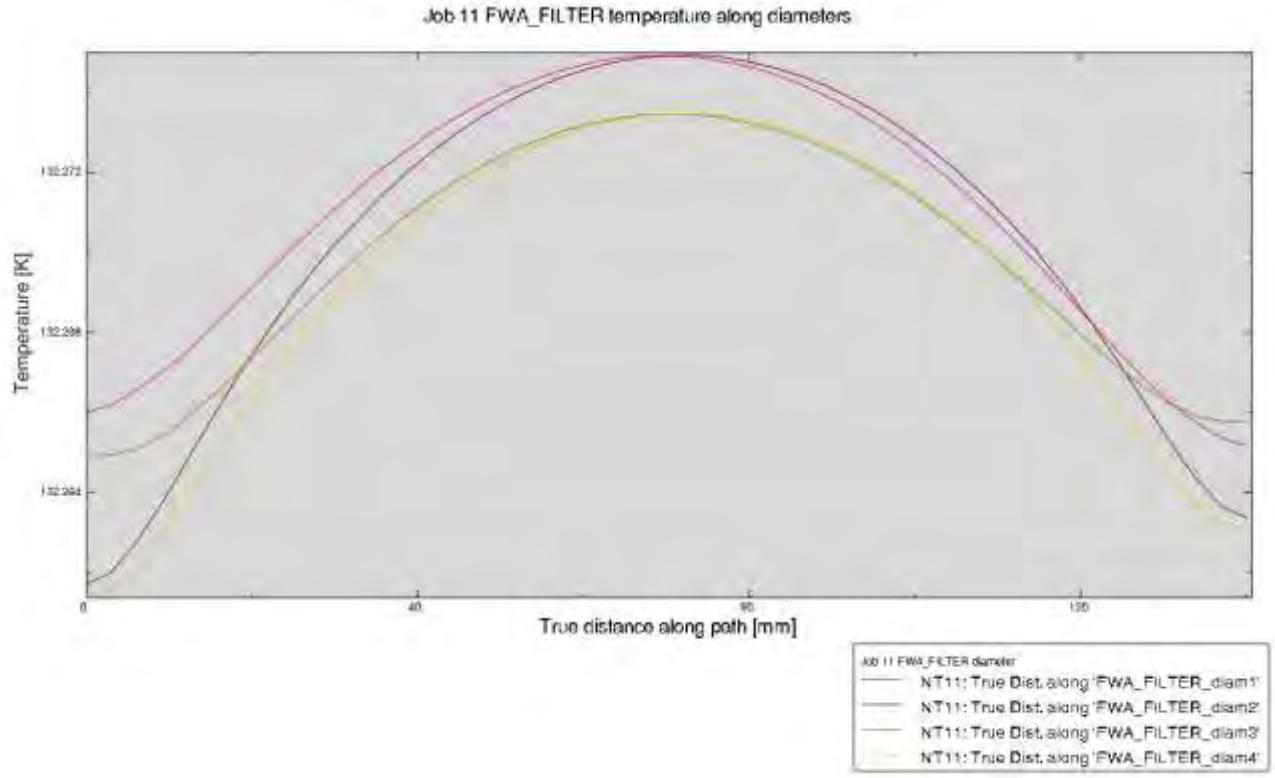
Job 11 FWA_FILTER temperature along diameters
Temperature [K]
True distance along path [mm]
Job 11 FWA_FILTER diameter
NT11: True Dist. along 'FWA_FILTER_diam1'
NT11: True Dist. along 'FWA_FILTER_diam2'
NT11: True Dist. along 'FWA_FILTER_diam3'
NT11: True Dist. along 'FWA_FILTER_diam4'

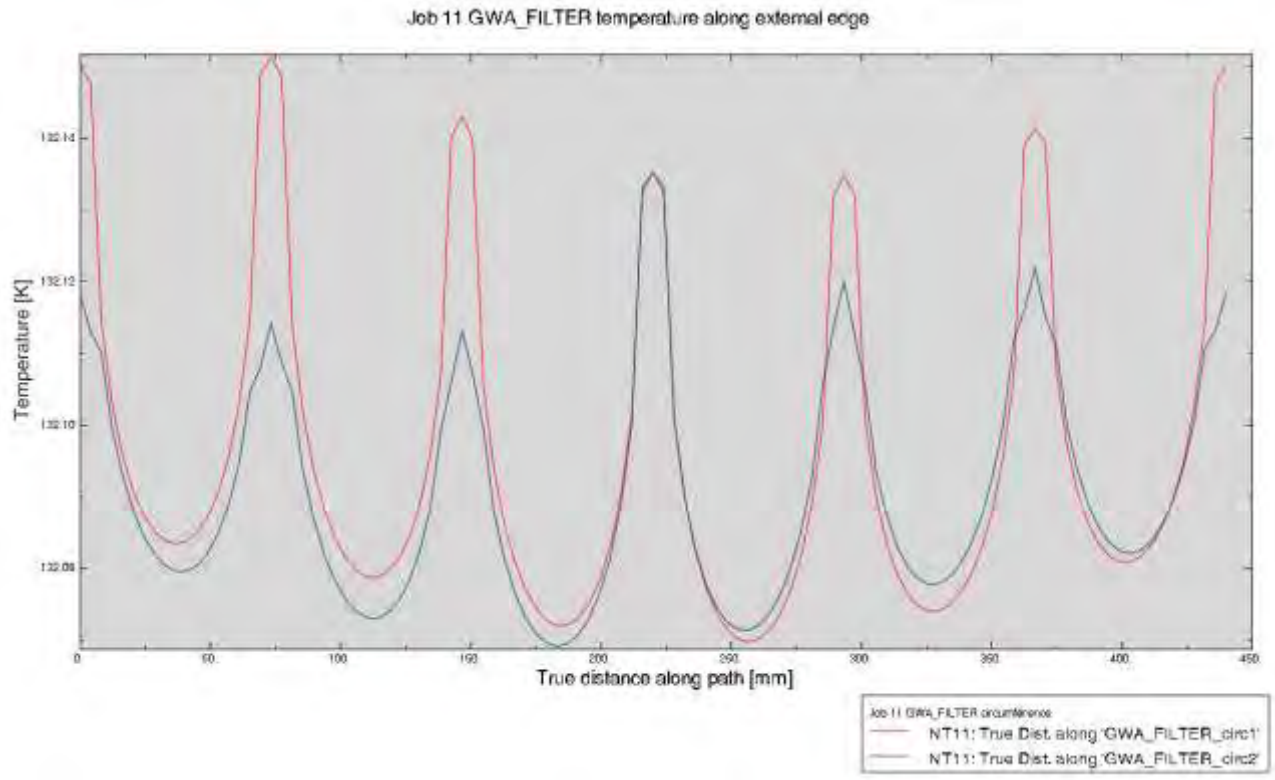
Job 11 GWA_FILTER temperature along external edge
Temperature [K]
True distance along path [mm]
Job 11 GWA_FILTER circumference
NT11: True Dist. along 'GWA_FILTER_circ1'
NT11: True Dist. along 'GWA_FILTER_circ2'

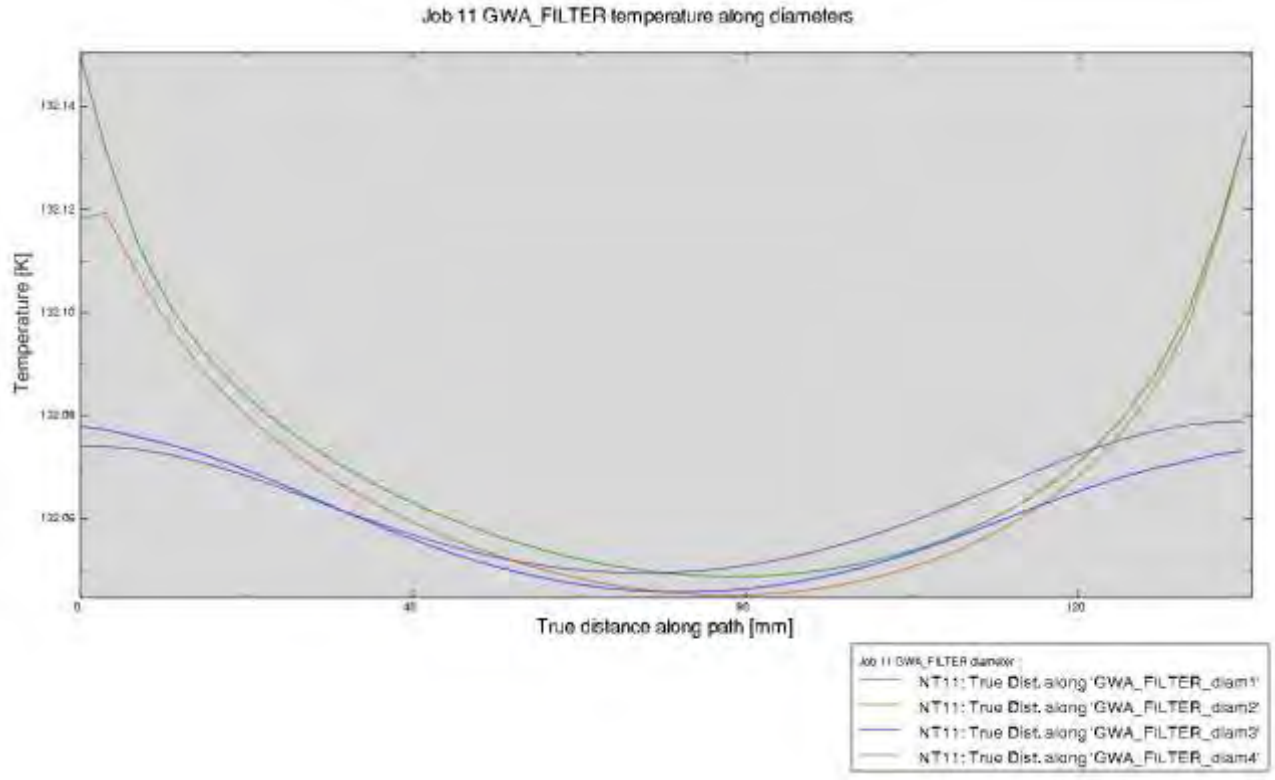
Job 11 GWA_FILTER temperature along diameters
Temperature [K]
True distance along path [mm]
Job 11 GWA_FILTER diameter
NT11: True Dist. along 'GWA_FILTER_diam1'
NT11: True Dist. along 'GWA_FILTER_diam2'
NT11: True Dist. along 'GWA_FILTER_diam3'
NT11: True Dist. along 'GWA_FILTER_diam4'

13.1.2. JOB 11 Heat Loads

Reaction fluxes at the boundaries: the following table reports the values of the reaction fluxes at the boundary condition IF's with fixed temperature.

Model name	Unit Name	Flux [mW]
NIDS_Detail 3D-572-1	BP6	6.797
NIDS_Detail 3D-573-1	BP5	6.771
NIDS_Detail 3D-585-1	BP3	8.138
NIDS_Detail 3D-586-1	BP4	8.162
NIDS_Detail 3D-598-1	BP1	8.024
NIDS_Detail 3D-599-1	BP2	8.005
NIDS_Detail 3D-772-1	SSS	-3941.990
NIDS_Detail 3D-889-1	CSS	-2131.170

In the following table are reported the minimum, maximum and mean temperature for some components.

Model name	Unit Name	Tmin	Tmax	Tmean
NIDS_Detail 3D-1-1	P1	132.19	132.29	132.21
NIDS_Detail 3D-31-1	P2	132.20	132.27	132.24
NIDS_Detail 3D-91-1	CaLA lens 1	130.76	130.76	130.76
NIDS_Detail 3D-92-1	CaLA lens 2	130.68	130.69	130.68
NIDS_Detail 3D-93-1	CaLA lens 3	130.14	130.27	130.18
NIDS_Detail 3D-126-1	CoLA lens	132.52	132.63	132.59
NIDS_Detail 3D-128-1	Filter Wheel	132.14	132.19	132.17
NIDS_Detail 3D-169-1	Filter	132.05	132.15	132.07
NIDS_Detail 3D-261-1	Grism	132.25	132.28	132.27
NIDS_Detail 3D-264-1	Grism Wheel	132.24	132.25	132.24
NIDS_Detail 3D-541-1	P3	131.91	131.96	131.93
NIDS_Detail 3D-761-1	P4	131.90	131.95	131.93
NIDS_Detail 3D-772-1	SSS	134.97	138.20	136.01
NIDS_Detail 3D-776-1	detector	95.35	96.11	95.44
NIDS_Detail 3D-777-1	detector	95.50	96.31	95.54
NIDS_Detail 3D-778-1	detector	95.50	96.22	95.54
NIDS_Detail 3D-779-1	detector	95.35	96.11	95.43
NIDS_Detail 3D-780-1	detector	95.39	96.16	95.47
NIDS_Detail 3D-781-1	detector	95.41	96.17	95.47
NIDS_Detail 3D-782-1	detector	95.31	96.05	95.39
NIDS_Detail 3D-783-1	detector	95.52	96.27	95.56
NIDS_Detail 3D-784-1	detector	95.51	96.26	95.54
NIDS_Detail 3D-785-1	detector	95.43	96.15	95.48
NIDS_Detail 3D-786-1	detector	95.52	96.27	95.56
NIDS_Detail 3D-787-1	detector	95.51	96.26	95.54

NIDS_Detail 3D-788-1	detector	95.43	96.15	95.48
NIDS_Detail 3D-789-1	detector	95.39	96.16	95.47
NIDS_Detail 3D-790-1	detector	95.41	96.18	95.47
NIDS_Detail 3D-791-1	detector	95.31	96.05	95.39
NIDS_Detail 3D-793-1	sidecar	137.42	137.75	137.66
NIDS_Detail 3D-798-1	sidecar	138.00	138.25	138.21
NIDS_Detail 3D-800-1	sidecar	138.01	138.25	138.21
NIDS_Detail 3D-802-1	sidecar	137.41	137.75	137.66
NIDS_Detail 3D-819-1	sidecar	135.70	135.98	135.90
NIDS_Detail 3D-824-1	sidecar	136.24	136.47	136.43
NIDS_Detail 3D-826-1	sidecar	136.24	136.47	136.43
NIDS_Detail 3D-828-1	sidecar	135.70	135.98	135.90
NIDS_Detail 3D-841-1	sidecar	137.00	137.33	137.24
NIDS_Detail 3D-846-1	sidecar	137.58	137.83	137.78
NIDS_Detail 3D-848-1	sidecar	137.58	137.82	137.78
NIDS_Detail 3D-850-1	sidecar	136.98	137.33	137.23
NIDS_Detail 3D-867-1	sidecar	135.69	135.97	135.89
NIDS_Detail 3D-872-1	sidecar	136.22	136.46	136.42
NIDS_Detail 3D-874-1	sidecar	136.22	136.46	136.42
NIDS_Detail 3D-876-1	sidecar	135.69	135.97	135.90
NIDS_Detail 3D-889-1	CSS	95.00	95.57	95.35

In the following table are reported the max and min temperatures among the three interfaces between CoLA structure and P2, and among the three interfaces between CaLA structure and P1.

	Tmin [K]	Tmax[K]
CoLA Structure - P2 interface	131.487	131.637
CaLA Structure - P1 interface	131.494	131.505

13.2. Job 12 – Steady state analysis, Max T Case, Instrument Off, Not-OP mode

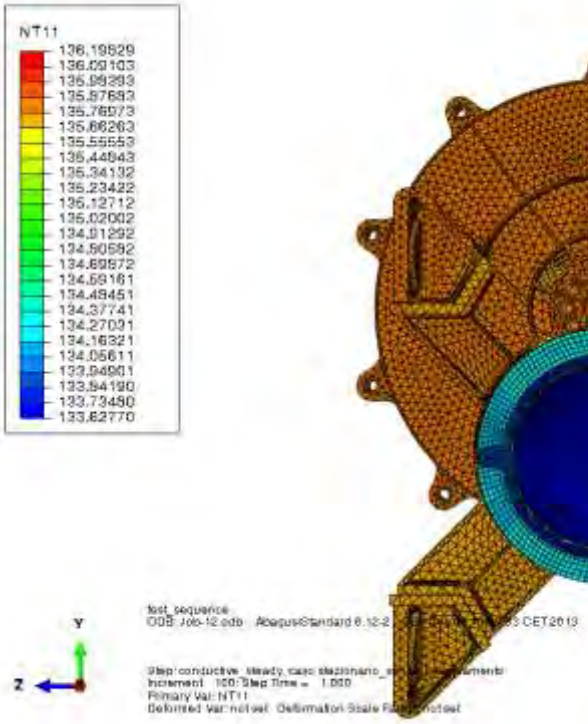

Figure 13-50 P1 and CaLA assembly Temperature distribution [K]

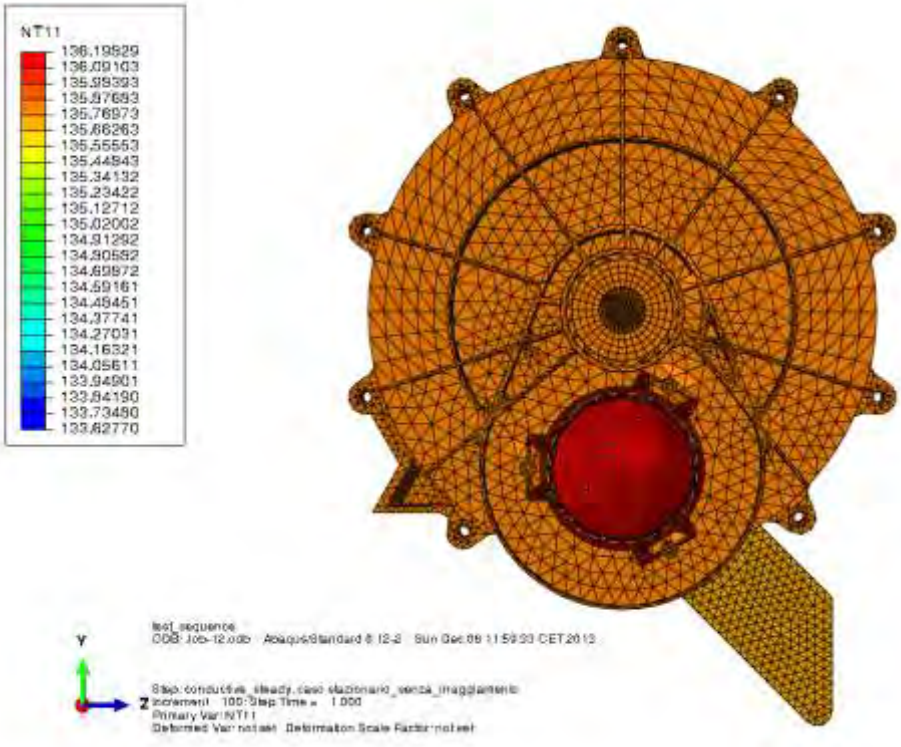

Figure 13-51 P2 and CoLA Assembly Temperature distribution [K]

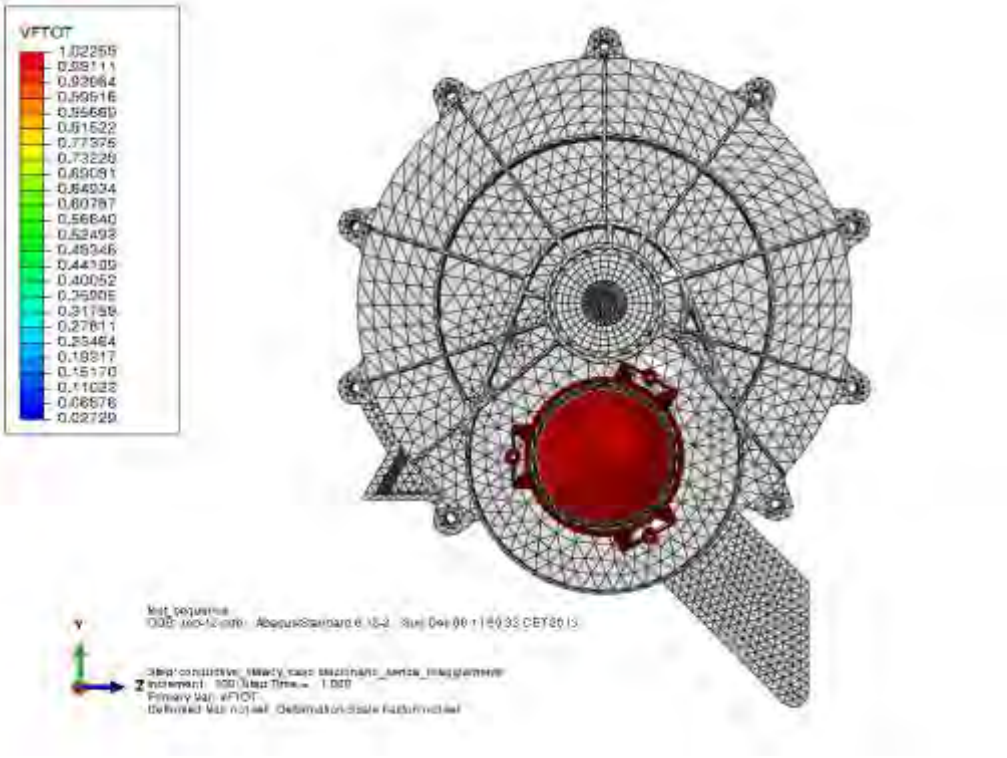

Figure 13-52 CoLA lens with support view factor

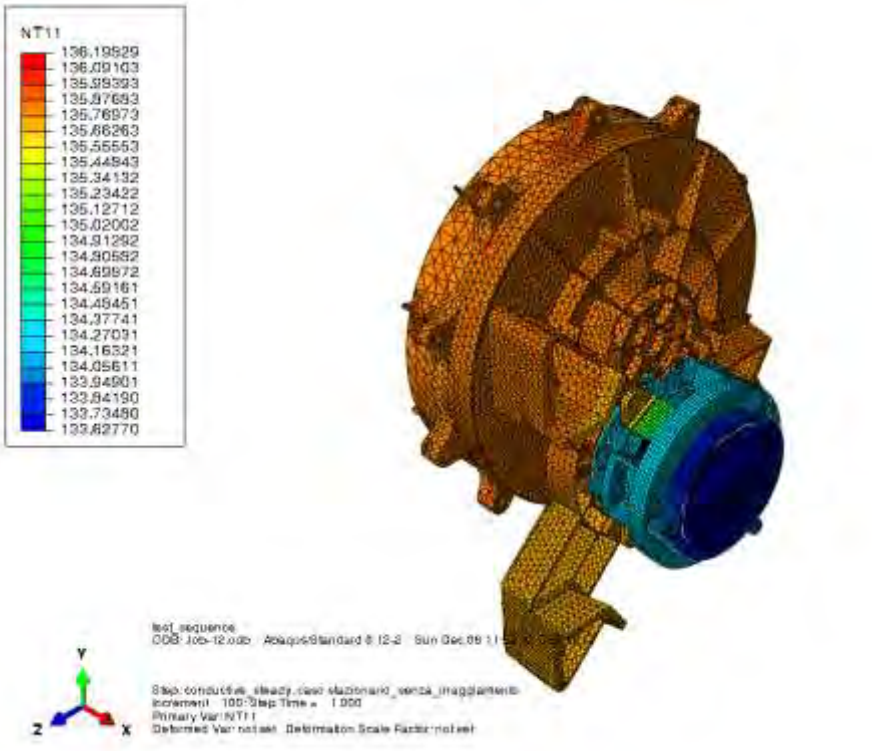

Figure 13-53 P1 and CaLA assembly Temperature distribution [K]

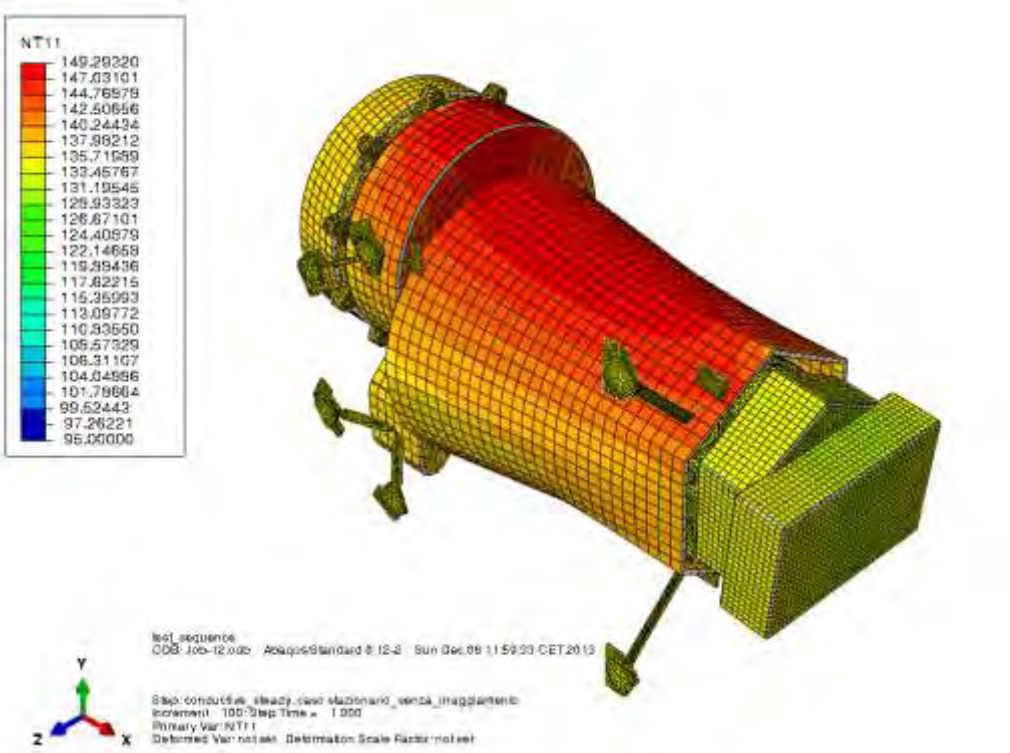

Figure 13-54 Full instrument assembly, with shrouds, temperature distribution [K]

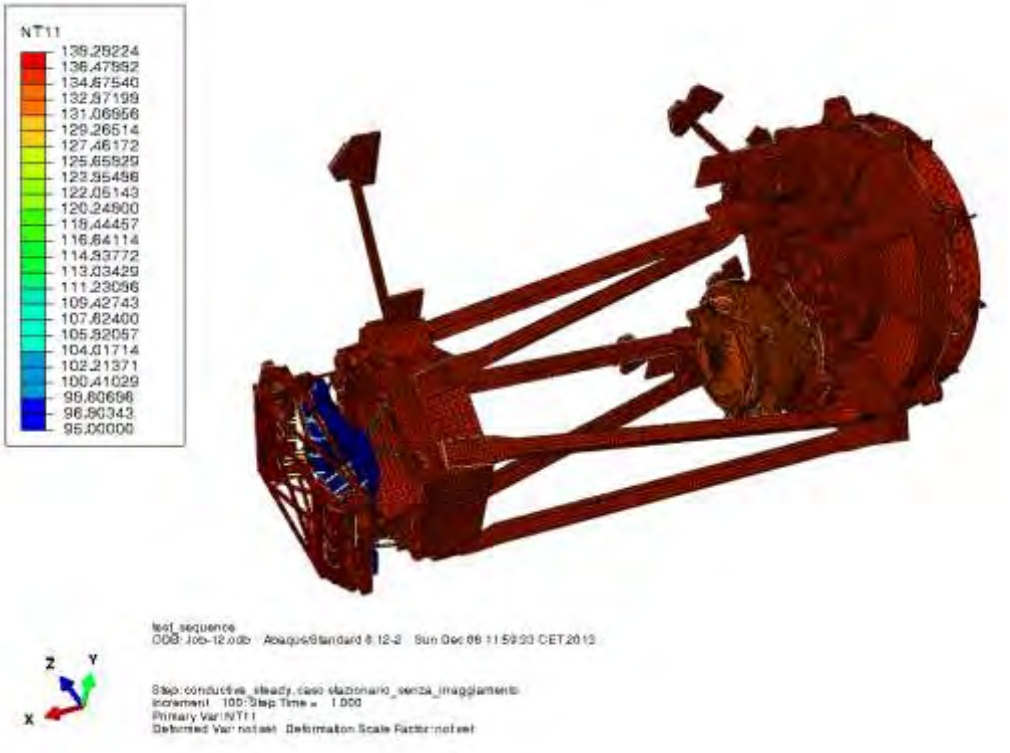

Figure 13-55 Full instrument assembly temperature distribution [K]

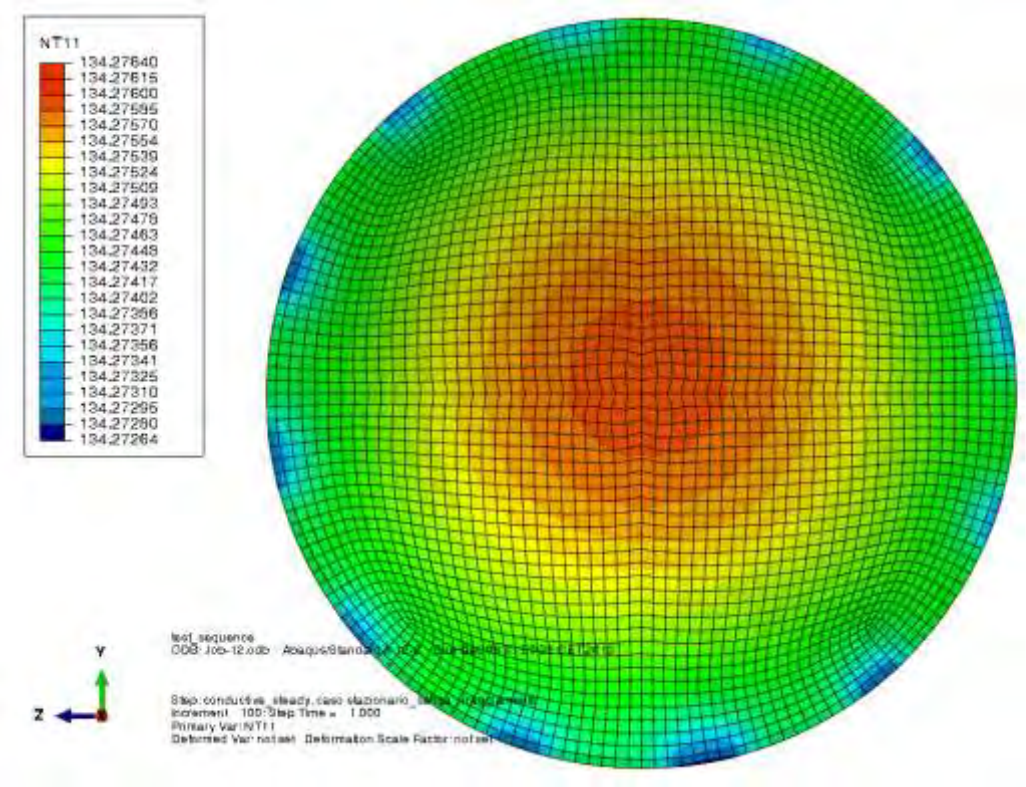

Figure 13-56 CaLA Lens 1 back temperature distribution [K]

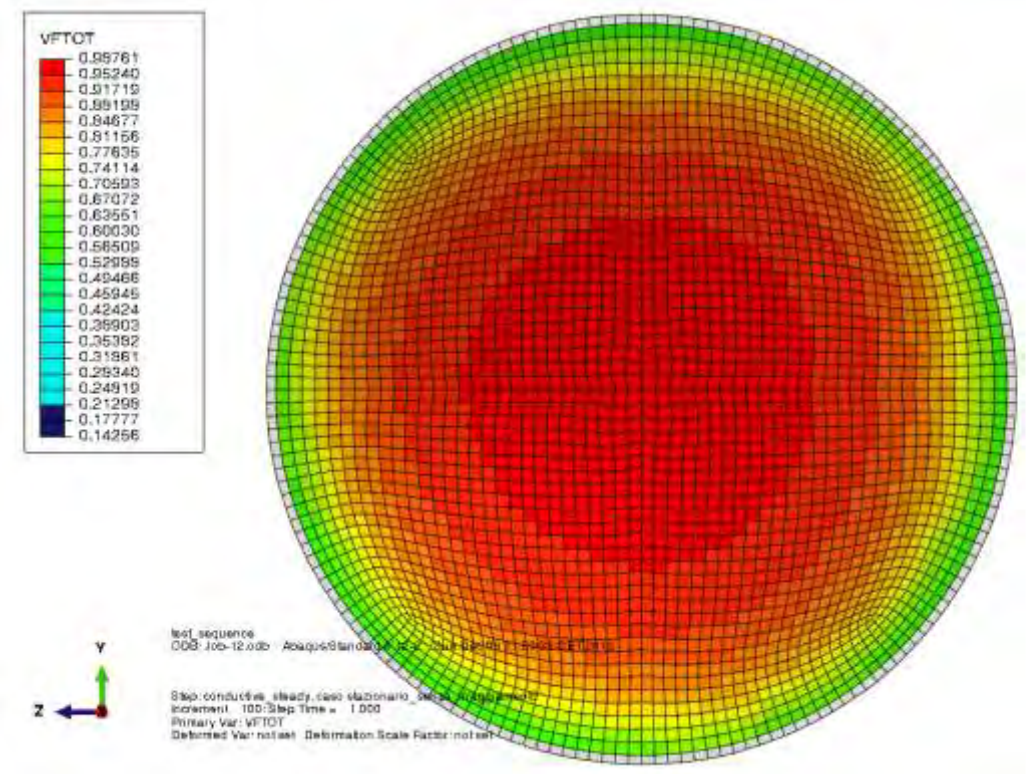

Figure 13-57 CaLA Lens 1 back view factor

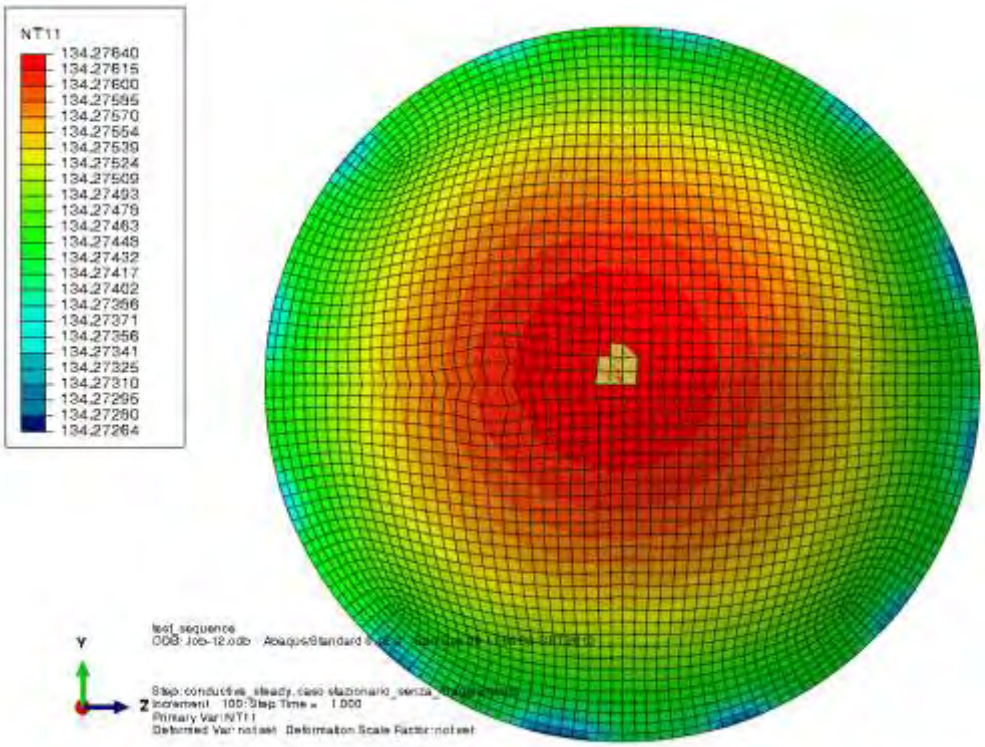

Figure 13-58 CaLA Lens 1 front temperature distribution [K]

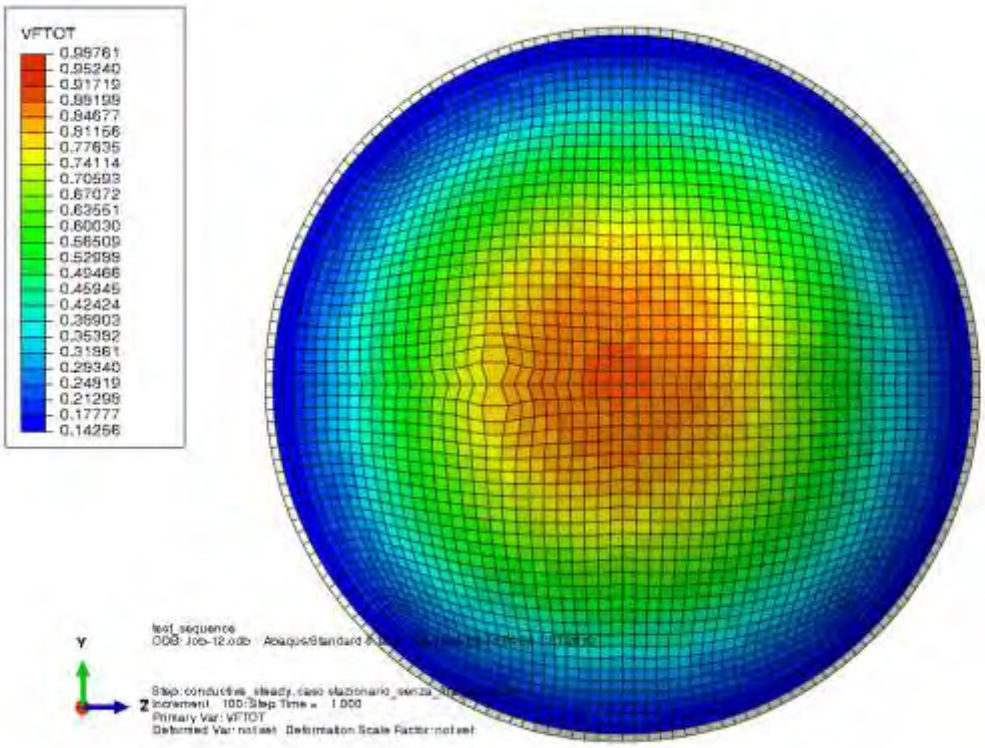

Figure 13-59 CaLA Lens 1 front view factor

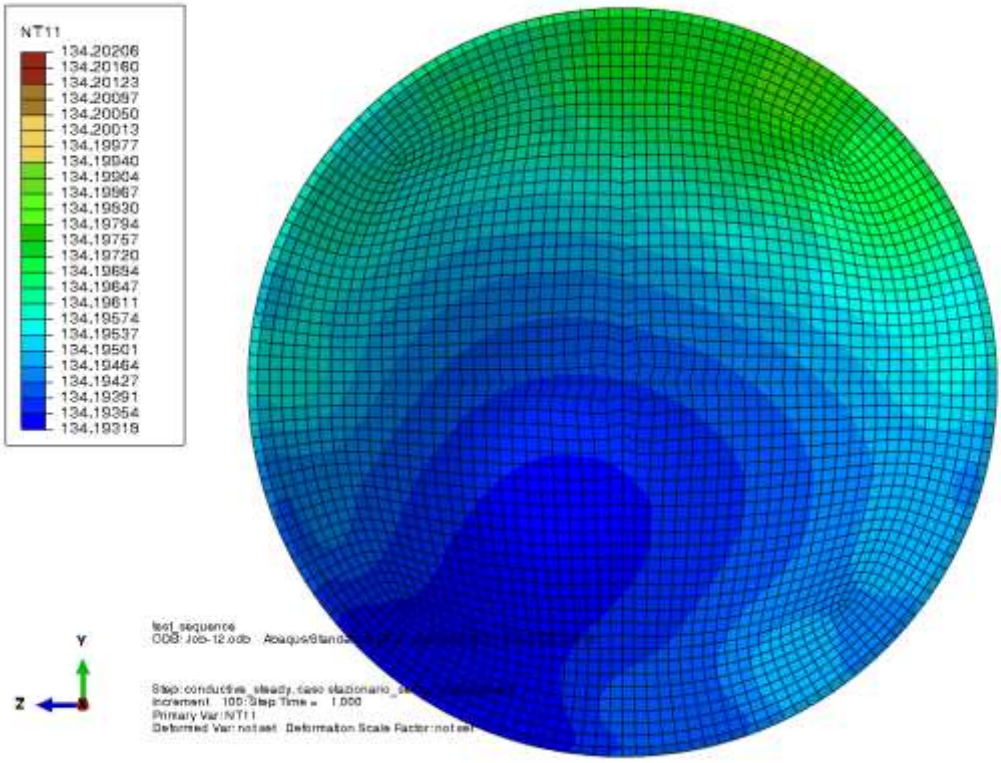

Figure 13-60 CaLA Lens 2 back temperature distribution [K]

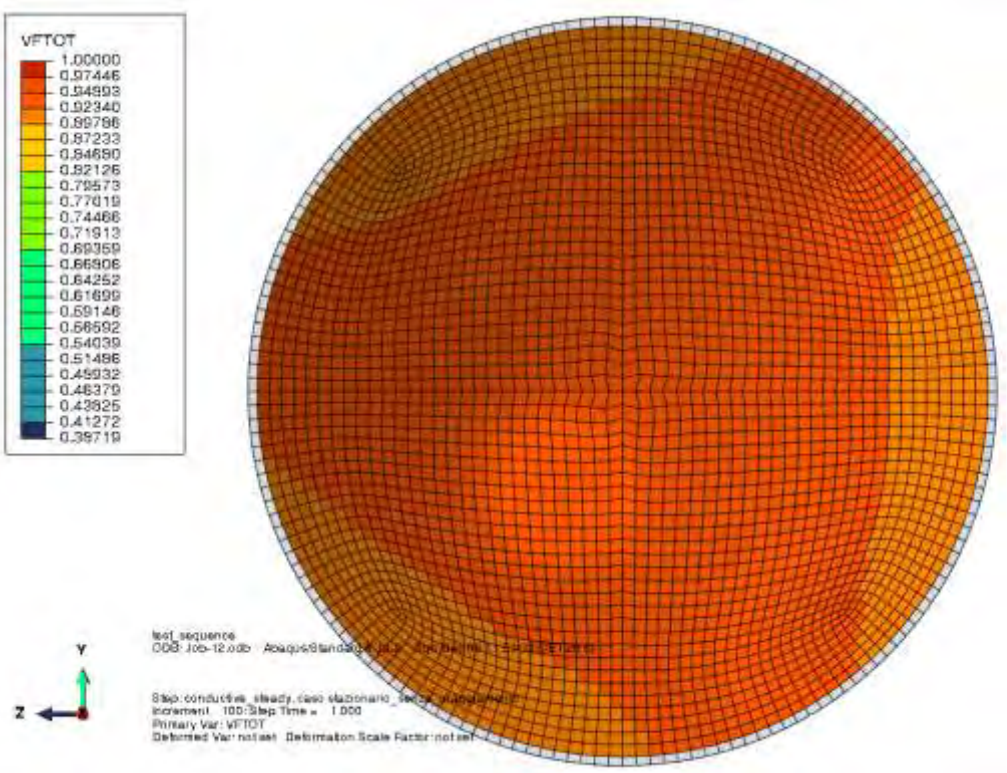

Figure 13-61 CaLA Lens 2 back view factor

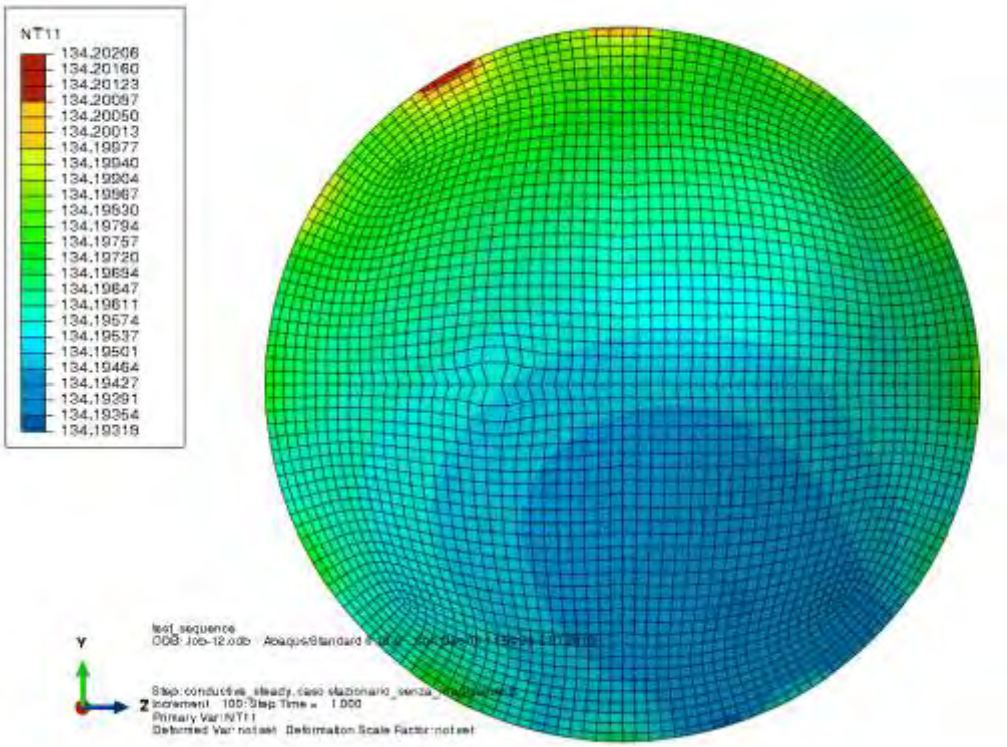

Figure 13-62 CaLA Lens 2 front temperature distribution [K]

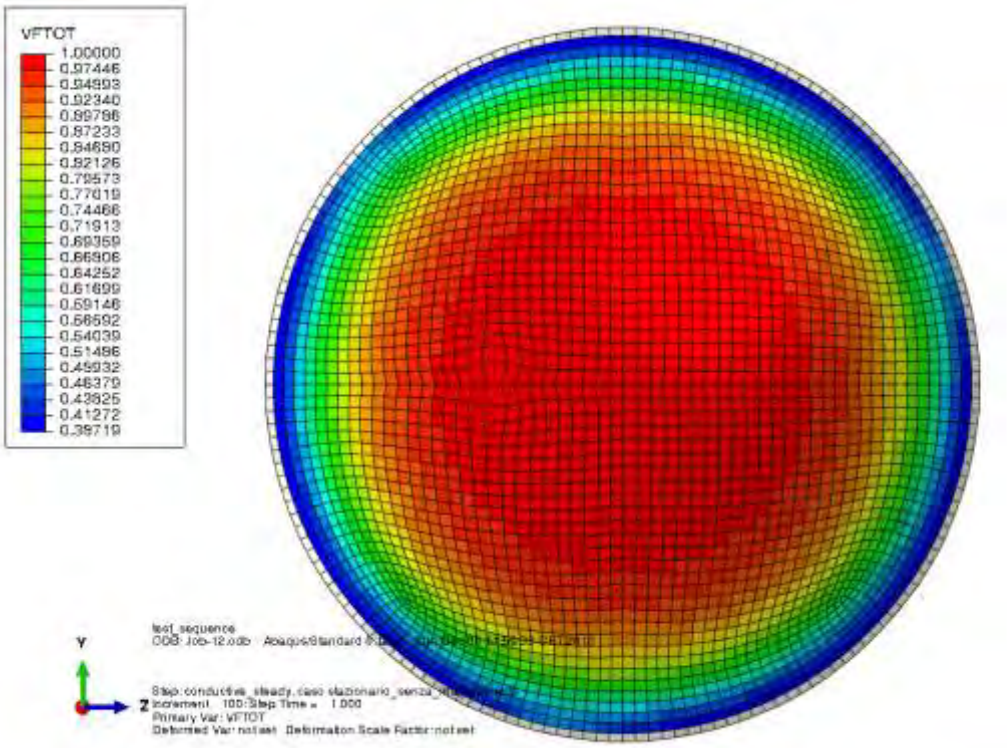

Figure 13-63 CaLA Lens 2 front view factor

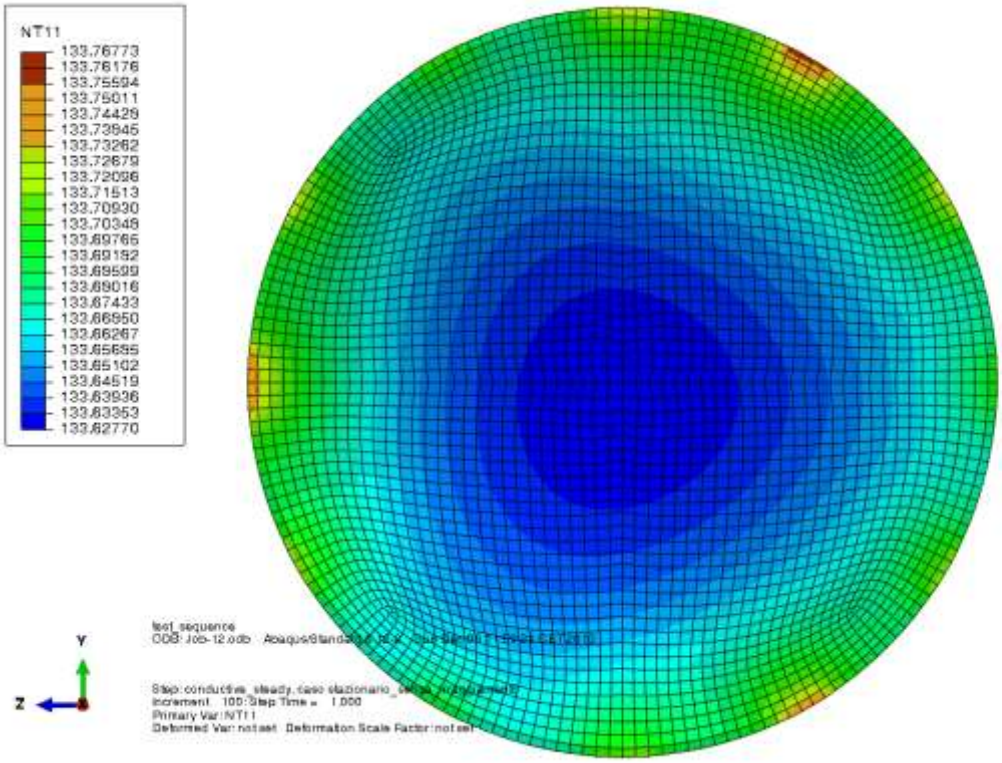

Figure 13-64 CaLA Lens 3 back temperature distribution [K]

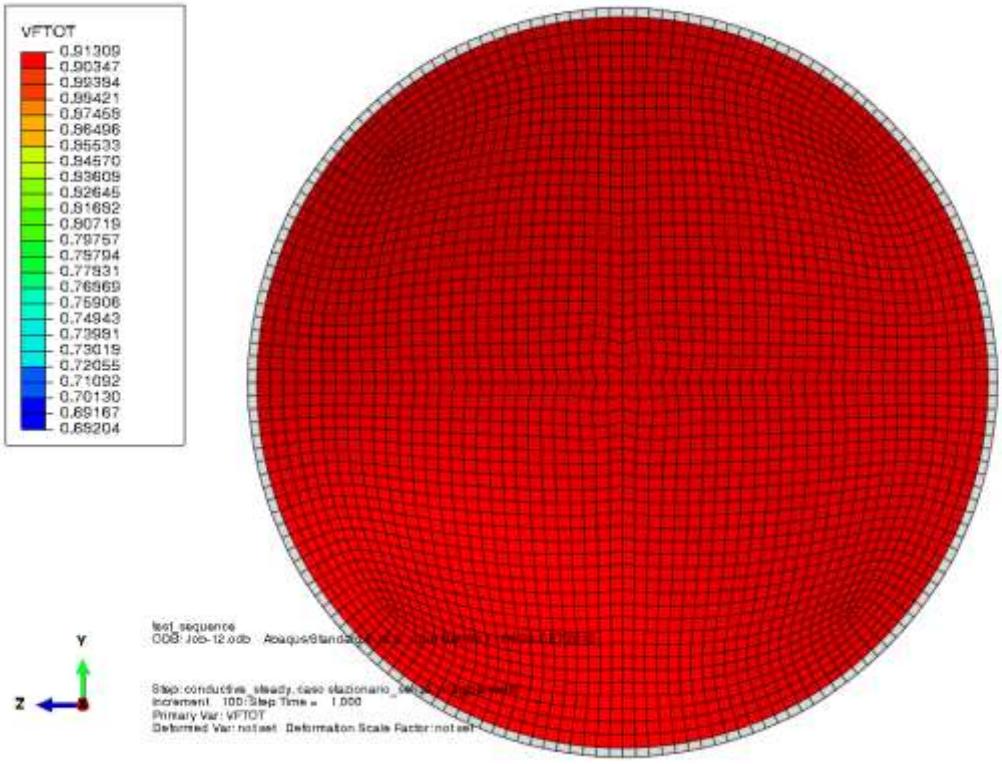

Figure 13-65 CaLA Lens 3 back view factor

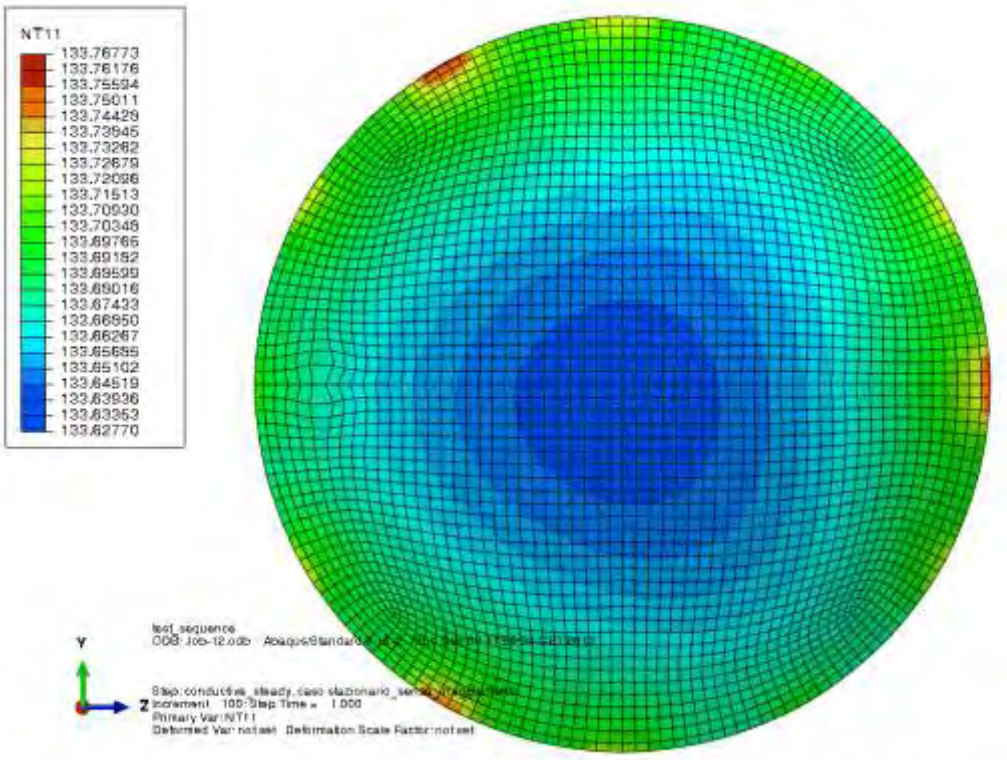

Figure 13-66 CaLA Lens 3 front temperature distribution [K]

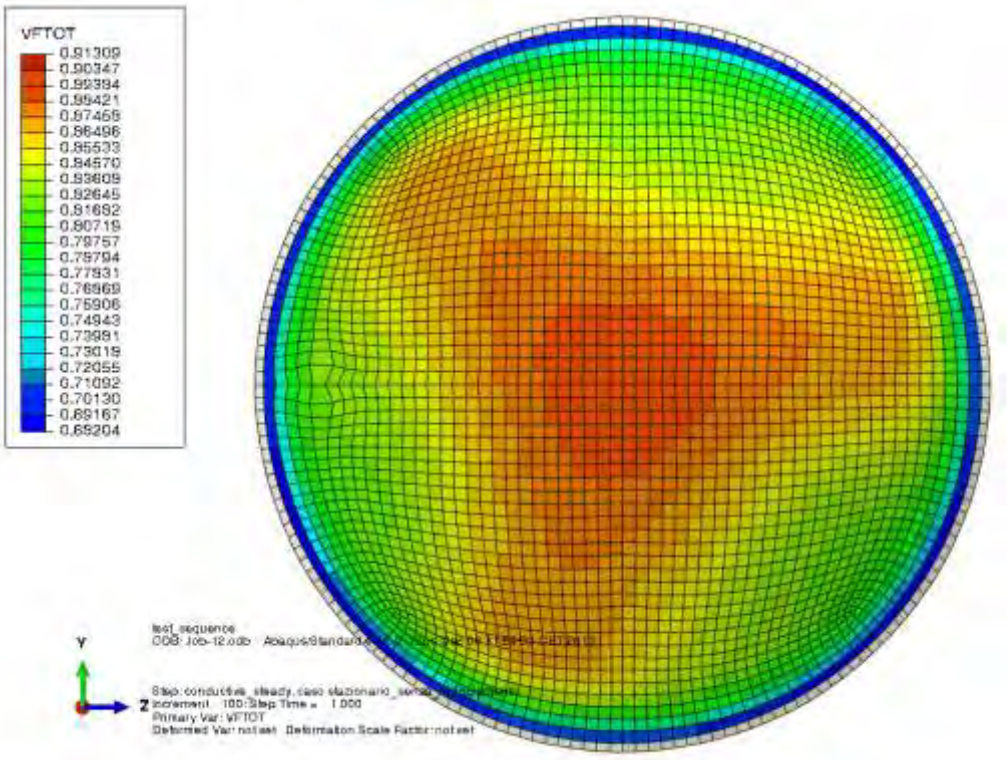

Figure 13-67 CaLA Lens 3 front view factor

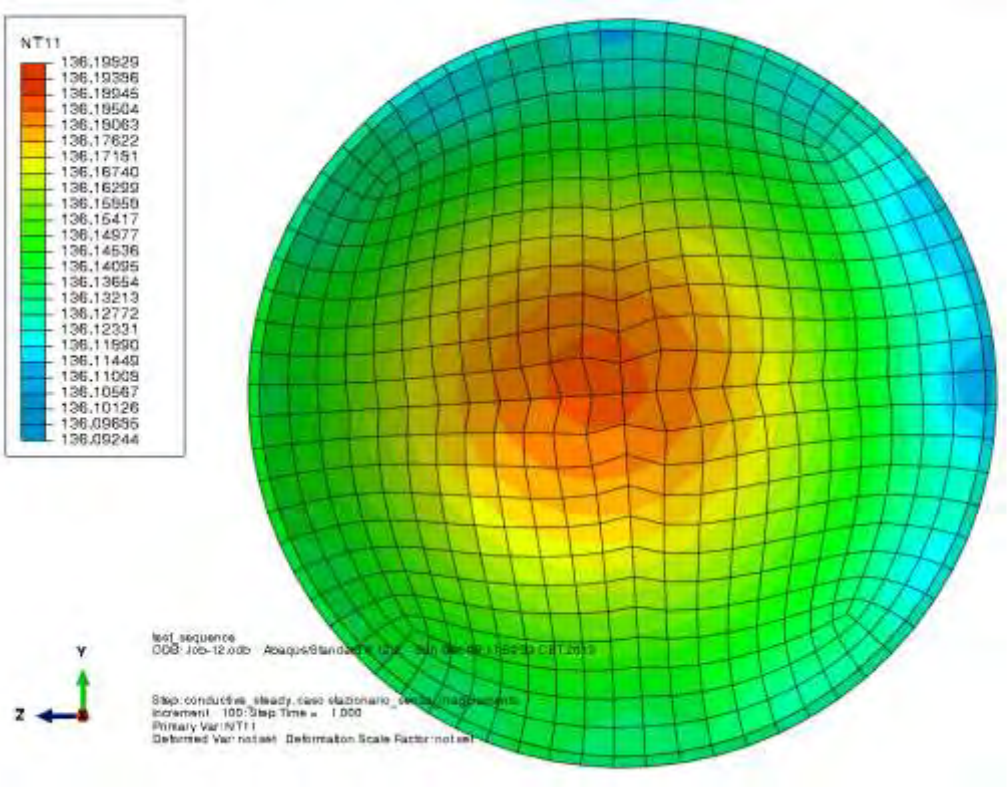

Figure 13-68 CoLA Lens back temperature distribution [K]

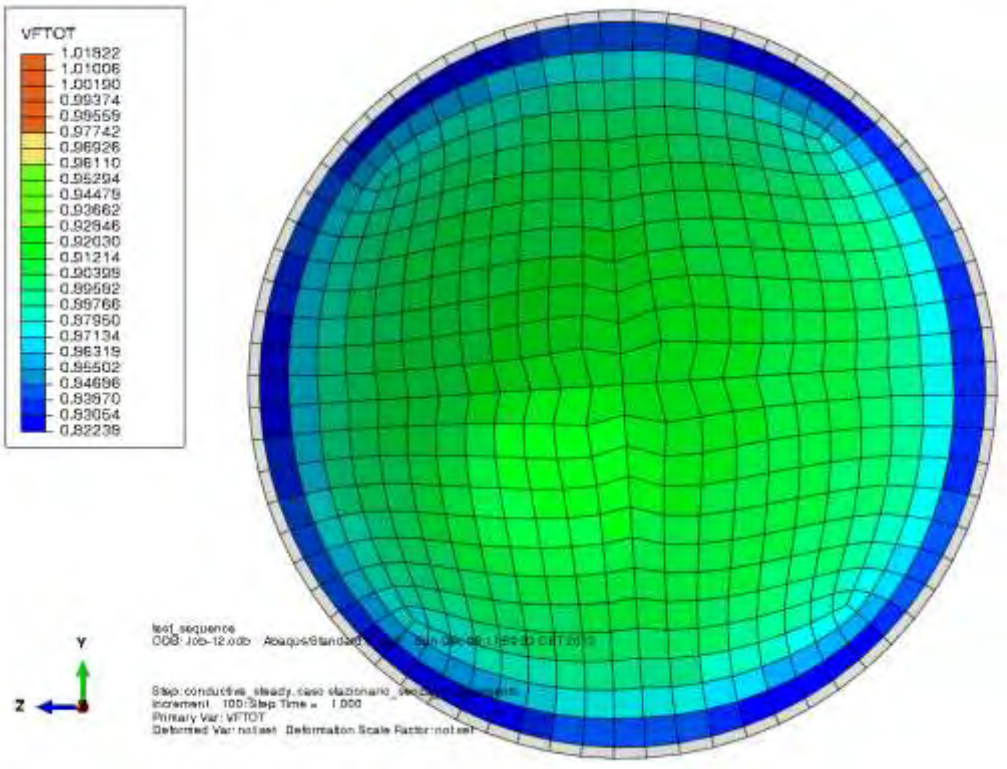

Figure 13-69 CoLA Lens back view factor

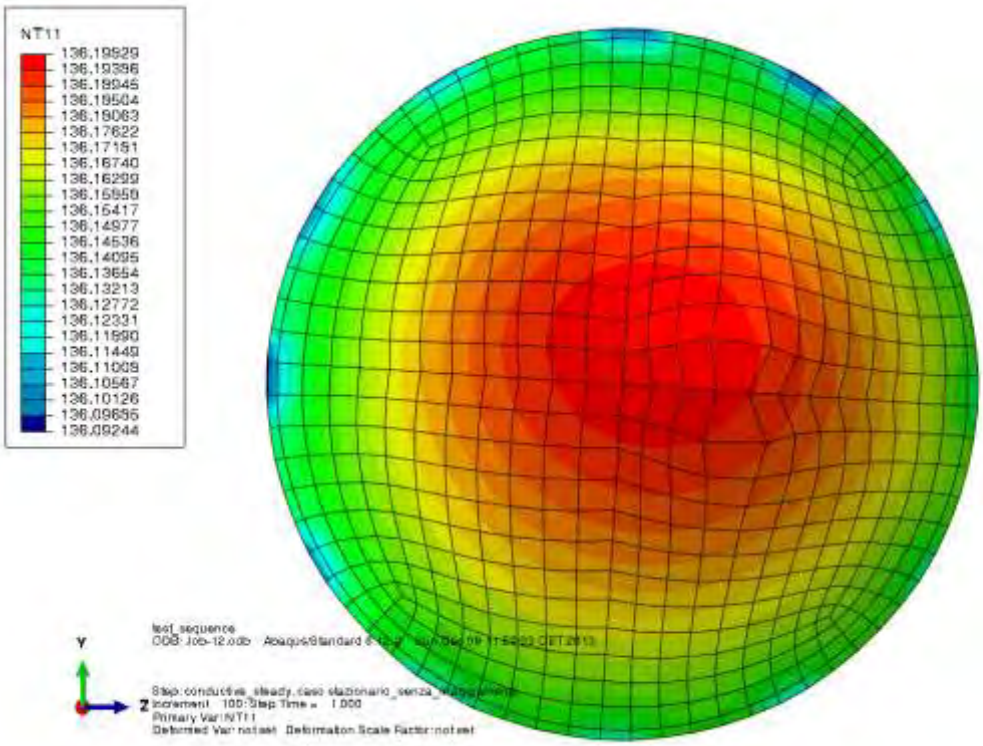

Figure 13-70 CoLA Lens front temperature distribution [K]

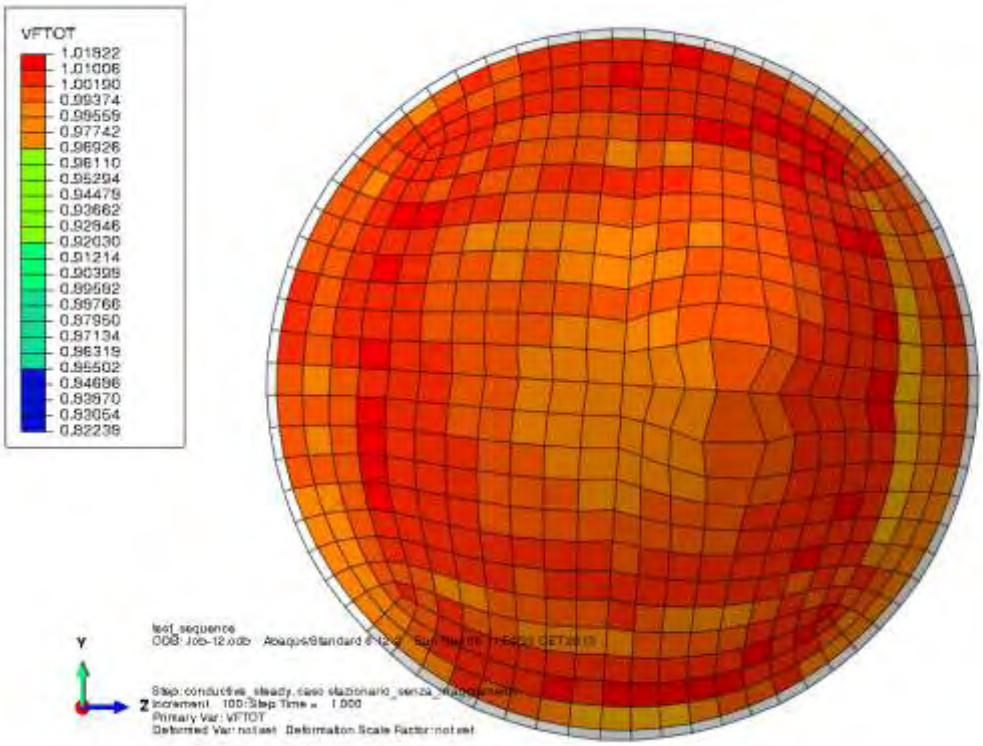

Figure 13-71 CoLA Lens front view factor

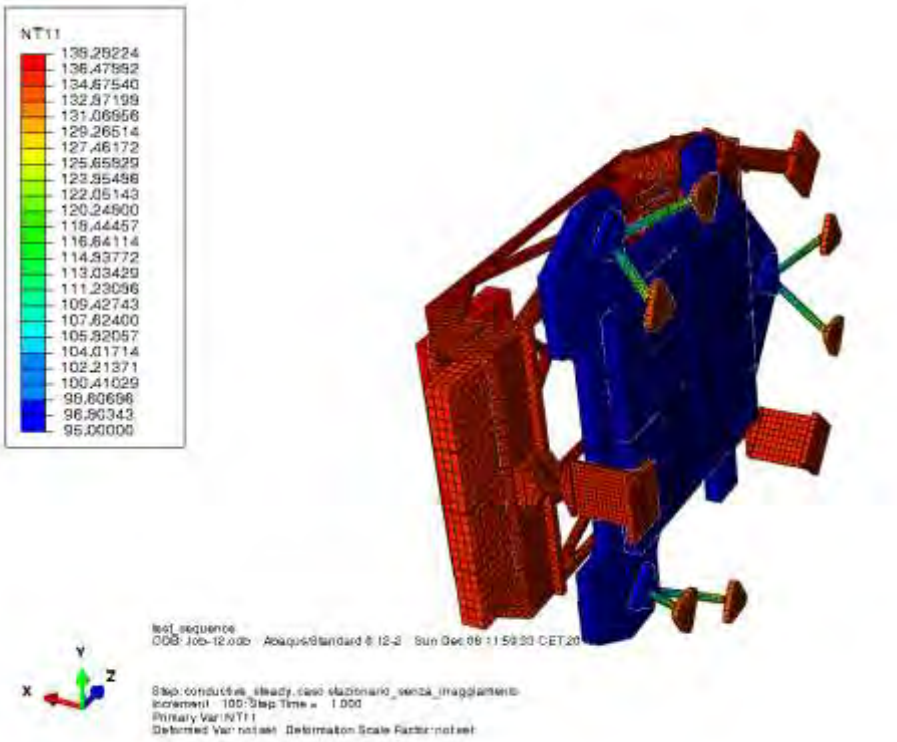

Figure 13-72 Detectors and Sidecars temperature distribution [K]

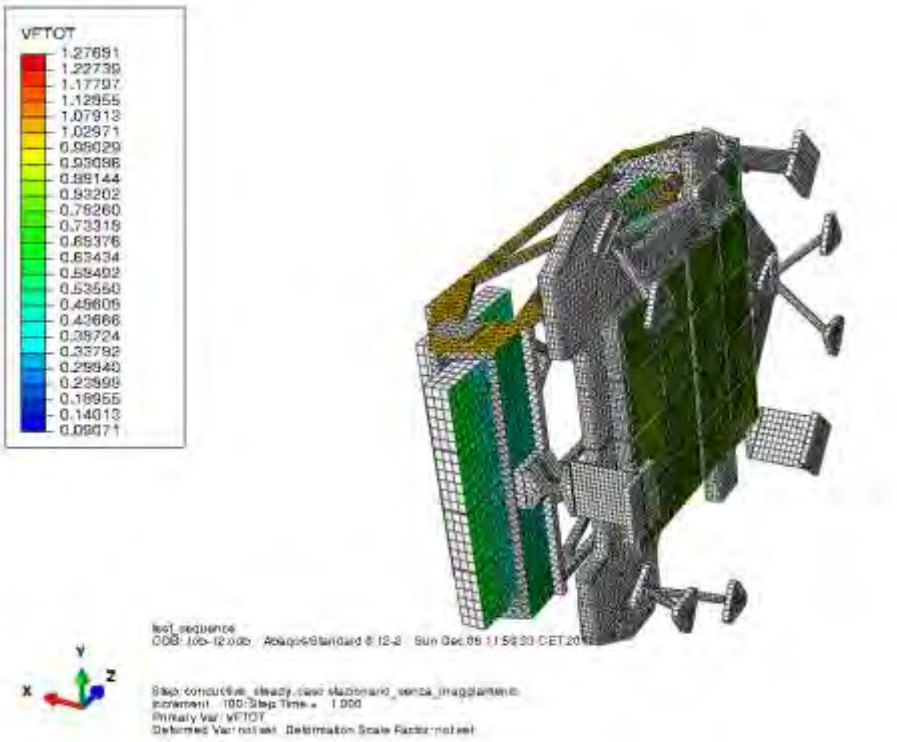

Figure 13-73 Detectors and Sidecars view factor

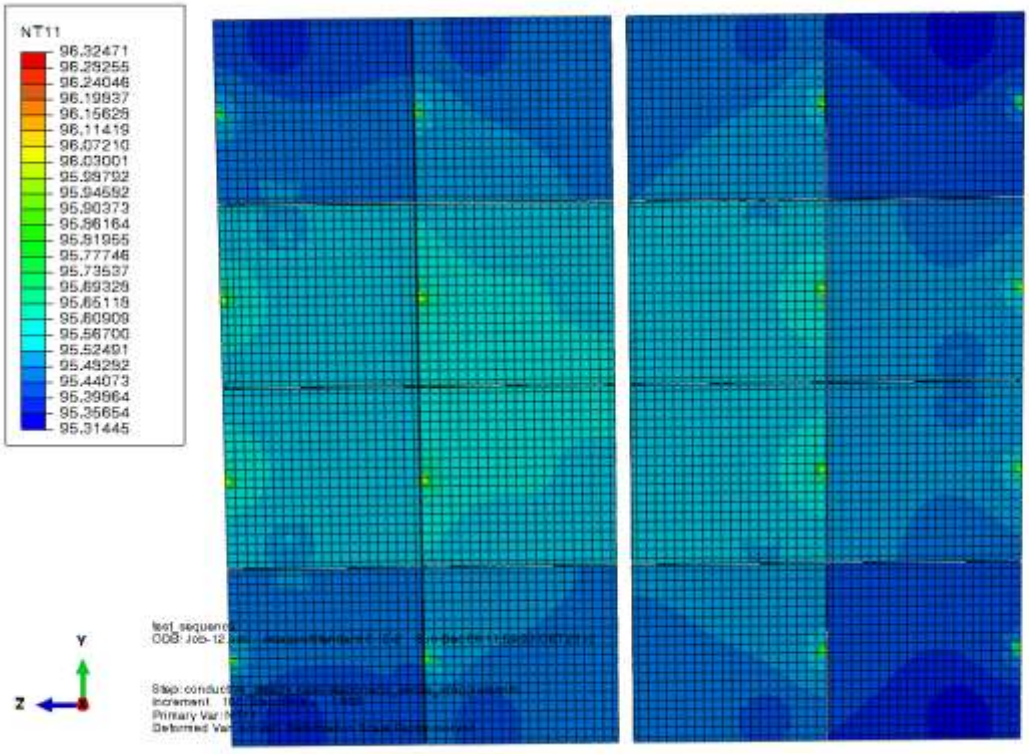

Figure 13-74 Detectors back temperature distribution [K]

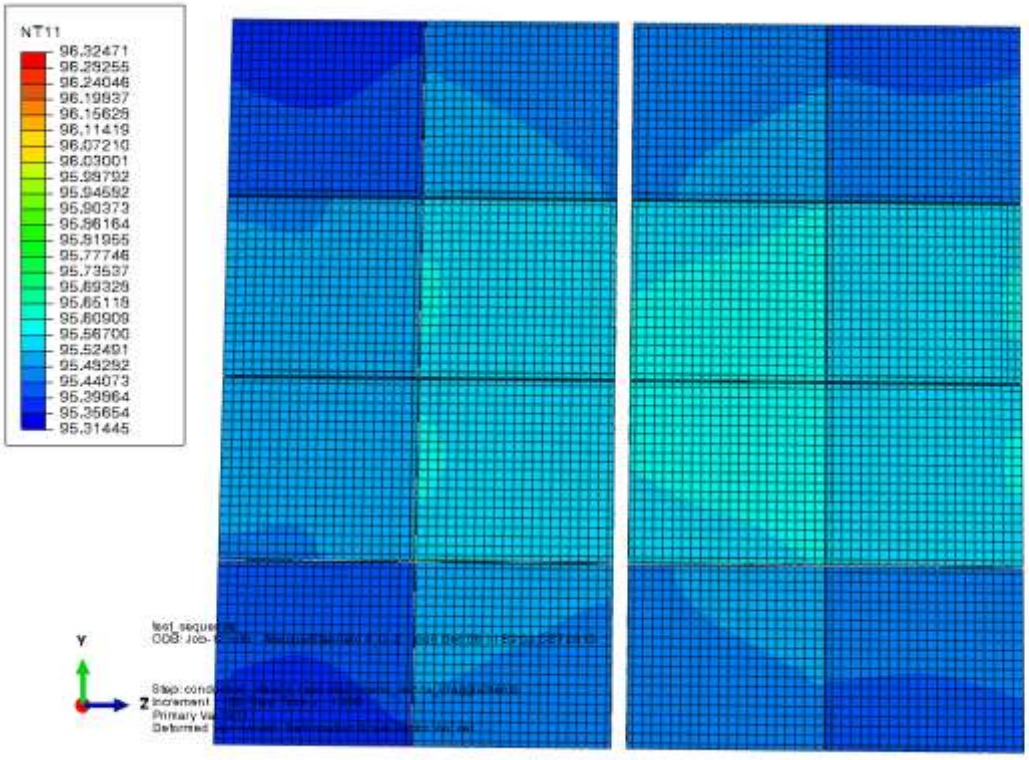

Figure 13-75 Detectors front temperature distribution [K]

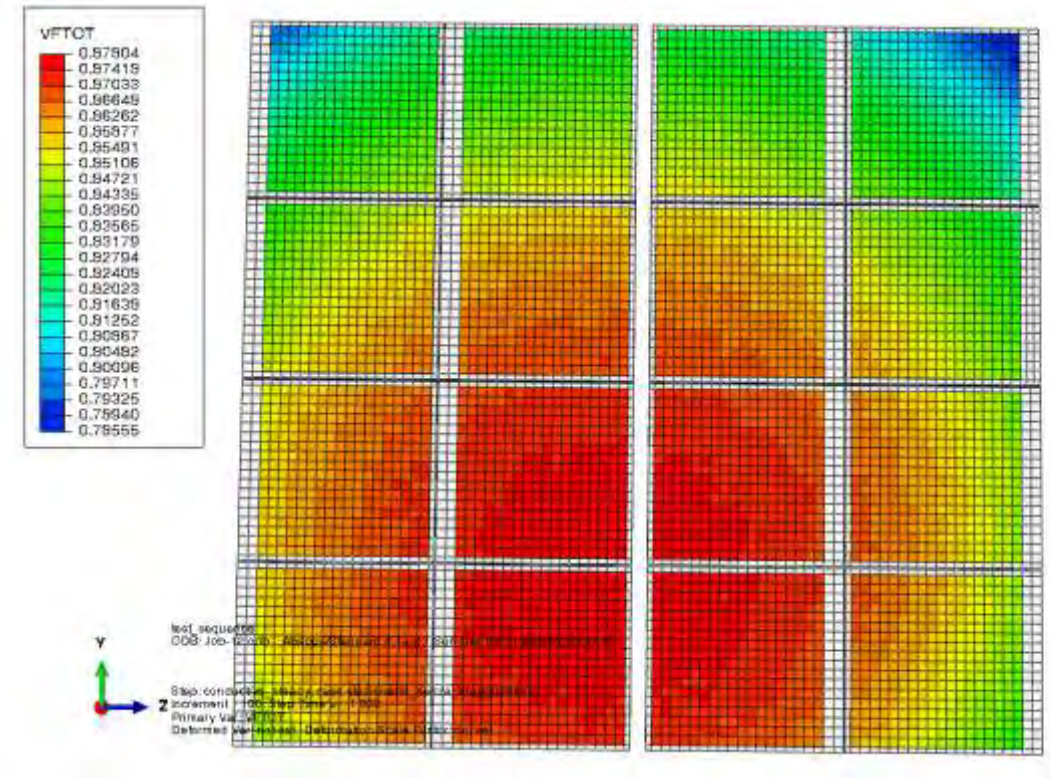

Figure 13-76 Detectors view factor

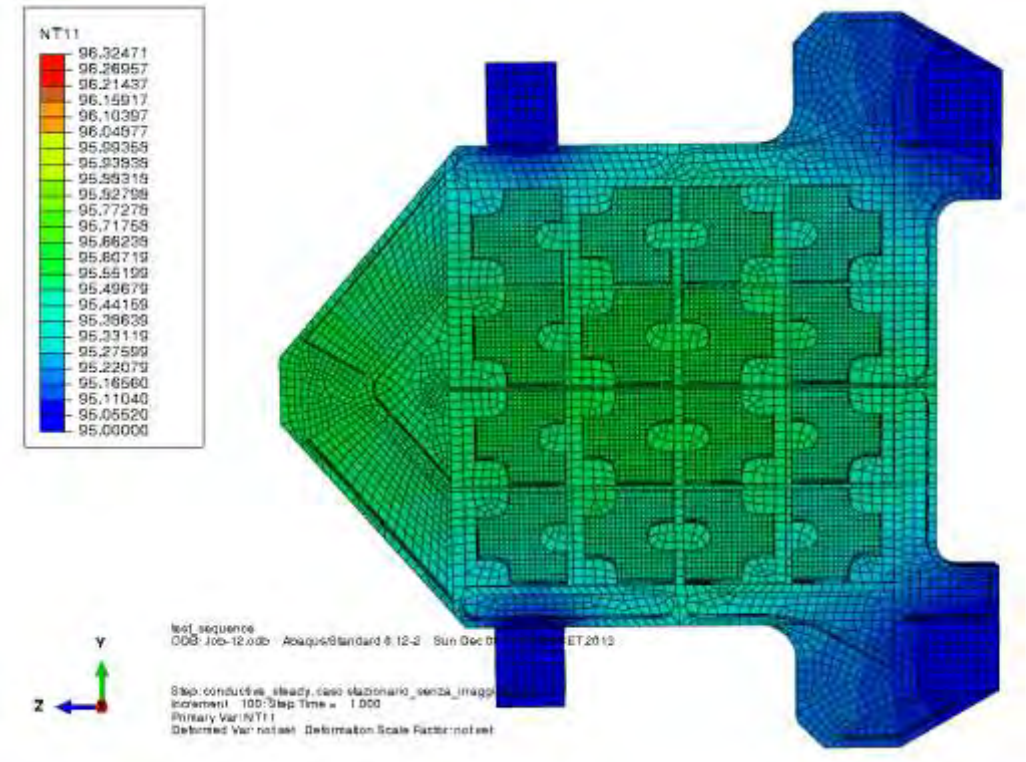

Figure 13-77 Detectors and CSS back temperature distribution [K]

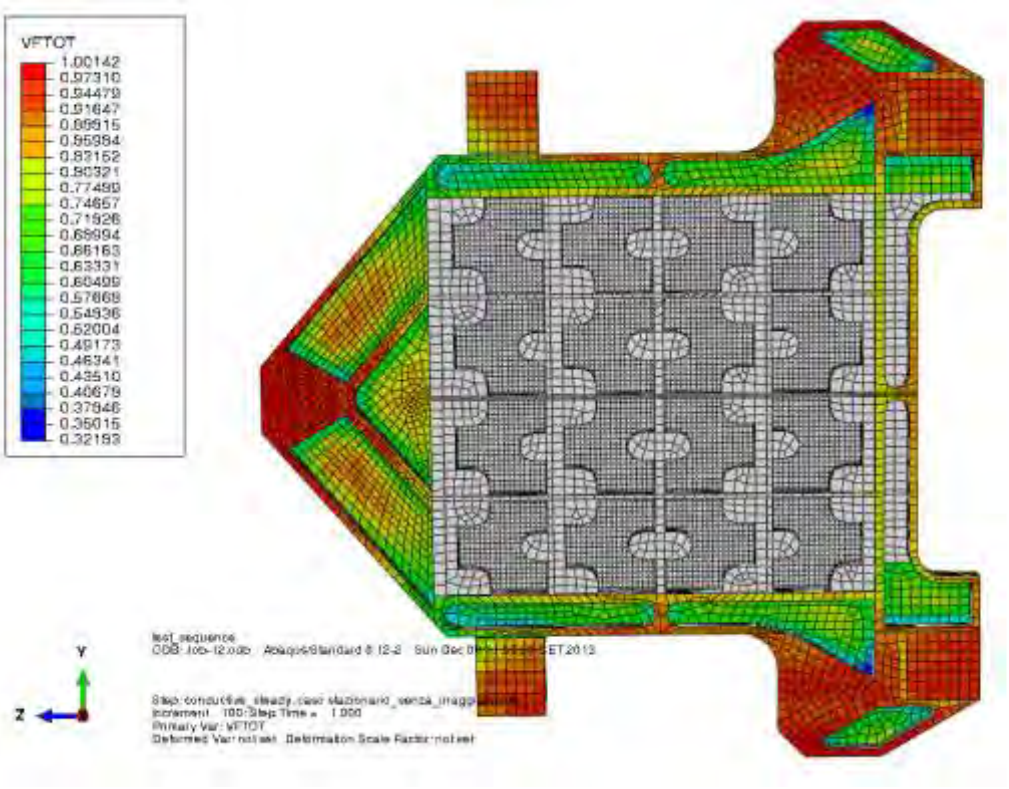

Figure 13-78 Detectors and CSS back view factor

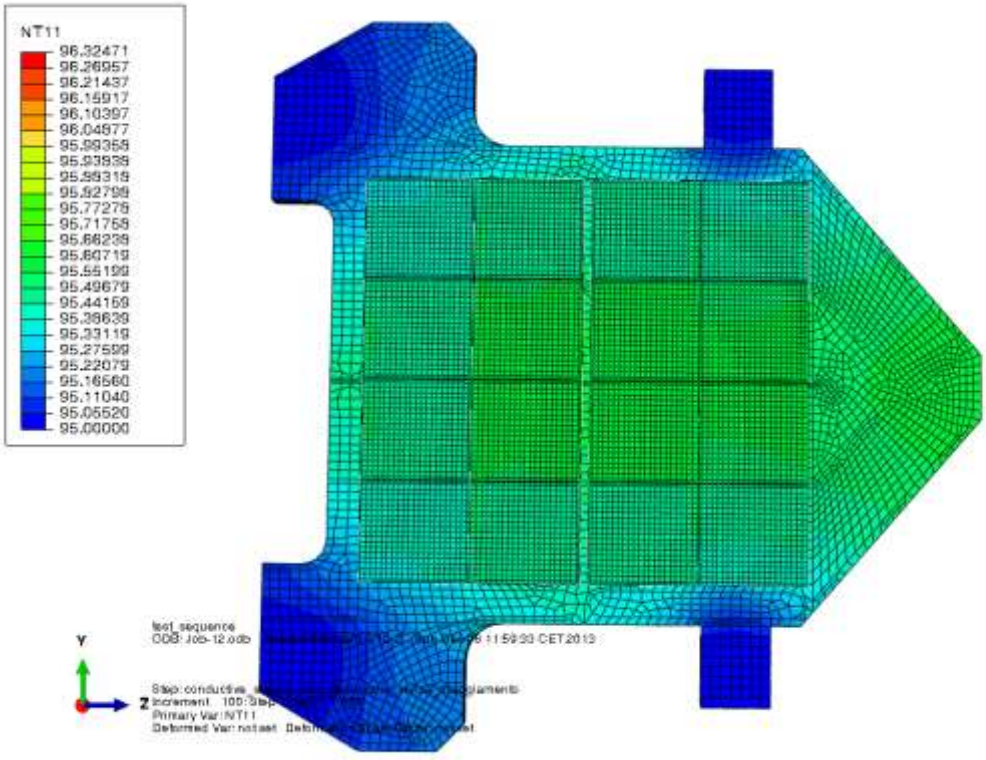

Figure 13-79 Detectors and CSS temperature distribution [K]

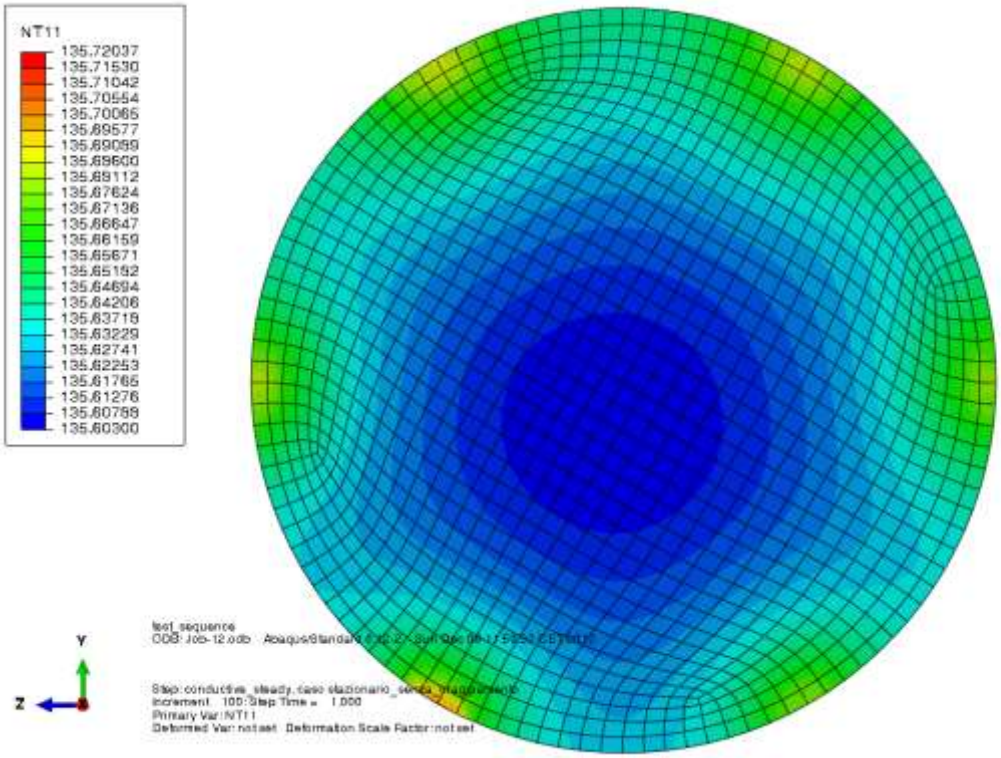

Figure 13-80 Filter back temperature distribution [K]

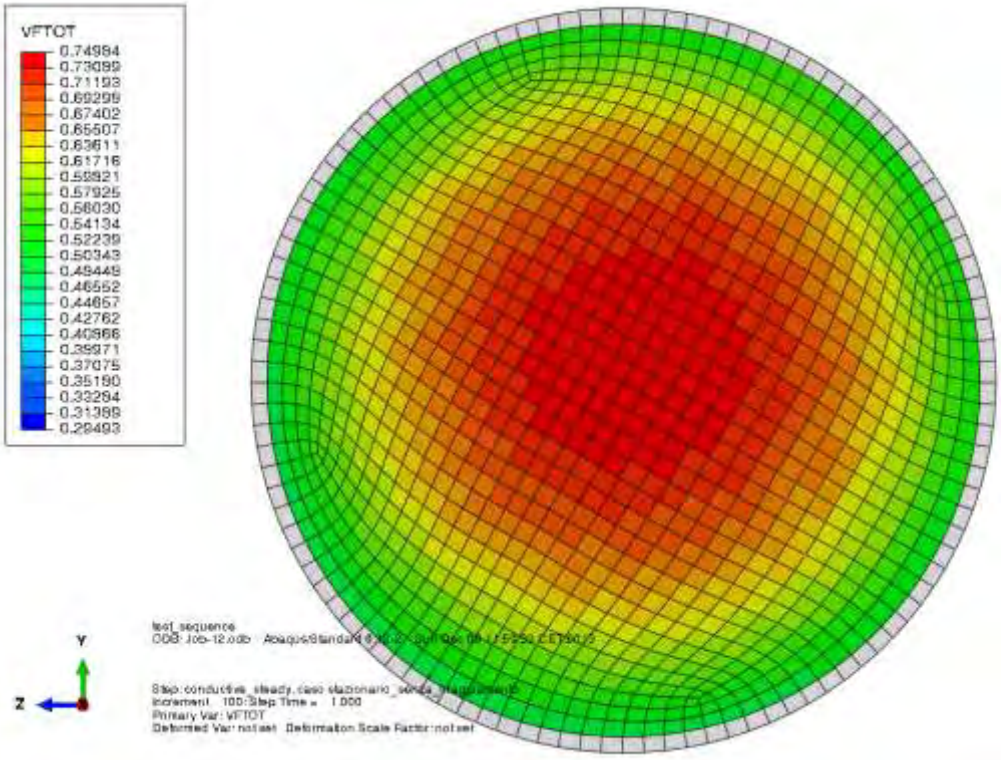

Figure 13-81 Filter back view factor

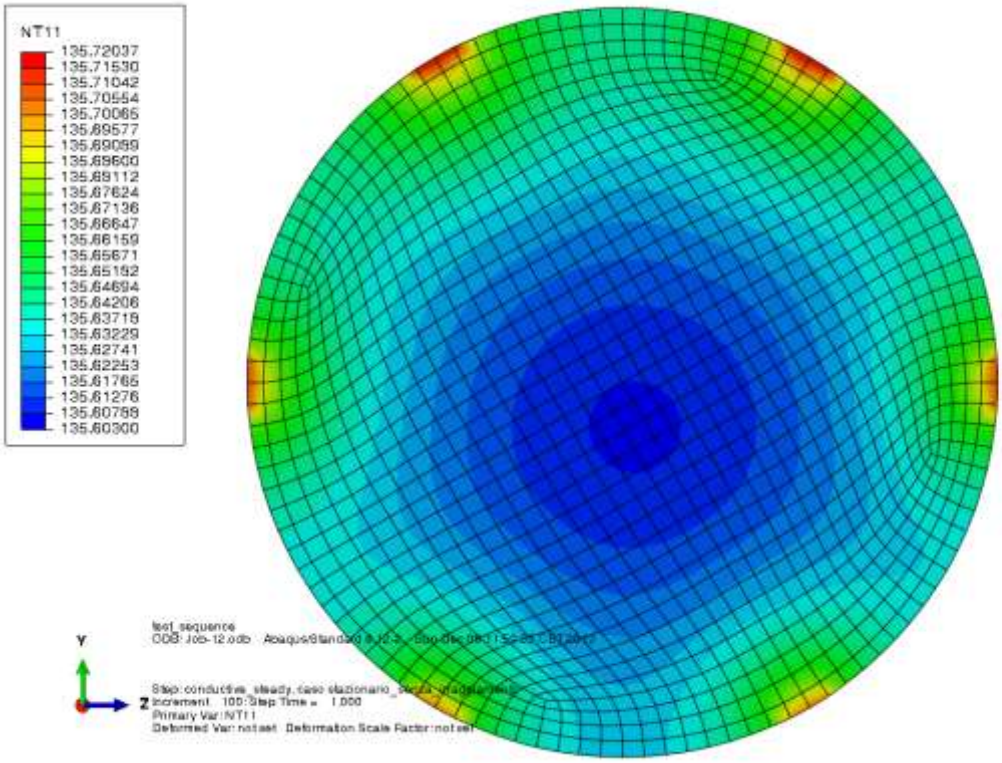

Figure 13-82 Filter front temperature distribution [K]

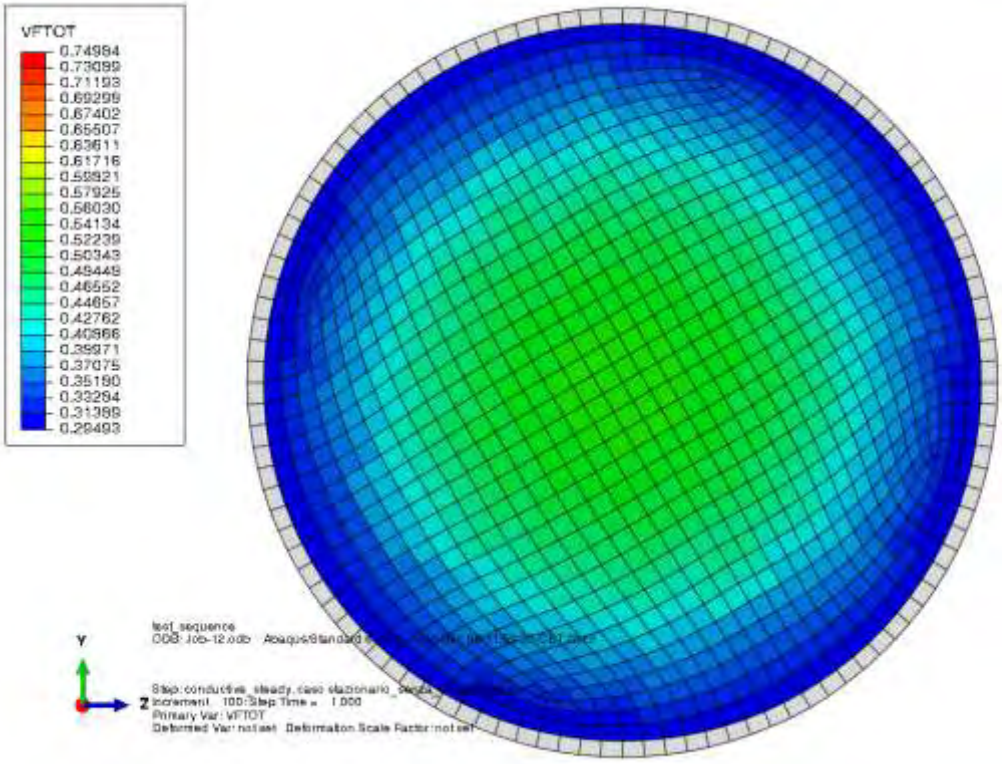

Figure 13-83 Filter front view factor

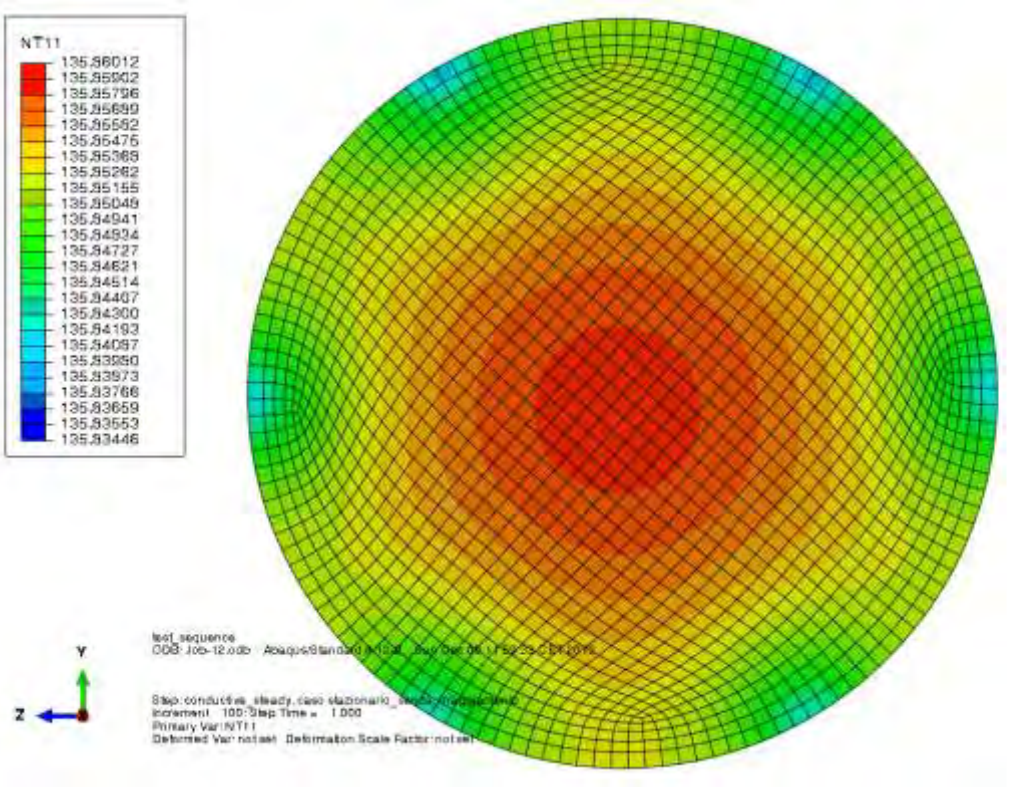

Figure 13-84 Grism back temperature distribution [K]

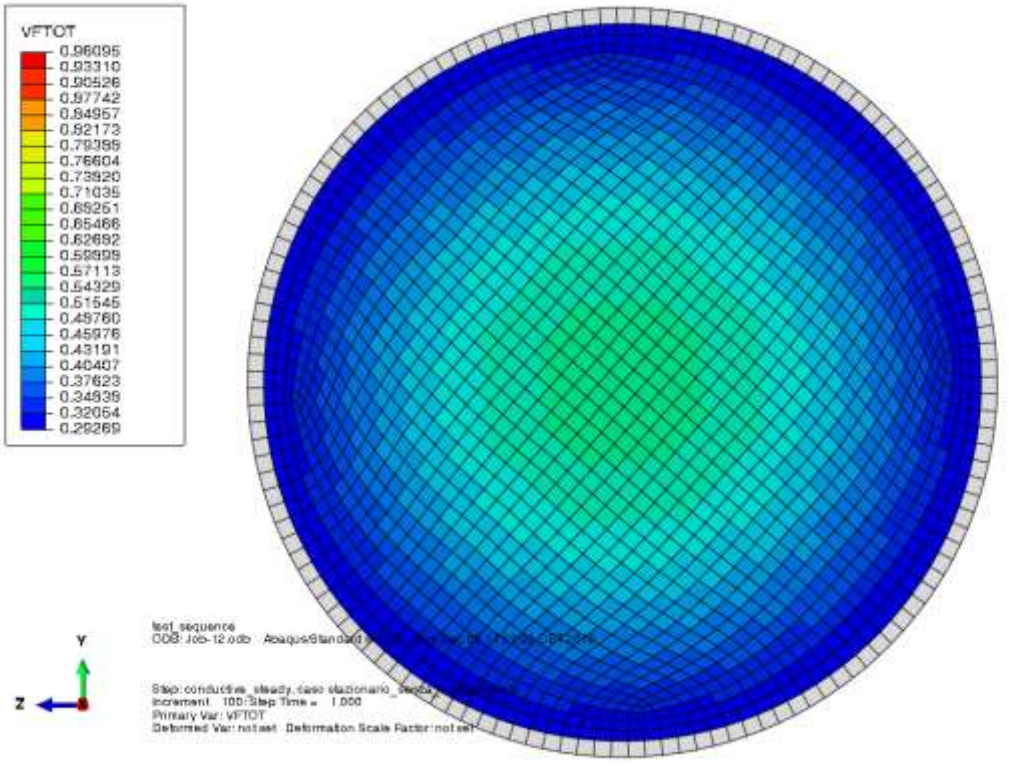

Figure 13-85 Grism back view factor

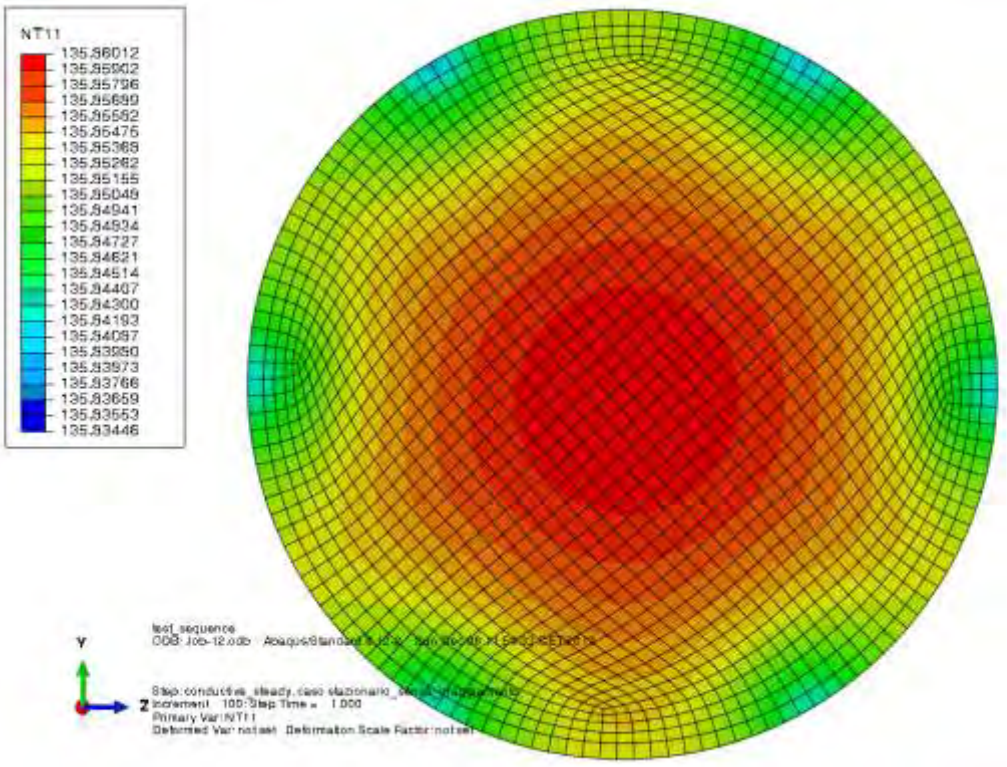

Figure 13-86 Grism back temperature distribution [K]

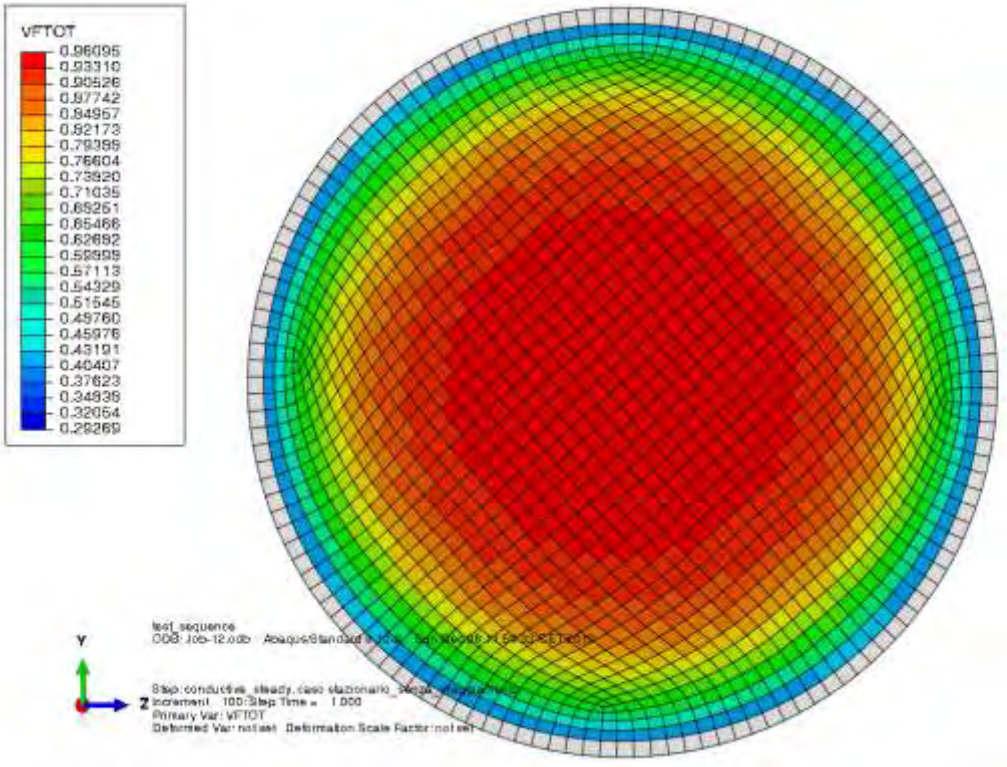

Figure 13-87 Grism back view factor

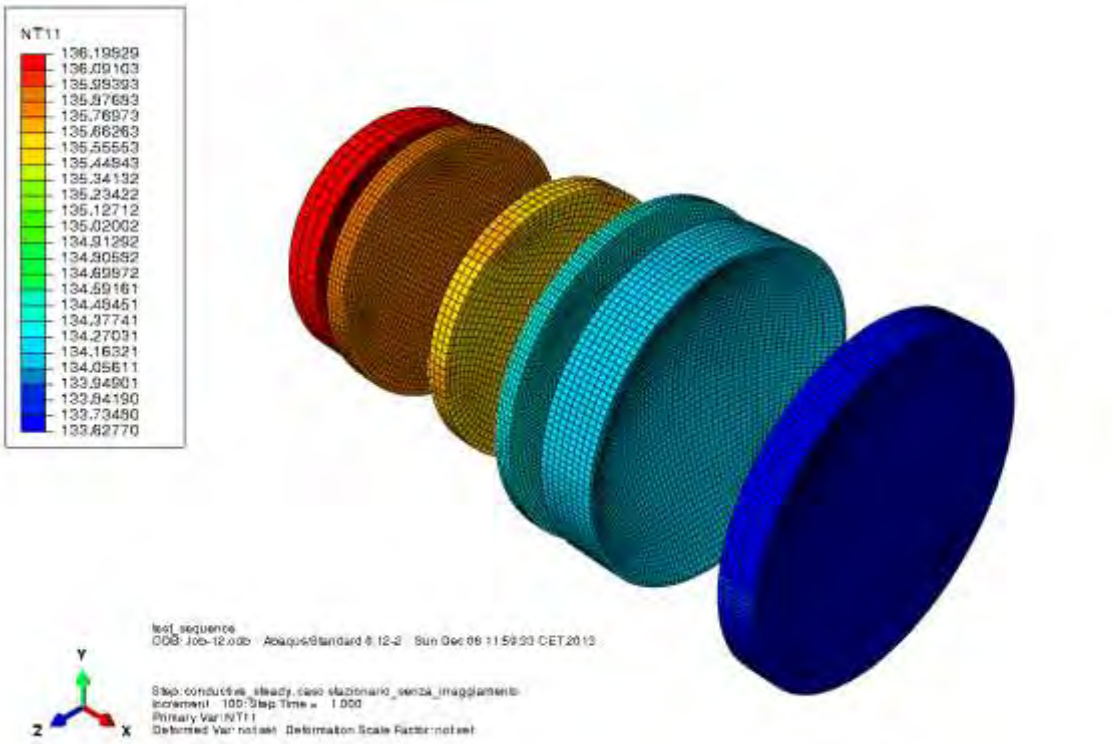

Figure 13-88 NI-OA lenses temperature distribution [K]

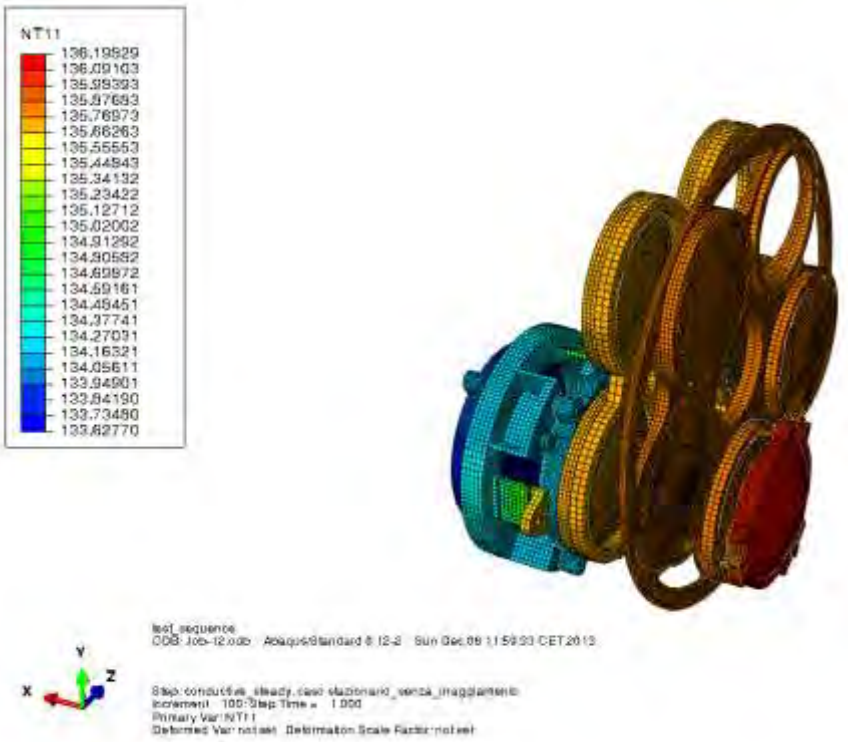

Figure 13-89 Wheels and lenses temperature distribution [K]

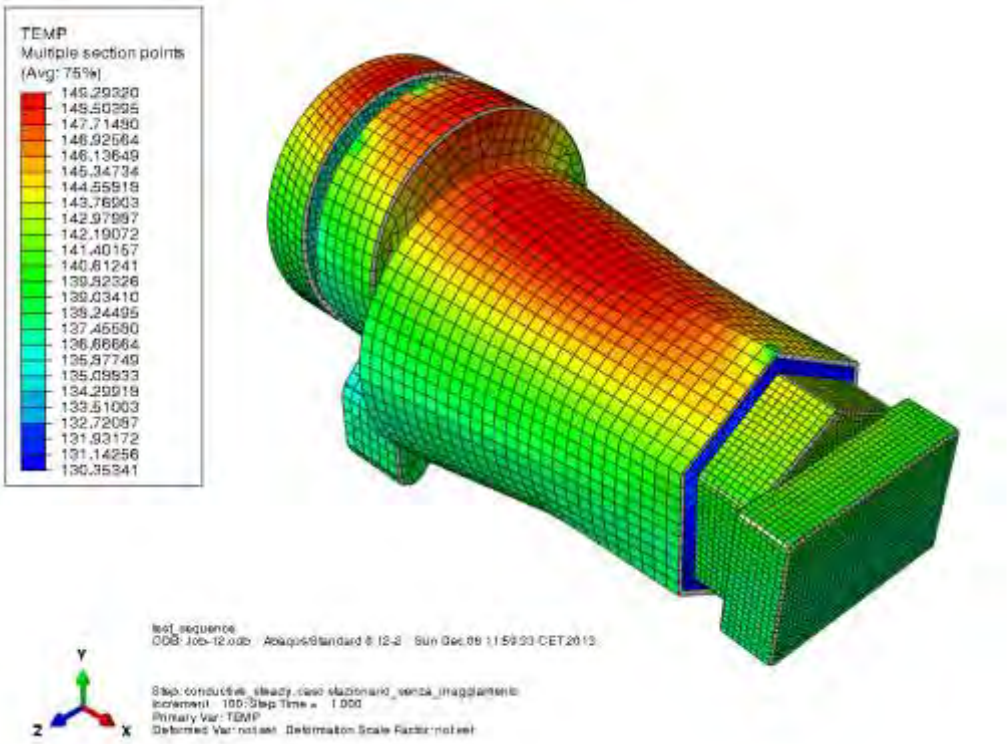

Figure 13-90 MLI Shields temperature distribution [K]

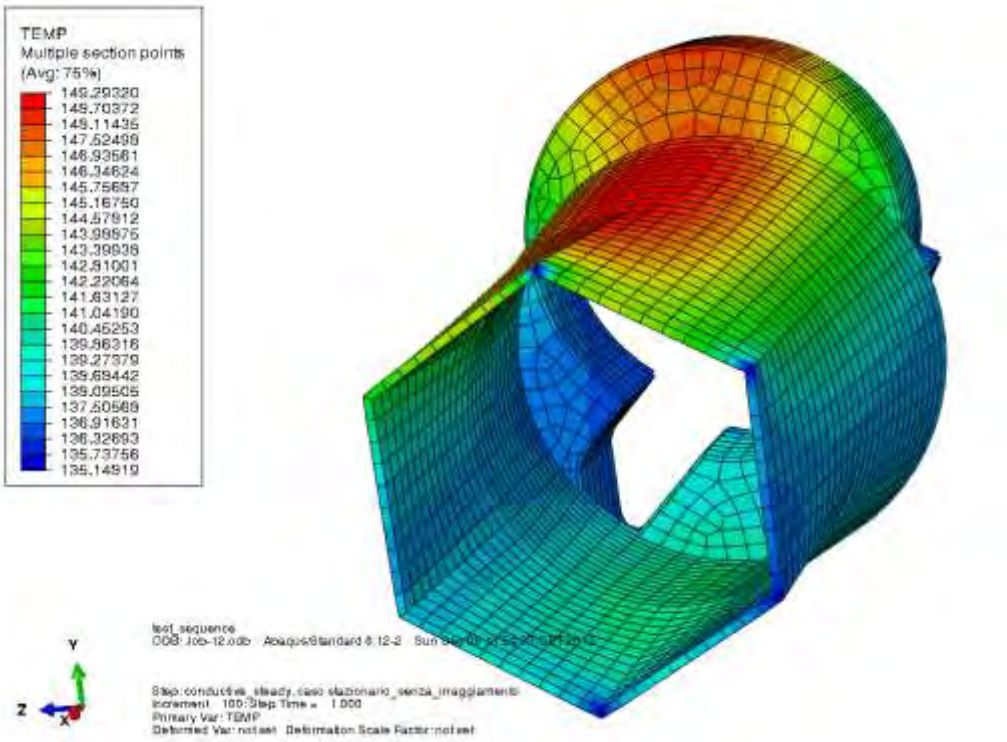

Figure 13-91 Main MLI Shield external temperature distribution [K]

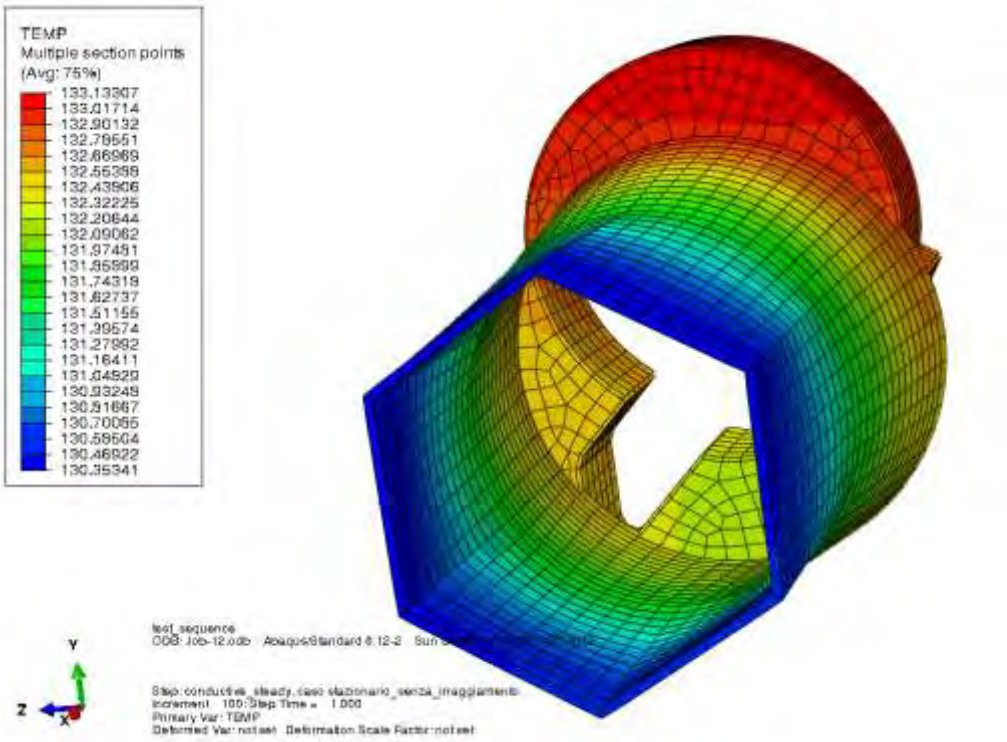

Figure 13-92 Main MLI Shield internal temperature distribution [K]

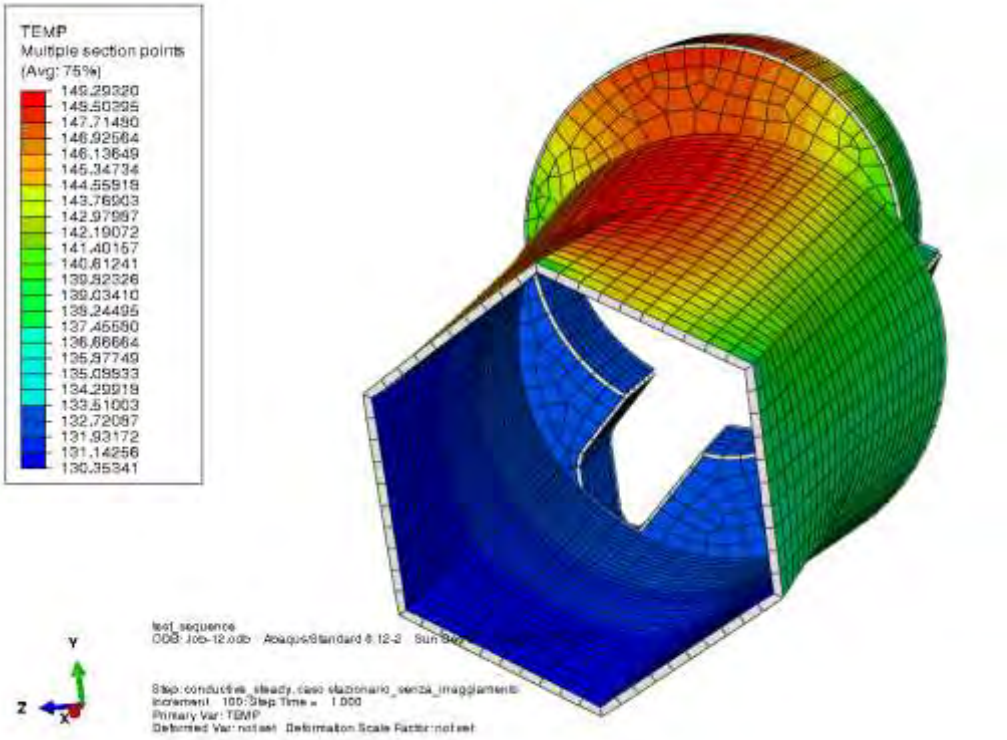

Figure 13-93 Main MLI Shield internal and external temperature distribution [K]

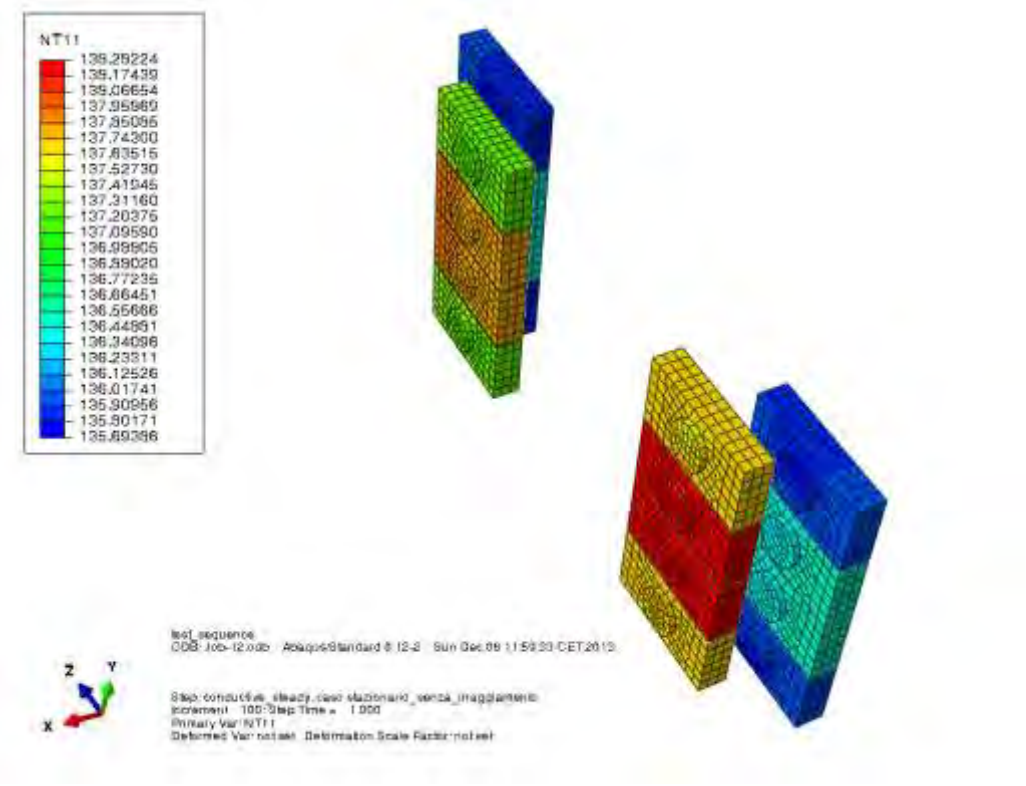

Figure 13-94 Sidecars temperature distribution [K]

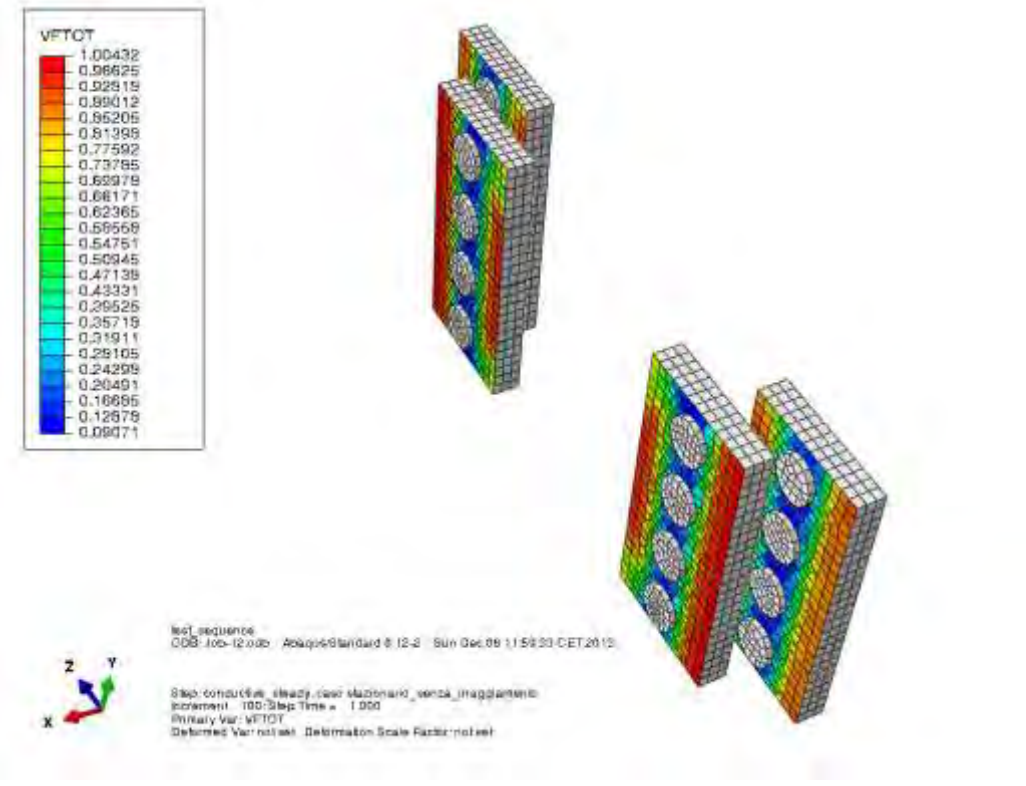

Figure 13-95 Sidecars view factor

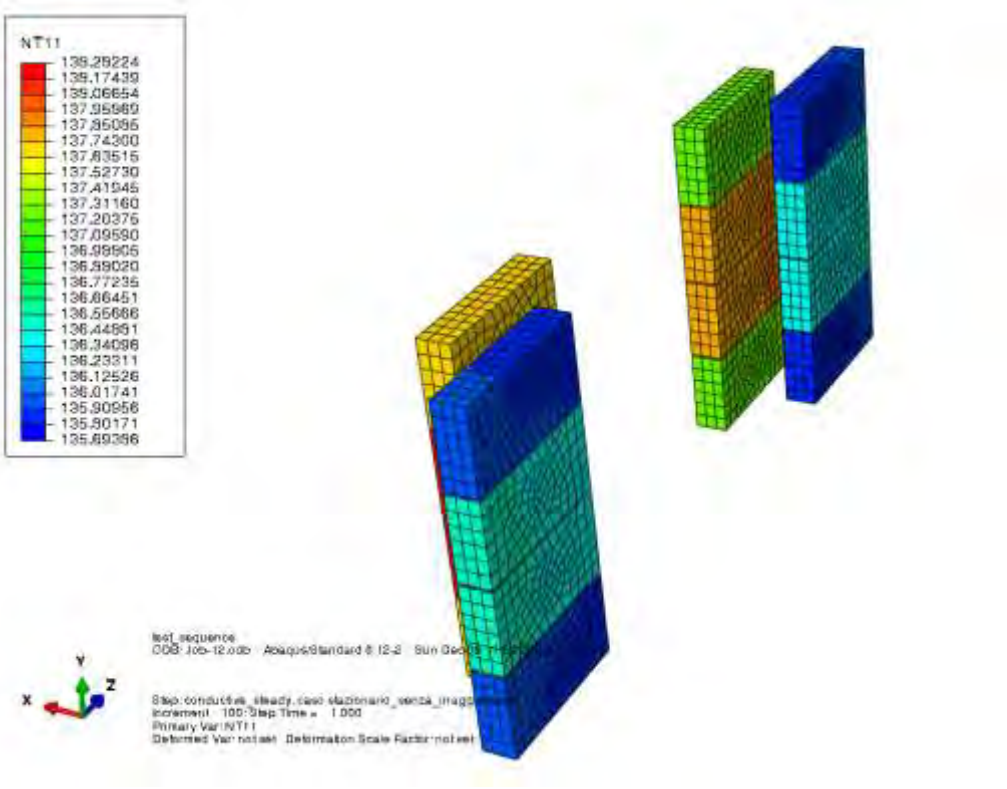

Figure 13-96 Sidecars temperature distribution [K]

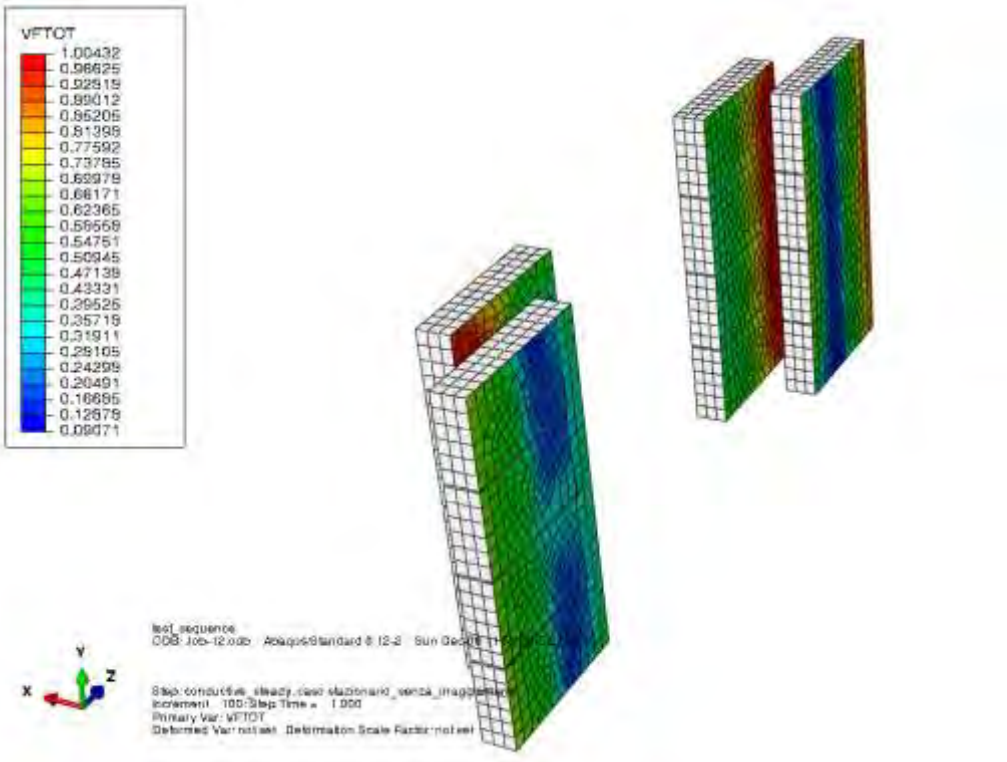

Figure 13-97 Sidecars view factor

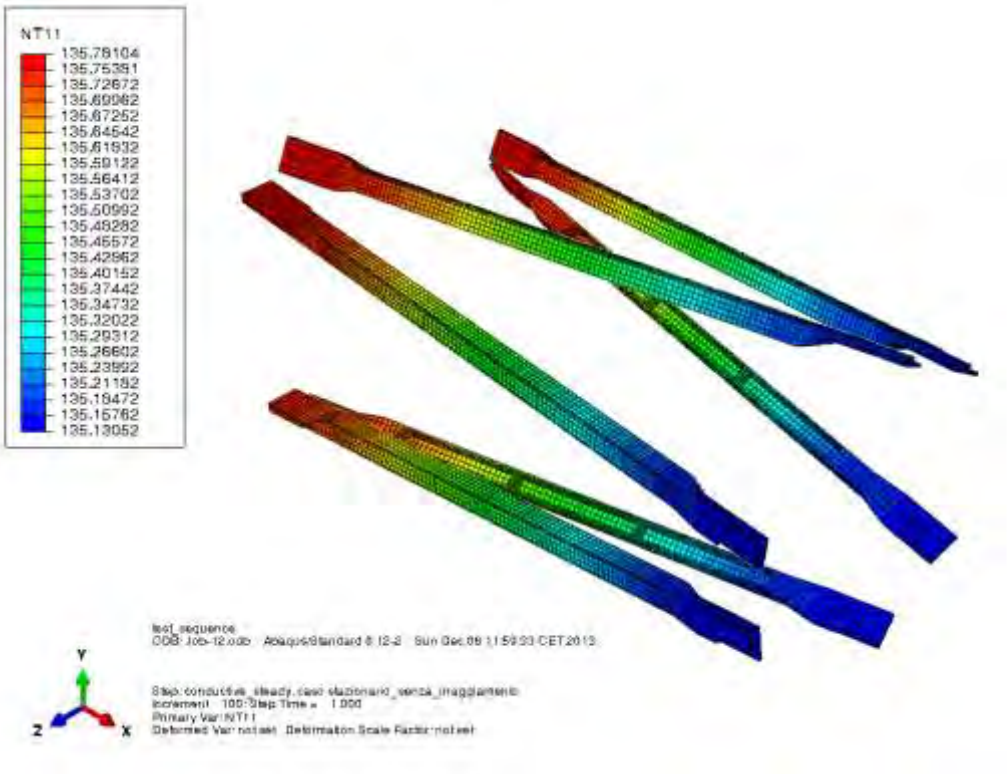

Figure 13-98 Structural beams temperature distribution [K]

13.2.1. JOB 12 temperature profiles on optical units

All the temperature profiles on the different units, calculated along the paths indicated in Chapter 11, are now shown in the next Figures. Captions and unit names are reported directly in the figures.

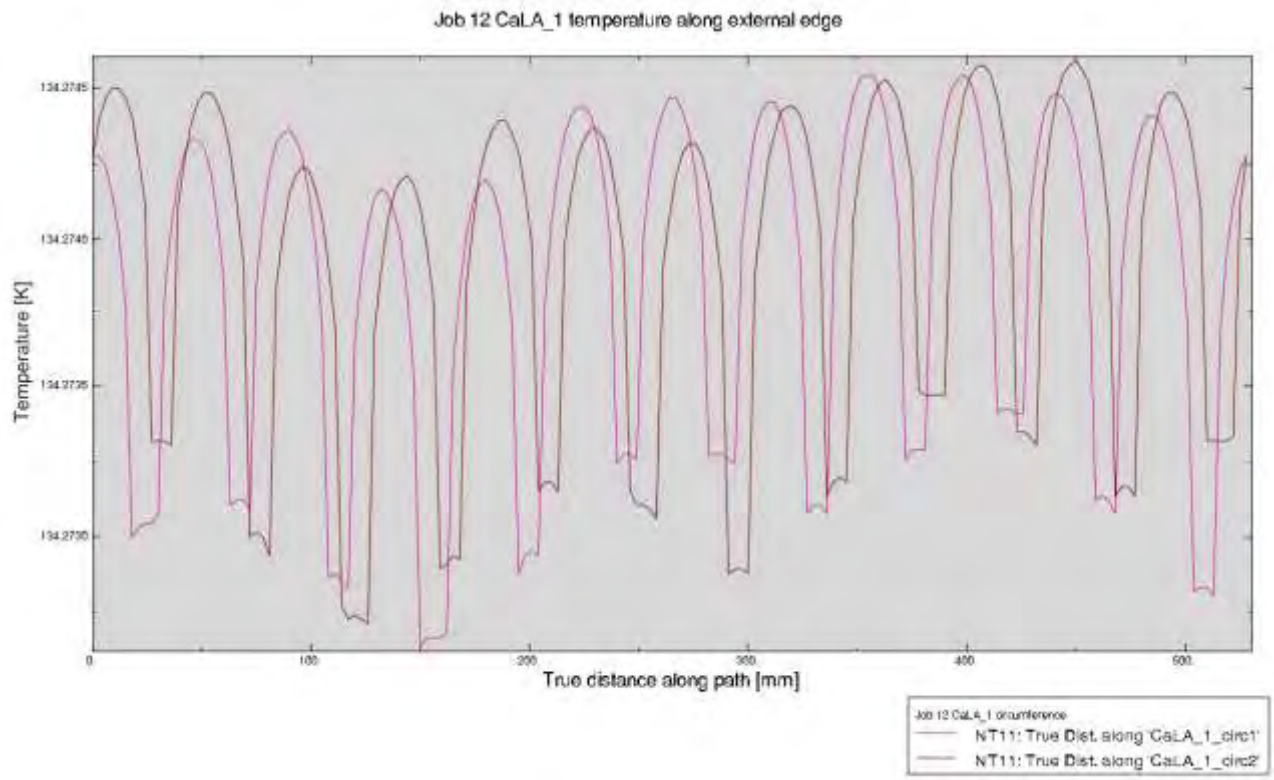

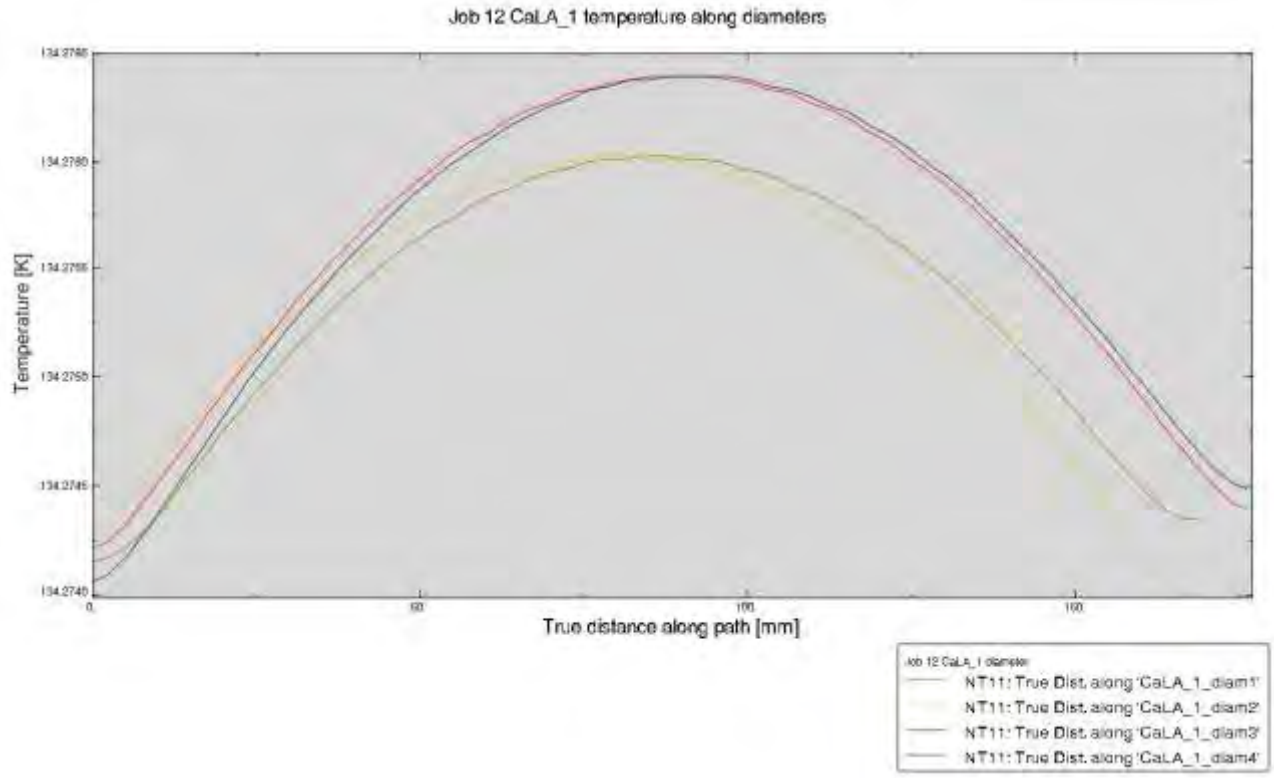

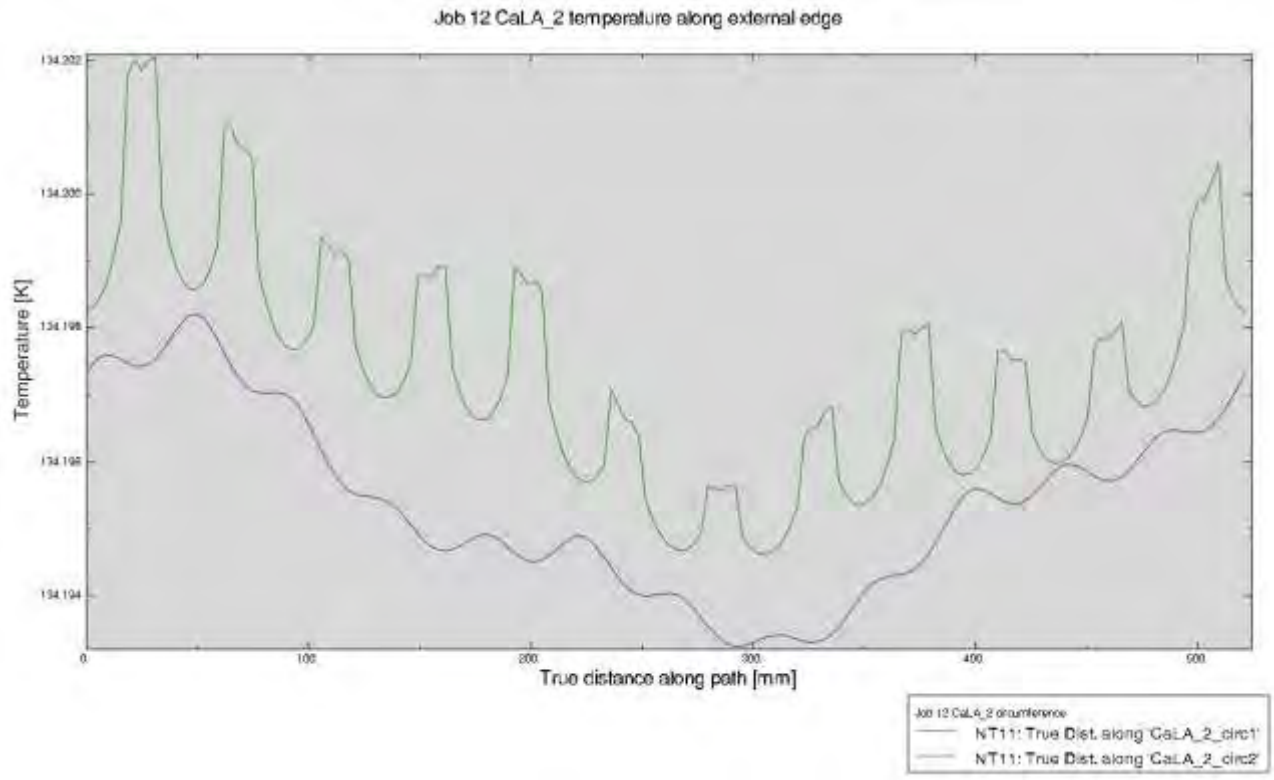
Job 12 CaLA_2 temperature along external edge
Temperature [K]
True distance along path [mm]
Job 12 CaLA_2 circumference
NT11: True Dist. along 'CaLA_2_circ1'
NT11: True Dist. along 'CaLA_2_circ2'

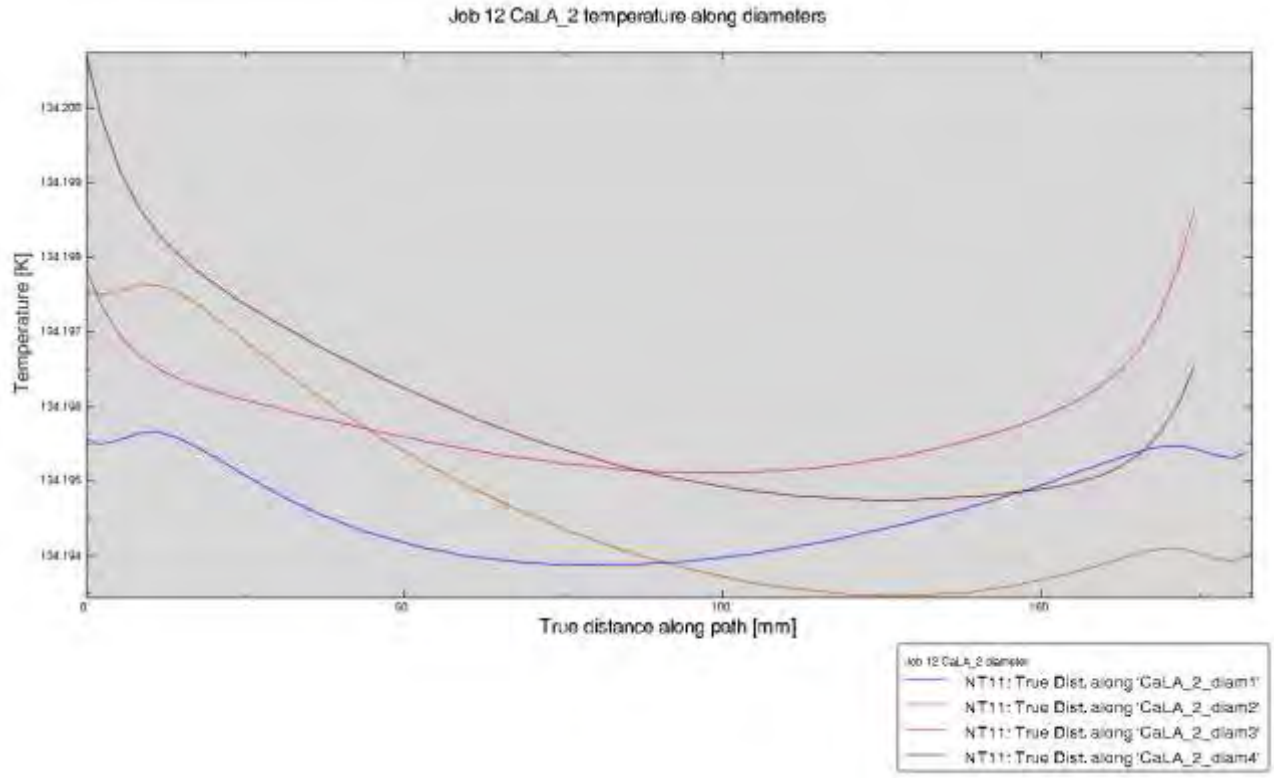
Job 12 CaLA_2 temperature along diameters
Temperature [K]
True distance along path [mm]
Job 12 CaLA_2 diameter
NT11: True Dist. along 'CaLA_2_diam1'
NT11: True Dist. along 'CaLA_2_diam2'
NT11: True Dist. along 'CaLA_2_diam3'
NT11: True Dist. along 'CaLA_2_diam4'

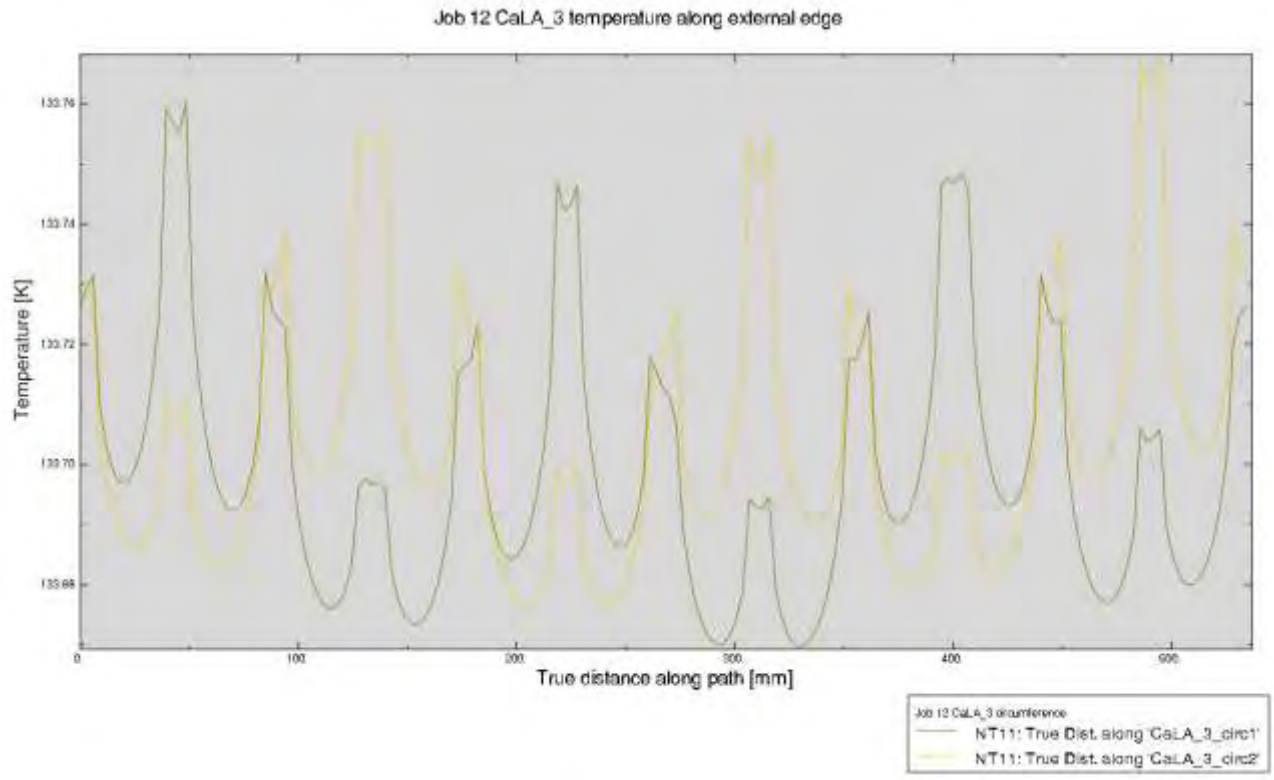
Job 12 CaLA_3 temperature along external edge
Temperature [K]
True distance along path [mm]
Job 12 CaLA_3 circumference
NT11: True Dist. along 'CaLA_3_circ1'
NT11: True Dist. along 'CaLA_3_circ2'

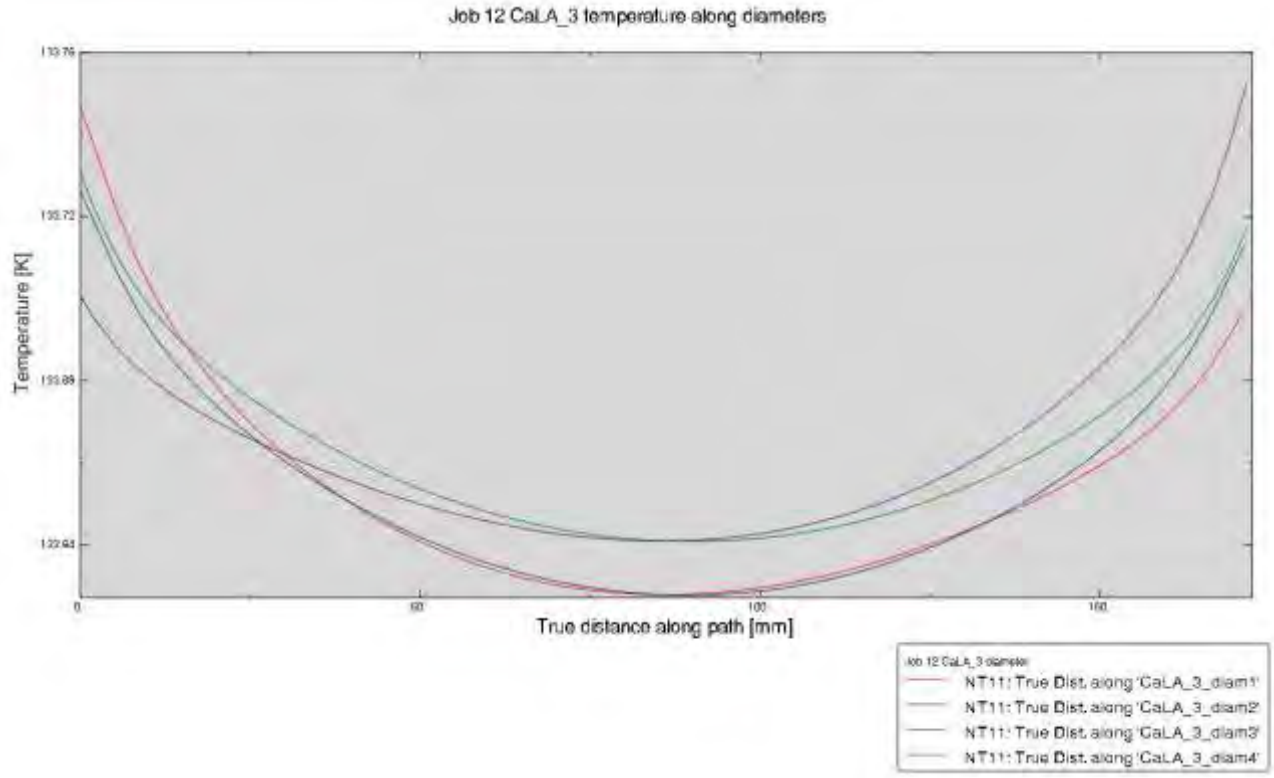
Job 12 CaLA_3 temperature along diameters
Temperature [K]
True distance along path [mm]
Job 12 CaLA_3 diameter
NT11: True Dist. along 'CaLA_3_diam1'
NT11: True Dist. along 'CaLA_3_diam2'
NT11: True Dist. along 'CaLA_3_diam3'
NT11: True Dist. along 'CaLA_3_diam4'

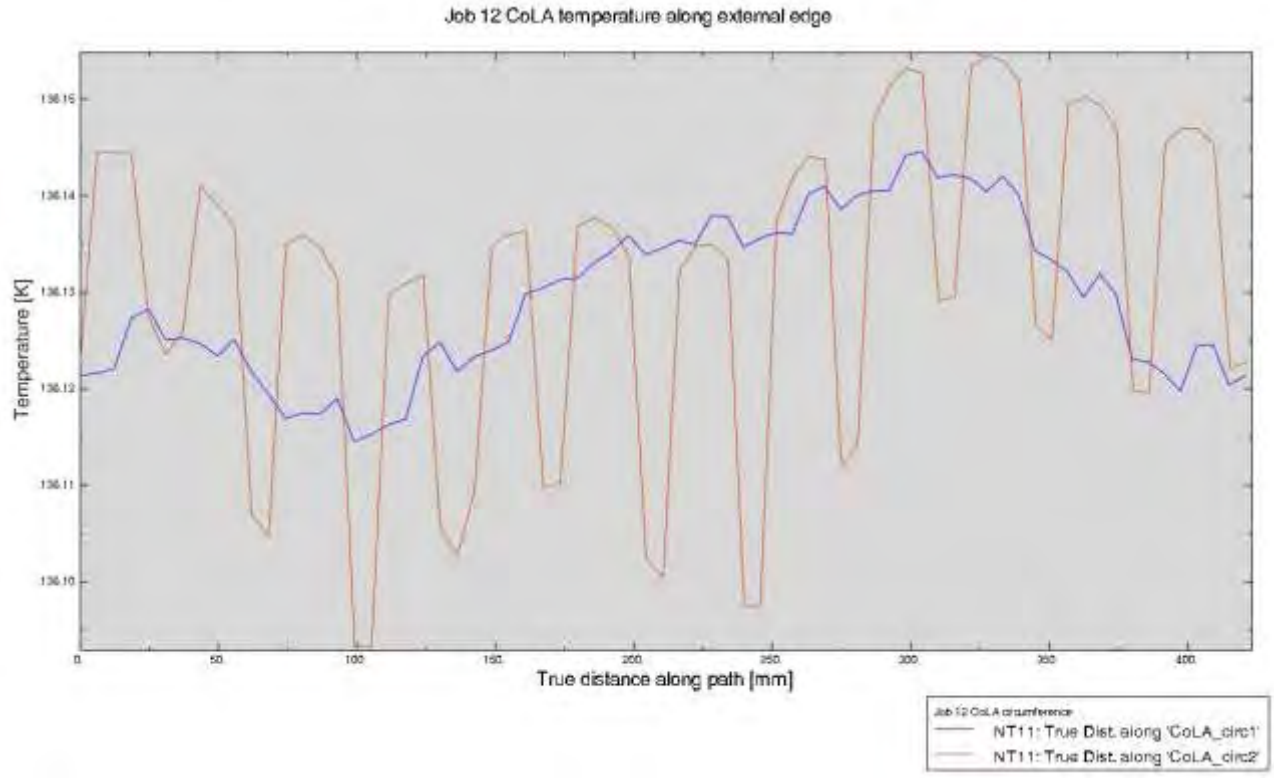
Job 12 CoLA temperature along external edge
Temperature [K]
True distance along path [mm]
Job 12 CoLA circumference
NT11: True Dist. along 'CoLA_circ1'
NT11: True Dist. along 'CoLA_circ2'

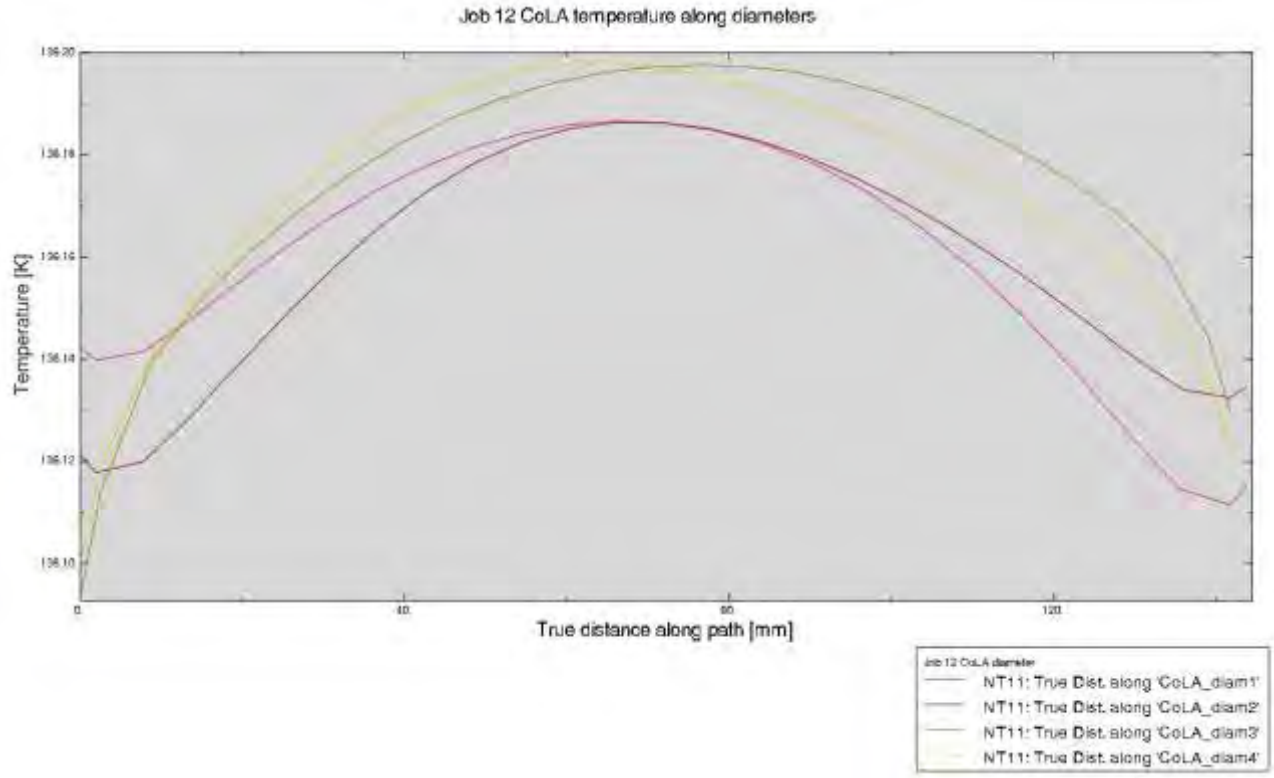
Job 12 CoLA temperature along diameters
Temperature [K]
True distance along path [mm]
Job 12 CoLA diameter
NT11: True Dist. along 'CoLA_diam1'
NT11: True Dist. along 'CoLA_diam2'
NT11: True Dist. along 'CoLA_diam3'
NT11: True Dist. along 'CoLA_diam4'

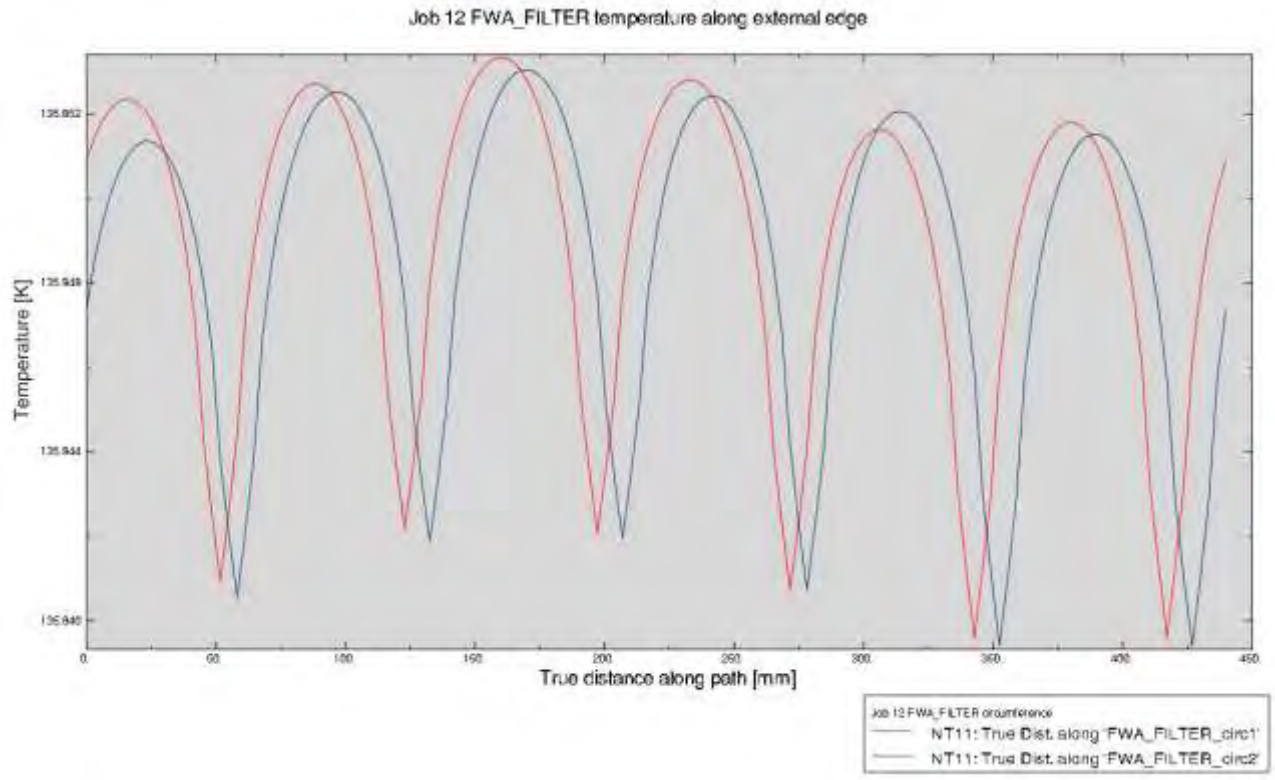
Job 12 FWA_FILTER temperature along external edge
Temperature [K]
True distance along path [mm]
Job 12 FWA_FILTER circumference
NT11: True Dist. along 'FWA_FILTER_circ1'
NT11: True Dist. along 'FWA_FILTER_circ2'

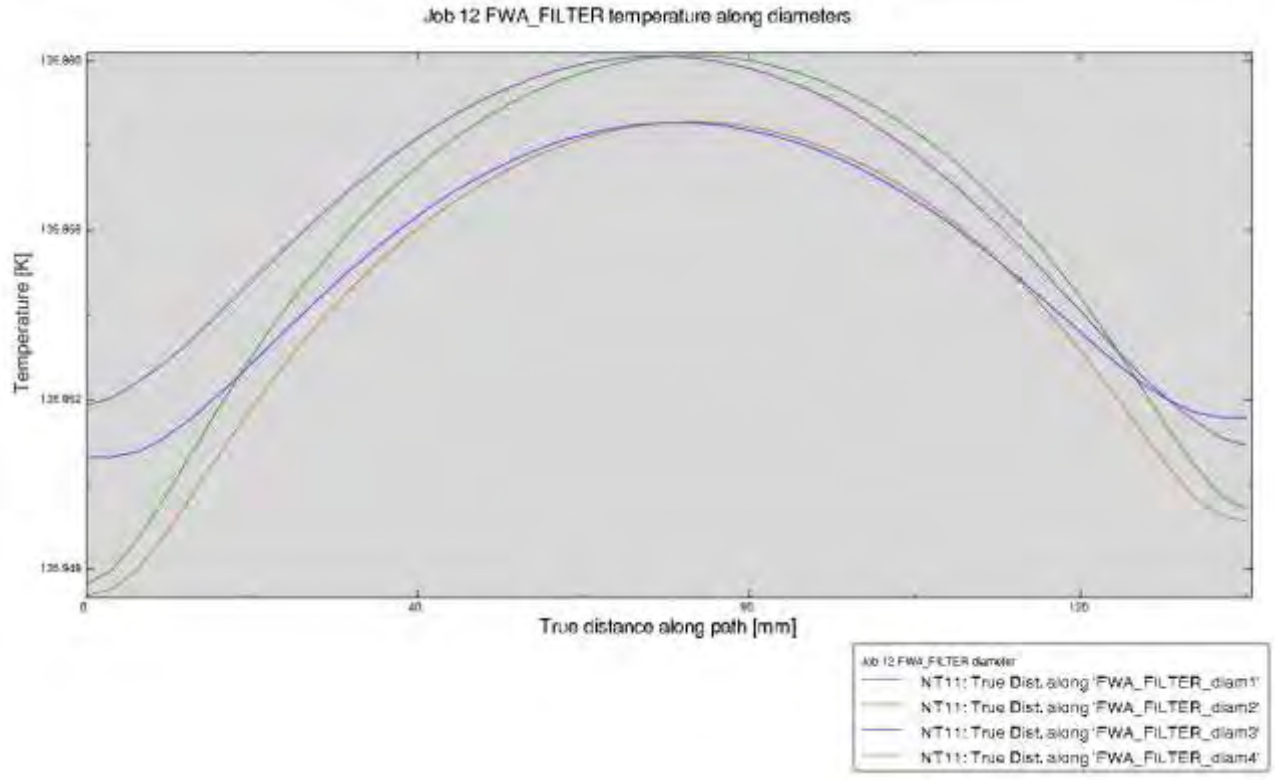
Job 12 FWA_FILTER temperature along diameters
Temperature [K]
True distance along path [mm]
Job 12 FWA_FILTER diameter
NT11: True Dist. along 'FWA_FILTER_diam1'
NT11: True Dist. along 'FWA_FILTER_diam2'
NT11: True Dist. along 'FWA_FILTER_diam3'
NT11: True Dist. along 'FWA_FILTER_diam4'

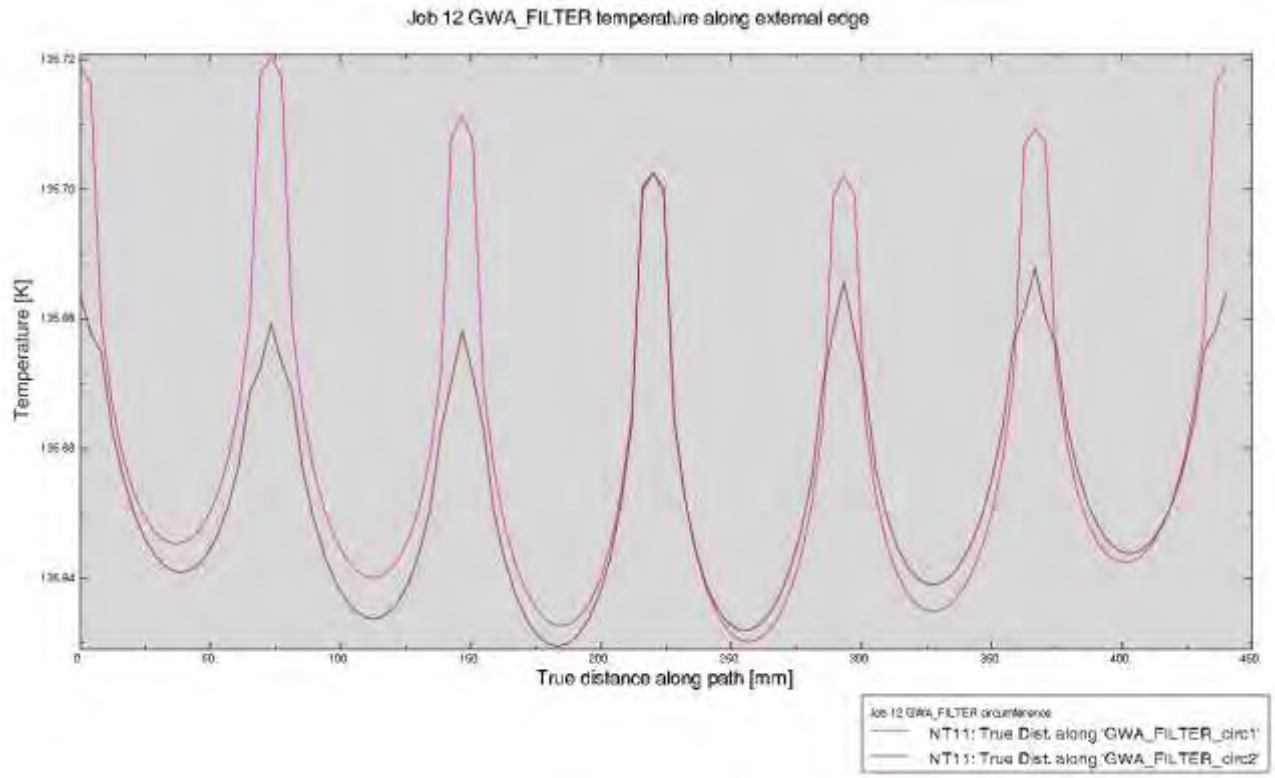
Job 12 GWA_FILTER temperature along external edge
Temperature [K]
True distance along path [mm]
Job 12 GWA_FILTER circumference
NT11: True Dist. along 'GWA_FILTER_circ1'
NT11: True Dist. along 'GWA_FILTER_circ2'

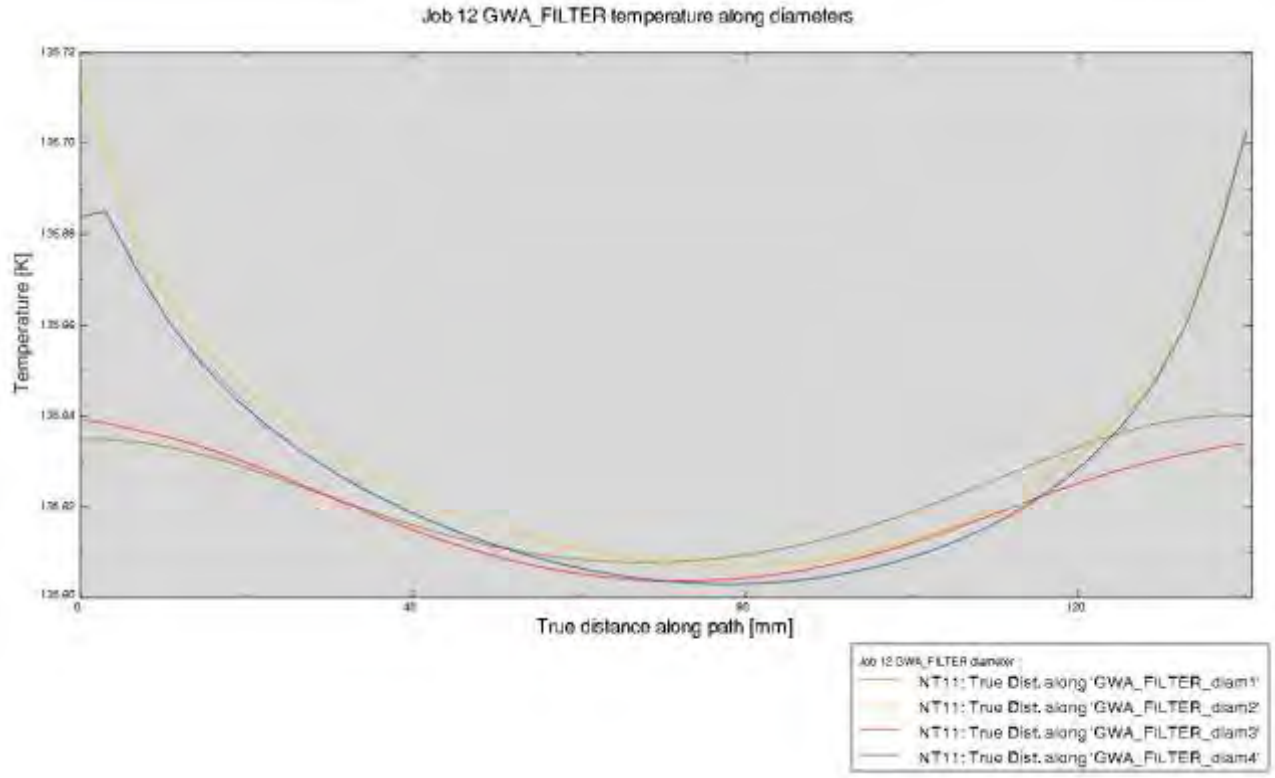
Job 12 GWA_FILTER temperature along diameters
Temperature [K]
True distance along path [mm]
Job 12 GWA_FILTER diameter
NT11: True Dist. along 'GWA_FILTER_diam1'
NT11: True Dist. along 'GWA_FILTER_diam2'
NT11: True Dist. along 'GWA_FILTER_diam3'
NT11: True Dist. along 'GWA_FILTER_diam4'